UNIVERSITY OF OKLAHOMA

GRADUATE COLLEGE

SEISMIC ANALYSIS OF SINGLE AND GROUPED HELICAL PILES IN DENSE SAND WITH SOIL-STRUCTURE INTERACTION

A DISSERTATION

SUBMITTED TO THE GRADUATE FACULTY

in partial fulfillment of the requirements for the

Degree of

DOCTOR OF PHILOSOPHY

By

MARYAM SHAHBAZI
Norman, Oklahoma
2020

SEISMIC ANALYSIS OF SINGLE AND GROUPED HELICAL PILES IN DENSE SAND WITH SOIL-STRUCTURE INTERACTION

A DISSERTATION APPROVED FOR THE
SCHOOL OF CIVIL ENGINEERING AND ENVIRONMENTAL SCIENCE

BY THE COMMITTEE CONSISTING OF

Dr. Amy B. Cerato, Chair

Dr. Kianoosh Hatami

Dr. Andy Madden

Dr. Gerald A. Miller

Dr. Kanthasamy K. Muraleetharan

To my *parents*,

for their unconditional love, support, and encouragement.

To my *husband*,

for his endless support, dedication, and sacrifices.

Acknowledgments

I would like to thank my dissertation advisor and committee chair, Professor Amy B. Cerato for her invaluable support and advice throughout my doctoral studies. Her continuous care and guidance made this endeavor successful. I also would like to extend my gratitude to Professors Gerald Miller, K.K. "Muralee" Muraleetharan, Kianoosh Hatami, and Andrew Elwood Madden at the University of Oklahoma for serving on my committee and their scientific guidance and technical advice.

I am thankful to Professor Hesham El Naggar and Mr. Moustafa El-Sawy at the University of Western Ontario for their contributions to the conduction of full-scale shake table test and their helpful comments on my research. I also gratefully acknowledge Dr. Hussam Mahmoud and Mr. Emad Hassan, at the Colorado State University for their cooperation and valuable assistance in the last part of my research on risk assessment and sharing the structural Opensees code.

Finally, I would like to express my heartful thank to my family for their constant support and sacrifice during my education all these years to pave my way toward my dreams.

Table of Content

List of Tables

List of Figures

Abstract

The successful performance of helical piles under many loading conditions, specifically earthquake motions, make them very popular. Nevertheless, only a few, limited, realistic and quantitative studies on their seismic behavior are available in the literature. The main objective of this research was to evaluate the seismic performance of helical piles by analyzing data from a full-scale experimental shake table test, as well as creating a calibrated model using the commercially available computer program DynaPile. In addition, the seismic performance of grouped helical piles supporting a superstructure was assessed through risk analysis.

A full-scale experimental testing program using a large shake table located at the University of California-San Diego was performed on ten steel piles including nine helical piles with varying geometry and one driven pile embedded in dense sand over five days. The test program was subjected to pulse, white noise excitation and two replicated earthquake motions with different frequency content (1994 Northridge California earthquake and 1995 Kobe earthquake). Different intensities of shakes were generated by scaling the original earthquake amplitudes (50%, 75%, and 100%). On Day 1, test sand was compacted in 30 cm-layers in a 6.7 m long, 3.0 m wide and 4.6 m high laminar box to achieve approximately 100% relative density. Several accelerometers were placed at various elevations and locations within the sand bed, as well as on the exterior side of the laminar box to record sand behavior and its dynamic properties. On Day 2, piles were installed in the soil and free-head piles were tested. On Day3 concrete blocks were placed on top of each individual pile to simulate inertial loads. Strain gauges attached to the exterior pile walls provided data for analyzing the behavior of piles. In order to evaluate group pile behavior, two sets of four same-diameter piles were tied together to form two 2x2 grouped helical piles. Each pile group was

connected by a steel skid placed atop the piles. Two accelerometers were placed on opposite sides of the skids near its center of mass and connected to the data acquisition system. On Day 4 each skid was connected to every pile head with two bolts to form a fixed connection. On Day 5, the top bolt of each connection was removed to simulate a pinned pile head connection with the same skids.

The dynamic responses were recorded and measured using both strain gauges on individual piles and accelerometers placed throughout the sand bed as well as on the laminar box and center-of-mass of the skids. Load-displacement and p-y curves were developed to evaluate the response of single and grouped helical piles mainly in terms of resistance and dynamic properties including natural frequency and damping ratio. Damping ratios were attained using four different methods including half-power bandwidth, logarithmic decrement, energy and modal analysis methods. The damping responses under small strain vibration (white noise) and large deformation motion (shakes) as well as the effect of deflection on damping were provided. A special emphasis was placed on the effect of pile slenderness ratio and type of pile-structure connections (i.e. pinned or fixed) on damping. The logarithmic decrement method for small strains and the half-power bandwidth method for both small and large strains were found to yield reasonable damping values for the piles and skids. However, when calculating damping for the soil medium itself, the half-power bandwidth method may not be preferable because the soil exhibits nonlinear behavior. When using the energy method to calculate damping ratio, developing hysteresis load-displacement curves using collected data from one single data recorder (e.g. accelerometer) attached to an appropriate place within the pile-soil-structure system, results in less errors than using data from strain gauges attached to various levels of each pile to develop p-y curves. Moreover, the experimental observations were analyzed to evaluate the soil-pile group-skid

stiffness. To that end, the slope of the line that connected two ends of the maximum loop was considered as experimental stiffness. Generally, piles with a pinned head connection showed higher energy dissipation, but lower stiffness. It was also found that piles with greater slenderness ratio (length/diameter) demonstrated lower value of stiffness. In addition to damping and stiffness, natural frequency of the system was found and compared using both Fast Fourier Transform (FFT) and Frequency Response Function (FRF).

A numerical model in a commercially available software program, DynaPile, was calibrated based on the experimental results. The model was then used to conduct a parametric study to gain a broader understanding of seismic behavior of helical pile groups under varying conditions. The experimental and numerical results were compared and the effects of varying different properties in a soil-pile-structure system's seismic response were discussed. Properties of soil (e.g. shear wave velocity) and structural characteristics including stiffness, damping and slenderness ratio were evaluated in detail. Understanding the parameters that effect the dynamic characteristics of soil-pile systems and quantifying the possible range that can occur under real earthquakes will allow engineers to choose appropriate pile geometry, group configuration and connection type to achieve a desired level of performance.

In addition, estimation of vulnerability of structures and foundations is necessary in seismic zones to have better judgment on the structural performance. Seismic fragility analysis is considered the main method in risk assessment, since it represents a measure for defining the safety margin of the structural system. Since high rise buildings are mostly supported by deep foundations, assessing vulnerability of structures supported by piles is essential even though risk assessment of helical piles has not been addressed in the literature yet. Most structural fragility curves do not take into consideration the contribution of pile foundation systems in the structural vulnerability. Therefore,

this study aims to modify existing fragility curves of a six-story fixed-base steel frame hospital building with buckling-restrained braces (BRBs), to incorporate the effect of helical pile group behavior on the fragility of the structure. To that end, a finite element model of the investigated structure was modified with results from a full-scale shake table test performed on two groups of helical piles embedded in dense sand supporting a superstructure. The primary results show that fixed base design may not be conservative for all conditions and soil-foundation interaction should be considered when creating fragility curves, especially for a stiff structure on soft soils where a high-intensity earthquake is anticipated.

Chapter 1 : INTRODUCTION

1.1 Problem description

Earthquake damage losses in recent decades have been estimated at $7 billion, $30 billion and $200 billion during the 1989 Loma Prieta, 1994 Northridge, and 1995 Kobe earthquakes respectively (Bertero and Bertero 2002). During the Northridge earthquake in 1994, a total of 107 highway bridges were damaged, including seven bridges experiencing partial collapse. The total repair cost for the damaged bridges was estimated to be about $150M USD (Brown et al., 2001). These immense losses and structural failures have prompted a wide investigation into increasing life safety performance of structures. More resilient and seismic resistant infrastructure design along with comprehensive seismic performance evaluations and risk assessment of structures are required to mitigate probable damage and develop recovery strategies.

One type of seismic resilient foundation that has worked in the Pacific Rim area for decades is helical piles. Helical piles are full displacement, drilled deep foundations that consist of a central steel shaft with one or more welded bearing plates. These plates help advance the pile as it is spun into the ground and provide individual bearing areas to increase its bearing capacity as needed. Helical piles have been used in seismically active zones located in Japan and New Zealand due to favorable performance during relatively large earthquakes in the past. Unfortunately, the lack of quantitative data about the seismic behavior of helical piles prevent some engineers from specifying this pile type within earthquake prone areas. Thus, further investigation on their seismic performance is necessary.

Another aspect that should be considered in order to design realistically and safely within seismic zones is soil-structure interaction (SSI). When an earthquake occurs, the ground motion and behavior of the structure and foundation are influenced by the structural, foundation and soil underlying and surrounding the foundation, which is defined as SSI. SSI includes kinematic and inertial interaction effects (Zhang and Wolf, 1998; Givens et al., 2012; Medina et al., 2013). The presence of a pile installed in the subsurface that causes ground motions to deviate from their original path, is defined as kinematic interaction. Base shear and moments due to inertial response of a structure causing displacement of the foundation relative to the free field is defined as inertial interaction. Although soil-pile-structure interaction significantly effects the response of the engineered system, this effect is typically ignored in conventional designs and the foundation and soil are considered rigid with the structure connected to a fixed base; in many cases, this does not reflect actual conditions. A reliable and realistic approach for studying the behavior of structures and piles under seismic loading with complex seismic SSI effects is physical full-scale modelling of instrumented piles and structures on a shake table subjected to actual earthquake motions. However, this kind of modeling and data collection are rare in the literature due to high costs and experimental difficulties.

In practice, piles are commonly applicable in groups e.g. for bridges and high-rise buildings, which behave differently than single piles. Therefore, not only the performance of single helical piles but the performance of helical pile groups is important to study in investigations. The geometry of the piles, spacing between piles, as well as pile-head connections are important factors controlling the response of piles that should be considered. Understanding the parameters that effect the dynamic characteristics of soil-pile systems and quantifying the possible range that can occur under real earthquakes will allow engineers to choose appropriate pile geometry, group

configuration and connection type to achieve a desired level of performance.

One method to visualize structural performance in seismic zones is to estimate the vulnerability of structures and foundations. This is done through seismic fragility analysis and is considered the main approach in risk assessment since it represents a measure for defining the safety margin of the structural systems. Most of the fragility analyses performed to date have assumed a fixed connection with the ground. However, we know that many structures, including high rise buildings, are mostly supported by deep foundations and those deep foundations affect how the structure feels the earthquake. Therefore, assessing how the foundation system influences the structure vulnerability is important, even though risk assessment of foundations, including helical piles, has not yet been addressed in the literature. The interaction between the soil and structure influences dynamic parameters such as energy dissipation of a system; when SSI is considered, the structure might experience different levels of damage (Nakhaei and Ghannad, 2008). An authentic response of a soil-pile-structure system subjected to an earthquake motion would better predict the level of damage rather than assuming a fixed base in all cases. Having this type of real data for different building and pile types is unrealistic, but it will be a significant engineering development to adjust existing fragility curves to account for the foundation system's influence using the available full-scale experimental data set from this study.

Therefore, to fill these knowledge gaps, large scale shake table field tests, along with simulations of single and grouped piles under superstructure load were conducted as part of a comprehensive study for understanding pile and structure behavior under earthquake motions. Generally, this research aims to 1) determine a range of quantitative data on dynamic parameters of single and grouped helical piles in dense sands, including natural frequency and damping ratio while taking into account SSI criteria such as shake strength, foundation geometry and connection

type; 2) evaluate different soil and pile properties on seismic performance of helical pile-structure systems with simulated models; and 3) modify existing structural fragility curves to more authentically assess vulnerability of the structure by including the effect of SSI.

1.2. Objectives and scope

The intention of this research is to offer insight on the seismic behavior of structures supported by deep foundations in order to mitigate seismic risk. Generally, this research aims to provide a comprehensive investigation on the seismic performance of single and grouped helical piles with consideration of soil-structure interaction using realistic experimental results and dynamic simulation.

The main objectives of this study are to:

1) Estimate natural frequencies and damping ratios of single and grouped piles under varying earthquake loads using different theoretical calculation methods and better understand the factors that affect the results.

2) Model the soil-pile system in ENSOFT's Dynapile software using experimental responses to evaluate the effect of SSI. Introduce quantitative values for spring stiffness between a structure and foundation in addition to finding the parameters that may influence the stiffness.

3) Utilize the calibrated model to simulate various soil-pile systems to examine the effect of soil, pile and structural properties.

4) Evaluate the effect SSI on existing fragility curves through a sensitivity study.

1.3 Dissertation outline

Each chapter following the comprehensive literature review is based on a peer reviewed paper or is being planned as a future publication. In addition to this chapter, this dissertation is organized into the following chapters:

Chapter 2 presents a broad literature review by summarizing previous research in the areas of seismic properties of pile foundations and seismic vulnerability and risk assessment of the structure founded on this type of foundations considering the effect of soil and piles.

Chapter 3 describes the conducted full-scale experimental test on helical piles with different geometry and configurations. Afterward, the methods that have been used to analyze seismic response of structure-piles system are explained and results (e.g. deflection and bending moment with depth; py curves) are provided.

Chapter 4 discusses various approaches to achieve damping ratios of the soil-helical pile system and compares these approaches. Moreover, the damping ratios of pile groups, as well as the structure, while considering their mutual interaction, are presented.

Chapter 5 describes the effect of SSI on the response of the structure and foundation. The soil-pile system, using a lumped mass to simulate the structure similar to the experimental geometry and configurations, were modeled in ENSOFT's Dynapile software. The responses from full-scale experimental tests have been applied to calibrate the model in DynaPile. The quantitative values for spring stiffnesses between the structure and foundation were presented. These models were used to simulate various soil-pile systems to highlight the significance of the various parameters for computing the stiffness of a system. The contributive parameters that may influence the structural and foundation's stiffness are evaluated.

Chapter 6 adopts the advantages of the structural stiffness values after considering soil and foundation interaction to investigate the vulnerability of a 6-story steel frame hospital located in Memphis, Tennessee. The developed modified fragility curves (with SSI consideration) are compared with existing fragility curve of fixed based structure from Hassan and Mahmoud (2018)'s study.

Chapter 7 summarizes this research and draws conclusions in addition to providing potential ideas for future work.

Chapter 2 : LITERATURE RIVIEW

This chapter provides a wide review of relevant studies to this research. First, a brief introduction to helical piles and their behavior under axial and lateral loading, specifically dynamic lateral soil-pile behavior, are presented followed by a discussion on the approaches for computation of dynamic properties of piles. In addition, the beneficial and detrimental effect of soil-foundation-structure are described according to the literature. Finally, this chapter ends with a detailed discussion on sensitivity studies and risk assessment of engineered structures.

2.1 Helical Piles

During the Northridge earthquake in 1994, 107 highway bridges were damaged including 7 bridges experiencing partial collapse. The total repair cost for the damaged bridges was estimated to be about $150,000,000 (Brown et al., 2001). Such structural failures due to earthquakes have motivated engineers to design safer and seismic resistant foundations.

Helical piles are one type of deep foundation that have shown favorable performance within seismically active zones, especially during relatively large earthquakes (Ridgley 2015; Cerato et al. 2017). Helical piles are composed of steel shafts fitted with one or more helical plates and are installed into the ground by applying torque and crowd to the pile head. This type of pile provides support through soil bearing on the plates and along the shaft. They come in many lengths and are often the foundation of choice for retrofitting existing buildings or new, urban construction, due to their small footprint and ability to create minimal disturbance to surrounding structures. The specific geometry of these piles leads to easy installation with less noise and no casing requirement

the presence of ground water (Elkasabgy and El Naggar, 2013).

The various resisting forces on the helical pile are lateral soil resistance around the pile shaft, bearing soil resistance on the bottom of plates, uplift soil resistance on the top of plates and frictional soil resistance on the surface of plates (Prasad and Rao, 1996). The excellent performance of infrastructure supported by slender helical piles during Pacific Rim earthquakes (e.g., 2011 Christchurch earthquake in New Zealand) and the undamaged helical piles exhumed from underneath the infrastructure, confirmed their suitability for resisting seismic loads (Ridgley, 2015; Cerato et al., 2017).

2.2 Ultimate axial capacity of helical pile

There have been many studies performed on the axial uplift and compressive capacities of single helical anchors and piles (Ghaly et al. 1991; Prasad and Rao 1994; Singh 1995; Vickars and Clemence 2000; Victor 2008) in varying subsurface types that have helped determine, for example, appropriate installation torque-to-capacity ratios, embedment depth and ultimate design loads. For example, comprehensive experimental tests and numerical finite element analyses on the axial capacity of 19 full-scale helical piles with square shafts subjected to both tensile and compressive loads were conducted by Livneh and El Naggar (2008) in different soils. The load-deflection of piles tested in compression proved its suitability for axial compression applications. Moreover, the correlation between the installation torque and compressive strength of helical piles in dense clayey silt was proposed. Thus, with monitoring torque during helical pile installation, the axial capacity can be predicted. Another experimental-numerical study on evaluation of compressive capacity of helical piles in sand and clay was performed (Elsherbiny and El Naggar 2013). The pile capacity, after considering group reduction and helix efficiency factors when the

settlement reached 5% of the helix diameter, was determined. Elkasabgy and El Naggar (2013) showed that the vertical dynamic load was mostly transferred through the shaft and the negligible load was transferred through the helix. Several other studies have extensively investigated the axial capacity of helical behavior using physical and numerical modeling (El Naggar and Abdelghany 2007; Sakr 2009; Sakr and Bartlett 2010; Sharnouby and el Naggar 2012; Salhi et al. 2013; Elkasabgy and El Naggar 2014).

2.3 Static and cyclic lateral capacity of helical piles

Lateral capacity of helical piles can either come from the central shaft pressing against the abutting soil like a typical deep foundation or the helical pile can be battered at some angle to allow the structural lateral load to be resolved along the axial length of the pile. In this study, we will only discuss the former. Soil resistance along the pile shaft and at the pile tip represents the main lateral static capacity of pile. Lateral capacity of single helical piles under horizontal static load have been studied in sand (Abdrabbo and El Wakil, 2016). It is concluded that lateral capacity of helical piles increases with embedment depth and shear strength of the soil. Moreover, in an experimental study, the lateral capacity of two models of steel helical piles (length = 0.5 m and shaft diameter 13 mm) with two and four helices (diameter = 22 mm) subject to static lateral load in clay were compared to a steel shaft with the same diameter. It was shown that the lateral capacity of the single straight shaft pile was 25 N and increased to 32 N and 40 N for helical piles with two helical plates and four helical plates, respectively, even though the helices were located close to the tip at a level of 26 D (Prasad and Rao, 1996). In this study, bearing resistance on the bottom of the helical plate and uplift resistance on the top of the helix was also depicted in the simulation. Similarly, a full-scale single and double- helix pile under axial compression, uplift, and lateral load indicated that helical piles can develop significant resistance to lateral loads, however, the lateral behavior

of helical piles was shown to be controlled mostly by the size of the shaft (i.e., diameter and thickness) and the helices had a minor effect (Sakr, 2009). Two helices were found as the optimum number of helices in lateral and axial loading, which increased axial compression capacity 40% higher than with a single helix. The lateral capacity may reduce, however, when there is more than two helices due to soil disturbance. Abdrabbo and El Wakil (2016) investigated the behavior of small-scale model of a single helical pile under static lateral loading in sand. It was concluded that the resistance of a helical pile under lateral loading is more significant compared to similar plain shaft pile.

Cyclic lateral loading consists series of repetitive lateral loads due to due to impact, waves, wind. Soil lateral resistance degradation due to the rearrangement of soil particles depends on frequency of loading (which is confined to 5 HZ) and number of cycles. There are many studies on behavior of helical piles subject to lateral cyclic load up to date (Ting 1987; Rao and Prasad 1993; Prasad and Rao 1994; Abdelghany 2008; Abdelghany and El Naggar 2010; Chandrasekaran et al. 2010; El Sharnouby and El Naggar 2011; Lee et al. 2019). It has been observed that the lateral deflection of helical piles is caused due to the plastic deformation of the soil primarily. Nevertheless, helical piles recover most of the deflection during unloading which indicates minimal structural damage (El Sharnouby and El Naggar 2011). Generally, helical piles were found to perform better than regular pipe piles after high cyclic lateral loads, as they exhibit higher pullout capacities than pipe piles (Prasad and Rao 1994).

2.4 Dynamic lateral behavior of piles

The lateral dynamic properties and behavior of pile and soil medium can be studied using either experimental testing or theoretical approaches. Experimental studies have been performed on

different types of piles and several theoretical methods have been implemented to interpret their results. In addition, analytical and numerical methods have been presented for predicting seismic response of conventional piles. Each of these methods has advantages and limitations and all demonstrate the need for realistic experimental results to use in the analyses. Therefore, relevant published experimental testing programs and theoretical investigations studying the characteristics of group pile lateral dynamic behavior are discussed and their salient features are highlighted.

2.4.1 Experimental approaches to determine the dynamic lateral behavior

Laboratory-scale tests of soil-foundation-structure seismic behavior, including their mutual interaction, can be implemented using 1g shake-table testing or dynamic excitation on centrifuge models. However, the limited size and boundary effects within these tests may affect the accuracy and validity of their results (e.g., radiation damping may not be present; fixed boundary conditions or modeling of axial and lateral stiffness of the piles may be improper). On the other hand, full-scale field testing avoids most of these pitfalls and provides realistic results. However, it is expensive, labor intensive and time consuming, and therefore not as commonly used as the smaller scale models. Several of these experiments and their analysis methods are discussed.

Yang et al. (2011) conducted a series of small-scale 1g shake table tests on single piles (1.2 m long) driven in dry and saturated dense sand. Based on the results, they proposed empirical equations to estimate the initial soil stiffness as a function of the soil friction angle and confining pressure. The scaled pile models provided a general insight into the seismic response and damage pattern of the piles. Guan et al. (2018) investigated the seismic behavior of a single concrete pile employing small-scale shake table tests and demonstrated that load-displacement curves based on

the experiment results underestimate the ultimate lateral loading capacity and overestimate the lateral displacement.

Full-scale tests are anticipated to yield more realistic results because of the inherent proper consideration of the important factors that affect the nonlinear behavior of piles during strong excitations (i.e. pile group interaction, weakened soil around the pile, contact conditions at soil-pile interface). These factors influence the resultant stiffness and damping of a pile (Han and Novak 1988; Shirato et al. 2008). A series of full-scale tests on lateral response of single and grouped piles in liquefiable soil were performed at Treasure Island in San Francisco, California before and after liquefaction increment (Rollins et al. 2001; Rollins et al. 2005; Rollins et al. 2006). The controlled blasting techniques using explosive charges at different levels far enough from experiment site was applied to induce liquefaction. As a result, after liquefaction the stiffness of soil-pile group (2x2 and 3x3 cast-in-steel-shell with 32.4 cm outside diameter) decreased by 70% to 80% compared to pre-liquefaction values. Stone columns installation as a ground improvement technique, increased the stiffness of pile foundation approximately three times compared to unimproved soil. Liang et al. (2017) conducted a large-scale shake table test (1:70 scaled) for a long span bridge supported by a pile foundation system, which showed that stiffness variation in a bridge structure influences the pile response remarkably. Elkasabgy and El Naggar (2013) conducted a full-scale dynamic vertical load tests on a 9.0 m double-helix helical pile and a driven steel pile to evaluate the piles' dynamic behavior. Using the experimental results, they examined the validity of the linear and nonlinear approaches for predicting the pile stiffness and damping constants. They demonstrated that nonlinear theoretical analysis approach provides a reasonable estimation for the pile response curves, stiffness and damping. The linear approach, on the other hand, overestimates the stiffness and damping and underestimates the dynamic response because

it ignores the weak bond between the pile and soil caused by the pile installation process. They also reported a stiffness increase of 42% and damping increase of 90% for the helical pile after nine months due to the stiffness and strength re-gain of soil around the pile. Elkasabgy and El Naggar (2018) published the results of dynamic full-scale load tests on 9 m long steel piles and proposed a methodology for data reduction to determine dynamic lateral stiffness of steel helical and driven piles embedded in clay. The equivalent-linear approach in this study was shown favorable in predicting the pile response since the soil disturbance due to pile installation could be well simulated. This model predicted a 60% increase in the lateral stiffness of a helical pile, nine months after installation due to strength regain of the disturbed zone of soil around the pile. These researchers recently (Elkasabgy and El Naggar 2019), in a similar study conducted five full-scale helical piles with 6 and 9 m length and 0.324 m diameter in cohesive soil. Both short- and long-term conditions were evaluated. Comparing the measured subgrade modulus from experiment p-y curves with estimated value from properties of the undisturbed soil showed that pile installation reduced the subgrade modulus. Thus, a resistance reduction factor accounting for degradation of initial subgrade modulus due to helical pile installation was offered to be incorporated in p-y curves in design. Thus, according to these studies, the scale of test medium and accuracy in collection of data (e.g. signal processing) in experiments are the main factors that may cause deviation from actual response and should be considered (Wilson 1998; El Naggar et al. 2005; Talukder 2009). .

All of the tests discussed so far have been performed on single piles and that is because, to date, the only published work on the dynamic behavior of grouped helical piles is from Shahbazi et al. (2019). All of the other literature on grouped behavior is on various other pile types; and only the steel pile results could be considered comparable to the behavior of helical piles. Novak and Grigg (1976) conducted site experiments with model steel single and grouped piles (2x2). The

piles were 2 m long with 0.06 m diameters. The testing program involved applying harmonic vertical or horizontal excitation using a Lazan mechanical oscillator. The dynamic stiffness and damping of the soil-pile system were obtained from the experimental results and were compared with the predictions of the plane strain theory proposed by Novak (1974). They reported a reasonable agreement between the theoretical predictions and the experimental observations when the effect of the pile group interaction was accurately considered. For deeper layers of soil where the soil shear modulus is greater, resonant frequencies and corresponding amplitude may be overestimated, while in uppermost layer of soil with lower values of shear modulus acceptable response was obtained.

Weissman and Prevost (1989) conducted centrifuge testing to simulate the seismic behavior of soil-structure systems and compared the results with those obtained from a full scale dynamic lateral loading of a soil-single steel driven pile system (Ting et al. 1987). They demonstrated that due to the large deflections and associated considerable strain softening, the dynamic stiffness and damping ratio obtained from their centrifuge models were different from the dynamic full-scale test results. Their results, however, have been affected by the boundary conditions and scaling effects. Abdoun and Dobry (2002) conducted centrifuge models of instrumented aluminum pile foundations in two- and three-layered soil subjected to lateral pressure, including single pile and pile groups under the effect of liquefaction. The results show remarkable agreement between centrifuge results and field experience. Kagawa et al. (2004) compared the responses obtained from dynamic centrifuge tests simulating large-scale soil– single concrete pile-structure models. They reported that centrifuge testing caused some discrepancies in the results in comparison with those obtained from large-scale tests. They attributed the discrepancies to scaling issues, boundary effects, acceleration variation within the model and

difficult detailed instrumentation due to its intrinsic small scale. Centrifuge testing, however, requires less time, cost and effort to conduct compared to large scale tests (Kagawa et al. 2004; Ubilla et al. 2011; Ebeido 2019).

2.4.2 Theoretical approaches to determine the dynamic lateral behavior

In the absence of experimental observations, validated numerical or analytical approaches can be used to understand the seismic behavior of piles. Theoretical methods employed for the dynamic and seismic behavior of pile include dynamic Beam on Nonlinear Winkler Foundation (BNWF), finite-element or finite-difference methods, continuum methods, and plasticity-based macro-models (Gajan et al. 2010; Stewart et al. 2012). These methods may either uncouple or fully couple the analysis of the superstructure and foundation (Gazetas and Dobry 1984; Kaynia and Mahzooni 1996; Mylonakis et al. 1997; Beltrami et al. 2005; Rovithis et al. 2009).

BNWF has been employed extensively for analysis of static and dynamic lateral pile response (Matlock 1970; Penzien 1970; Cox et al. 1974; Matlock and Foo 1978; Nogami et al. 1992; Boulanger et al. 1999). In BNWF models, the pile is simulated as a series of discrete linear elastic beam-column elements and the surrounding soil is modeled by a series of non-linear detachable Winkler springs and dashpots on each side of the pile to represent the soil stiffness and damping (Boulanger et al. 1999; Talukder 2009). Although, the BNWF approach is widely used because of its simplicity and effective ability to predict the soil-foundation-structure interaction particularly in soft soils (Boulanger et al. 1999), it only considers deformations and strains of pile and soil in only one dimension. However, the soil deformations and reactions as well as energy dissipation are three-dimensional (Nghiem 2009; Heidari and El Naggar 2018). There is a study by Raychowdhury and Hutchinson (2009) that implemented analysis of a BNWF model into

OpenSees (McKenna et al. 2000) in two dimensions. Talukder (2009) developed a simplified BNWF model employing the finite element program ABAQUS (version 6.7) that captured soil-pile interaction observed in the dynamic centrifuge experiments on two different single piles in saturated sand. The uncertainties in signal processing of the experiment, however, caused some deviation in the comparison of model and experimental results. He reported that their simplified BNWF ignored the effect of pore pressure on soil stiffness. It was shown that seismic soil-pile interaction couldn't be analyzed realistically because of the uncoupling of free field, soil and pile in their presented BNWF model; in their case, a 3D continuum finite element approach was suggested. Allotey and El Naggar (2008) developed a modified BNWF that accounts for pile nonlinear behavior, gapping between pile and soil, soil strength degradation as well as radiation damping. They validated the model predictions through comparisons with results of published full pile load tests and concluded that this model is suitable for evaluating seismic response of piles. El Naggar et al. (2005) investigated the nonlinear seismic response of offshore piles embedded in layered soil considering different aspects of pile–soil interaction. They proposed a simplified BNWF model employing the general finite element analysis software ANSYS. They reported good agreement between the model predictions and the results of centrifuge tests.

Finite element method (FEM) is another widely used method that can simulate the behavior of soil and structure properly even for complicated geometry and loading conditions (Seed and Lysmer 1978; Lou et al. 2011). The continuum approach is the most computationally involved method that has been utilized in limited studies to analyze the response of piles (Borja and Wu 1994; Jeremic et al. 2009). Novak (1974) and Novak and Nogami (1977) developed closed-form formulas to approximately determine pile dynamic stiffness and damping assuming linear elasticity. Kaynia (1982) has also presented a linear elastic formulation to determine the dynamic

stiffness of pile groups.

Nova and Montrasio (1991) proposed the method called Plasticity-based macro-element to capture the plastic behavior of the pile under strong excitation. This method was verified using some experimental results (Cremer et al. 2001; Houlsby and Cassidy 2002; Chatzigogos et al. 2009; Pecker and Chatzigogos 2010). However, it is only applicable for the nonlinear response analysis of foundations by considering the shear failure mode. Additionally, this method cannot account for the variation of damping due to the stress change.

2.5 Dynamic parameters of a soil-pile system

The behavior of a structure is dependent on stiffness and damping provided by soil and foundation (Novak 1974). Thus, determination of soil-pile dynamic parameters, such as damping, are required to accurately predict and analyze the dynamic behavior of a structure on pile foundations. For strong earthquake motions, damping of the soil-foundation system plays an important role in dissipating energy and may reduce the response of a structure. The main factors that influence the soil-pile damping are the soil's shear strain amplitude, the deflection of piles, pile head displacement, as well as pile slenderness ratio, i.e. pile length divided by pile radius (Hardin and Drnevich, 1972; Novak, 1974). The steel piles provide very little damping themselves. When installed into soil, however, the interaction between the pile and soil promotes energy dissipation, which contributes to significant damping (Cremer and Heckl, 1973). Therefore, piles with larger slenderness ratios may dissipate more energy because of increased interaction with the surrounding soil in addition to experiencing more deflection and strain. This phenomenon was confirmed through observations of damaged piles that were exhumed from three earthquakes in Japan (Miura, 1997). Based on these observations, Miura (1997) concluded that a "[a flexible pile] is better than

a pile with higher rigidity [during the range of allowable deformation] when they are subjected to the same ground motion."

The dynamic stiffness and geometric damping of piles rely on soil-pile interaction and are governed by the following dimensionless parameters: specific mass of the soil over specific mass of the pile (mass ratio), shear wave velocity in the soil over longitudinal wave velocity in the pile (wave velocity ratio), length of the pile (thickness of the soil layer) over pile radius (slenderness ratio), pile static load over Euler's buckling load (load ratio), and the dimensionless frequency (Novak, 1974). Stiffness and hysteretic damping parameter of sand is independent of load type (static or dynamic), frequency and water content (Bolton and Wilson, 1990; El Naggar and Abdelghany, 2007) but it depends on strain, stress level, void ratio and number of loading cycle (Brennan et al., 2005). However, Rollins et al. (2009) and Lundgreen (2010) showed that the number of cycle is less effective on the magnitude of damping ratio. Furthermore, confining pressure was found as another effective factor which can result in hysteretic damping reduction (Rollins et al., 1998). In addition, the research on vertical vibration of pile groups (Boominathan and Lakshmi, 2000) show that, damping and group stiffness lean on load frequency and spacing between piles. Damping is high at the low frequencies and decreases with the increase of the frequency, but it decreases as the spacing between piles decreases.

2.5.1 Approaches to calculate damping ratio

The damping ratio (ζ), is commonly used in geotechnical engineering to describe the dissipation of energy in a system subjected to dynamic loading. There are various approaches to calculate the damping ratio from dynamic test results (Ashmawy et al., 1995; Chopra, 1995) which will be discussed in the following:

The logarithmic decrement method uses the exponential decay of motion amplitude with time to determine ζ. The damping evaluation using this approach can be affected by the presence of aperiodic peaks, which confuse the selection of peaks to be considered in calculating the damping ratio, ζ (Ge and Sutherland, 2013; Tweten et al., 2014). To accurately determine the damping ratio and minimize the errors caused by disordered peaks, decay curve fitting to a response curve is suggested (Ostadan et al., 2004; Ge and Sutherland, 2013). In addition, Tweten et al. (2014) proposed a method to establish the ideal number of periods for choosing the second peak that can be used to determine the damping ratio in logarithmic decrement calculations.

Alternatively, ***the equivalent or energy method*** can be used to determine the damping ratio. It is based on calculating the area enclosed by hysteretic loops of stress-strain (force-displacement) curves. The area of the loop represents the dissipated energy and is used as a measure of the damping. This method is simple but approximate (Novak and Hifnawy, 1983; Chopra, 1995), because the actual response of a structure does not often yield an ideal symmetric elliptical loop (Lin et al., 1988). The method has been shown to overestimate damping by more than 50% depending on the soil-foundation conditions, especially in small-strain shake events (Novak and Hifnawy, 1983).

The half power bandwidth method is also employed to evaluate damping. In this method, the peak amplitude in the frequency response curve (i.e. resonant amplitude) is used to compute ζ. This is because the influence of damping on the dynamic response is most salient near resonance condition. The half power bandwidth method is appropriate for systems that have frequency dependent stiffness such as foundations in or on layered soil deposits (e.g., pile groups) (Saitoh, 2007; Olmos and Roesset, 2010). However, highly nonlinear soils often exhibit skewness in the

shape of the frequency response curve due to the inconsistency in recorded response at some frequencies (Ashmawy et al., 1995).

Modal analysis is another method used for calculating damping ratio, which involves a mathematical approach using complex eigenvalues. The MATLAB functions "modalfrf" and "modalfit" can be used to conduct the required calculations (Pavelka et al., 2017). Peak picking (pp) and least squares complex exponential (lsce) are two methods of curve fitting implemented in MATLAB, which give local and global estimates of damping, respectively (Kerschen and Golinval, 2005; Siemens Industry Software). Using peak picking as a fitting method influences the damping calculation significantly but has been shown to provide sufficiently acceptable fitting when the modes are well separated (Pavelka et al., 2017).

2.5.1.1 Studies on evaluation of damping ratios using different methods

Several studies have used one or more of these methods to determine the damping ratios of soil-pile systems. The half power bandwidth method was used to determine the damping ratio of a 3 x 3 pile group installed in soft clay induced by bi-directional sinusoidal vibration, and the damping ratio ranged from 17% to 19% (Halling et al., 2000), however, the shear strains were not reported. The half power bandwidth method was also used to calculate the damping ratios of pile foundations during actual statnamic load tests (Lin et al., 2004; Tsai et al., 2011). Additionally, Tsai et al. (2011) numerically simulated the tested 81.1 m long cast-in-place 1.5 m diameter pile in sand resting on clay under axial statnamic loads (with maximum of 19 MN). The variation of the damping ratios with time during the test was evaluated, and the maximum ζ was found to be 17%, which coincided with the instant of maximum displacement of pile head (17 mm).

The half bandwidth and log decrement method with decay fitting curves were used to determine the damping ratio of a circular 18.3 m diameter shallow foundation resting on homogenous soil and subjected to impulse loading (Ostadan et al., 2004). The calculated damping ratio was applied in a dynamic structural analysis model to evaluate the validity of the calculated foundation damping for similar dynamic load conditions. The results demonstrated that the calculated damping under impulse load could be used for dynamic analysis of structures, accounting for soil structure interaction.

The energy method was used to calculate the damping ratio of 3x3 groups of steel pipe piles (O.D. 32.4 cm) subjected to cyclic loading. The estimated damping ratios were around 20% and 18 to 28 % in natural and treated soil, respectively (Lundgreen, 2010) that corresponded to pile group shear strains of 0.21, 0.05 and 0.27 %, respectively. In a more recent full-scale field test (Fleming et al., 2016), a 32.4 cm diameter steel pipe pile installed in soft clay was subjected to cyclic lateral loading before and after deep soil mixing treatment of soil adjacent to the pile. The calculated damping ratio using the energy method demonstrated an increase of 650% in the damping ratio due to the soil improvement compared to the pile in native soil. It was found that at the maximum pile head displacement of 12 cm, ζ = 4.5% and 29% for the pile in native and improved soil, respectively (Fleming et al., 2016). The damping of an offshore wind turbine foundation installed in marine deposited mud was calculated based on logarithmic decrement method (Hemmati et al., 2017). It was concluded that the soil damping contributions to the resistance of mudline peak moment and base shear force were 20% and 7-10 %, respectively.

2.6 Soil-pile-structure interaction in dynamic response of engineered systems

The seismic response of a structure resting on a pile foundation relates to a complex mechanism defined as soil-structure interaction (SSI). In order to have more realistic dynamic structural response it is required to consider the effect of mutual interaction of soil, pile and structure in analysis and design. SSI includes the inertial interaction between the structure and the pile foundation and the kinematic interaction between piles and the surrounding soil. Zhang and Wolf (1998) suggest that in a low intensity ground motion, the inertial component is significant, while under a high intensity shake, kinematic effects are dominant. In another parametric study, pile-soil-pile interaction was modeled by 3-D Green's function formulation to monitor the forces in the piles during a seismic event (Kaynia and Mahzooni, 1996). Structures with varying values of natural frequency founded on 5x5 pile groups with different spacing and rigidity values were studied. The main results showed that the kinematic interaction is a prime contributor to shear force and bending moment of piles except at frequencies close to the natural frequency of the soil-structure system. In those frequencies, the effect of inertial interaction is dominant.

SSI influences the dynamic properties of the ground motion and connected structural systems, which leads to a variation of a system's period, stiffness and damping; especially under earthquake motions (Stewart et al. 2012). The degree of influence of SSI on building response can be related to the factors summarized as the following (Miura, 1997; Boulanger et al., 1999; Jeremic et al., 2009; Stewart et al., 2012; Badry and Satyam, 2017): 1) Size of the foundation footprint, 2) Kinematics: soil and foundation properties (e.g., soil stiffness, pile rigidity), 3) Inertia: dynamic properties and geometry of structure (e.g., period lengthening, damping ratio, flexible versus stiff), 4) Non-linear behavior of soil, 5) Uncertainty. The more nascent studies are discussed herein.

SSI becomes notable when the interface of a foundation and structure is extensive, the footing is embedded (kinematic effect) and the superstructure is heavy (inertial effect) (Anand and Satish Kumar, 2018). As the connection area between soil and foundation increases, the effect of SSI grows and becomes more complicated (Miura, 1997; Jeremic et al., 2009). Comparing the seismic response of a structure founded on spread footings versus single piles using an analytical procedure illustrated that the damping of structures founded on piles can be twice the damping of a structure on spread footings (Maravas et al. 2007). However, Van Nguyen et al. (2017) showed that even though a pile foundation produces more damping, longer piles do not necessarily result in a safer design under strong motion because the longer piles exhibit more lateral deflection and bending moment. The high contact surface of a long pile with the surrounding soil dissipate, but also transfer, more of the earthquake's energy to the superstructure, which may cause larger shear forces in the columns and increases in inter-story drift. Cast in situ reinforced concrete single and grouped piles with different lengths of 1, 1.5 and 2 m were subjected to strong horizontal excitations in Manna and Baidya (2010)'s study. In their study, it was concluded that the stiffness and damping of the pile group system either increases or decreases depending on the pile configuration and the pile-soil-pile interaction. Both stiffness and damping of the pile increased when the cap embedment increased. Reduction in stiffness and damping of the pile system occurred as load intensity increased, which was primarily due to the development of the weak boundary zone around the pile and the separation between the pile and soil.

Period lengthening and changes in damping are two major results of inertial interaction which is presented by Eq. (2-1) (Stewart et al., 2012).

$$\frac{T_{SSI}}{T} = \sqrt{1 + \frac{k}{k_x} + \frac{kh^2}{k_{yy}}} \qquad 2\text{-}1$$

where, h and k are structural height and lateral stiffness respectively. T and T_{SSI} are respectively structural period and SSI period. k_x and k_{yy} are horizontal and rotational soil springs.

According to the equation above, it is obvious that as structure-to-soil stiffness ratio ($h/(V_sT)$) increases, the period increases subsequently. Hence, SSI in flexible structures on stiff soil or rock is negligible, while it is significant for stiff structures located on soft soil (Givens et al., 2012; Stewart et al., 2012). Moreover, neglecting SSI in stiff superstructures can lead to significant underestimation of displacement (De Carlo et al., 2000). Results of a study by Papalou et al., (2012) showed that more flexible structures are insensitive to SSI. They illustrate that, during the 1985 earthquake in Mexico City, the combined effects of soil-structure interaction and vertical inertial loading contributed to increase the ductility demands of fixed-base structures with natural periods between 1.0s and 1.5s. Therefore, soil-structure interaction was found significant for only less flexible structures; especially those of low or moderate height with a first mode period of 0.5s located on soft flexible soil. Rigid and heavy structures on soft soil is where SSI should be considered critical. The dynamic characteristics of pile-structure systems including SSI contribution have been studied by Rainer (1975) using mathematical modeling. The structure-to-soil stiffness ratio was found to be a primarily effective parameter in defining the natural frequency and the damping ratio of a foundation-structure system. Another study on the estimation of periods and damping of a building founded on piles considering SSI contributions (Medina et al., 2013) was performed by analyzing the structure while it was excited by vertically incident S waves. As a result, for taller structures, the stiffer pile groups (larger number of piles, larger embedment ratio and lower pile slenderness ratio) yielded lower periods in a coupled system, which was in the opposite of what was found for short buildings. Generally, slender buildings, as well as soft soils, magnified the effect of SSI. When SSI was considered, the maximum base shear force could be

lower than that of a fixed-base condition in short buildings, but when the structure's slenderness ratio (L/d) was large, the opposite was true.

Boulanger et al. (1999) also reported that SSI can be important in evaluating the seismic response of pile-supported structures, particularly in soft clay or liquefying sand. The effect of SSI in fully saturated sand was found to be important due to the presence of pore water pressure (Sáez et al., 2013). It was shown that SSI seems to be very important when the mean period of an inelastic structure is close to the first elastic period of soil. Additionally, the effect of SSI on a reinforced concrete (RC) building that was shaken strongly by the 1994 Northridge earthquake was modeled (Givens et al., 2012). This 13-story building with a two-level basement was supported by friction pile foundations in alluvial sediments. As a result, the responses, such as shear forces and drifts below the ground surface, were more sensitive to SSI effects compared to the above ground structure. This sensitivity depends on the spring distribution and ground motion; the greatest effect of SSI occurs with the stiffest structure.

Another contributing parameter to SSI during a seismic event is the nonlinear behavior of soil, which makes the case more complicated. It was reported that the nonlinearity of soil has significant effects on the pile response for lower and moderate frequencies of excitations ($a_0 \left(= \frac{\omega d}{V_s}\right) < 0.6$), while at higher frequencies its effects are not as significant (Maheshwari et al., 2005). One of the main explanations for nonlinear behavior in the seismic response of piles is the separation between the pile and soil (gapping) and subsequent lack of bonding at the pile–soil interface (Naggar et al., 2005; Elkasabgy and El Naggar, 2013). Because of this gapping at the top of the pile, specific elements are required (depends on kind of soil) to model the gap and separate it from the soil springs on each side of pile, which controls how the soil and pile can move. Piles in clay experience gaps when soil is in tension, while in sand (cohesionless soil) the gap created

from the movement of the pile is filled by soil and the gaps heal themselves (Naggar et al., 2005). Ladhane and Sawant (2016) carried out a dynamic analysis and parametric study of pile groups in different configurations using a 3D finite element program. The transferred stress between the soil and pile during the application of a lateral load was simulated. It was shown that the natural frequency of a pile group tends to decrease with reduction in soil stiffness due to nonlinear behavior of the soil-pile system during yielding.

2.6.1 Damages due to neglecting SSI

Since seismic soil-structure interaction is closely related to the safety evaluation of many sensitive engineering structures built to resist earthquakes, such as dams and bridges, SSI is a significant topic in structural seismic design (Miura, 1997; Zhang and Wolf, 1998). Traditionally, ignoring SSI has been considered a conservative design due to the enhancement of the structural period and damping ratio (Jennings and Bielak, 1973; Veletsos and Meek, 1974; Ghalibafian et al., 2008; Anand and Satish Kumar, 2018). Leaving SSI out of design considerations and codes (API; FEMA) relegated SSI to a mere perceived benefit in the seismic response of a structure instead of an integral part of its overall behavior. Some studies, however, have found that limiting the use of SSI in design may not be conservative and does not necessarily reduce the structural response even if increase in fundamental period of a structure occurs (Gazetas and Mylonakis, 2001). It has also been argued that the perceived beneficial role of SSI is an oversimplification of reality and indeed is incorrect for different soil–structure systems and earthquake motions that may lead to an unsafe prediction of seismic performance of structures (Bielak, 1974; Mylonakis and Gazetas, 2000; Gazetas and Mylonakis, 2001). The repercussions of not considering SSI in design has been observed in earthquake events such as 1989 Loma Prieta, 1995 Kobe Earthquakes and 2015 Nepal earthquake (Yashinsky, 1998; Gazetas and Mylonakis, 2001; Tabatabaiefar and Fatahi 2014).

Damaged structures supported by piled raft foundations during the 2015 Nepal earthquake show that the effect of SSI is intensified when a superstructure is asymmetric (Badry and Satyam, 2017). One of the reasons for the Hanshin expressway piers' collapse during the 1995 Kobe earthquake was because the type of soil modified the propagated waves and enhanced the natural period of the bridge, which led to an amplified response (Gazetas and Mylonakis, 2001). In another study (De Carlo et al., 2000), it was concluded that slender bridge piers may experience large top displacements due to base rotational motion and cause dislocation of the bridge deck after an earthquake, which is another reason explaining the collapse of the Hanshin expressway. Thus, SSI may be either beneficial or detrimental to a structural response under earthquake loading depending on the individual structure and soil properties which should never be ignored in design.

The risk of underestimating the structural response associated with ignoring soil-structure interaction and its nonlinear effects has been reported by Moghaddasi et al. (2011) using a probablistic evaluation under 40 earthquake excitations from 4.08 million analyses. The seismic response of structures with soil–shallow foundation–structure models is estimated by modifying the period and associated damping of the corresponding fixed base system. There is 30–50% probability for an increase in the total structural displacement of over 10% due to SSI, 10–30% probability for amplification of greater than 25% and 2–15% for an increase of over 50% in this response. This study illustrates that an increase in the value of the structural aspect ratio (h_{eff}/r) and structure-to-soil mass ratio ($m_{str}/\rho_s r^3$), reduces the probability for detrimental soil–foundation–structure interaction scenarios. It can therefore be observed that there is an essential need to consider SSI in design of inelastic structures in order to evaluate precise dynamic behavior of soil-structure-foundation system.

In addition, Far (2017) presents a review of applicable modelling and numerical techniques including their advantages and disadvantages for dynamic soil-structure interaction analysis. These modelling which are economical methods are well established and applied in numerous studies without conducting expensive large-scale experiments (Boulanger et al. 1999; Talukder 2009; Givens et al. 2012; Stewart et al. 2012; Carbonari et al. 2017; Michel et al. 2018).

In 1978 the Applied Technology Council (ATC) suggested the reduction in design base shear to model fixed base structures more realistically, which is only acceptable for elastic structures (ATC); later, the National Earthquake Hazard Reduction Program (NEHRP) recommended a cap for this reduction as a guideline for design with consideration of SSI. In this regard, a smaller base shear reduction should be applied for inelastic buildings (Anand and Satish Kumar, 2018).

2.7 Risk Analysis, Fragility curves

Seismic fragility analysis is considered the primary method for assessing risk and vulnerability, since it represents a measure for defining the safety margin of the structural systems (Porter, 2016). If the applied seismic force exceeds the capacity of a structure, it is defined as a seismically vulnerable structure (Behnamfar and Banizadeh, 2016). A fragility curve is a plot of the probability of structural damage due to earthquakes in a certain damage state against the level of seismic excitation e.g. PGA (peak ground acceleration) or PGV (peak ground velocity). These curves give a reasonable prediction of damage to the building due to post-earthquake phenomenon, which assist in estimation of a damage level for a specific ground motion and can assess vulnerability of a structure (Karim and Yamazaki, 2001; Mekki et al., 2016). These curves graphically represent the probability that the demand on a structure will exceed its capacity. The curve is commonly in

the form of a log-normal cumulative probability density function (Mander, 1999; Porter, 2016). The fragility or probability of failure (p_f), is developed by a lognormal cumulative distribution function (CDF) (method-of-moments) (Eq. (2-2)):

$$P_R = \Phi\left[\frac{\ln X-\lambda}{\zeta}\right] \quad 2\text{-}2$$

where Φ is the standard normal distribution, X is the ground motion indices (PGA or PGV, etc.), λ and ζ are the mean and standard deviation of ln X. Two parameters of the distribution (i.e., λ and ζ) are obtained by the least-squares method on a lognormal probability paper (Karim and Yamazaki, 2001).

And in the more general format (Nielson, 2005; Padgett, 2007) (Eq. (2-3)):

$$P_f = \Phi\left(\frac{\ln S_D/S_C}{\sqrt{\beta_D^2+\beta_C^2}}\right) \quad 2\text{-}3$$

where Φ [·] is the standard normal probability integral, S_C is the median value of the structural capacity, β_C is its associated logarithmic standard deviation of structural capacity, S_D is the seismic demand, and β_D is the associated logarithmic standard deviation for the demand.

There are three approaches for creating lognormal CDF fragility curves: 1) lognormal CDF fit by method-of-moments (MM); 2) lognormal CDF fit by minimizing weighted sum of squared error (SSE); and 3) Lognormal CDF fit by maximum likelihood estimation (MLE). These mentioned approaches are described and compared in detail by Lallemant et al. (2015).

2.7.1 Damage states

Five points (A, B, C, D and E) are used to define the behavior of structural RC members according to FEMA (Giannopoulos, 2009) (Figure 2.1). Point B corresponds to the nominal steel yield

strength. The slope of line BC is usually taken equal to between 0% and 10% of the initial slope (line AB). Point C has resistance equal to the nominal strength. Line CD corresponds to initial failure of the member. It may be associated with phenomena such as fracture of the bending reinforcement or spalling of concrete. Line DE represents the residual strength of the member. It may be non-zero in some cases, or practically zero in others. Point E corresponds to the deformation limit. However, usually initial failure at C defines the limiting deformation, and in that case point E is a point having deformation equal to that at C but with zero resistance.

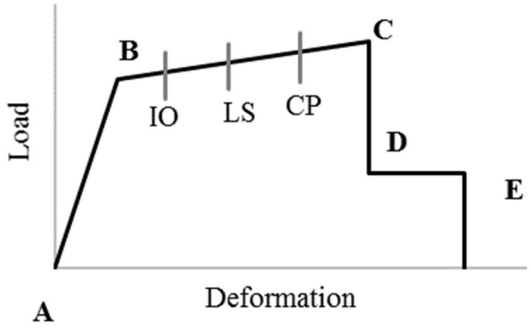

Figure 2.1. Typical load–deformation relation and performance levels (Giannopoulos, 2009)

Levels of performance have been defined in various formats. Table 2.1 presents examples of damage states according to average inter-story drifts of high-rise concrete moment frame buildings; similar tables for all types of construction are recommended in HAZUS (2003) (Table 2.1). HAZUS uses the terms, ‘slight,’ ‘moderate,’ ‘extensive,’ and ‘complete,’ to define their structural damage state thresholds as a function of average inter-story drift.

These general levels of performance have been defined differently by others. In one particular study, (Kinali and Ellingwood, 2007; Karapetrou et al., 2015), three different levels of performance, or limit states, in terms of response measurements (such as inter story drifts, floor

accelerations, joint rotations, etc.) were defined as Immediate Occupancy (IO), Life Safety (LS) and CP (Collapse Prevention) (Figure 2.2).

Table 2.1. Structural damage state thresholds (fragility medians) of generic building type C1H (High-Rise Concrete Moment Frame) (HAZUS, 2003)

Seismic Design Level	Elastic Period (sec.)	Average Inter-Story Drift Ratio					
		Capacity Curve Control Points		Structural Damage State Thresholds (Fragility Medians)			
		Yield	Plastic	Slight	Moderate	Extensive	Complete
Special High-Code	1.45	0.0035	0.0419	0.0031	0.0063	0.0188	0.0500
High-Code	1.45	0.0023	0.0279	0.0025	0.0050	0.0150	0.0400
Moderate-Code	1.45	0.0012	0.0105	0.0025	0.0043	0.0117	0.0300
Low Code	1.46	0.0006	0.0044	0.0025	0.0040	0.0100	0.0250
Pre-Code	1.46	0.0006	0.0052	0.0020	0.0032	0.0080	0.0200

Damage is dependent on both permanent deformation and absorbed energy in hysteretic cycles loading (Park, 1985; Park et al., 1985). Terms, slight, moderate, extensive, and complete, as in the case of Hazus-MH can be used to categorize damage states (HAZUS, 2003) (Table 2.2).

Nazri and Alexander (2014) also developed the plot showing correlation between damage index and drift for two- and four-story steel frame buildings (Figure 2.3).

Table 2.2. Relationship between damage index (Park, 1985) and damage state (Mekki et al., 2016)

1 Damage index	2 Damage state
DI_Park $\leqslant$ 0.1	No damage
0.1 < DI_Park $\leqslant$ 0.25	Slight
0.25 < DI_Park $\leqslant$ 0.40	Moderate
0.40 < DI_Park $\leqslant$ 1.00	Severe
DI_Park > 1.00	Collapse

a) b)

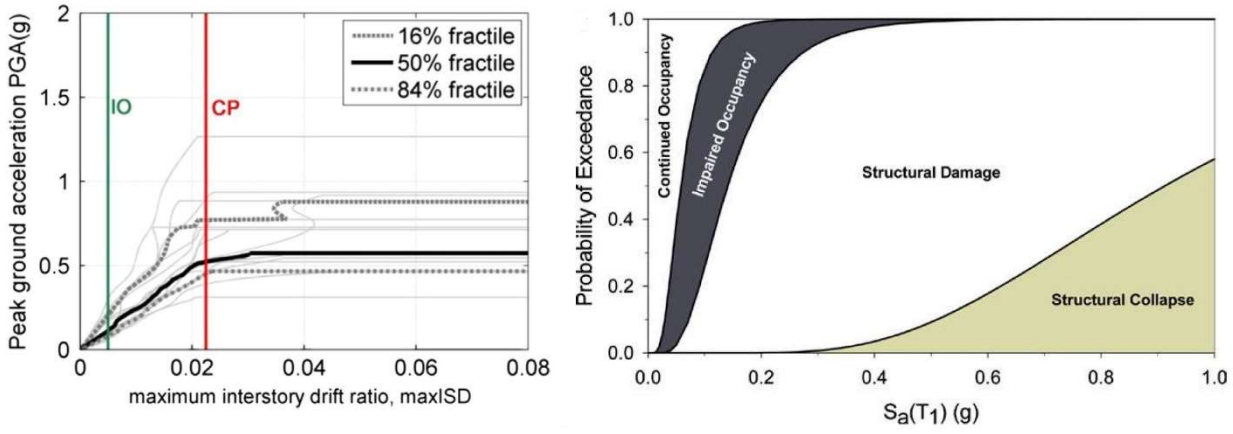

Figure 2.2. IDA curves for the prototype fixed base models by a) Karapetrou et al. (2015); b) Kinali and Ellingwood (2007)

a) b)

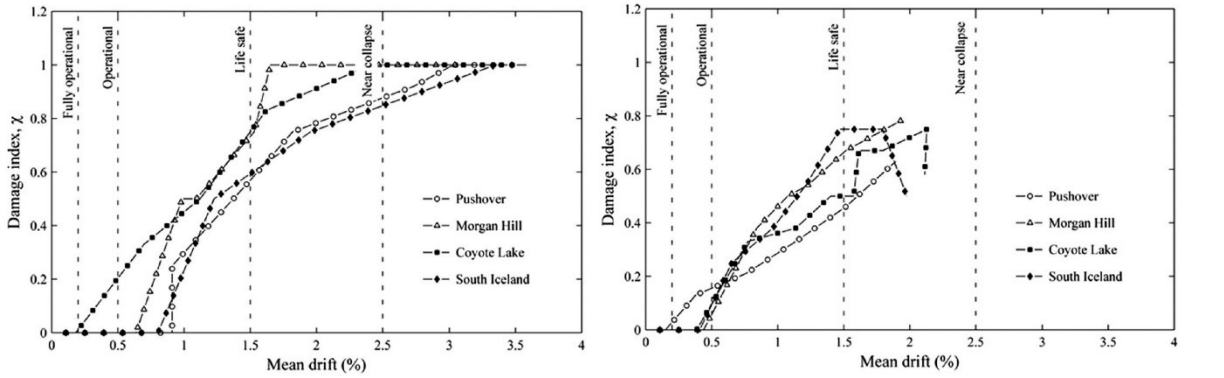

Figure 2.3. Correlation between damage index and drift for a) two-story building; b) four story building (Nazri and Alexander, 2014)

2.7.2 Types of fragility curves

Development of fragility curves requires the following factors: 1) professional judgment; 2) quasi-static and design code analysis; 3) utilization of damage data associated with past earthquakes; and 4) numerical simulation of the seismic response of structures based on dynamic analysis

(Shinozuka et al., 2000). Depending on the source of data used to develop fragility curves, they can be categorized as 1) heuristic; 2) empirical; 3) analytical.

-Heuristic fragility curves: These curves are the least reliable type of fragility functions based on expert opinion where the experts guess or judge failure probability. ATC-13 (Applied Technology Council 1985) compiles many judgment-based fragility functions for California buildings, which were some of the first examples of fragility functions (Porter, 2016). Experts were asked to estimate a probability of certain damage occurrence in highway bridges. These functions are only for Californian infrastructure; its application in other zones is questionable (Nielson, 2005). Also, FEMA P-58 and HAZUS-MH technical manual also offer a large suite of component fragility functions (Porter, 2016). Hazard U.S. (HAZUS, 2003) presents generalized fragility curves of some structure types like bridges. However, for an accurate analysis of a structure, a more analytical method must be used.

-Empirical fragility curves: These curves are based on post-earthquake damage evaluation data. This type of fragility curve is generated from actual earthquake data or a simulated laboratory shake (Nielson, 2005; Porter, 2016). While these fragility curves are more accurate than the expert-based functions, there are still some limitations. The empirical fragility curves do not specify the structural performance (static and dynamic) and variation of input ground motion, and may not be applicable for estimating probability of damage for specific structures because it is difficult to find enough damaged structures of a certain type with the same material, design and construction method to obtain statistically acceptable results (Karim and Yamazaki, 2001). Another cause of error is the inconsistency of recorded ground motion levels, e.g. data created by USGS and Woodward-Clyde Federal Services (WCFS) might show different earthquake magnitude at the same location. Similarly, bridge damage levels varied from inspector to inspector (Nielson, 2005).

Finally, empirical fragility curves can only be developed after significant seismic events. Less earthquake prone areas that have not experienced an intense earthquake do not have enough data to develop their own fragility curves. Furthermore, the fragility curves for a specific zone may not be used for other areas due to the different structure, soil and motion types. Figure 2.4 is the example of empirical fragility curve developed by Shinozuka et al. (2000) based on Kobe earthquake data and damages.

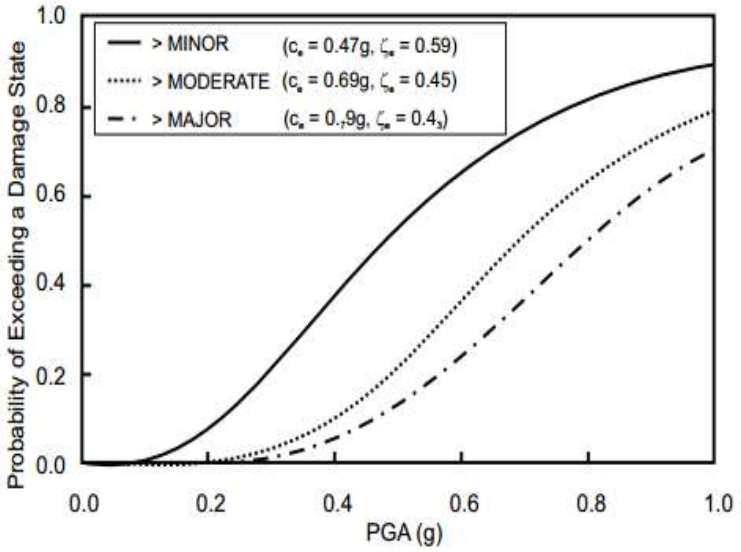

Figure 2.4. Empirical fragility curves based on bridge column damage data from Kobe earthquake

***-Analytical fragility curves*:** These kinds of fragility curves are based on structural modeling and analysis in the absence of adequate empirical data from actual ground motion data and structure damage levels. In order to get responses, simulations and resultant damage are developed (Nielson, 2005). The most reliable, but also most time-consuming method for developing analytical fragility curves, is non-linear time history analysis (NTHA). Through this method, the response of the structure to a suite of ground motion time histories is determined. Shinozuka et al. (2000), Karim and Yamazaki (2003), Nielson (2005), Kinali (2007) and Padgett (2007) have applied this method

for bridge fragility assessment. For nonlinear dynamic analyses of a structure under seismic load, incremental dynamic analysis (IDA) is another approach that scale the earthquake records upward from the elastic range to reveal the behavior of the structure under very large demands up to the collapse and global dynamic instability to assess the seismic vulnerability of the given structure under the influence of SSI and site effects. This method can be considered as a sequential form of NTHA. A plot of damage measure quantity (i.e. engineering demand parameter (EDP) such as roof displacements, inter story drift angle, etc.) vs. intensity measure (IM), generally measured by Sa(T1) (first mode spectral acceleration, at T1 = 1 s) are developed through this approach (Kinali, 2007; Karapetrou et al., 2015). Figure 2.5 illustrates an example of a bridge's analytical fragility curves (Mander, 1999).

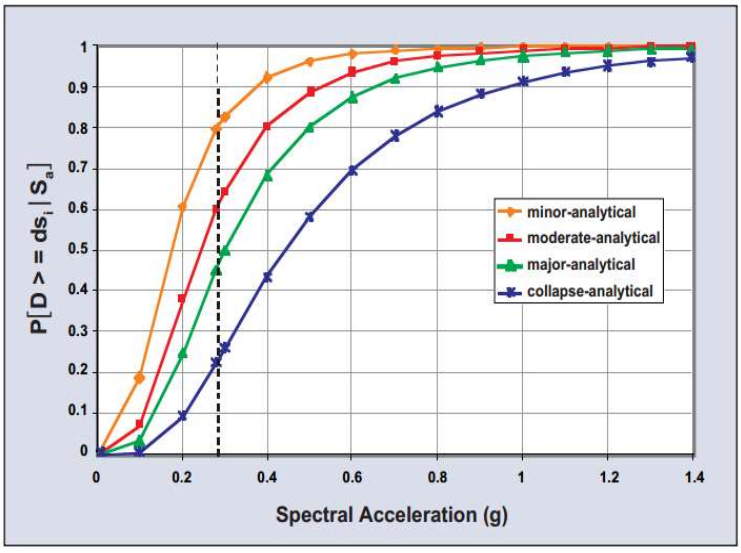

Figure 2.5. Example of bridge's analytical fragility curve (Mander, 1999)

2.7.3 Effect of soil-structure interaction on fragility curves

As discussed previously, there is some research that assert SSI impact is positive and generally reduces the vulnerability of structure (Tang and Zhang, 2011; Mekki et al., 2016). The damage

probability of a shear wall was found to decrease on a flexible foundation, especially when soil nonlinearity is considered (Tang and Zhang, 2011). In fact, several studies on seismic vulnerability of structures with consideration of SSI illustrate that the conventional way of calculating fragility assuming a fixed base structure may lead to unconservative results (Mouroux and Brun, 2003; Rajeev and Tesfamariam, 2012; Karapetrou et al., 2015; Behnamfar and Banizadeh, 2016; Mekki et al., 2016). The effect of SSI, soil parameters and geometrical foundation uncertainties on seismic fragilities of three, five and nine-story reinforced concrete (RC) frames on shallow foundations in dense silty sand have been studied (Rajeev and Tesfamariam, 2012). However, uncertainties in the modeling for SSI effects such as spring spacing, and stiffness intensity ratio were not considered. The results show that the influence of SSI on fragility is higher for three and nine-story frame than the five-story frame. The consideration of the SSI has significant influence on the fragilities; the probability of exceedance of a specific damage state in SSI model was found greater than in a fixed base model. The vulnerability of a nine-story reinforced concrete building including the effect of site and SSI was also studied (Karapetrou et al., 2015). In the model, a set of 15 real ground motion records with moment magnitude (Mw) and epicentral distance (R) that range between $5.8<Mw<7.2$ and $0<R<45$ km, respectively, were selected. The IDA approach, under the influence of SSI and site effects, was applied. When considering soil nonlinearity, the derived seismic response at the base of the structure was decreased compared to the free field motion. SSI effect introduced additional damping to the system due to the energy dissipation. The effect of SSI depends on ground motion, soil and structure dynamic characteristics; the building on harder soil is less vulnerable during an earthquake than one on soft soil as Mouroux and Brun (2003) concluded. Mekki et al. (2016) found that for specific spectral displacement, the probability of reaching or exceeding a specific damage state decreases when soil stiffness decreases. Moreover,

the nonlinear dynamic analysis of 5 buildings consisting of 3, 5, 6, 8, and 9 stories built on both soft and very soft soil under 20 suites of 10 ground motions with shear wall and moment resisting lateral load bearing systems were also implemented (Behnamfar and Banizadeh, 2016). They concluded that the shear modulus of soft soils reduces drastically at large strains due to increasing peak ground accelerations. In general, when SSI was accounted for, plastic deformation (i.e. seismic damage) was larger in shorter buildings on softer soil that included shear walls. In addition, SSI increases the lateral displacement of structures. In conclusion, consideration of SSI during both linear and nonlinear soil behavior is important because it influences the seismic vulnerability of structures.

2.8 Summary of the chapter

As discussed earlier, several researchers have studied the performance of single helical piles the effect of helices under different loading configurations and examined their lateral, compressive and uplift resistance experimentally and theoretically. The research project described herein has led to the one published study on the behavior of grouped helical piles under dynamic loads. According to these studies, helical piles show satisfactory results in all these loading conditions; especially dynamic lateral loading. Their efficient performance and reports on no or slight damage in seismic regions have increased their popularity in the United States as seismic resistant piles. The seismic characteristics and performance of helical piles, especially in groups, however, require additional study and their usage remains limited in some parts of the world. This lack of published information hinders proper design of helical pile foundations in seismic applications.

There have been several studies providing results of centrifuge or small-scale pile foundation tests and yet other papers discussing the validity of theoretical and numerical models.

From the results of these previous studies the assumptions that are used in a purely numerical analysis may cause inaccuracies in design due to many uncertainties. It is important to have repeatable, full-scale testing with actual seismic loading to provide a realistic understanding of deep foundation responses subject to earthquakes and provide a solid foundation to build a model from. This is especially important when the data set includes complicating factors, such as boundary effects and the effect of inertial load of structure. However, experimental data can be complicated by SSI; whether SSI affects the system positively or negatively according to the condition and characteristics of the combination of soil, foundation and structure needs to be carefully assessed.

Consequently, the numerical modeling with experimental validation is essential to allow engineering professionals the opportunity to understand how grouped helical piles will behave under different structures and in different subsurfaces. Moreover, assessing the vulnerability of structures supported by helical piles with consideration of SSI can provide comprehensive and reliable data on predicting behavior of structures under future earthquakes with a range of peak ground accelerations (PGA).

2.9 References

Abdelghany, Y. 2008. "Monotonic and cyclic behaviour of helical screw piles under axial and lateral loadings.", London, Ontario, Canada: The University of Western Ontario.

Abdelghany, Y., and M. H. El Naggar. 2010. "Monotonic and cyclic behavior of helical screw piles under axial and lateral loading."

Abdoun, T., R. J. S. D. Dobry, and E. Engineering. 2002. "Evaluation of pile foundation response to lateral spreading." 22(9-12), 1051-1058.

Abdrabbo, F.M., El Wakil, A.Z., 2016. Laterally loaded helical piles in sand. Alexandria Engineering Journal.

Allotey, N., and M. H. El Naggar. 2008. "Generalized dynamic Winkler model for nonlinear soil–structure interaction analysis." Canadian Geotechnical Journal, 45(4), 560-573.

Allred, S. M. 2018. "Seismic performance of grouped helical piles in fixed and pinned connections." University of Oklahoma.

Anand, V., Satish Kumar, S.R., 2018. Seismic Soil-structure Interaction: A State-of-the-Art Review. Structures, 16: 317-326.

Arya, A., and A. S. Arya. 1991. "Pile Group Stiffness for Seismic Soil-Structure Interaction." 2nd International Conferences on Recent Advances in Geotechnical Earthquake Engineering and Soil Dynamics, Missouri University of Science and Technology Scholars' Mine, Missouri.

Ashmawy, A., Salgado, R., Guha, S., Drnevich, V., 1995. Soil damping and its use in dynamic analyses.

Badry, P., Satyam, N., 2017. Seismic soil structure interaction analysis for asymmetrical buildings supported on piled raft for the 2015 Nepal earthquake. Journal of Asian Earth Sciences, 133: 102-113.

Beltrami, C., C. G. Lai, and A. Pecker. 2005. "A Kinematic Interaction Model For a Large-Diameter Shaft Foundation: An Application to Seismic Demand Assesment of a Bridge Subject to Coupled Swaying-Rocking Excitation." Journal of Earthquake Engineering, 9(spec02), 355-393.

Bielak, J., 1974. Dynamic behaviour of structures with embedded foundations. Earthquake Engineering & Structural Dynamics, 3(3): 259-274.

Boominathan, A., and R. Ayothiraman. 2005. "Dynamic behaviour of laterally loaded model piles in clay." Proceedings of the Institution of Civil Engineers-Geotechnical Engineering, 158(4), 207-215.

Borja, R. I., and W.-H. Wu. 1994. "Vibration of foundations on incompressible soils with no elastic region." Journal of geotechnical engineering, 120(9), 1570-1592.

Boulanger, R.W., Curras, C.J., Kutter, B.L., Wilson, D.W., Abghari, A., 1999. Seismic Soil-Pile-Structure Interaction Experiments and Analyses J. Geotech. Geoenviron. Eng., 125(9): 750-759.

Brown, D.A. et al., 2001. Static and dynamic lateral loading of pile groups. TRB Washington, DC, USA.

Carbonari, S., Morici, M., Dezi, F., Gara, F., Leoni, G., 2017. Soil-structure interaction effects in single bridge piers founded on inclined pile groups. Soil Dynamics and Earthquake Engineering, 92: 52-67.

Cerato, A., T. Vargas, and S. Allred. 2017. "A critical review: State of knowledge in seismic behaviour of helical piles." DFI Journal-The Journal of the Deep Foundations Institute, 11(1), 39-87.

Chandrasekaran, S., A. Boominathan, G. J. G. Dodagoudar, and G. Engineering. 2010. "Experimental investigations on the behaviour of pile groups in clay under lateral cyclic loading." 28(5), 603-617.

Chatzigogos, C. T., A. Pecker, and J. Salençon. 2009. "Macroelement modeling of shallow foundations." Soil Dynamics and Earthquake Engineering, 29(5), 765-781.

Chopra, A.K., 1995. Dynamics of structures, a primer, 2. Earthquake Engineering Research.

Chowdhury, I., Dasgupta, S., 2008. Dynamics of structure and foundation - A unified approach: 2. fundamentals, 1-617 pp.

Cox, W. R., L. C. Reese, and B. R. Grubbs. 1974. "Field testing of laterally loaded piles in sand." Proc., Offshore Technology Conference, Offshore Technology Conference.

Cremer, C., A. Pecker, and L. Davenne. 2001. "Cyclic macro-element for soil–structure interaction: material and geometrical non-linearities." International Journal for Numerical and Analytical Methods in Geomechanics, 25(13), 1257-1284.

De Carlo, G., Dolce, M., Liberatore, D., 2000. Influence of Soil–Structure Interaction on the Seismic Response of Bridge Piers, Proceeding of the 12th World Conference on Earthquake Engineering/Auckland, New Zealand.

Ebeido, A. A. 2019. "Lateral-Spreading Effects on Pile Foundations: Large-scale Testing and Analysis." UC San Diego.

Edwin Richart, F., D Wood, R., J. R, H., 1970. Vibrations of soils and foundations / F. E. Richart, R. D. Woods, J. R. Hall.El-sawy, M. 2017. "Seismic performance of steel helical pile." Master of science, The University of Western Ontario.

El Sawy, M.K., El Naggar, M.H., Cerato , A.B., Elgamal, A.W., 2019. Seismic performance of helical piles in dry sand from large scale shake table tests. Geotechnique: 18-P-001.

Elkasabgy, M., El Naggar, M.H., 2013. Dynamic response of vertically loaded helical and driven steel piles. Canadian Geotechnical Journal, 50(5): 521-535.

Elkasabgy, M., and M. H. El Naggar. 2018. "Lateral Vibration of Helical and Driven Steel Piles Installed in Clayey Soil." Journal of Geotechnical and Geoenvironmental Engineering, 144(9), 06018009.

Far, H., 2017. Advanced computation methods for soil-structure interaction analysis of structures resting on soft soils. International Journal of Geotechnical Engineering: 1-8.

Gajan, S., P. Raychowdhury, T. C. Hutchinson, B. L. Kutter, and J. P. Stewart. 2010. "Application and validation of practical tools for nonlinear soil-foundation interaction analysis." Earthquake Spectra, 26(1), 111-129.

Gazetas, G., Mylonakis, G., 2001. Soil-structure interaction effects on elastic and inelastic structures.

Ghalibafian, H., Ventura, C.E., Foschi, R.O., 2008. Effects of nonlinear soil-structure interaction on the inelastic seismic demand of pile-supported bridge piers, The 14th World Conference on Earthquake Engineering, Beijing, China.

Ghaly, A., A. Hanna, and M. J. J. o. g. e. Hanna. 1991. "Uplift behavior of screw anchors in sand. II: hydrostatic and flow conditions." 117(5), 794-808.

Ghosh, B., Madabhushi, S.P.G., 2007. Centrifuge modelling of seismic soil structure interaction effects. Nuclear Engineering and Design, 237(8): 887-896.

Giannopoulos, P., 2009. Seismic Assessment of RC Building according to FEMA 356 and Eurocode 8, 16th Conference on Concrete, TEE, ETEK, pp. 21-23.

Givens, M.J., Stewart, J.P., Haselton, C.B., Mazzoni, S., 2012. Assessment of soil-structure interaction modeling strategies for response history analysis of buildings. UCLA Civil and Environmental Engineering: Retrieved from: http://escholarship.org/uc/item/019523j6.

Guan, Z., X. Chen, and J. Li. 2018. "Experimental investigation of the seismic performance of bridge models with conventional and rocking pile group foundations." Engineering Structures, 168, 889-902.

Halling, M. W., K. C. Womack, I. Muhamad, and K. M. Rollins. 2000. "Vibrational testing of a full-scale pile group in soft clay." Proc. 12th World Conference on Earthquake Engineering, Auckland.

Han, Y., and M. Novak. 1988. "Dynamic behaviour of single piles under strong harmonic excitation." Canadian Geotechnical Journal, 25(3), 523-534.

Hardin, B.O., Drnevich, V.P., 1972. Shear modulus and damping in soils: measurement and parameter effects. Journal of Soil Mechanics & Foundations Div, 98(sm6).

HAZUS, 2003. Multi-hazard loss estimation methodology earthquake model, Washington, DC: FEMA-National Institute of Building Sciences.

Houlsby, G. T., and M. J. Cassidy. 2002. "A plasticity model for the behaviour of footings on sand under combined loading." Géotechnique, 52(2), 117-129.

Jennings, P.C., Bielak, J., 1973. Dynamics of building-soil interaction. Bulletin of the seismological society of America, 63(1): 9-48.

Jeremic, B., Jie, G.Z., Preisig, M., Tafazzoli, N., 2009. Time domain simulation of soil-foundation-structure interaction in non-uniform soils. Journal of Earthquake Engineering and Structural Dynamics, 38: 699-718.

Jin, S., Lutes, L., Sarkani, S., 2000. Response variability for a structure with soil–structure interactions and uncertain soil properties. Probabilistic Engineering Mechanics, 15(2): 175-183.

Kagawa, T., M. Sato, C. Minowa, A. Abe, and T. Tazoh. 2004. "Centrifuge simulations of large-scale shaking table tests: case studies." Journal of Geotechnical and Geoenvironmental Engineering, 130(7), 663-672.

Karapetrou, S.T., Fotopoulou, S.D., Pitilakis, K.D., 2015. Seismic vulnerability assessment of high-rise non-ductile RC buildings considering soil–structure interaction effects. Soil Dynamics and Earthquake Engineering, 73: 42-57.

Karim, K.R., Yamazaki, F., 2001. Effect of earthquake ground motions on fragility curves of highway bridge piers based on numerical simulation. Earthquake Engng Struct. Dyn., John Wiley & Sons, 30: 1839–1856.

Karim, K.R., Yamazaki, F., 2003. A simplified method of constructing fragility curves for highway bridges. Earthquake Engineering & Structural Dynamics, 32(10): 1603-1626.

Kaynia, A. M. 1982. "Dynamic stiffness and seismic response of pile groups." Massachusetts Institute of technology.

Kaynia, A.M., Mahzooni, S., 1996. Forces in pile foundations under seismic loading. Journal of Engineering mechanics, 122(1): 46-53.

Kerschen, G., Golinval, J.C., 2005. Experimental modal analysis. Lecture Notes. (http://www.ltas-vis.ulg.ac.be/cmsms/uploads/File/Mvibr_notes.pdf) (Sep. 10, 2018).

Kinali, K., 2007. Seismic Fragility Assessment of Steel Frames in the Central and Eastern United States, Georgia Institute of Technology, Georgia Institute of Technology.

Kinali, K., Ellingwood, B.R.J.E.s., 2007. Seismic fragility assessment of steel frames for consequence-based engineering: A case study for Memphis, TN. 29(6): 1115-1127.

Kramer, S. 1996. "Geotechnical Earthquake Engineering. Prentice-Hall, Inc." New Jersey, 348-422.

Ladhane, K.B., Sawant, V.A., 2016. Effect of Pile Group Configurations on Nonlinear Dynamic Response. International Journal of Geomechanics, 16(1): 04015013.

Lallemant, D., Kiremidjian, A., Burton, H., 2015. Statistical procedures for developing earthquake damage fragility curves. Earthquake Engineering & Structural Dynamics, 44(9): 1373-1389.

Lee, J., O. Kwon, I. Kim, G. Kim, and J. J. A. O. R. Lee. 2019. "Cyclic pullout behavior of helical anchors for offshore floating structures under inclined loading condition." 92, 101937.

Liang, F., Y. Jia, L. Sun, W. Xie, and H. Chen. 2017. "Seismic response of pile groups supporting long-span cable-stayed bridge subjected to multi-support excitations." Soil Dynamics and Earthquake Engineering, 101, 182-203.

Lin, M.-L., Ni, S.-H., Wright, S.G., Stokoe, K.H., 1988. Characterization of material damping in soil, Proceddings of Ninth World Conference on Earthquake Engineering, Tokyo-Kyoto, Japan.

Loria, A.F.R., Laloui, L., 2017. The equivalent pier method for energy pile groups. Géotechnique, 67(8): 691-702.

Lou, M., H. Wang, X. Chen, and Y. Zhai. 2011. "Structure–soil–structure interaction: Literature review." Soil Dynamics and Earthquake Engineering, 31(12), 1724-1731.

Lysmer, J., and F. E. Richart. 1966. "Dynamic response of footings to vertical loading." Journal of Soil Mechanics & Foundations Div.

Maheshwari, B., Truman, K., Gould, P., El Naggar, M., 2005. Three-dimensional nonlinear seismic analysis of single piles using finite element model: Effects of plasticity of soil. International Journal of Geomechanics, 5(1): 35-44.

Mander, J.B., 1999. Fragility curve development for assessing the seismic vulnerability of highway bridges. Research Progress and, 89.

Manna, B., Baidya, D., 2010. Nonlinear dynamic response of piles under horizontal excitation. Journal of geotechnical and geoenvironmental engineering, 136(12): 1600-1609.

Maravas, A., Mylonakis, G., Karabalis, D., 2007. Dynamic characteristics of structures on piles and footings, 4th International conference on earthquake geotechnical engineering. Thessaloiki-Greece, pp. 25-28.

Matlock, H. 1970. "Correlations for design of laterally loaded piles in soft clay." Offshore Technology in Civil Engineering Hall of Fame Papers from the Early Years, 77-94.

Matlock, H., and S. H. Foo. 1978. "Simulation of lateral pile behavior under earthquake motion." Proc., From Volume I of Earthquake Engineering and Soil Dynamics, Proceedings of the ASCE Geotechnical Engineering Division Specialty Conference, Pasadena, California.

Medina, C., Aznárez, J.J., Padrón, L.A., Maeso, O., 2013. Effects of soil–structure interaction on the dynamic properties and seismic response of piled structures. Soil Dynamics and Earthquake Engineering, 53: 160-175.

Mehanny, S., Ayoub, A., 2008. Variability in inelastic displacement demands: Uncertainty in system parameters versus randomness in ground records. Engineering Structures, 30(4): 1002-1013.

Mekki, M., Elachachi, S.M., Breysse, D., Zoutat, M., 2016. Seismic behavior of R.C. structures including soil-structure interaction and soil variability effects. Engineering Structures, 126: 15-26.

Michel, P., Butenweg, C., Klinkel, S., 2018. Pile-grid foundations of onshore wind turbines considering soil-structure-interaction under seismic loading. Soil Dynamics and Earthquake Engineering, 109: 299-311.

Mitropoulou, C.C., Kostopanagiotis, C., Kopanos, M., Ioakim, D., Lagaros, N.D., 2016. Influence of soil–structure interaction on fragility assessment of building structures. Structures, 6: 85-98.

Miura, F., 1997. Lessons from the damage caused by past earthquakes, International Workshop on Micropiles, Seattle.

Moghaddasi, K., Cubrinovski, M., Pampanin, S., Carr, A., Chase, G., 2009. Monte Carlo simulation of SSI effects using simple rheological soil model.

Moghaddasi, M., Cubrinovski, M., Chase, J.G., Pampanin, S., Carr, A., 2011. Probabilistic evaluation of soil–foundation–structure interaction effects on seismic structural response. Earthquake Engineering & Structural Dynamics, 40(2): 135-154.

Mouroux, P., Brun, B.L., 2003. RISK-UE. An advanced approach to earthquake risk scenarios with applications to different European towns.

Mylonakis, G., Gazetas, G., 2000. Seismic soil-structure interaction: beneficial or detrimental? Journal of Earthquake Engineering, 4(3): 277-301.

Naggar, M.H.E., Shayanfar, M.A., Kimiaei, M., Aghakouchak, A.A., 2005. Simplified BNWF model for nonlinear seismic response analysis of offshore piles with nonlinear input ground motion analysis. Canadian Geotechnical Journal, 42: 365-380.

Nakhaei, M., Ghannad, M.A., 2008. The effect of soil–structure interaction on damage index of buildings. Engineering Structures, 30(6): 1491-1499.

Nazri, F.M., Alexander, N.A.J.C.J.o.C.E., 2014. Exploring the relationship between earthquake intensity and building damage using single and multi-degree of freedom models. 41(4): 343-356.

Nielson, B.G., 2005. Analytical Fragility Curves for Highway Bridges in Moderate Seismic Zones.

Nghiem, H. M. 2009. "Soil-Pile-Structure Interaction Effects on High rise Under Seismic Shaking." Doctor of Philosophy, University of Colorado Denver.

Nogami, T., and M. Novak. 1977. "Resistance of soil to a horizontally vibrating pile." Earthquake Engineering & Structural Dynamics, 5(3), 249-261.

Nogami, T., J. Otani, K. Konagai, and H.-L. Chen. 1992. "Nonlinear soil-pile interaction model for dynamic lateral motion." Journal of Geotechnical Engineering, 118(1), 89-106.

Nova, R., and L. Montrasio. 1991. "Settlements of shallow foundations on sand." Géotechnique, 41(2), 243-256.

Novak, M., 1974. Dynamic stiffness and damping of piles. Canadian Geotechnical Journal, 11(4): 574-598.

Novak, M., and R. F. Grigg. 1976. "Dynamic experiments with small pile foundations." Canadian Geotechnical Journal, 13(4), 372-385.

Novak, M., and T. Nogami. 1977. "Soil-pile interaction in horizontal vibration." Earthquake Engineering & Structural Dynamics, 5(3), 263-281.

Novak, M., Hifnawy, L.E., 1983. Effect of soil-structure interaction on damping of structures. Earthquake engineering & structural dynamics, 11(5): 595-621.

Padgett, J.E., 2007. Seismic Vulnerability Assessment of Retrofitted Bridges Using Probabilistic Methods, Georgia Institute of Technology.

Papalou, A., Bielak, J., Bazán, E., 2012. Effects of Isolated Spread Footings on the Dynamics of Soil-Structure Interaction. Journal of Geotechnical and Geoenvironmental Engineering, 138(8): 1033-1036.

Park, Y.-J., 1985. Seismic Damage Analysis and Damage-Limiting Design for R/c Structures (Earthquake, Building, Reliability, Design), University of Illinois at Urbana-Champaign.

Park, Y.-J., Ang, A.H.-S., Wen, Y.K., 1985. Seismic damage analysis of reinforced concrete buildings. J Struct Eng ASCE, 111(4): 740-757.

Pavelka, P., Huňady, R., Kučinský, M., 2017. Modal Analysis Using the Signal Processing Toolbox of Matlab 2017. American Journal of Mechanical Engineering, 5(6): 312-315.

Pecker, A., and C. T. Chatzigogos. 2010. "Non Linear Soil Structure Interaction: Impact on the Seismic Response of Structures "Dordrecht: Springer Netherlands, Dordrecht.

Penzien, J. 1970. "Soil-pile foundation interaction." Earthquake engineering, 11.

Porter, K., 2016. A Beginner's Guide to Fragility, Vulnerability, and Risk, University of Colorado Boulder

Poulos, H.G., Civil, U.o.S.S.o., Engineering, M., Civil, U.o.S.S.o., Research, M.E.C.f.G., 1993. Settlement Prediction for Bored Pile Groups. University of Sydney, Centre for Geotechnical Research.

Prasad, Y., and S. N. Rao. 1994. "Pullout behaviour of model pile and helical pile anchors subjected to lateral cyclic loading." *Canadian geotechnical journal*, 31(1), 110-119.

Prasad, Y.V.S.N., Rao, S.N., 1996. Lateral Capacity of Helical Piles in Clays. Journal of Geotechnical Engineering, 122(11).

Prendergast, L. J., D. Hester, K. Gavin, and J. O'sullivan. 2013. "An investigation of the changes in the natural frequency of a pile affected by scour." Journal of Sound and Vibration, 332(25), 6685-6702.

Puri, V. K., and S. Prakash. 1992. "Observed and predicted response of piles under dynamic loads." Proc., Piles under dynamic loads, ASCE, 153-169.

Rainer, J., 1975. Simplified analysis of dynamic structure–ground interaction. Canadian journal of civil engineering, 2(3): 345-356.

Rajeev, P., Tesfamariam, S., 2012. Seismic fragilities of non-ductile reinforced concrete frames with consideration of soil structure interaction. Soil Dynamics and Earthquake Engineering, 40: 78-86.

Randolph, M.F., 1994. Design methods for pile group and piled rafts. Proc. 13th Int. Conf. on SMFE, 5: 61-82.

Rao, S. N., and Y. J. J. o. g. e. Prasad. 1993. "Uplift behavior of pile anchors subjected to lateral cyclic loading." 119(4), 786-790.

Raychowdhury, P., and T. C. Hutchinson. 2009. "Performance evaluation of a nonlinear Winkler-based shallow foundation model using centrifuge test results." Earthquake Engineering & Structural Dynamics, 38(5), 679-698.

Richart, F. E., R. D. Wood, and J. R. Hall. 1970. "Vibrations of soils and foundations

Ridgley, N. 2015. "Practice Note 28: Screw Piles: Guidelines for Design, Construction & Installation." The Institution of Professional Engineers New Zealand Inc.

Rollins, K. M., S. A. Ashford, and J. Lane. 2001. "Full-scale lateral load testing of deep foundations using blast-induced liquefaction."

Rollins, K. M., T. M. Gerber, J. D. Lane, S. A. J. J. o. G. Ashford, and G. Engineering. 2005. "Lateral resistance of a full-scale pile group in liquefied sand." 131(1), 115-125.

Rollins, K. M., L. J. Hales, S. A. Ashford, and I. Camp, William M 2006. "PY curves for large diameter shafts in liquefied sand from blast liquefaction tests." *Seismic Performance and Simulation of Pile Foundations in Liquefied and Laterally Spreading Ground*, 11-23.

Rovithis, E., K. Pitilakis, and G. Mylonakis. 2009. "Seismic analysis of coupled soil-pile-structure systems leading to the definition of a pseudo-natural SSI frequency." Soil Dynamics and Earthquake Engineering, 29(6), 1005-1015.

Sáez, E., Lopez-Caballero, F., Modaressi-Farahmand-Razavi, A., 2013. Inelastic dynamic soil–structure interaction effects on moment-resisting frame buildings. Engineering structures, 51: 166-177.

Sakr, M., 2009. Performance of helical piles in oil sand. Canadian Geotechnical Journal, 46(9): 1046-1061.

Seed, H. B., and J. Lysmer. 1978. "Soil-structure interaction analyses by finite elements—State of the art." Nuclear Engineering and Design, 46(2), 349-365.

Shahbazi, M., A. B. Cerato, S. Allred, M. H. El Naggar, and A. Elgamal. 2019. "Damping Characteristics of Full-Scale Grouped Helical Piles in Dense Sands Subject to Small and Large Shaking Events." Canadian Geotechnical Journal.

Shahbazi, M., M. Rowshanzamir, S. M. Abtahi, and S. M. J. A. C. S. Hejazi. 2017. "Optimization of carpet waste fibers and steel slag particles to reinforce expansive soil using response surface methodology." 142, 185-192.

Shamsabadi, A., Taciroglu, E., 2013. A Frequency-Time Domain Handshake Method For Seismic Soil-Foundation-Structure Interaction Analysis of Long-Span Bridges, Proceeding 7th National Seismic Conference on Bridges and Highways.

Shinozuka, M., Feng, M.Q., Lee, J., Naganuma4, T., 2000. STATISTICAL ANALYSIS OF FRAGILITY CURVES. J. Eng. Mech., ASCE, 126(12): 1224-1231.

Shirato, M., Y. Nonomura, J. Fukui, and S. Nakatani. 2008. "Large-scale shake table experiment and numerical simulation on the nonlinear behavior of pile-groups subjected to large-scale earthquakes." Soils and foundations, 48(3), 375-396.

Shirgir, V., A. Ghanbari, M. Amiri, and A. Derakhshandi. 2017. "Effect of Pile Foundation on Natural Frequency of Soil Layer." Journal of Engineering Geology, 10(4), 3839.

Shome, N., Cornell, C.A., Bazzurro, P., Carballo, J.E., 1998. Earthquakes, Records, and Nonlinear Responses. Earthquake Spectra, 14(3): 469-500.

Siemens Industry Software, ,Estimation of modal parameters. Rev 16 A.

Singh, S. K. 1995. "Behavior of Screw Pile Anchors in Sand." Kurukshetra University, Kurukshetra.

Stewart, J. et al., 2012. Soil-Structure Interaction for Building Structures

Stewart, J.P., Kim, S., Bielak, J., Dobry, R., Power, M.S., 2003. Revisions to soil-structure interaction procedures in NEHRP design provisions. Earthquake Spectra, 19(3): 677-696.

Tabatabaiefar, H.R., Fatahi, B., 2014. Idealisation of soil–structure system to determine inelastic seismic response of mid-rise building frames. Soil Dynamics and Earthquake Engineering, 66: 339-351.

Talukder, M.K., 2009. Seismic response of pile foundation in saturated sand using Beam on Nonlinear Winkler Foundation approach, Canada.

Tamori, S. i., M. Iiba, and Y. Kitagawa 2001. "A Simplified Method for Dynamic Response Analysis of Soil-Pile-Building Interaction System in Large Strain Levels of Soils-Analysis for Building with Embedment and Pile." Proceedings Third UJNR Workshop on Soil-Structure Interaction, California, USA.

Tang, Y., Zhang, J., 2011. Probabilistic seismic demand analysis of a slender RC shear wall considering soil–structure interaction effects. Engineering Structures, 33(1): 218-229.

Ting, J. 1987. "Full-scale cyclic dynamic lateral pile responses." *Journal of Geotechnical engineering*, 113(1), 30-45.

Ting, J. M., C. R. Kauffman, and M. Lovicsek. 1987. "Centrifuge static and dynamic lateral pile behaviour." Canadian Geotechnical Journal, 24(2), 198-207.

Ubilla, J., T. Abdoun, and R. Dobry. 2011. "Centrifuge scaling laws of pile response to lateral spreading." International Journal of Physical Modelling in Geotechnics, 11(1), 2-22.

Vamvatsikos, D., Cornell, C.A.J.E.E., Dynamics, S., 2002. Incremental dynamic analysis. 31(3): 491-514.

Van Nguyen, Q., Fatahi, B., Hokmabadi, A.S., 2017. Influence of size and load-bearing mechanism of piles on seismic performance of buildings considering soil–pile–structure interaction. International Journal of Geomechanics, 17(7): 04017007.

Vargas Castilla, T.M., 2017. Understanding the seismic response of single helical piles in dry sand using a large-scale shake table test, Master of science, University of Oklahoma.

Veletsos, A.S., Meek, J.W., 1974. Dynamic behaviour of building-foundation systems. Earthquake Engineering & Structural Dynamics, 3(2): 121-138.

Vickars, R. A., and S. P. Clemence 2000. "Performance of helical piles with grouted shafts." *New technological and design developments in deep foundations*, 327-341.

Victor, R. T. 2008. " Helical Anchors as Wind Tower Guyed Cable Foundations." Master Thesis, University of Oklahoma, University of Oklahoma.

Wilson, D. 1998. "Soil-pile-superstructure interaction in soft clay and liquefiable sand." Rep. No. UCD/CGM-98, 4.

Wolf, J.P., 1985. Dynamic soil-structure interaction. Englewood Cliffs (N.J.) : Prentice-Hall.

Yang, E.-K., J.-I. Choi, S.-Y. Kwon, and M.-M. Kim. 2011. "Development of dynamic py backbone curves for a single pile in dense sand by 1g shaking table tests." KSCE Journal of Civil Engineering, 15(5), 813.

Yang, E.-K., S.-Y. Kwon, J.-I. Choi, and M. M. Kim 2010. "Natural Frequency Calculation of a Pile-Soil System in Dry Sand Under an Earthquake Loading." 5th International Conference on Recent Advances in Geotechnical Earthquake Engineering and Soil Dynamics, Missouri University of Science and Technology Scholars' Mine.

Yashinsky, M., 1998. The Loma Prieta, California, Earthquake of October 17, 1989, 3. US Government Printing Office.

Zhang, C., Wolf, J.P., 1998. Dynamic soil-structure interaction: Current research in China and Switzerland. Elsevier, Amsterdam.

Chapter 3 : FULL-SCALE SHAKE TABLE TEST AND DATA REDUCTION

This chapter describes the full-scale tests conducted on the large high-performance outdoor 12 m by 7.6 m shake table (LHPOST) located at the University of California – San Diego's Englekirk structural research lab. The data reduction of recorded data to analyze seismic performance of helical piles will be discussed in detail.

3.1 Experimental test set up

Pile instrumentation- Helical piles were provided by Torcsill Foundations LLC and Ram Jack pile manufacturer. In order to stick the stain gages on each pile effectively, the specified location on each pile were sanded. Holes then were drilled at those locations to feed the strain gage wiring through the hollow inside of the piles. The locations of strain gages were wiped off from any residue and dirt with acetone and lacquer thinner saturated paper towel. After sticking gages to the pile surface at marked locations by especial glue, the epoxy coat was applied to fix the gages in place (Figure 3.1). To avoid sheering off the stain gages from the pile surface during screwing pile into the soil, strain gages were wrapped with fiber glass fabric and resin. All strain gages were tested by multimeter to make sure all were working before installation and starting the test (Allred 2018). Thus, at each level, two strain gauges connected as quarter bridges were attached successfully on opposite sides of the exterior wall of each pile shaft in the shaking direction (east-west). A total of 152 strain gauges were used: either six or seven coupled strain gauges along each pile length. The locations of strain gages are displayed in Figure 3.2.

Figure 3.1. Fiber glass fabric and resin wrapped around each stain gage

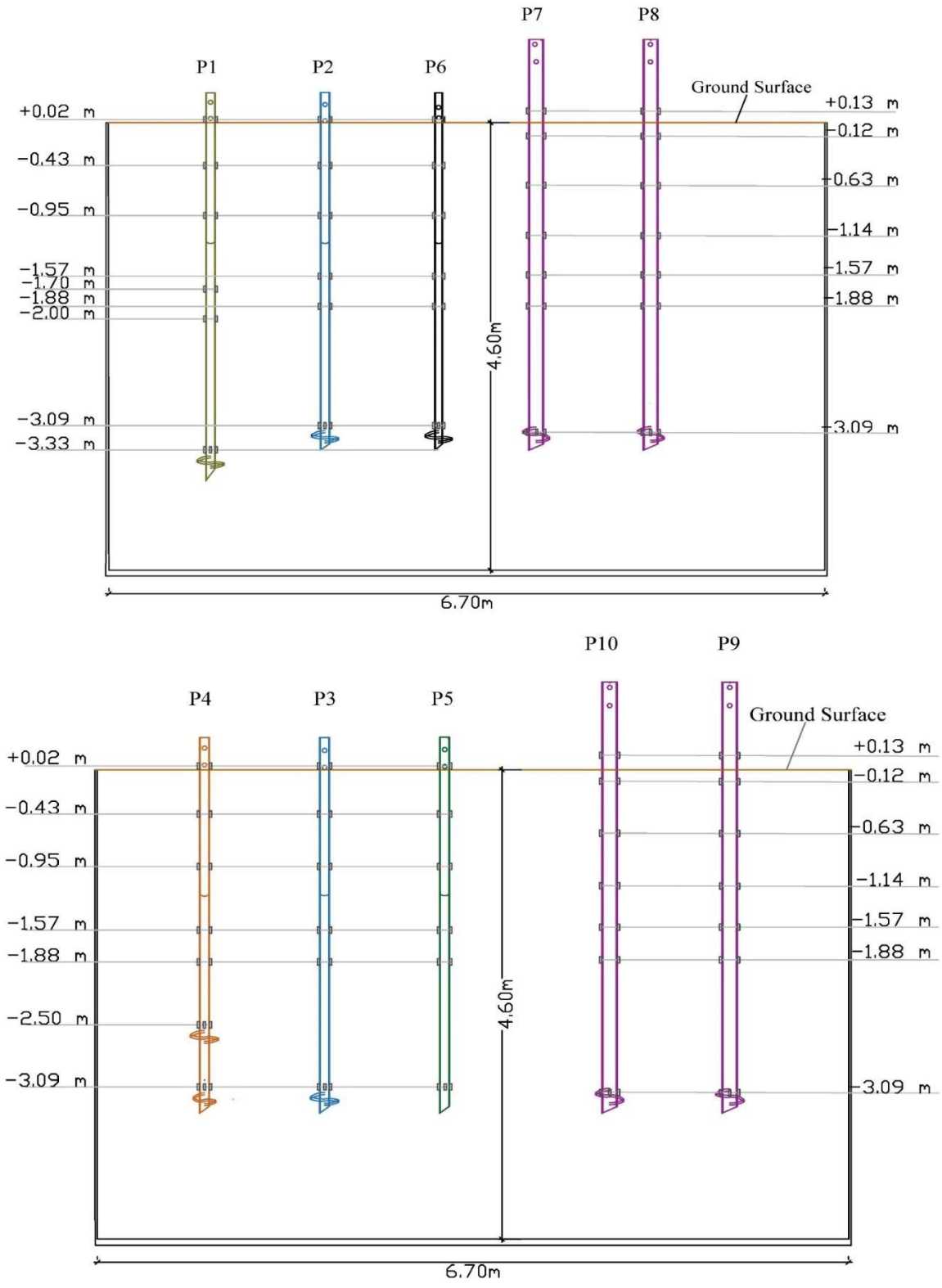

Figure 3.2. Elevation view of pile with strain gages

Dense sand construction in laminar box- Direct shear (ASTM D3080) under a normal stress of 50, 100, 150 kPa as well as other standard laboratory tests including moisture content tests (ASTM D 4643) and sieve analysis (ASTM D 6913) were conducted to determine the engineering properties of the well graded sand provided by UCSD. The results are presented in Table 3.1 and Figure 3.3. Test sand were compacted in every 30 cm-layer and was enclosed in a 6.7 m long, 3.0 m wide and 4.6 m high laminar box to achieve approximately 100% relative density. Several accelerometers were placed at various elevations on the east, center and west sides of sand bed as well as on the exterior of the laminar box to record sand behavior and its dynamic properties. Figure 3.4 displays a schematic elevation of the sand box showing the locations of the accelerometers within the sand bed and on the exterior of the laminar box. Accelerometers were connected to data acquisition system to record and save sand and laminar box response. Pulse and white noise (0.07 g root-mean-square (RMS)) excitations was applied to shake sand bed at 0.1 g peak acceleration. Pulses were transmitted through the sand and at each accelerometer level within the sand bed the peak wave arrival times were recorded. Shear wave velocity was then calculated after each motion.

Table 3.1. Sand properties

Property	Value
Average natural water content, ωn (%)	5.5
Friction angle direct shear, $\emptyset_{ds}$ (°)	47.6
Average grain size, D50 (mm)	0.85
Fines content (Fc) (%)	4.5
Unit weight, γ (kN/m3)	19.5
Relative density, Dr (%)	100

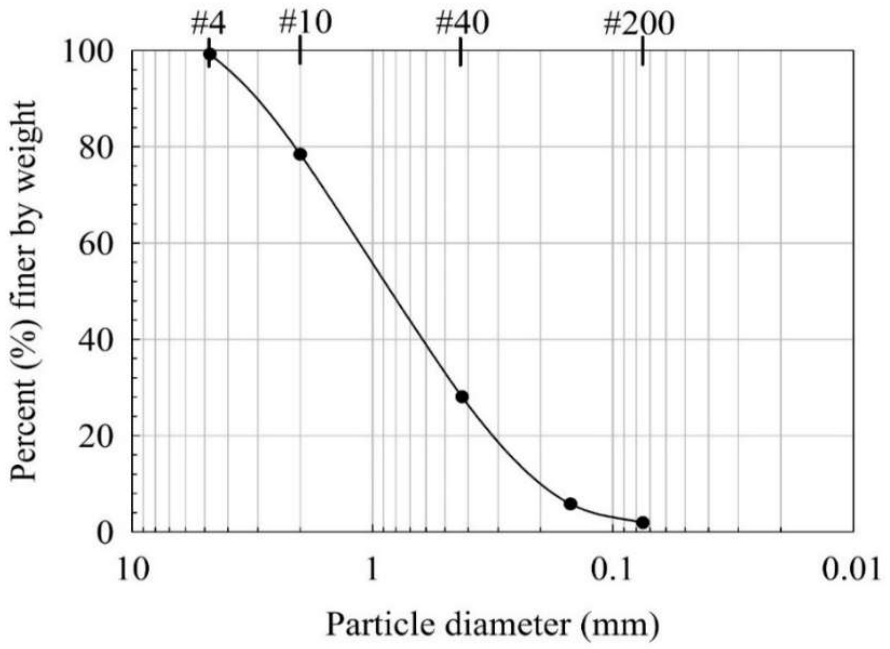

Figure 3.3. Grain size distribution of sand

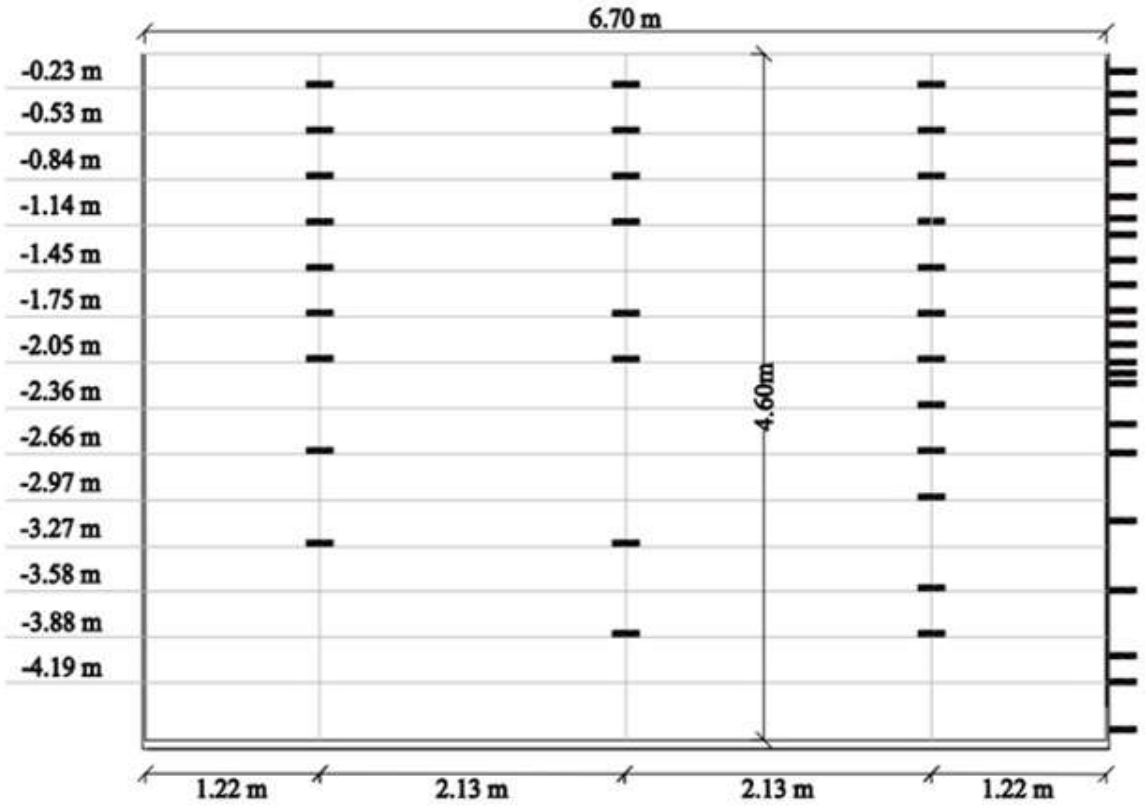

Figure 3.4. Elevation view of sand-bed and box accelerometer layout

Pile installation- Ten instrumented steel piles including nine helical piles and one driven pile were installed in the soil by applying a mechanical torque to each pile head (Figure 3.5). All piles' lead and extension part were coupled with bolt except pile 1 which was threaded. The geometry and engineering properties of piles are summarized in Table 3.2. Yield strength, Young's modulus and steel grade of the helical pile were certified by the steel mill and measured and defined by manufacturers who provided the piles. Figure 3.2 demonstrates the piles' layout within the sand box and their configuration and instrumentation. The spacing to diameter ratio of piles are more than 8D to minimize pile interaction effects that can be seen in plan-view of piles layout in Figure 3.6. After installation, a dynamic cone penetration test was performed. All strain gauges were connected to a data acquisition system to record simultaneous readings of strain along the shaft of all piles during the tests.

Figure 3.5. Pile installation image at UCSD

Table 3.2. Pile properties

Pile	Type	Outside diameter (mm)	Wall thickness (mm)	Length of pile (m)	Pile head above ground (cm)	Helix level (m)	Yield strength, F_y (MPa)
P1	Circular, single helix, single bolt	88	5	3.96	30	-3.40	448
P2	Circular, single helix, double bolt	88	5	3.66	30	-3.15	448
P3	Circular, single helix, double bolt	88	5	3.66	30	-3.15	448
P4	Circular, double helix, double bolt	88	5	3.66	30	-3.15	448
P6	Square, single helix	76	5	3.66	30	-3.15	414
P7	Circular, single helix, double bolt	140	10.5	4.27	86	-3.15	552
P8	Circular, single helix, double bolt	140	10.5	4.27	86	-3.15	552
P9	Circular, single helix, double bolt	140	10.5	4.27	86	-3.15	552
P10	Circular, single helix, double bolt	140	10.5	4.27	86	-3.15	552

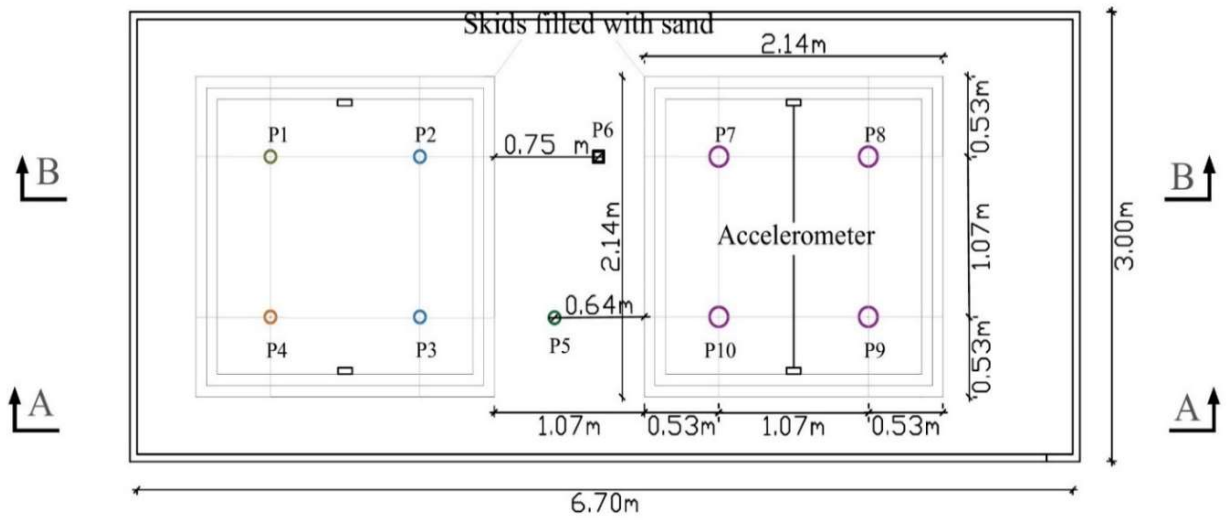

Figure 3.6. Plan view of test laminar box layout and skid condition

Shake table test schedule- The dynamic and seismic tests were conducted over five days. As mentioned, on Day 1, the dense sand bed enclosed in the laminar shear box was subjected to two pulses and a white noise motion to establish the dynamic properties of the soil. On Day 2, piles were installed and were subjected to different excitations without inertial masses. On Day 3, concrete blocks were placed on top of each pile head to provide inertial mass to simulate loading conditions of the piles (Figure 3.7). The weights applied to each single pile are presented in Table 3.3. On Day 4, four helical piles with outer diameter of 0.088 m were connected by a steel skid that weighed 62 kN placed atop the piles to form Group 1 (2x2). Another four helical piles with outer diameter of 0.140 m were connected by another steel skid that weighed 98 kN placed atop the piles to form Group 2 (2x2). Two accelerometers on opposite sides of the skids near its center of mass were located and connected to data acquisition. Figures 3.8 to 3.10 show the setup of the pile groups. For both Group 1 and Group 2, on Day 4 the skid was connected to each pile head with two bolts to form a fixed connection. Both pile groups (with fixed connection) were subjected to different excitations with different frequency contents and intensities. On Day 5, the top bolt of each connection was removed to simulate a pinned connection with the same skids. The pile groups were then subjected to the same set of excitations. The connections are illustrated in Figure 3.11.

Table 3.3. Weights on each pile head

Pile	Weight (kN)
P1	7.50
P2	7.35
P3	7.65
P4	7.35
P5	3.63
P6	4.27
P7	12.11
P8	7.70
P9	6.86
P10	12.21

Figure 3.7. Single piles with inertial load on Day 3 of test

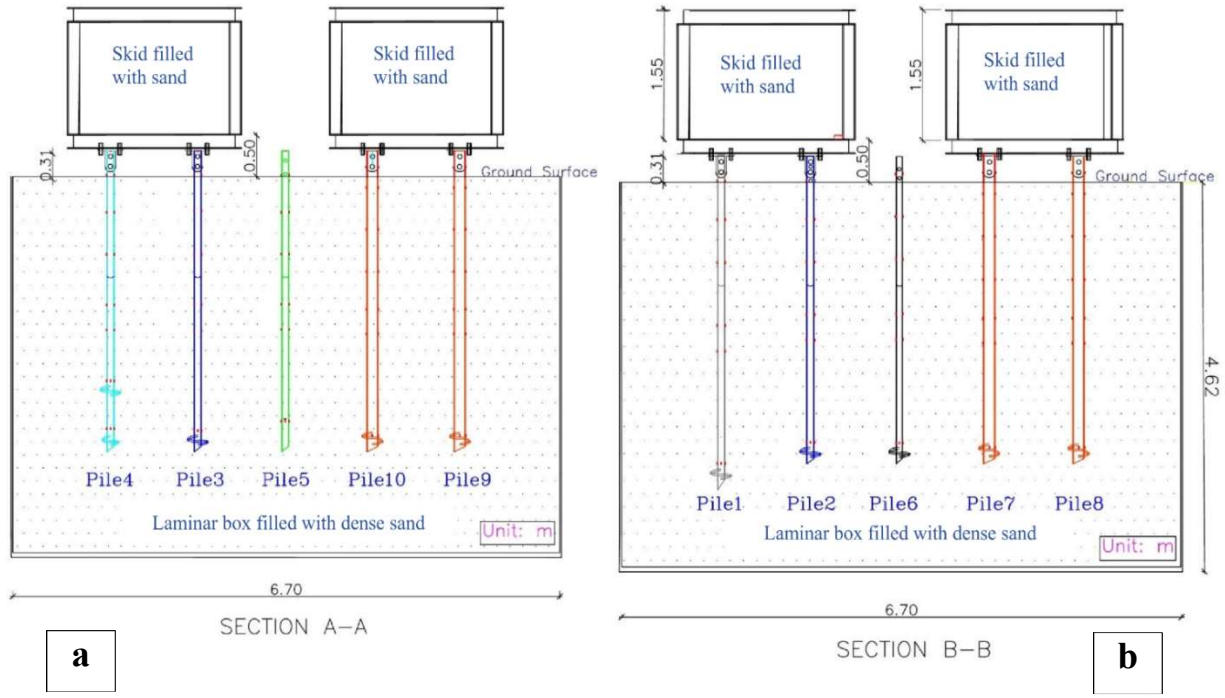

Figure 3.8. Day4 and 5 set up: (a) section view (A-A); (b) section view (B-B)

Figure 3.9. Grouped piles with sand-filled skid load on Day 4 and 5 of test

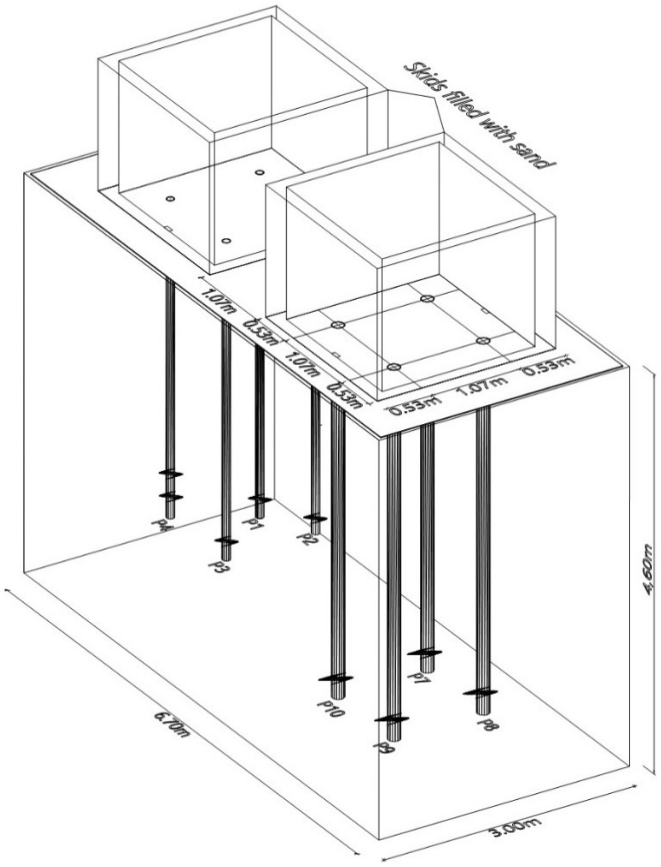

Figure 3.10. 3D view of shake table

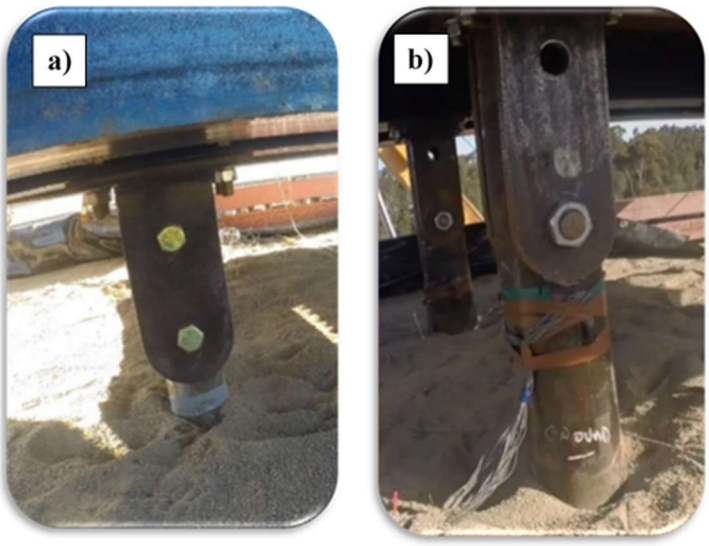

Figure 3.11. Illustration of: (a) fixed connection (double bolt) on Day 4 and (b) pinned connection (single bolt) on Day 5

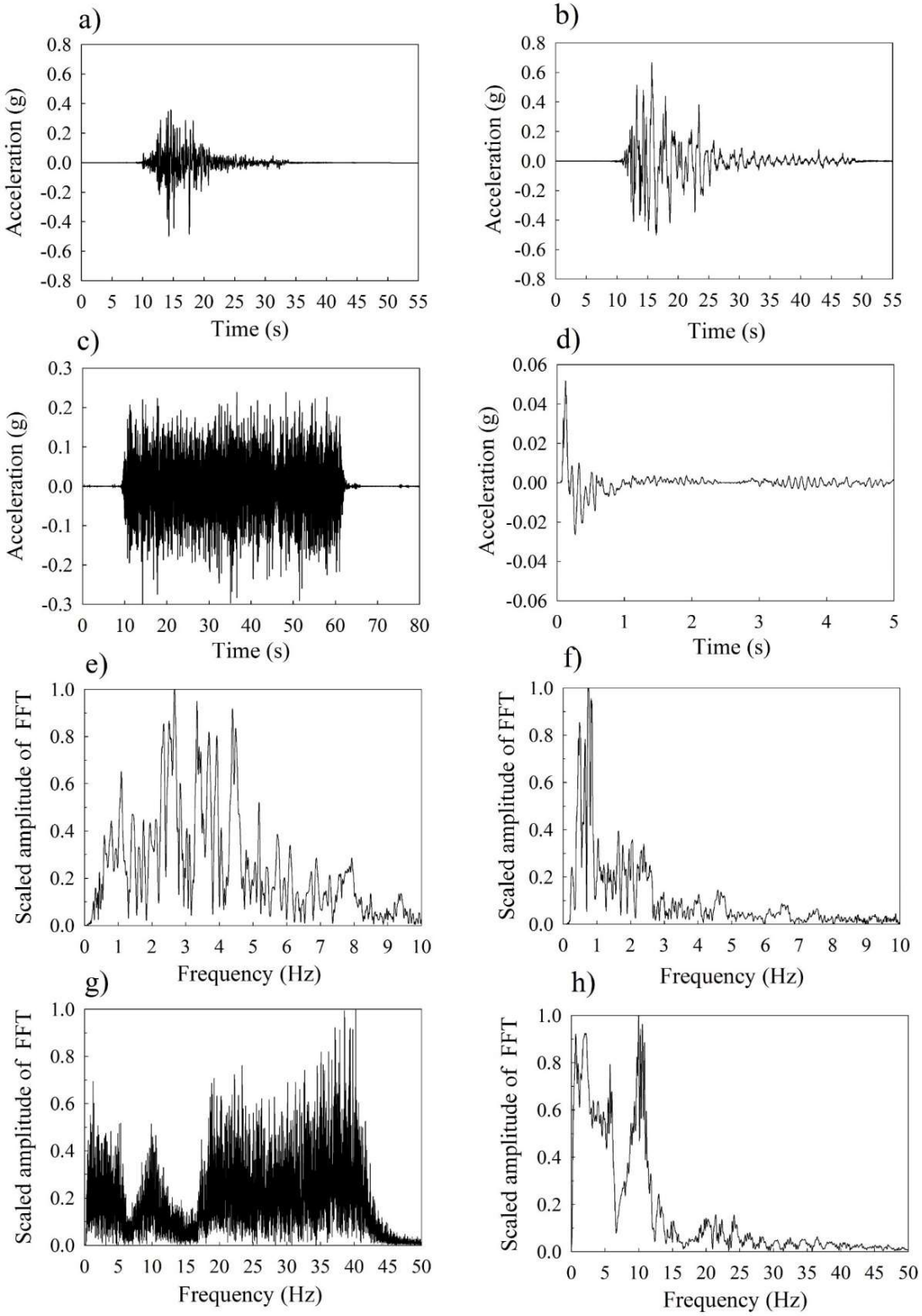

Figure 3.12. (a) unscaled Nor. time history; (b) unscaled Tak. time history; (c) unscaled white noise time history; (d) unscaled pulse time history; (e) Nor. frequency content; (f) Tak. frequency content; (g) white noise frequency content; (h) pulse frequency content

The first input motion each day consisted of random signal with a constant intensity for a frequency bandwidth of 0 to 40 Hz, as white noise excitation (0.07 g root-mean-square, RMS) followed by variations of two replicated earthquake motions with known ground acceleration data; the 1994 Northridge California earthquake (Fire Station 108, 12520 Mulholland Dr., USC station 5314, Component 35 degrees) and the 1995 Kobe earthquake (Takatori station, Component 0 degree). Figure 3.12 presents the unscaled earthquake records considered in the tests. These ground motions were applied at graduating intensity of 50%, 75% and 100% of the peak ground acceleration (PGA) amplitude for both earthquakes. After each shake pulse was applied. Results show that the changes in wave velocity after each shake were negligible. Thus, it is assumed that shear wave velocity remained constant throughout the testing sequence and repeated shaking did not seem to change sand bed properties such as shear modulus and stiffness.

More information on the pile test set-up can be found in Allred (2018), El-sawy (2017) and Vargas Castilla (2017)'s studies.

3.2 Data reduction and analysis

Data filtering and analysis- The collected stain gage and accelerometers reading were filtered in order to remove noise signals. A 4^{th} degree Butterworth filter with band pass between 0.25 to 8 HZ were performed. This range seemed to be adequate to assure removing of high frequency noise without missing any earthquake signal.

It has been found that the p-y curve method, where p is the soil reaction and y is the pile lateral deflection, can be used to estimate the lateral performance of helical piles (Perko 2009, Sakr 2009). To calculate p and y, strain readings are required. The bending moment at each strain gauge location was calculated using recorded strain gauges readings (Eq.(3-1)).

$$M(z) = \frac{E_p I_p (\varepsilon_1 - \varepsilon_2)}{d} \quad 3\text{-}1$$

where $\varepsilon_1, \varepsilon_2$ are the filtered strain gauge readings at east and west sides of the pile, E_p, I_p are the elastic modulus and cross-sectional moment of inertia of pile, and d is outer pile's diameter.

These bending moments were fit with the function of depth at each time step using several curve-fitting methods. Between all methods attempted, a 4th order (cubic) spline was shown to provide well fitted curves using moment at strain gauge elevations and artificial points. Artificial points were added to satisfy boundary conditions at the center of mass and near the pile tip and assumed to have zero moment. The resulting curves were used to determine the soil reaction, p, and the pile deflection, y, by double differentiating and double integrating of bending moment function using Eq. (3-2) and (3-3), respectively. MATLAB (MathWorks, 2016) was used to filter and analyze the data.

$$p(z) = \frac{d^2 M(z)}{dz^2} \quad 3\text{-}2$$

$$y_p(z) = \iint \frac{M(z)}{E_p I_p} dz \quad 3\text{-}3$$

The bending moment, pile deflection and soil reaction versus depth along the pile length are obtained using cubic spline interpolation in MATLAB program. A few results from the responses of piles including p-y curves for Takatori 75% and Northridge 100% (which both have same intensity (peak acceleration = 0.5g)) are presented in Figures 3.13 to 3.24. The effect of pile geometry, connection and other conditions can be estimated by comparing the provided results. The rest is provided in attached appendix where the p-y curves are shown approximately where the maximum bending moment occurs.

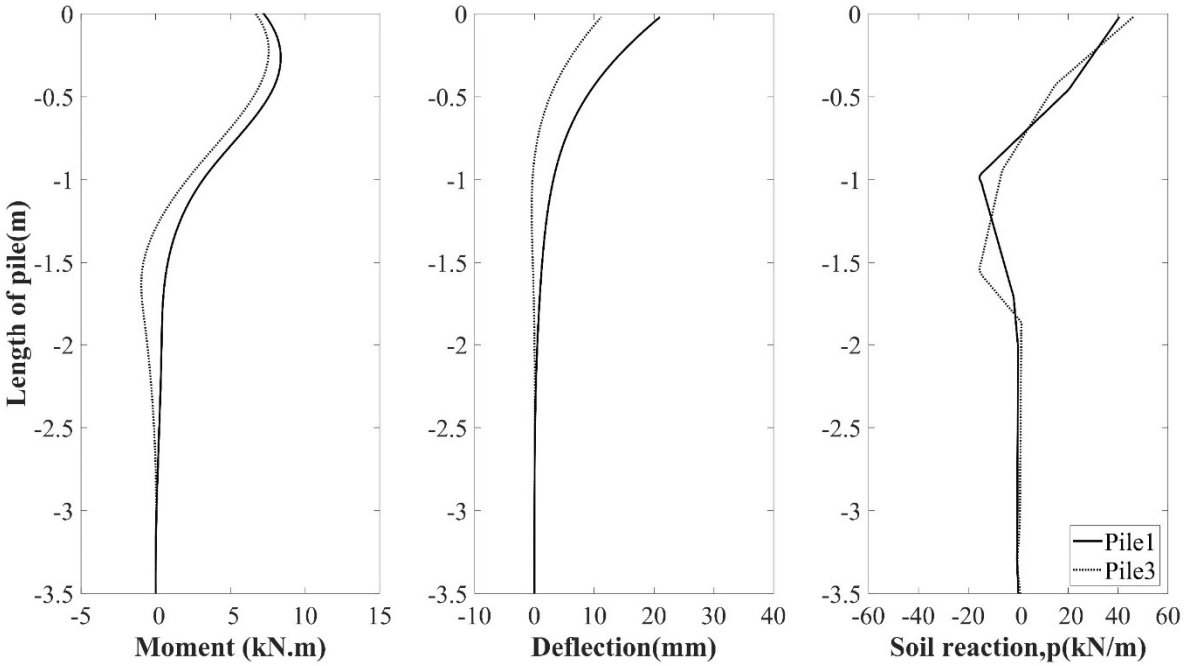

Figure 3.13. Bending moment, deflection and soil reaction of P1 and P3 with depth for Northridge 100%

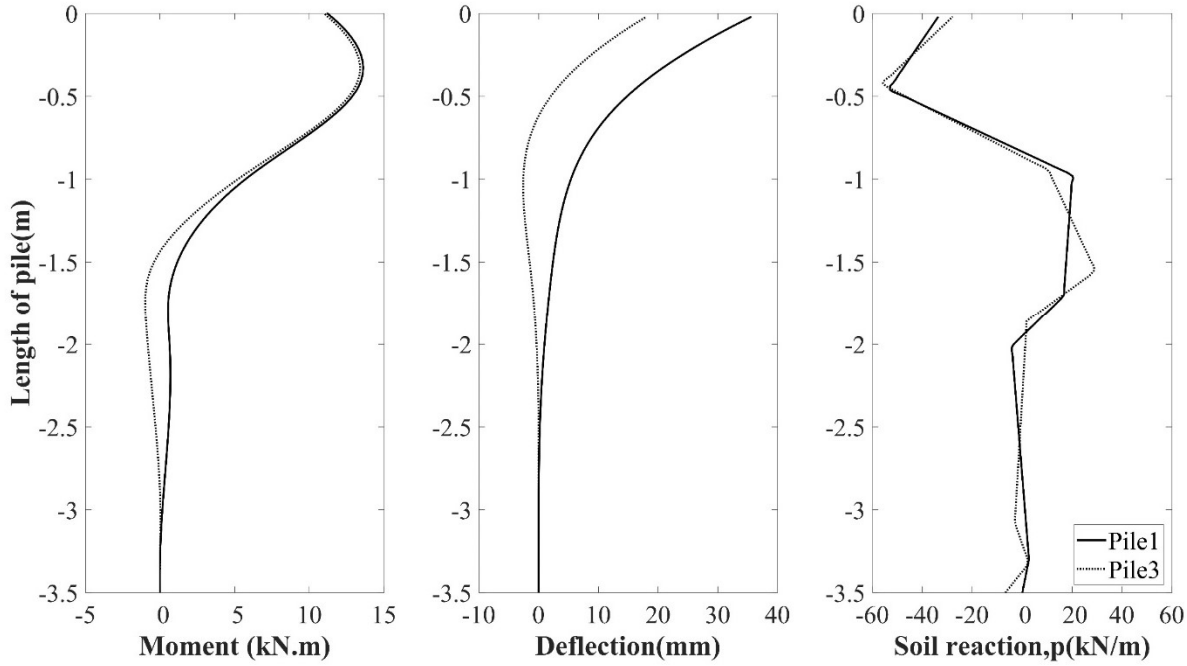

Figure 3.14. Bending moment, deflection and soil reaction of P1 and P3 with depth for Takatori 75%

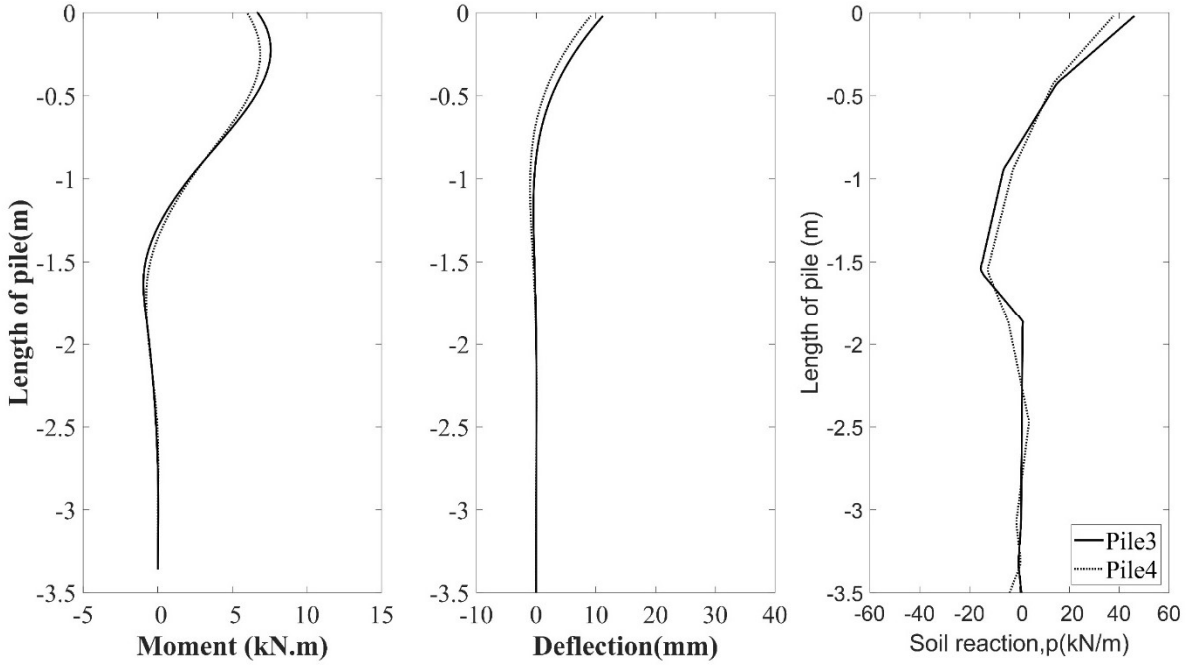

Figure 3.15. Bending moment, deflection and soil reaction of P3 and P4 with depth for Northridge 100%

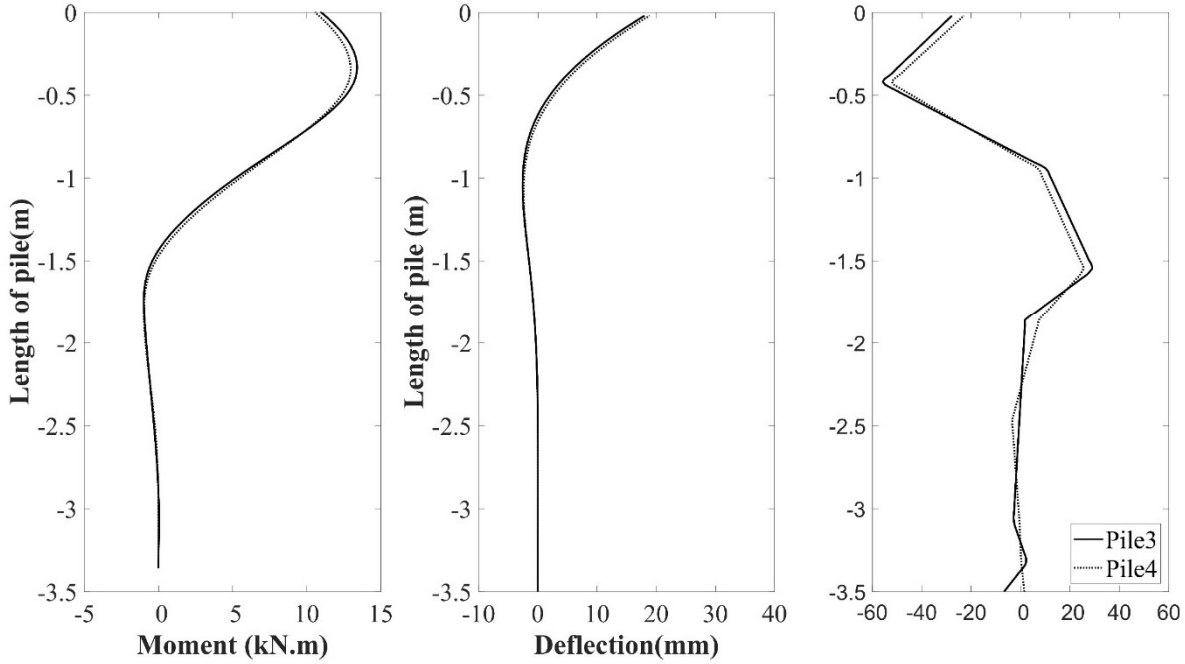

Figure 3.16. Bending moment, deflection and soil reaction of P3 and P4 with depth for Takatori 75%

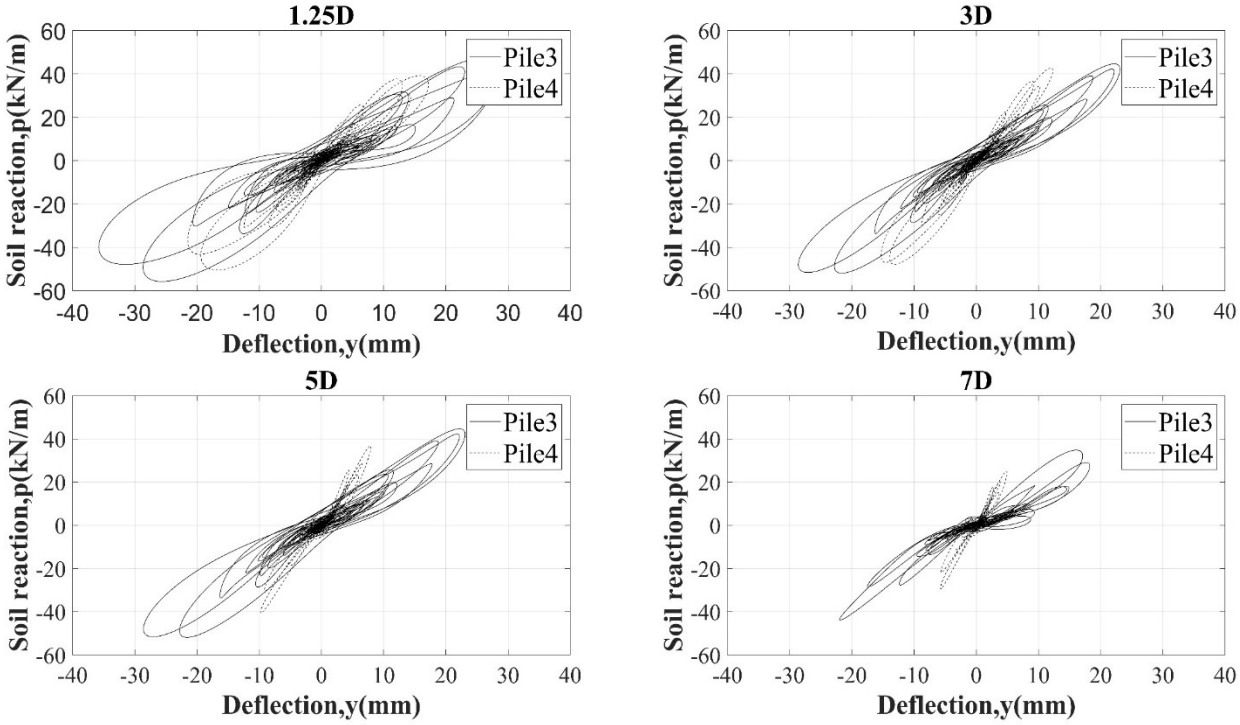

Figure 3.17. Dynamic p-y curves during Takatori 75% for P3 and P4 at different depths: 1.25D, 3D, 5D, and 7D. Note: D=diameter of pile

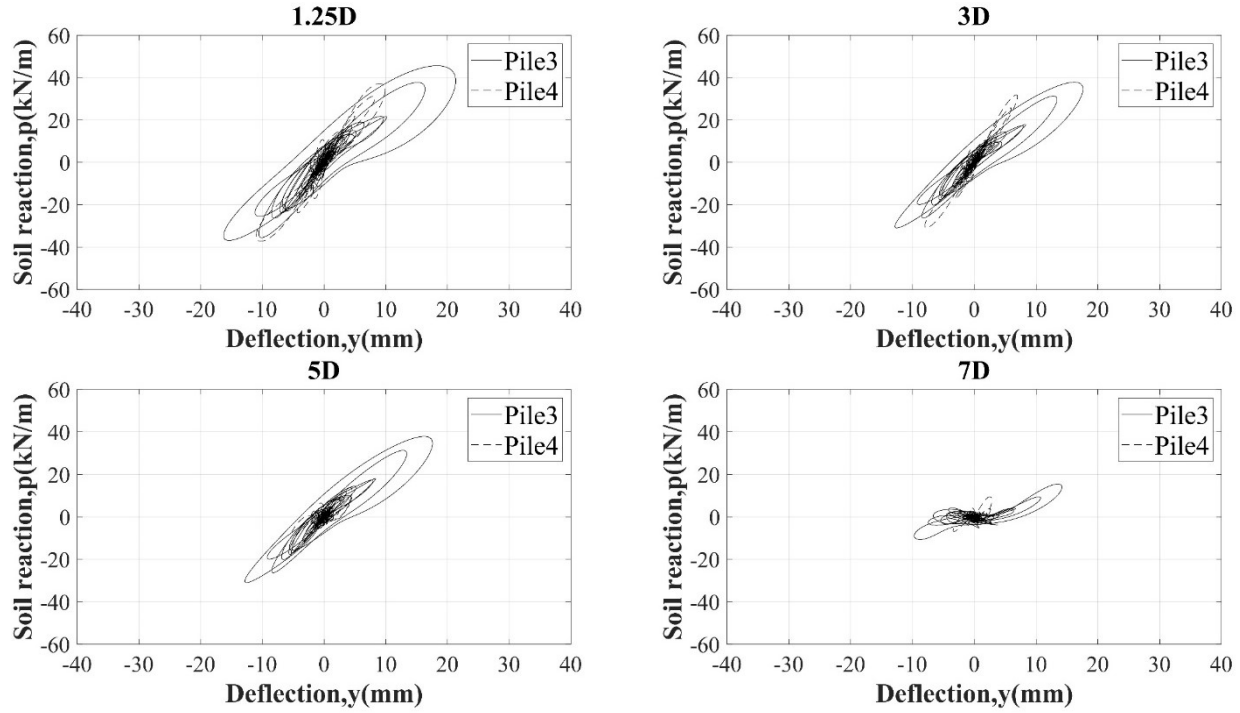

Figure 3.18. Dynamic p-y curves during Northridge 100% for P3 and P4 at different depths: 1.25D, 3D, 5D, and 7D. Note: D=diameter of pile

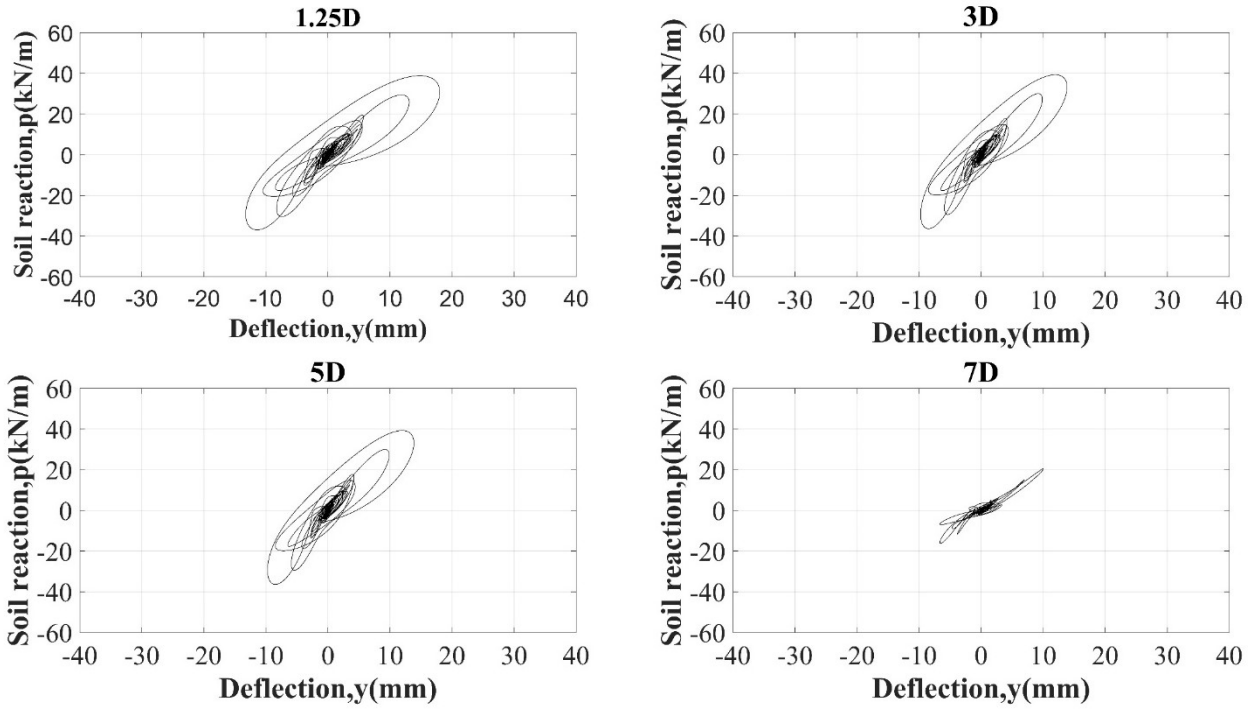

Figure 3.19. Dynamic p-y curves during Northridge 100% for P1 on Day 3 at different depths: 1.25D, 3D, 5D, and 7D. Note: D=diameter of pile

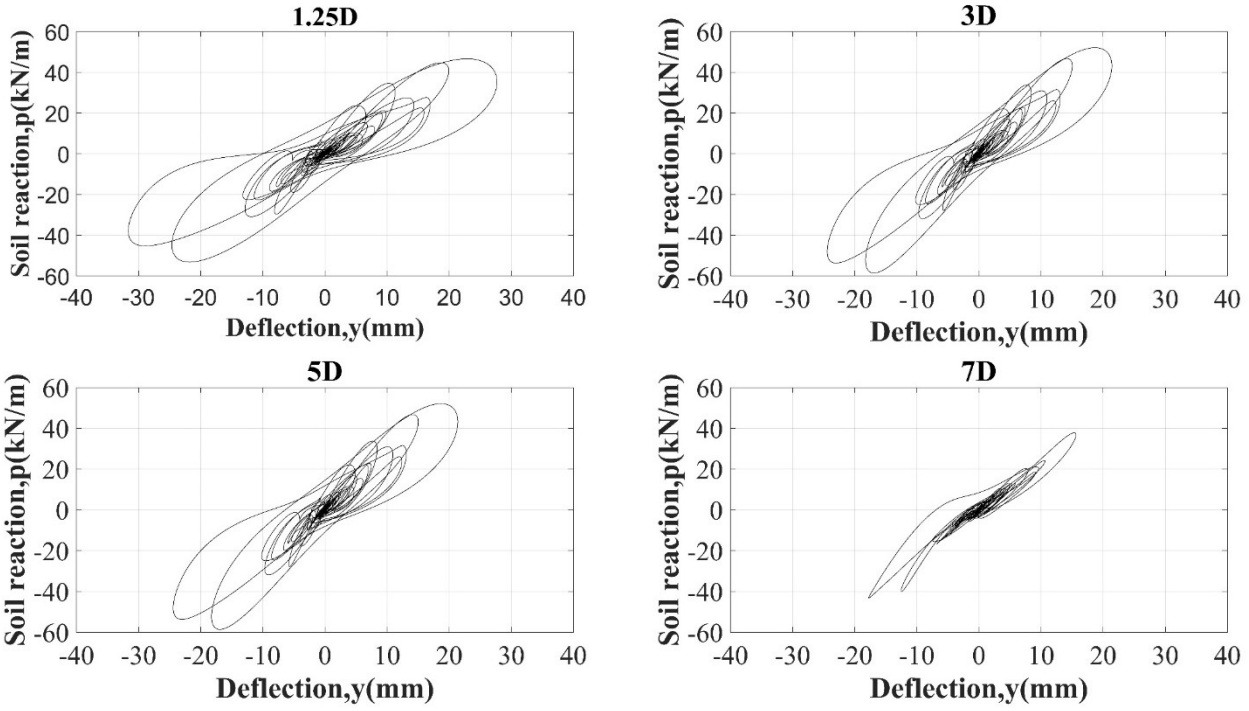

Figure 3.20. Dynamic p-y curves during Takatori 75% for P1 on Day 3 at different depths: 1.25D, 3D, 5D, and 7D. Note: D=diameter of pile

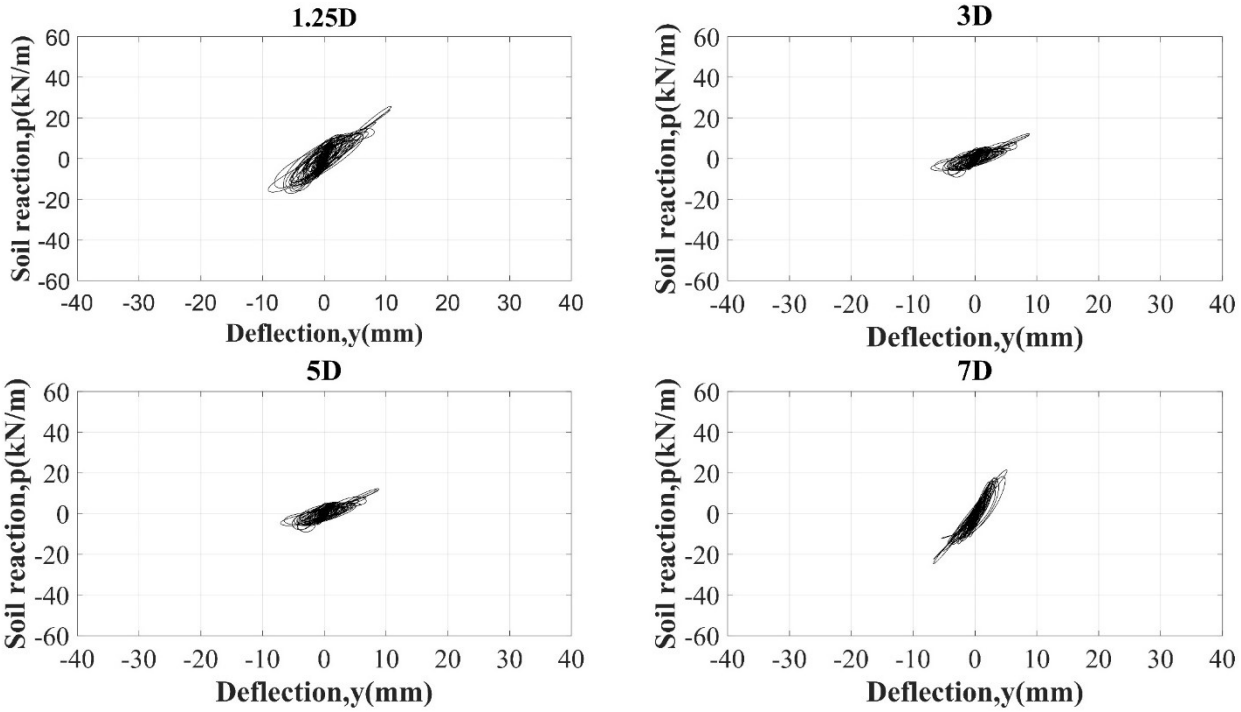

Figure 3.21. Dynamic p-y curves during Northridge 100% for P1 on Day 4 at different depths: 1.25D, 3D, 5D, and 7D. Note: D=diameter of pile

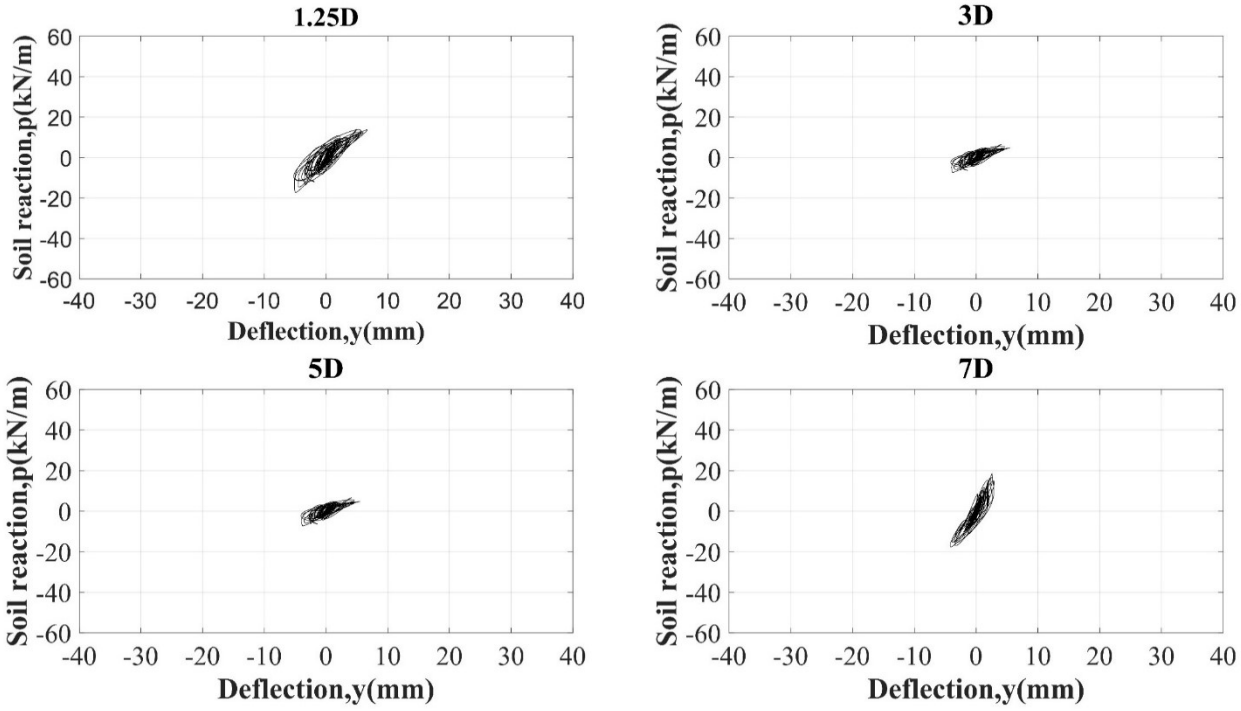

Figure 3.22. Dynamic p-y curves during Takatori 75% for P1 on Day 4 at different depths: 1.25D, 3D, 5D, and 7D. Note: D=diameter of pile

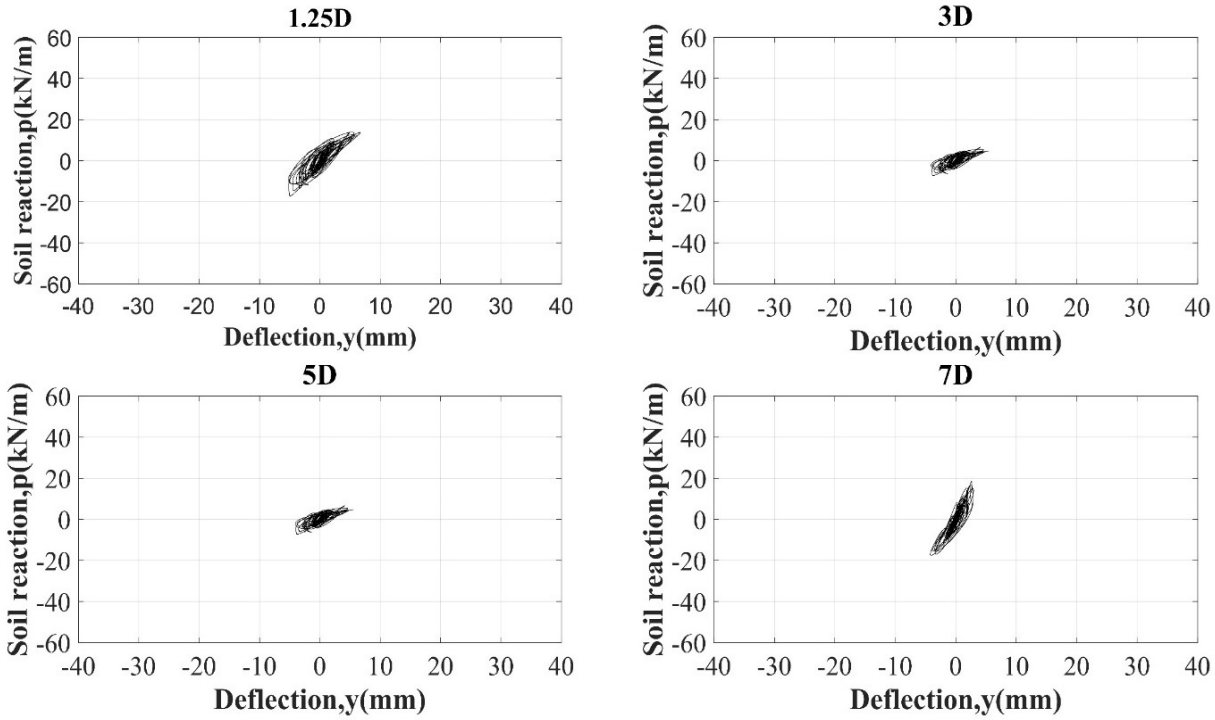

Figure 3.23. Dynamic p-y curves during Northridge 100% for P1 on Day 5 at different depths: 1.25D, 3D, 5D, and 7D. Note: D=diameter of pile

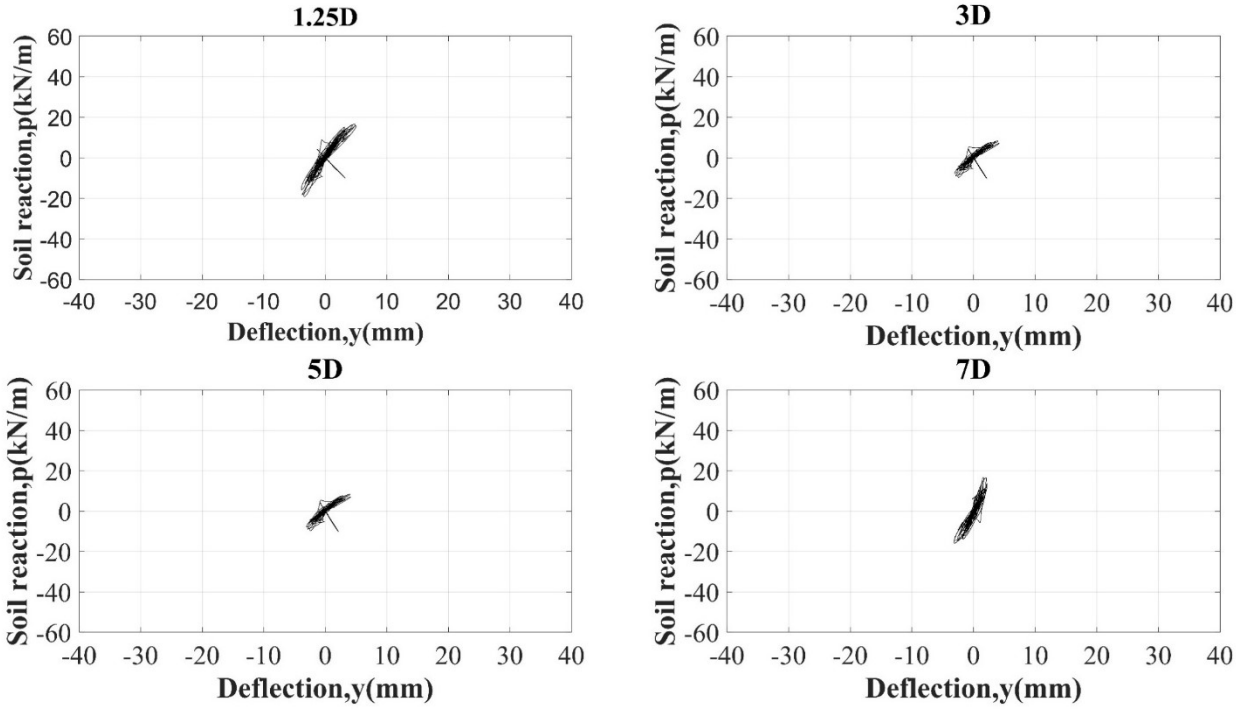

Figure 3.24. Dynamic p-y curves during Takatori 75% for P1 on Day 5 at different depths: 1.25D, 3D, 5D, and 7D. Note: D=diameter of pile

3.3 References

Allred, S. M. (2018). "Seismic performance of grouped helical piles in fixed and pinned connections." Master of Science, University of Oklahoma.

El-sawy, M. (2017). "Seismic performance of steel helical pile." Master of science, Master of science, The University of Western Ontario.

El Sawy, M. K., El Naggar, M. H., Cerato , A. B., and Elgamal, A. W. (2019). "Seismic performance of helical piles in dry sand from large scale shake table tests." *Geotechnique*, 18-P-001.

Perko, H. A. (2009). "Helical piles: a practical guide to design and installation."

Sakr, M. (2009). "Performance of helical piles in oil sand." *Canadian Geotechnical Journal*, 46(9), 1046-1061.

Vargas Castilla, T. M. (2017). "Understanding the seismic response of single helical piles in dry sand using a large-scale shake table test." Master of science, University of Oklahoma.

Chapter 4 : DAMPING CHARACTERISTICS OF FULL-SCALE GROUPED HELICAL PILES

4.1 Abstract

A full-scale pile testing program was implemented using the large outdoor shake table at the University of California-San Diego. Nine steel helical piles with varying geometry were embedded in dense sand and tested individually and in 2x2 groups comparing fixed and pinned pile head connections. The test piles were subjected to shake motions ranging from pulses and white noise to replicated earthquakes. Strain gauges attached to the exterior pile walls and accelerometers placed on the pile caps and within the soil provided data for analyzing the behavior of these piles. Foundation damping (herein soil-pile system) is a substantial parameter in seismic design of the foundation-structure. Therefore, the damping characteristics of the soil bed along with the combined soil-pile system consisting of single and grouped helical piles are discussed based on the experimental pulse, white noise and shake excitations. Several methods, including logarithmic decrement, half power bandwidth and energy (equivalent) methods were implemented to estimate the damping ratio over a range of strains. Based on the experimental data gathered from this study, the suitability and accuracy of different computational methods to determine damping ratio as well as the effect of type and location of instrumentation on the calculated damping ratio were evaluated.

4.2 Introduction

Determination of soil-pile dynamic parameters, such as damping, are required to accurately predict and analyze the dynamic behavior of pile foundations. For strong earthquake motions, damping of the soil-foundation system plays an important role in dissipating energy and may reduce the response of a structure. Two factors that influence the soil-pile damping are the soil's shear strain amplitude, the deflection of piles and pile head displacement, as well as pile slenderness ratio, i.e. pile length divided by pile radius (Hardin and Drnevich, 1972; Novak, 1974). The steel piles provide very little damping themselves. When installed into soil, however, the interaction between the pile and soil promotes energy dissipation, which contributes to significant damping (Cremer and Heckl, 1973). Therefore, piles with larger slenderness ratios may dissipate more energy because of increased interaction with the surrounding soil in addition to experiencing more deflection and strain. This phenomenon was confirmed through observations of damaged piles that were exhumed from three earthquakes in Japan (Miura, 1997). Based on these observations, Miura (1997) concluded that a "[a flexible pile] is better than a pile with higher rigidity [during the range of allowable deformation] when they are subjected to the same ground motion."

The excellent performance of infrastructure supported by slender helical piles during Pacific Rim earthquakes (e.g. 2011 Christchurch earthquake in New Zealand) and the undamaged helical piles exhumed from underneath the infrastructure, confirmed their suitability for resisting seismic loads (Ridgley, 2015; Cerato et al., 2017). However, the damping characteristics of helical piles have not been quantified. In fact, the seismic performance of helical pile groups has never been examined before. This lack of information hinders proper design of helical pile foundations in seismic applications.

The main objective of this part of study is to provide quantitative and qualitative

evaluations of the damping characteristics of single and grouped helical piles installed in a dense dry sand. Full-scale single- and double-helix piles of varying diameters were subjected to dynamic and seismic loadings with varying intensities and frequency content. The piles were tested as single piles and as groups with both fixed and pinned head conditions. The dynamic response was measured using both strain gauges on individual piles and accelerometers placed on the cap of the pile group. The effect of strain on damping, as well as the variation of the damping ratio with soil depth, are investigated. A special emphasis is placed on the effect of pile slenderness ratio and type of pile-structure connections (i.e. pinned or fixed) on damping.

Damping ratios estimated using different methods have been shown in Chapter 2 (Section 2.5) to be affected by soil type and condition (treated or untreated) as well as foundation shape, size and configuration. Each experimental or numerical study, however, has used only one or two methods of calculating damping ratio in analyzing the soil-foundation system. There are no comprehensive studies that compare and evaluate all existing methods together on single or grouped piles subjected to pulse, white noise and earthquake motions. In addition, there is still a significant lack of experimental studies in the literature assessing the dynamic performance of helical piles. Therefore, the current study aims to evaluate the seismic performance of single and grouped helical piles established from full scale shake table tests using multiple damping ratio calculation methods, which could provide quantitative data for better seismic design guidelines.

4.3 Methodology: applied methods for calculating damping ratio (ζ)

After conducting shake table test on the full-scale physical model of helical piles and performed data reduction and initial analysis (Chapter 3), the methods applied to calculate dynamic properties of piles. This will be discussed in detail in the following.

4.3.1 Logarithmic decrement method

The time history responses of accelerometers embedded in soil and those attached to the skids are utilized to calculate ζ through the soil and the pile group, respectively. In the logarithmic decrement method, the damping is obtained from the natural logarithm of the ratio of two peaks' amplitudes, i.e.:

$$\delta = \ln \frac{X_N}{X_{N+1}} \quad \text{or} \quad \delta = \frac{1}{N} \ln \frac{(X_1)}{(X_N)} \tag{4-1}$$

$$\boldsymbol{\zeta = \frac{1}{\sqrt{1+(\frac{2\pi}{\delta})^2}}} \tag{4-2}$$

where N is the number of periods between two peaks; X_N is the amplitude of nth peak, X_1 is the amplitude of first peak and δ is the amplitude of the peaks. Exponential decay curve fitting is also applied as shown in Figure 4.1 to define the amplitudes of peaks accurately. Due to the inconsistency between the peaks during the decay, curve fitting to the peaks in the response curve and using the average δ is suggested to minimize errors and obtain the exact value for X_N (Eq. (4-1)) (Ge et al., 2013). "The ideal maximum number of peaks" from the first peak (the largest magnitude) as Tweten et al. (2014)'s study suggests, are used in this paper to calculate δ. In this regard, δ's was calculated using the first peak with each successive peak (e.g., 1st with second and 1st with third, etc.) and the average of these δ's was determined and designated δ_1. Also, the average of δ applying each two successive peaks to reach the "ideal maximum number of peaks" (e.g., 1st with 2nd, 2nd with 3rd, etc.) were taken as δ_2. Finally, the average of δ_1 and δ_2 was estimated to be the δ applied in Eq. (4-2) to produce acceptable estimates of ζ.

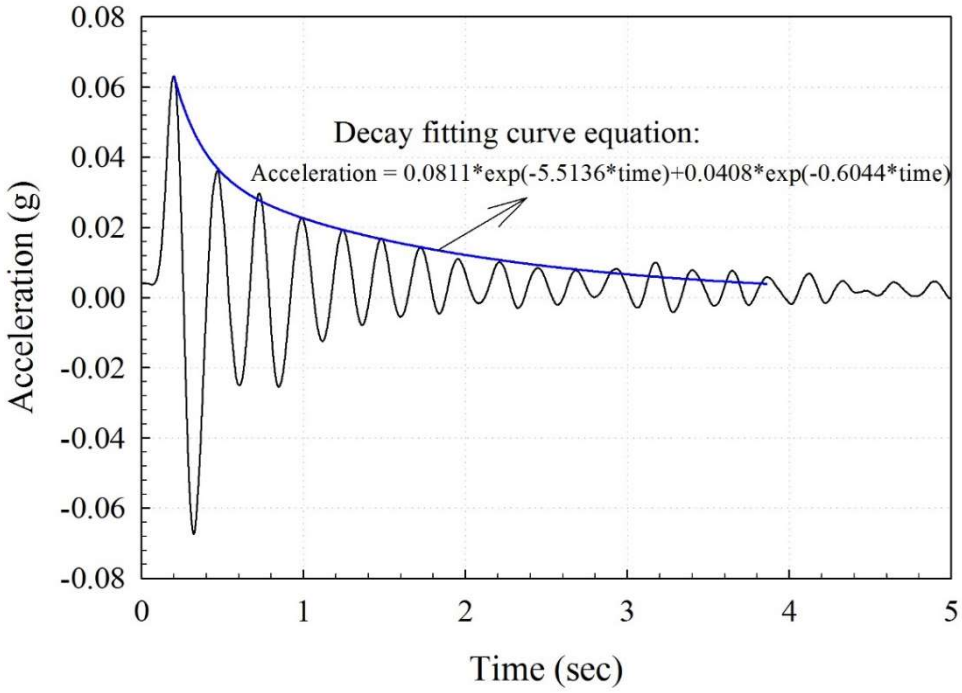

Figure 4.1. Decay curve fitting in logarithmic decrement

4.3.2 Equivalent or energy method

The energy method is carried out in the time domain (i.e. using measured response time history) to calculate ζ. The equivalent ζ can be calculated as the area of a hysteresis loop generated from the force-displacement curve of a soil-pile system normalized by the strain energy represented by the area linear elastic response curve of a soil-pile system as shown in Eq. (4-3) and Figure 4.2.

$$\boldsymbol{\zeta = \frac{E_D}{4\pi E_s}} \qquad 4\text{-}3$$

where E_D is the area of the hysteresis loop, which manifests energy loss and E_S represents the maximum strain energy. The force-displacement response curve (hysteresis) can be developed by means of strain gauge or accelerometer records. Strain readings obtained from the strain gauges attached to the piles can be used to derive soil reaction and pile deflection (hysteretic p-y curve) at every strain gauge level along the pile by obtaining bending moments through specific

mathematical procedures using the following equations (Eq. (4-4), (4-5) and (4-6)):

$$M(z) = \frac{EI(\varepsilon_1 - \varepsilon_2)}{d} \quad 4\text{-}4$$

$$p(z) = \frac{d^2 M(z)}{dz^2} \quad 4\text{-}5$$

$$y(z) = \iint \frac{M(z)}{EI}\, dz \quad 4\text{-}6$$

where $\varepsilon_1, \varepsilon_2$ are the strain gauge readings at each side of the pile, E and I are the elastic modulus and cross-sectional moment of inertia of the pile, and d is the outer pile diameter. These bending moments were fit with the function of depth at each time step using quintic spline interpolation in MATLAB since this spline provided the best fit (El-sawy, 2017; Vargas Castilla, 2017; Allred 2018). Therefore, bending moment with time at each elevation along the pile can provide p and y at that level during loading, which reveals hysteretic behavior.

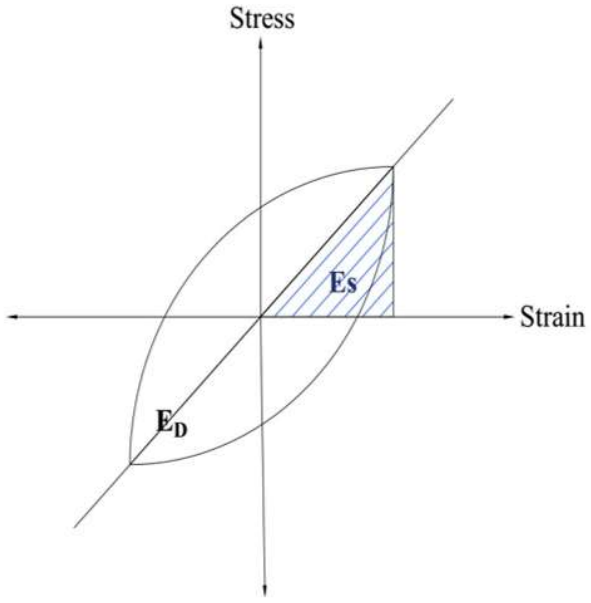

Figure 4.2. Ideal hysteresis loop in energy method (after Chopra (1995))

The p-y curve at the ground surface for each pile is used along with Eq. (4-3) to obtain the ζ of each pile including the interaction of the surrounding soil. For a pile group, the damping ratio is calculated by the summation of the individual pile's ζ (Boominathan and Lakshmi, 2000). For evaluating ζ of a pile group by means of accelerometer measurements, the record of the single accelerometer at the center of mass from each skid is adequate and displacement can be calculated directly by double integration of the acceleration. For both approaches and their respective hysteretic loops, the ideal shape of the maximum loop and its enclosed area are defined by the MATLAB code (polyarea function). To acquire the maximum ζ, the envelope loop, which occurs at maximum deflection or maximum force, was extracted (Figure 4.3).

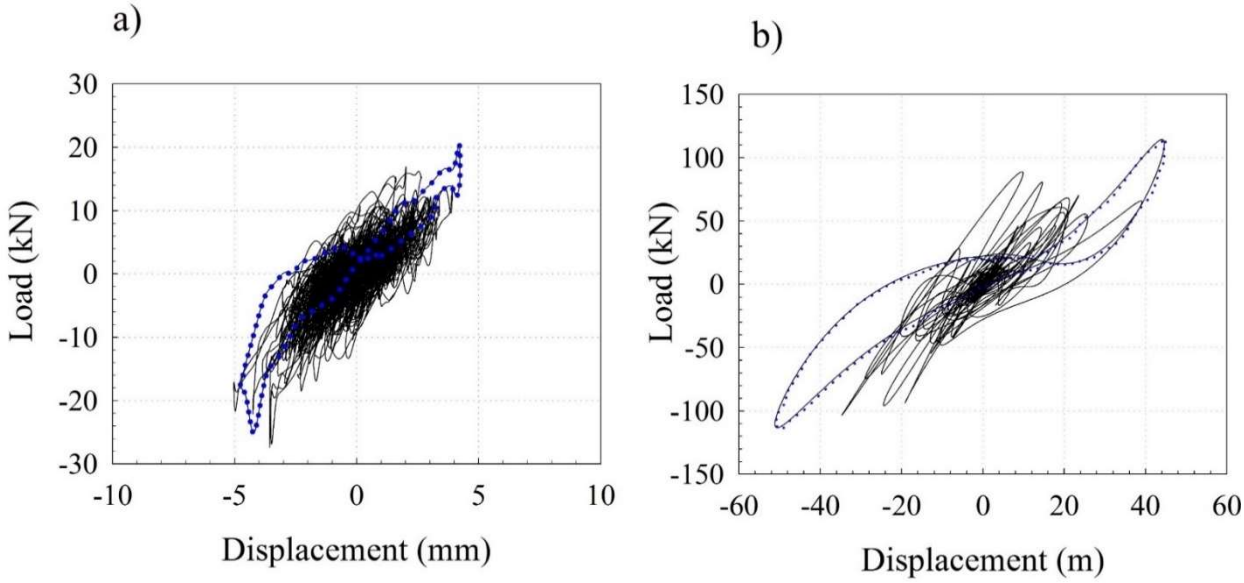

Figure 4.3. Finding the loop of maximum, deflection in load-displacement curve: (a) white noise; (b) Northridge 100%. (Note varying scale)

Alternatively, a complete cycle of sine or cosine wave can be traced in the load-time and displacement time history results under white noise (Figure 4.4). The maximum peaks of these waves in both load-time and displacement-time records can then be used to develop a load-displacement curve as shown in Figure 4.4. This method is accurate but time consuming and the

MATLAB procedure is preferred. Both methods for obtaining the hysteretic loops were used to determine ζ under white noise and individual earthquake record shakes, respectively.

4.3.3 Half power bandwidth method

The data recorded by the accelerometers in the frequency domain are used for this method. In this regard, the frequency response function (FRF) and consequently, frequency response curve, are derived by normalizing the fast Fourier transform (FFT) of the response by the FFT of the input motion. The global properly fitted curve that captures the local peaks in the frequency response curve is used to estimate ζ. The frequencies where the amplitude is $\frac{1}{\sqrt{2}}$ times the resonant amplitude is identified as shown in Figure 4.5, and Eq. (4-7) is used to determine ζ:

$$\boldsymbol{\zeta = \frac{f_b - f_a}{2 f_n}} \qquad 4\text{-}7$$

4.3.4 Modal analysis method

The function "modalfrf" in MATLAB (MathWorks, 2018) is utilized to perform the modal analysis procedure. The FRF is developed utilizing the response signals from accelerometer records as inputs. Subsequently, the FitMethod of lsce as a global fitting method is applied as an input in "modalfit" function to achieve the damping ratio matrix as one of the modal parameters. The maximum value in the given damping matrix is presented as the ζ, which can be compared with the maximum damping ratios from the half power results; they were found to be similar.

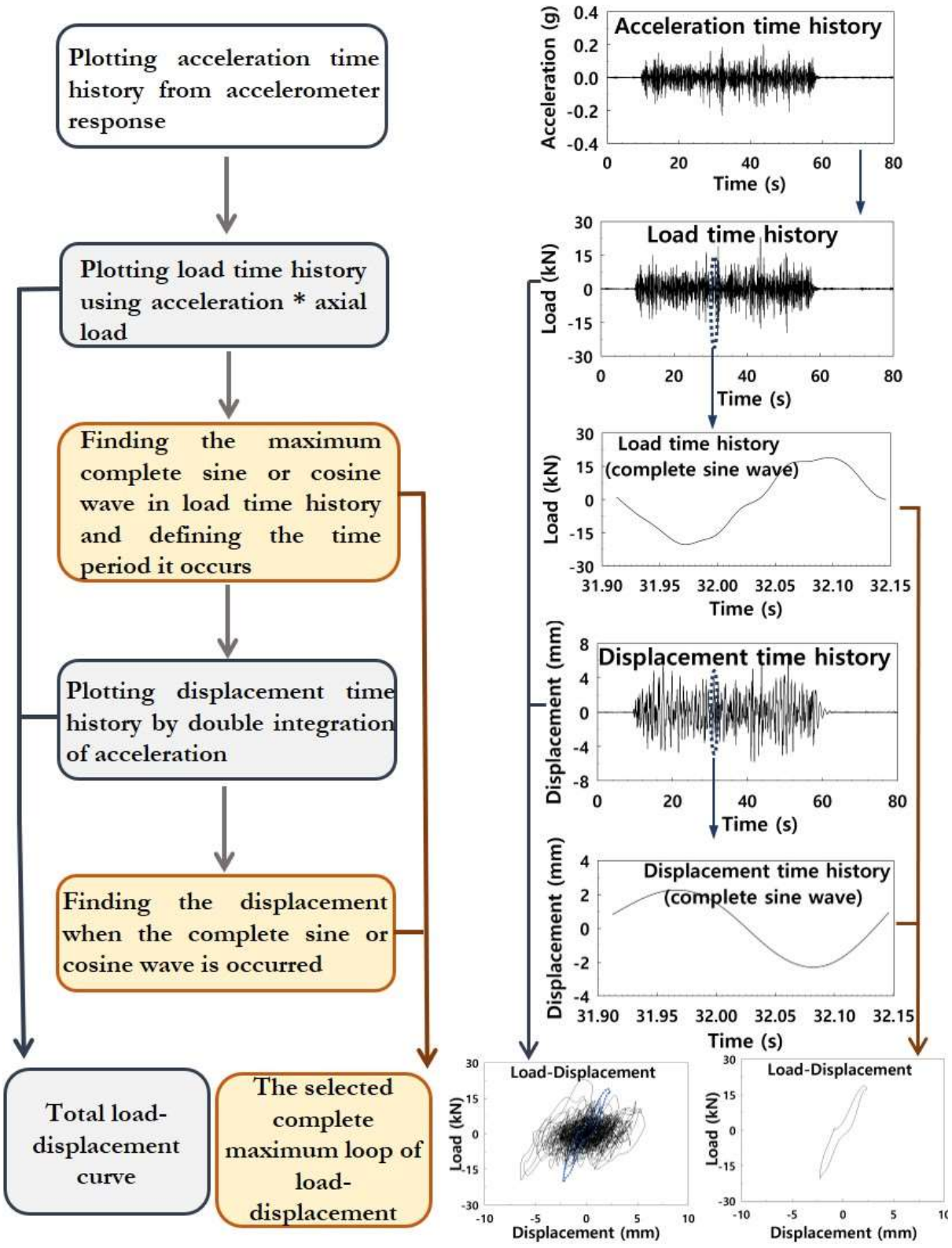

Figure 4.4. Extracting the complete load-displacement loop from acceleration time history

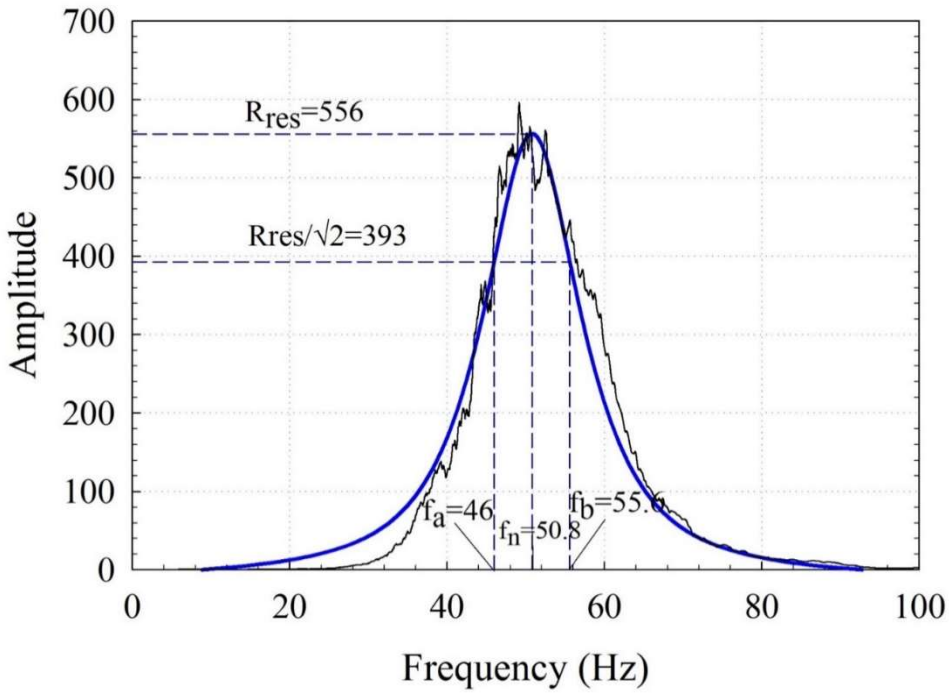

Figure 4.5. Fitting curve and finding values in half power bandwidth method

4.4 Results and discussion

4.4.1 Pile group damping ratios based on strain amplitude

The magnitude of damping ratio depends primarily on shear strain and confining stress (e.g., Kumar et al. 2017). Shear strain were computed based on the method discussed in Brennan et al. (2005). In this study, the confining stress stayed the same throughout the testing sequence, but the shake intensity changed and therefore, the damping ratio was assessed over moderate and intense motions. To evaluate the efficiency of the previously discussed methods under a smaller value of strain, values of ζ for pile groups subjected to either a pulse or white noise are computed and presented in Table 4.1. The different results from log decrement and half bandwidth methods are attributed to the type of loading, which causes a difference in strain (log decrement and half power use the response to pulse and white noise, respectively). These differences may also be attributed

to employing time domain data in the log decrement data method, while using frequency domain data in the half power method (Ostadan et al., 2004). In addition, determination of the exact peak in the half bandwidth method is sometimes difficult, and the curve fitted to the peaks is not unique, which may cause some discrepancies in values. Nonetheless, Novak and Hifnawy (1983) suggested the half bandwidth method as a good approach to determine the damping ratio for systems that have frequency dependent characteristics (Olmos and Roesset, 2010). However, even in highly controlled laboratory conditions and during field tests, scattered results and discrepancies are inevitable.

The energy method may not produce consistent measurements of the damping ratio due to the asymmetrical experimental (realistic) loop. Additionally, the equation gives equivalent and inherently approximate ζ values. In this study, the energy method was applied employing two approaches for finding a complete loop and the calculated ζ values are compared. The loop picking method, in which the complete sine wave is utilized, resulted in higher ζ values compared to the loop determined at maximum deflection. Novak and Hifnawy (1983) reported similar findings and concluded that the energy method tends to overestimate damping. On the other hand, utilizing the point of maximum deflection to define the loop does not yield the maximum ζ, and may provide a reasonable estimate of an equivalent maximum ζ. These values are similar to values derived from the half power bandwidth method. Modal analysis may not be appropriate for determining damping of foundations that exhibit strong soil-structure interaction, such as pile groups, because it requires several well-defined and separated modes as input. Since the modes were not clearly separated in this experimental set, the method can only provide largely approximate values. This might be due to the linear assumptions made in the superposition principle in a modal analysis, while the soil-pile system may exhibit nonlinear behavior.

Table 4.1. Damping values calculated at approximately 3.5 mm deflection under pulse or white noise using different methods (Day 4 γ_{avg} = 0.016% and Day 5 γ_{avg} = 0.05%)

Method	Day4		Day5	
	Group1	Group2	Group1	Group2
Energy [a]	5.5	5.3	6.6	6.2
Energy [b]	9.3	9.4	10.6	10.9
Half power bandwidth	5.6	5.3	6.5	6.3
Log decrement	4.9	3.1	5.1	4.8
Modal analysis	9.5	8.9	12.6	10.3

[a] Using maximum loop where maximum deflection occurs (by accelerometer records)

[b] Using one complete cycle of sine or cos wave (by accelerometer records)

Calculating damping during smaller strains is important for establishing baseline damping ratios. Among the different methods considered herein, the log decrement method resulted in the lowest ζ value and the energy method utilizing the loop at the maximum deflection as well as the half-power bandwidth method provided higher values. From a design perspective, it seems that for loading conditions producing a smaller range of strain, the log decrement method can provide a conservative estimate of the damping ratio for pile groups installed in dense sand, while the half-power bandwidth method and energy equivalent method (based on the loop at maximum deflection) provide average damping ratios based on comparing the values within this data set.

The energy method was used to evaluate the large-strain damping considering the maximum loop at maximum displacement by analyzing both the skid accelerometer response and the individual pile strain gauge response (

Table 4.2). While ζ of the pile group can be obtained directly using the skid accelerometers, using the individual pile strain gauge response requires evaluating each pile's p-y curve and then adding together the damping calculated from each p-y curve to produce the pile group damping.

This method typically results in a larger damping ratio than using the center-of-mass group accelerometer. It is important to acknowledge the potential accumulation in error when utilizing discrete strain gauge measurements on different individual piles to calculate pile group damping. Individual pile strain gauges may not produce the same damping ratio as a single accelerometer at the center of structure mass because each p-y curve is produced indirectly by differentiation and integration operations of the discrete bending moment measurement. Additionally, a p-y curve is developed along the pile and the method requires that a curve fitting method be employed, which requires certain boundary conditions at the pile head and pile tip. Thus, for a reasonable derivation of a pile p-y curve, at least six strain gauge measurements along the length of the pile are required. Hence, a minimum of twenty-four strain gauge readings are required to obtain the ζ of a four-pile group, in contrast with just one accelerometer reading that can give the entire behavior with minimum instrumentation error. Therefore, from the perspective of a large experimental instrumentation project, the results from accelerometer records are easier to collect and less likely to have processing errors. When using the single center-of-mass accelerometer data, the half bandwidth results are relatively close to the energy equivalent method. Consequently, the half bandwidth and energy method applying the maximum loop approach from the load-displacement curve of the pile cap accelerometer are offered as appropriate methods to use in large shake motions. Like the observations for the smaller strain cases, the modal analysis method consistently produced the highest damping ratio. This confirms the method may not be suitable for determining the damping of piled foundations as they do not exhibit well separated modes.

In order to simplify the comparison between damping values of soil-pile-skid under small strain motions and large shake, Table 4.1 and Table 4.2 are graphically summarized in Figure 4.6.

Table 4.2. Large strain damping values using different methods (shear strain calculated close to ground surface and center of skid)

Method	Day4		Day5	
	Group1	Group2	Group1	Group2
Northridge 100%				
Deflection:	*45 mm*	*40 mm*	*50 mm*	*47 mm*
Average soil shear strain:	*0.39%*	*0.14%*	*0.51%*	*0.32%*
Energy [a]	16.2	13.2	17.8	16.6
Energy [b]	11.5	9.2	13.0	11.0
Half power bandwidth [b]	9.8	9.5	10	9.8
Modal analysis [b]	17.8	18.6	20.7	19.3
Takatori 75%				
Deflection:	*51 mm*	*48 mm*	*58 mm*	*53 mm*
Average soil shear strain:	*0.89%*	*0.60%*	*0.95%*	*0.62%*
Energy [a]	19.1	16.7	22.5	19.8
Energy [b]	12.1	10.6	14.2	12.0
Half power bandwidth [b]	10.5	9.8	12.3	11.2
Modal analysis [b]	20.5	23	22.9	21.5

[a] Sum of single pile damping in each group using attached strain gauge responses under corresponding shake.
[b] Response of skid accelerometer under the corresponding shake.

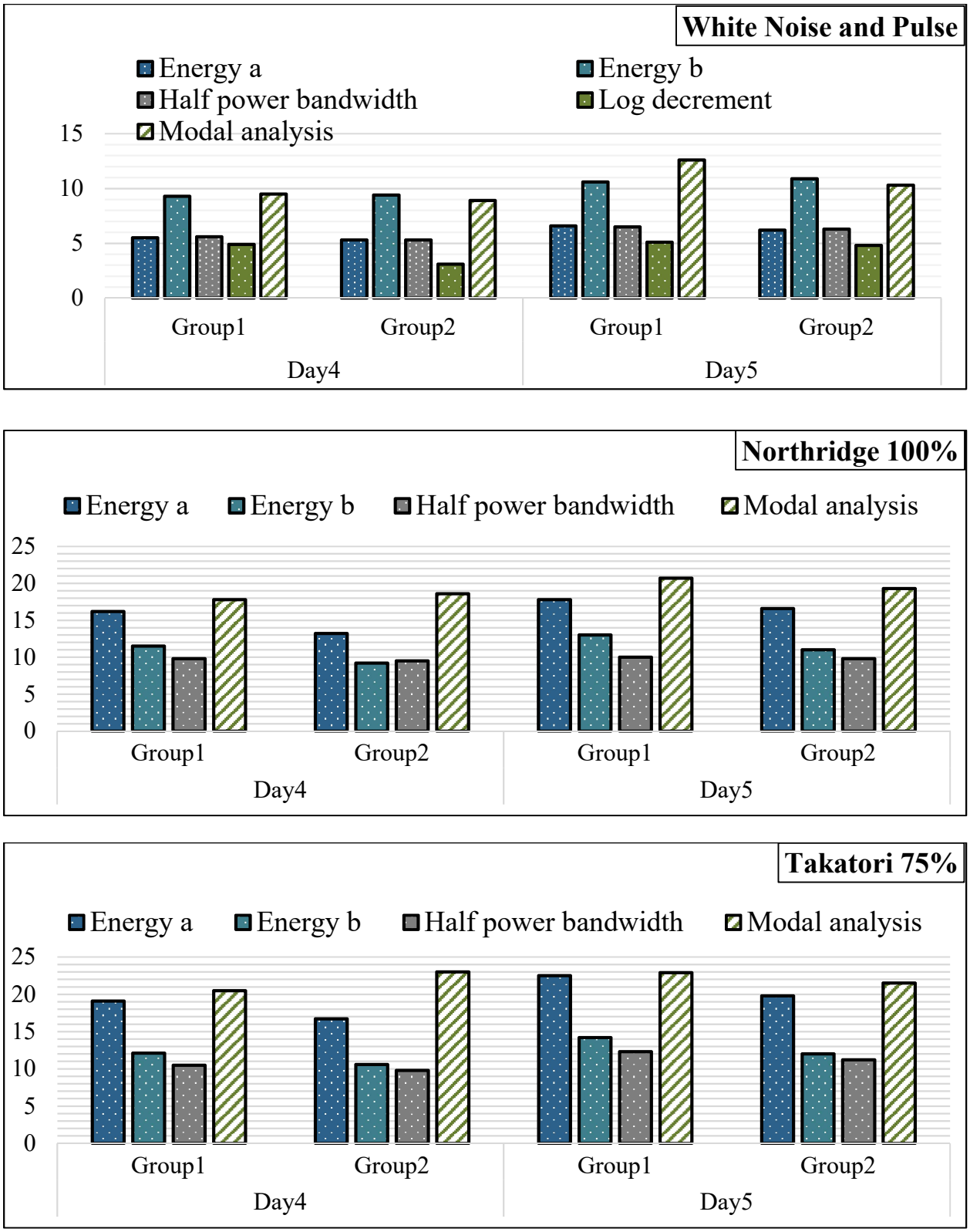

Figure 4.6. Summary of damping values for soil-pile-skid

4.4.2 Effect of pile head connection

The damping ratios obtained for fixed pile heads on Day 4 testing are consistently different from damping ratios obtained for pinned pile heads on Day 5 testing. Comparing the results in Table 4.1 and

Table 4.2, both groups with fixed pile heads exhibited lower ζ than for the same groups with pinned pile heads for both small and intense excitations. This can be attributed to the larger displacement at pile head with pinned connection. This is an important finding because many pile-structure connections in earthquake prone areas are constructed as fixed pile-cap connection. The results obtained herein suggest that allowing some flexibility at the connection, i.e. pinned connection, should increase the damping and hence improves the structural response during the seismic event. More investigations involving structures supported by flexible helical piles with variable cap connections should be performed in order to further verify this observation.

4.4.3 Group effect on damping

To better understand the group effect on energy dissipation and the damping ratio, test records for individual piles from Day 3 testing were used to calculate ζ for individual piles and the results are compared with those obtained for the pile groups. Table 4.3 summarizes the values of ζ for single piles and for individual piles in a group. Although, the maximum pile deflection was larger at the same deflection (5mm) when piles were tested in the single condition compared to when they were connected in a group (Figure 4.7), all individual piles within a group demonstrated higher ζ compared to the same single piles. This may be due to the larger soil pressure bulb present in the middle of the pile group (Kaynia, 1982).

Table 4.3. Damping ratio values of single piles (Day 3) and individual piles in a group (Days 4 and 5) under Northridge 100% at 5-mm deflection (P1-4 γ_{avg} = 0.3% and P7-10 γ_{avg} = 0.14% as calculated from Day 3)

Pile No.	Slenderness ratio	Damping ratio[a]		
		Day 3: Single pile	Day 4: Individual pile fixed head	Day 5: Individual pile pinned head
Pile 1	90	9.5	11.8	12.5
Pile 2	83	8.2	11.2	10.1
Pile 3	83	8.5	12.1	10.9
Pile 4	83	7.2	8.9	9.1
Pile 7	61	6.7	9.0	9.6
Pile 8	61	7.3	9.2	8.5
Pile 9	61	6.1	8.5	9.7
Pile 10	61	7.5	9.7	10.3

[a] ξ calculated using the energy method using individual pile p-y curves

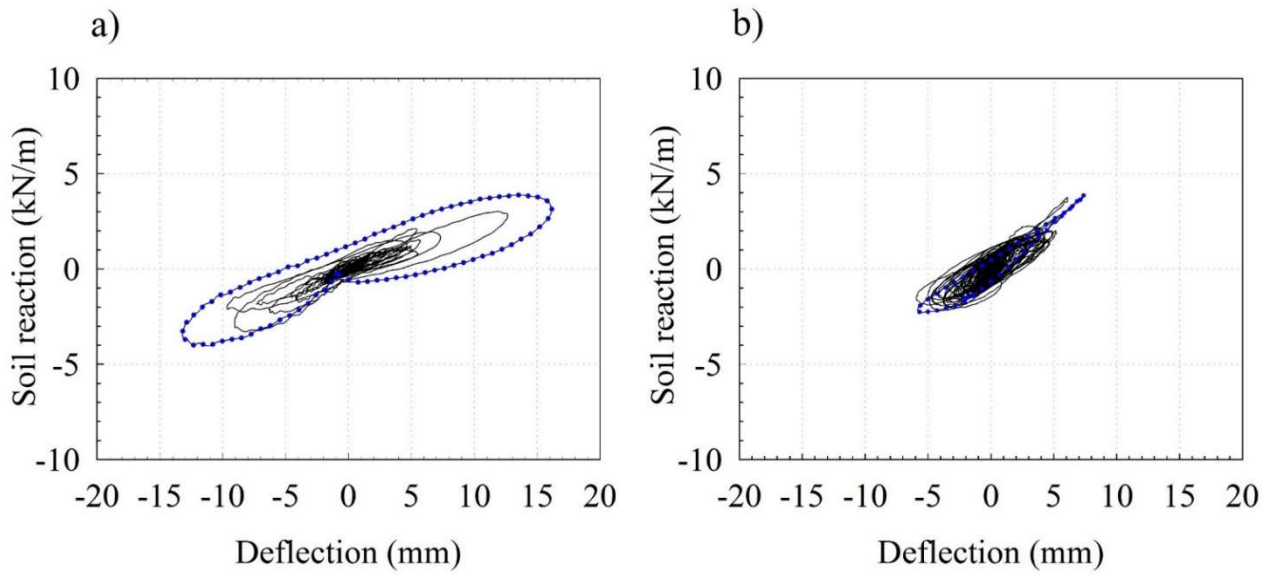

Figure 4.7. Behavior of pile 1 under Nor. 100 % as (a) single pile (Day 3); and (b) in group (Day 4)

There are several factors that influence the stiffness and damping of a pile group such as the number of piles, spacing between piles, loading frequency, pile cap connection and cap width

(Kaynia, 1982). In the current study, just the pile connection influence was evaluated. The overall ζ of piles within a group was determined at the same deflection (herein 5 mm) from the hysteretic load-displacement loop generated during the Northridge 100% shake (Table 4.3). The test sequence in this study only measured horizontal motion, but it is important to keep in mind that in a true seismic event, damping is associated with horizontal, vertical, rocking and torsional motion (Kaynia, 1982). According to the results of single pile damping ratios presented in Table 4.3, one can conclude that the rigid connection may either increase or decrease total damping of an individual pile compared to the same pile in a pinned condition.

4.4.4 Effect of pile geometry

Not only is the damping ratio affected by the strain magnitude, the pile-structure connection and whether the pile is acting individually or in a group, but it is affected by the pile geometry. On both Day 4 and Day 5, group 1 demonstrated a greater ζ than group 2. The explanation for this phenomenon may lie in the slenderness ratio of the piles. The slenderness ratio (l/r) is 90 for pile 1 (the longest pile in group 1) and 83 for the other three piles in group 1. For group 2, in which all piles have the same geometry (length and diameter), this ratio is 61. Since this slenderness ratio is higher for group 1, the behavior is more flexible with more deflection and more energy dissipation, while Group 2 has stiffer behavior with lower ζ. Furthermore, based on slenderness ratio (Table 4.3), the single piles (Day 3) and individual piles in the groups (Days 4 and 5) follow the same damping ratio trends when using the energy method. Accordingly, pile 1 with the largest slenderness ratio has the largest ζ. Comparison of piles with identical geometry and similar conditions (e.g., inertial masses) result in similar ζ's that validate the tests and methods used and indicates repeatability; for example, pile 2 (ζ =9.1; m = 750 kg) with pile 3 (ζ =10.4; m = 780 kg) and pile 8 (ζ =6.4; m = 785 kg) with pile 9 (ζ =5.8; m = 700 kg). The differences in ζ are most

likely due to the different inertial masses placed on top of the piles which would create a varying degree of soil-structure interaction, affecting the damping ratio. In addition, pile 4 (ζ =6.3; m = 750 kg), with two helices, is more rigid than piles with the same single-helix geometry (pile 2 and 3) as can be seen by the lower damping ratio but same inertial mass. Thus, adding one more helix to the single helical pile caused at least 12% reduction in damping ratio in our case study.

4.4.5 Damping ratios based on strain in soil

Damping ratios of soil were calculated at the locations where soil-bed accelerometers were placed. These maximum damping ratios were calculated using different methods and the average values are tabulated in Table 4.4. The results show that log decrement (for pulse) and energy method (for shakes - using the loop from the location of maximum deflection) are appropriate for soil with or without piles. The half bandwidth method, which seemingly underestimates ζ in this case, is not a desirable method for calculating the damping ratio of soil due to the nonlinearity, which causes skewed-shaped frequency response curves (Ashmawy et al., 1995), and is therefore not presented. This method does seem to work rather well, however, when calculating the damping ratios of piles and pile groups (Novak and Hifnawy, 1983; Olmos and Roesset, 2010). Typically, ζ increases regardless of structure type when motions become increasingly vigorous, which is attributed to the increase in deflections. Kumar et al. 2017 did, however, present cyclic triaxial laboratory data on saturated sand that showed a bell-curved damping ratio trend with increasing shear strain; damping ratio decreased after the shear strain reached 0.75%. Nonetheless, in this study, greater ζ's were calculated from a shake with large intensity (Nor. 100%) compared to a white noise excitation, (Table 4.4). As can be seen from the increase in damping ratio from the soil bed alone to the soil box with piles installed, piles not only can improve ultimate bearing capacity but also can help energy dissipation in soil about 17% in our case study.

Table 4.4. Comparison of average damping ratio through 3.6 m depth of soil using different methods

Method	White noise or pulse			Large shake [a] (Nor. 100)	
Average shear strain through depth (%):	Day 1 0.07	Day 2 0.13	Day3 0.17	Day 2 0.64	Day 3 0.73
Energy	6.9	8.1	8.1	11.9	12.6
Log decrement	5.9	7.4	7.5	-	-
Half power bandwidth	4.1	4.8	4.4	9.5	8.3

[a] On Day 1, large shakes are not applied.

The relationship of damping ratio versus shear strains from this study of a dense sand bed within the large laminar box subjected to pulses and white noise was compared with previous laboratory studies on sand and non-plastic soils (e.g. resonant column test and cyclic triaxial test) (Seed and Idriss, 1970; Kokusho, 1980; Rollins et al., 1998; Darendeli, 2001; Senetakis et al., 2013) in Figure 4.8. Sand in this study was compacted to 100% relative density, and Day 1 shakes encompassed only the sand bed. While the laboratory tests presented damping ratios over the shear strain range of 0.0001%-1%, this field-scale study shook the Day 1 sand bed to produce only shear strains between 0.02-0.13%; smaller input motions to fall within the definition of small strain (Seed, 1970; Seed et al., 1986) were not available and larger shakes were not performed until the piles were installed. Over this small range of tested shear strains on Day 1 (0.02-0.13%), the previous laboratory studies show sand bed damping ratios varied between 1 and 18% while this field-scale study using the laminar box shows the damping ratio stays between 4.5-9.5%. The damping ratios of the Day 1 sand bed fall well within the range of measured values from laboratory tests, although do not show a singular trend with increasing shear strain. This could be because the large laminar box sand bed with many more areas of disturbance (e.g., accelerometers,

accelerometer wires, etc.) was more variable than a small, experimental laboratory device. The difference may also be explained by the difference in soil bed characteristics, including density, gradation and confining pressures (Seed et al., 1986; Zhang and Aggour, 1996; Cheng and Leong, 2018;). The effect of confining pressures alone can be seen in the resonant column tests presented in Figure 4.8; the higher the confining pressure on sand, the lower the damping ratios are (Darendeli, 2001; Senetakis et al., 2013). More work should be done to understand a damping ratio response during shear strain increases to optimize foundation design. Ideally, it would be beneficial to have a high damping ratio over a larger range of strains, but there may be an optimal strain range for a foundation system to enter before the damping ratio either decreases (e.g., Kumar et al. 2017) or increases to a constant level.

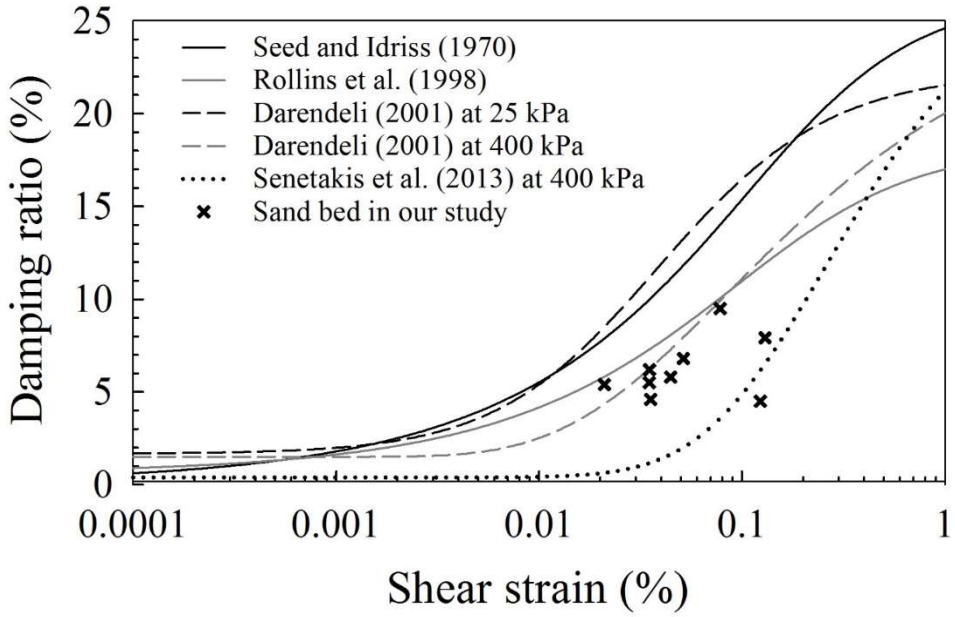

Figure 4.8. Comparing damping ratio values of Day 1 sand-bed response in this study with laboratory test results on sand from other researchers over a large range of shear strain

4.4.6 Relationship of damping ratio of soil and its strain with depth

Using the log decrement method for smaller strains and the energy equivalent method with the loop calculated at the maximum deflection point, the relationship of maximum shear strain amplitude (γ) and damping ratio (ζ) with sand bed depth is illustrated in Figure 4.9 and Figure 4.10 during pulses and large strain shakes (Nor. 100%), respectively. In general, shear strain initially increases with depth and then decreases. Since soil is heterogeneous, anisotropic and behaves nonlinearly in nature, wave propagation, and consequently shear strain, are complex and not consistent throughout the subsurface. ζ varies with shear strain and the maximum occurs at maximum shear strain. Day 1 shaking of just dense sand demonstrates significantly lower γ and ζ compared to Day 2 and 3 with piles installed in the soil for both small and large shakes. The damping ratio and shear strain increased with just the piles installed (Day 2), and then increased again when the inertial weights were added (Day 3) for both small and large shakes. This phenomenon may be explained by the piles further transmitting energy through the soil providing more damping.

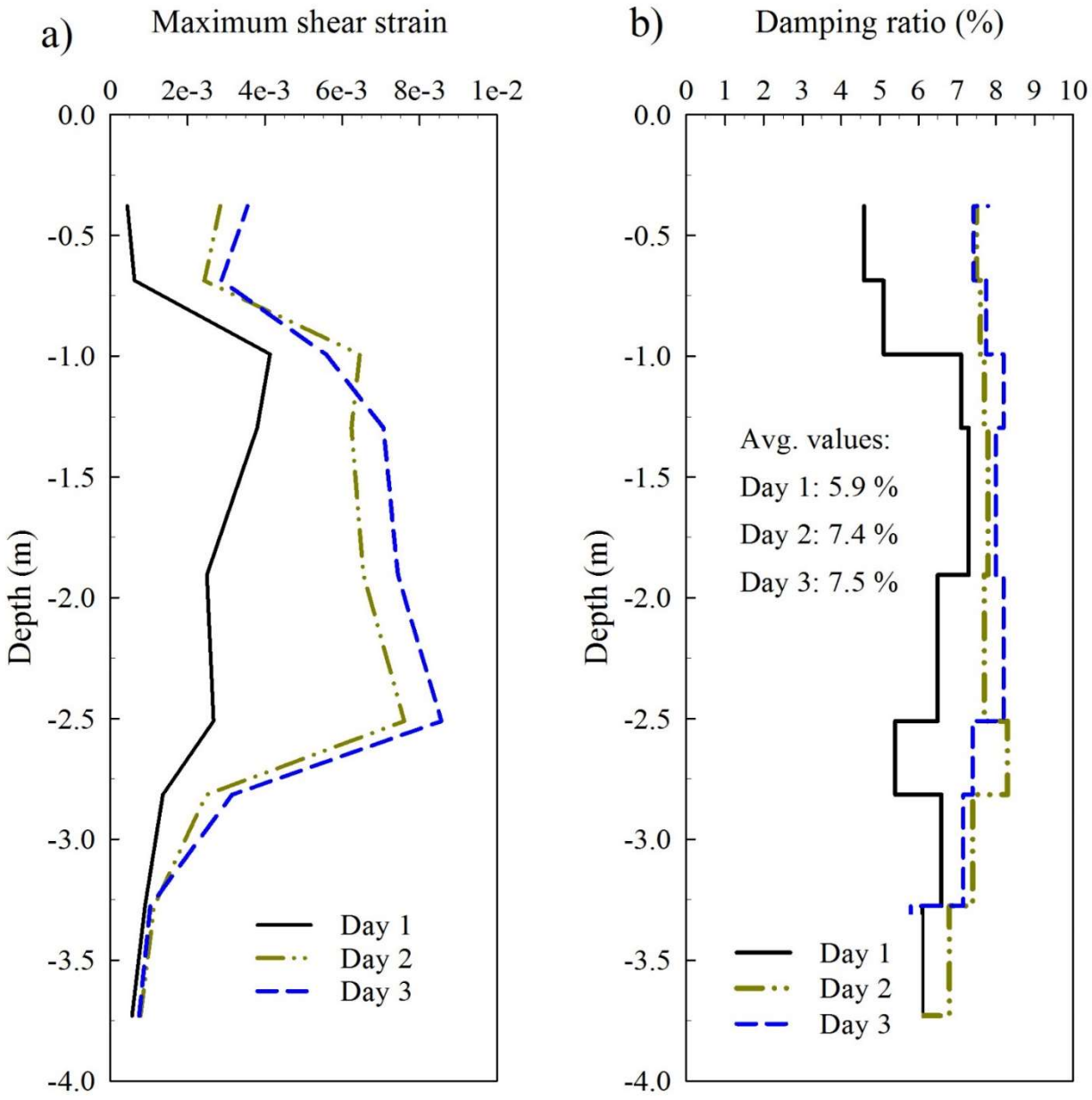

Figure 4.9. (a) shear strain and (b) damping ratio values along the pile in the soil experiencing small strain (Pulse) (log decrement)

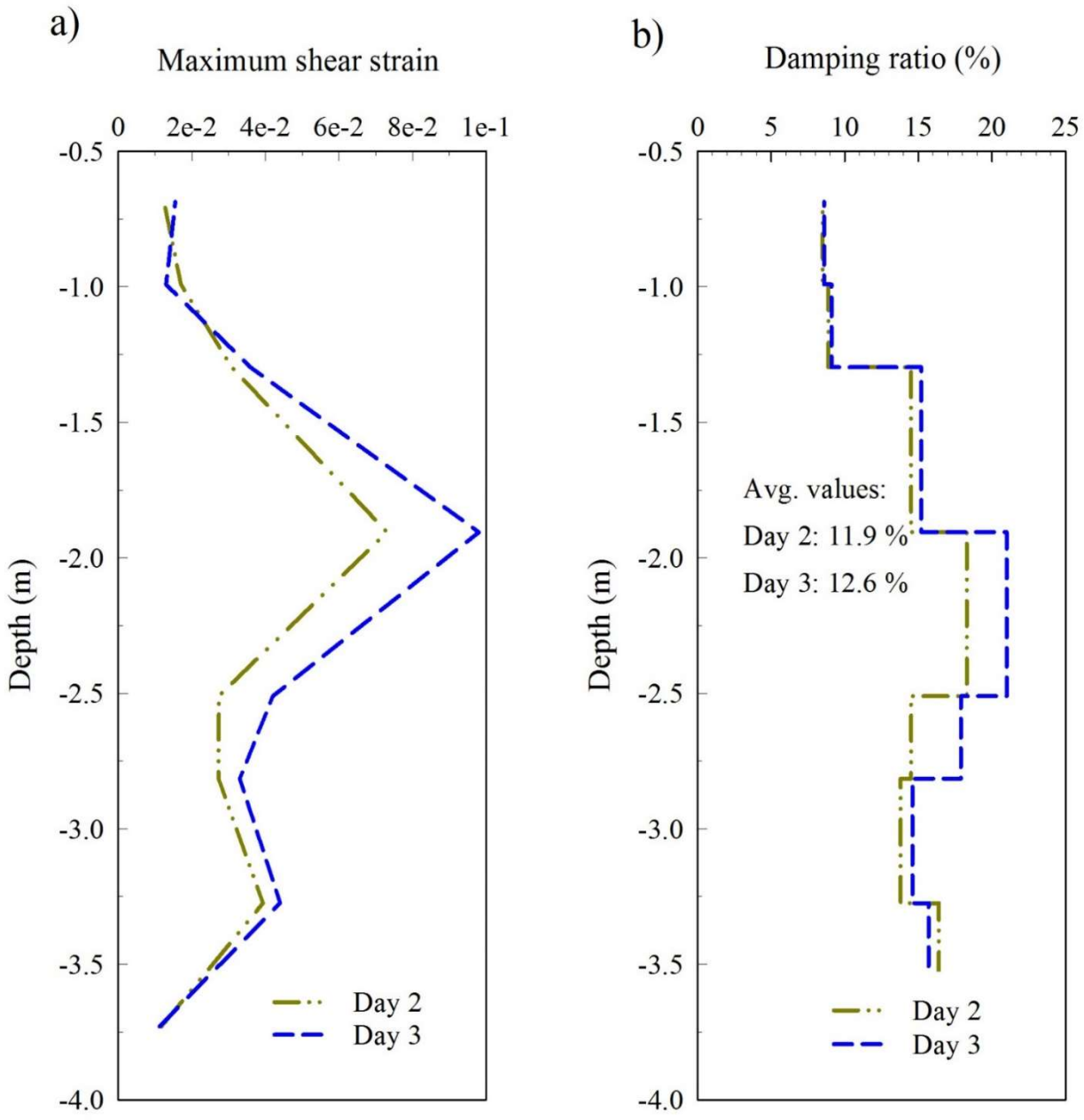

Figure 4.10. (a) shear strain and (b) damping ratio values along the pile in the soil experiencing large strain (Northridge 100%) (energy method)

4.5 Conclusions

The experimental data from a full-scale field study on the seismic behavior of helical piles in dense sands were analyzed to determine damping ratios of individual and grouped helical piles. Various

methods of calculating the damping ratio of piles and soil with inherent effect of soil-structure interaction were used and discussed. These damping ratios were the quantity used to better understand the seismic behavior of helical pile groups and study the effect of several parameters on behavior, including strain magnitude, instrumentation type and location, pile-structure connection, pile slenderness ratio and soil depth. Based on the results reported, the following conclusions can be drawn:

- Each damping calculation method has its own limitations, assumptions and approximations. Using data from this study, however, suggest that these methods are all valid to be used in assessing the seismic behavior of a soil-pile system, based on specific conditions. The log decrement method appeared to be appropriate for smaller strain applications during the pulse input motions. The half power bandwidth method seems to work well for a wider range of strain responses for a soil-pile system, but not for a soil system alone, due to the development of increasing nonlinear behavior. The energy method, in which the corresponding maximum deflection loop is considered in calculations, provides a good estimation of "equivalent" maximum damping for both small and large vibrations on piles and through soil when it is compared to values from other methods. Finally, modal analysis does not seem to show reasonable results on the tested soil-pile system during either white noise or earthquake input motions. There is not one method that is appropriate for all conditions, and therefore, a careful consideration of how to match each method with experimental data set is warranted.
- ζ increases regardless of structure type when motions become increasingly vigorous, which is attributed to the incremental increase in deflection. Thus, greater deflection contributes to greater ζ. This deflection depends on the intensity and frequency content of load and natural frequency of system.

- When comparing the results of damping ratios calculated from individual pile strain gauges and single accelerometers at the center of a structure mass, it was found that the individual pile strain gauges produced a much larger damping ratio than using the center-of-mass group accelerometer. When deciding on instrumentation needs on a large-scale foundation project, it may be appropriate to consider that a single accelerometer may provide results with less errors than using a mathematical fitting method through multiple pile strain gauges.
- The type of connection between the pile and structure significantly affect the performance of the structure, quantified by damping ratio. Both pile groups on Day 4 (Fixed connection) exhibit stiffer behavior (lower ζ) compared to the same pile group on Day 5 (pinned connection) in all applied methods regardless of the amount of deformation.
- All piles in this study, regardless of their geometries, demonstrate more flexible behavior (higher ζ) when they act individually. However, pile groups were observed to show higher energy dissipation overall compared with single piles.
- On both Day 4 (fixed connection) and Day 5 (pinned connection), the pile group (Group 1) containing piles with higher slenderness ratios (83-91) demonstrated a greater ζ than group 2 (piles with slenderness ratios of 61). The higher the slenderness ratio, the higher the flexibility, which allows the pile more deflection and energy dissipation. This trend was true as well for individual piles. Adding a second helix, while not changing the slenderness ratio, increases the stiffness and as a result, the damping ratio decreased.
- In general, shear strain initially increases with soil depth and then decreases. ζ varies with shear strain and the maximum occurs at the maximum shear strain. Shaking the laminar box containing just dense sand demonstrates significantly lower γ and ζ compared to Days 2-5, when there were piles in the soil.

Understanding the parameters that effect the damping characteristics of soil-pile systems and quantifying the possible range of damping that can occur under real earthquakes will allow engineers to choose appropriate pile geometry, group configuration and connection type to achieve a desired level of performance.

4.6 References

Allred, S.M., 2018. Seismic performance of grouped helical piles in fixed and pinned connections, Master of Science, University of Oklahoma.

Ashmawy, A., Salgado, R., Guha, S., Drnevich, V., 1995. Soil damping and its use in dynamic analyses.

Boominathan, A., Lakshmi, T., 2000. Dynamic characteristics of pile group under vertical vibration, The 12th World Conference on Earthquake Engineering, pp. 1-8.

Brennan, A., Thusyanthan, N., Madabhushi, S., 2005. Evaluation of shear modulus and damping in dynamic centrifuge tests. Journal of Geotechnical and Geoenvironmental Engineering, 131(12): 1488-1497.

Cerato, A., Vargas, T., Allred, S., 2017. A critical review: State of knowledge in seismic behaviour of helical piles. DFI Journal-The Journal of the Deep Foundations Institute, 11(1): 39-87.

Cheng, Z., Leong, E., 2018. Determination of damping ratios for soils using bender element tests. Soil Dynamics and Earthquake Engineering, 111: 8-13.

Chopra, A.K., 1995. Dynamics of structures, a primer, 2. Earthquake Engineering Research.

Cremer, L., Heckl, M., 1973. Structure-borne sound: structural vibrations and sound radiation at audio frequencies. Springer Science & Business Media.

Darendeli, M.B., 2001. Development of a new family of normalized modulus reduction and material damping curves.

El-sawy, M., 2017. Seismic performance of steel helical pile, Master of science, The University of Western Ontario.

ElSawy, M.K., El Naggar, M.H., Cerato, A.B., and Elgamal, A.W. 2019a. Seismic Performance of Helical Piles in Dry Sand from Large Scale Shake Table Tests. *Geotechnique.* https://doi.org/10.1680/jgeot.18.P.001.

ElSawy, M.K., El Naggar, M.H., Cerato, A.B., and Elgamal, A.W. 2019b. Data Reduction and Dynamic p-y curves of Helical Piles from Large Scale Shaketable Tests. *ASCE Journal of Geotechnical and GeoEnvironmental Engineering.*

Fleming, B.J., Sritharan, S., Miller, G.A., Muraleetharan, K.K., 2016. Full-scale seismic testing of piles in improved and unimproved soft clay. Earthquake Spectra, 32(1): 239-265.

Ge, C., Sutherland, S., 2013. Application of Experimental Modal Analysis to Determine Damping Properties for Stacked Corrugated Boxes. Mathematical Problems in Engineering, 2013: 8.

Halling, M.W., Womack, K.C., Muhamad, I., Rollins, K.M., 2000. Vibrational testing of a full-scale pile group in soft clay, Proc. 12th World Conference on Earthquake Engineering, Auckland. Paper.

Hardin, B.O., Drnevich, V.P., 1972. Shear modulus and damping in soils: measurement and parameter effects. Journal of Soil Mechanics & Foundations Div, 98(sm6).

Hemmati, A., Khorasanchi, M., Barltrop, N., 2017. Analysis of Offshore Wind Turbine Foundations With Soil Damping Models, ASME 2017 36th International Conference on Ocean, Offshore and Arctic Engineering. American Society of Mechanical Engineers, pp. V07BT06A037-V07BT06A037.

Kaynia, A.M., 1982. Dynamic stiffness and seismic response of pile groups, Massachusetts Institute of technology.

Kerschen, G., Golinval, J.C., 2005. Experimental modal analysis. Lecture Notes. (http://www.ltas-vis.ulg.ac.be/cmsms/uploads/File/Mvibr_notes.pdf) (Sep. 10, 2018).

Kokusho, T., 1980. Cyclic triaxial test of dynamic soil properties for wide strain range. Soils and foundations, 20(2): 45-60.

Kumar, S.S., Krishna, A.M., Dey, A., 2017. Evaluation of dynamic properties of sandy soil at high cyclic strains. Soil Dynamics and Earthquake Engineering, 99: 157-167.

Lin, M.-L., Ni, S.-H., Wright, S.G., Stokoe, K.H., 1988. Characterization of material damping in soil, Proceddings of Ninth World Conference on Earthquake Engineering, Tokyo-Kyoto, Japan.

Lin, S.-S., Hong, J., Lee, W.F., Chang, Y., 2004. Capacity evaluation of statnamic tested long piles. Soil dynamics and earthquake engineering, 24(11): 829-838.

Lundgreen, C.C., 2010. Damping ratio for laterally loaded pile groups in fine grained soils and improved soils, Master of Science, Brigham Young University.

MATLAB and Statistics Toolbox Release 2018, The MathWorks, Inc., Natick, Massachusetts, United States.

Miura, F., 1997. Lessons from the damage caused by past earthquakes, International Workshop on Micropiles, Seattle.

Novak, M., 1974. Dynamic stiffness and damping of piles. Canadian Geotechnical Journal, 11(4): 574-598.

Novak, M., Hifnawy, L.E., 1983. Effect of soil-structure interaction on damping of structures. Earthquake engineering & structural dynamics, 11(5): 595-621.

Olmos, B.A., Roesset, J.M., 2010. Evaluation of the half-power bandwidth method to estimate damping in systems without real modes. Earthquake Engineering & Structural Dynamics, 39(14): 1671-1686.

Ostadan, F., Deng, N., Roesset, J.M., 2004. Estimating total system damping for soil-structure interaction systems, Third UJNR Workshop on Soil-Structure Interaction, Menlo Park, California.

Pavelka, P., Huňady, R., Kučinský, M., 2017. Modal Analysis Using the Signal Processing Toolbox of Matlab 2017. American Journal of Mechanical Engineering, 5(6): 312-315.

Ridgley, N., 2015. Practice Note 28: Screw Piles: Guidelines for Design, Construction & Installation, The Institution of Professoinal Engineers New Zealand Inc.

Rollins, K.M., Evans, M.D., Diehl, N.B., III, W.D.D., 1998. Shear modulus and damping relationships for gravels. Journal of Geotechnical and Geoenvironmental Engineering, 124(5): 396-405.

Saitoh, M., 2007. Simple model of frequency-dependent impedance functions in soil-structure interaction using frequency-independent elements. Journal of Engineering Mechanics, 133(10): 1101-1114.

Seed, H.B., Idriss, I.M., 1970. Soil moduli and damping factors for dynamic analysis, Rep. No. EERC 70-10, University of California, Berkeley, CA.

Seed, H.B., Wong, R.T., Idriss, I., Tokimatsu, K., 1986. Moduli and damping factors for dynamic analyses of cohesionless soils. Journal of geotechnical engineering, 112(11): 1016-1032.

Senetakis, K., Coop, M.R., Todisco, M.C., 2013. The inter-particle coefficient of friction at the contacts of Leighton Buzzard sand quartz minerals. Soils and Foundations, 53(5): 746-755.

Siemens Industry Software, ‚Estimation of modal parameters. Rev 16 A.

Tsai, P.-h., Feng, Z.-y., Lin, S.-y., 2011. A wavelet based method for estimating the damping ratio in statnamic pile load tests. Computers and Geotechnics, 38(2): 205-216.

Tweten, D.J., Ballard, Z., Mann, B.P., 2014. Minimizing error in the logarithmic decrement method through uncertainty propagation. Journal of Sound and Vibration, 333(13): 2804-2811.

Vargas Castilla, T.M., 2017. Understanding the seismic response of single helical piles in dry sand using a large-scale shake table test, Master of science, University of Oklahoma.

Zhang, X., Aggour, M., 1996. Damping determination of sands under different loadings, Eleventh World Conference of Earthquake Engineering.

Chapter 5 : DYNAMIC CHARACTERIZATION OF MODELED GROUPED HELICAL PILES WITH SOIL-STRUCTURE INTERACTION

5.1 Abstract

A full-scale shake table testing program was performed with two helical pile groups supporting model structures to better understand the dynamic properties of a soil-pile-group-structure system. Each group had four piles embedded in dry, dense sand confined in a 6.7m L x 3.0m W x 4.6m H laminar box. One group was comprised of 8.8 cm diameter and 3.66 m long helical piles, while the second group had 14 cm diameter and 4.27 m long helical piles. To investigate the influence of the pile head fixity condition on group behavior, both pinned head and fixed head connections were implemented and tested. White noise excitation and two replicated strong earthquake motions were used to determine the natural frequency and observe the seismic behavior of the soil-pile-group-structure system, respectively. The experimental observations were analyzed to evaluate structural natural frequency and pile group stiffness and damping. . The experimental results were used to calibrate a numerical model, which was then used to conduct a parametric study to gain a broader understanding of the seismic behavior of helical pile groups under varying conditions. The experimental and numerical results were compared and the effects of varying different properties in a soil-pile-structure system, including their system seismic response, are discussed.

5.2 Introduction

The literature review in Chapter 2 (sections: 2-2, 2-3, 2-4) clearly indicates that it is important to have realistic full-scale testing with actual seismic loading in order to better understand the seismic

response of piles and to provide the basis of a robust analytical or numerical model. Only Shahbazi et al. (2019) has published results on the seismic behavior of grouped helical piles. Helical piles have exhibited favorable performance during recent relatively large earthquakes (Ridgley 2015; Cerato et al. 2017). However, the utilization of these seismically resilient foundations is hindered by the absence of comprehensive quantitative studies on their dynamic behavior.

Realistic experimental results and suitable analysis methods are important for understanding seismic helical pile group behavior and for developing proper modeling and design procedures accessible to practicing engineers. Therefore, the work presented herein attempts to fill the knowledge gap that exists regarding group helical pile behavior and discusses appropriate tools for interpreting the results. It aims to evaluate the seismic performance of grouped helical piles from full scale shake table tests including the contribution of the inertial effect of a model structure on the pile foundation. In this regard, shake table tests were conducted on full-scale grouped helical piles supporting a model superstructure which subjected to earthquake motions. A dynamic model was then established using the commercially available ENSOFT Dynapile software and calibrated with the experimental results to conduct a parametric study and to calculate the spring stiffness of a single degree freedom lumped mass simulating the structure in order to gain a broader understanding of the seismic behavior of helical pile groups under varying conditions. This part of research was performed after obtaining results out of Chapter 3 and 4.

5.3 Experimental dynamic lateral stiffness of model structure supported by helical pile group

The lateral stiffness of the model structure was determined from the experiment. The record of the single accelerometer at the center of mass of each skid from individual shakings was used to

develop load-displacement curve for each specific condition. The displacement was calculated directly by double integration of the time history acceleration and load was obviously the weight of the skid times recorded acceleration. All this calculation was conducted in MATLAB (Shahbazi et al. 2019). The stiffness was then derived from the experimental load-displacement curves of the model structure supported by the soil-pile system that shows soil-pile resistance to the global system movement (Figure 5.1). The lateral stiffness was calculated as the slope of the maximum hysteretic loop from the dynamic load-displacement curves, i.e.

$$k_x = \frac{\Delta\, Load}{\Delta\, Displacement} = \frac{Load(\max) - Load(\min)}{Displacement(\max) - Displacement(\min)} \qquad 5\text{-}1$$

Table 5.1 presents the lateral stiffness values as well as maximum displacement according to the maximum loop hysteresis obtained from the experiments.

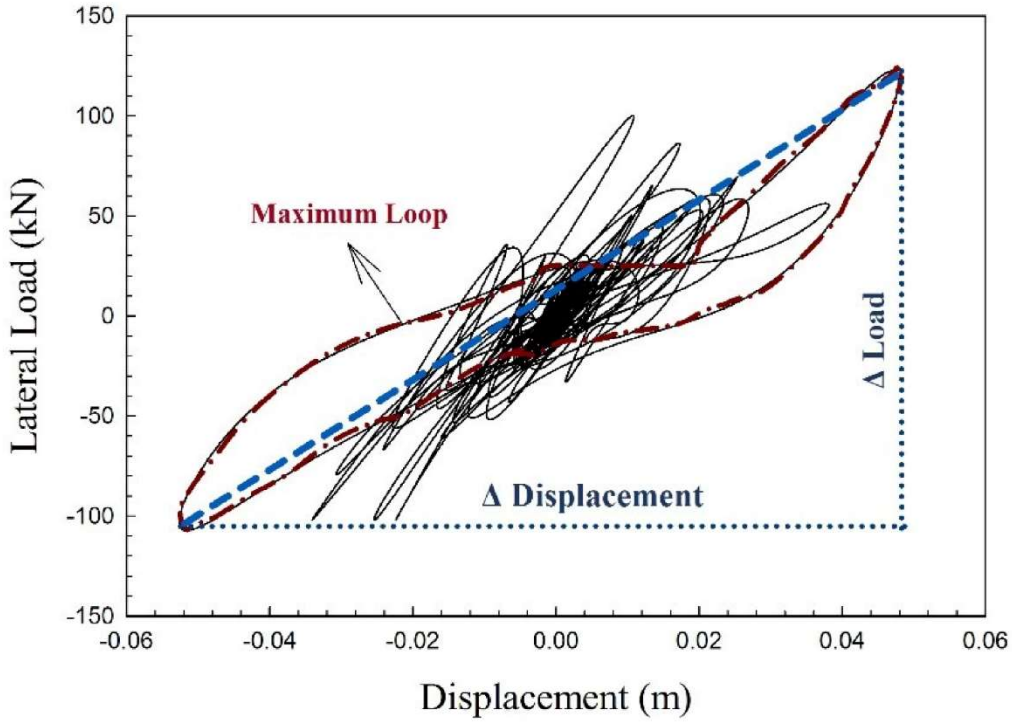

Figure 5.1. Calculation of lateral stiffness using hysteresis load-displacement curve

Table 5.1. Maximum structural lateral stiffness, k_x

Properties			Response		
Pile head	pile group	Shake	Max structure displacement in experiment (mm)	Field lateral structural stiffness, k_x (kN/m)	*DynaPile's* lateral structural stiffness, k_x (kN/m)
Fixed Headed	***Group1***	N100	45	2220	2600
		N75	30	2630	3200
		N50	22	2635	3530
		T100	82	855	1275
		T75	58	860	1575
		T50	32	1250	1925
	Group2	N100	67	1400	2925
		N75	43	1510	3165
		N50	30	1500	3470
		T100	100	1300	1685
		T75	72	1390	1905
		T50	48	1460	2240
Pinned Headed	***Group1***	N100	40	2250	2540
		N75	30	2330	2740
		N50	19	2475	3310
		T100	78	795	1065
		T75	57	840	1325
		T50	30	1270	2095
	Group2	N100	57	1405	2720
		N75	37	1515	3460
		500	28	1500	3790
		T100	91	825	1575
		T75	69	970	1875
		T50	42	1260	2140

Note: “N” and “T” refer to Northridge and Takatori earthquakes, respectively. The number follows the notation shows the scaled intensity of original motion (e.g. N75: Northridge 75%).

5.4 Numerical prediction of dynamic lateral stiffness of model structure represented as lumped mass

The experimental data were used to verify a numerical model established using ENSOFT's Dynapile (2016). The ENSOFT Dynapile software package is a computational software that uses the consistent boundary-matrix method (Blaney et al. 1976) to analyze the seismic response of single and grouped piles.

The complete SSI model, including the grouped helical pile foundation and surrounding soil medium, are modeled in DynaPile as shown in Figure 5.2. The pile and soil properties can be seen in this figure. This program is a graphical commercial program that performs dynamic analysis of single and multi-pile groups in finite or semi-infinite multi layered media. The program outputs are dynamic responses of pile foundation (e.g. time history response, frequency response curve) and dynamic stiffnesses of pile foundations under seismic motions. Each group of piles was modeled separately. The material in this model were soil and steel with densities of 19.5 and 80 kN/m^3, respectively; the other properties are presented in Figure 5.2. The pile cross sections were defined as in the experiment as presented in Table 3.2. The soil layer was then defined in 18 sublayers as a 4.6 m deep dense sand bed. Piles length and layout were specified for two pile groups according to the experiment (Table 3.2, Figure 3.6 and 3.8). In this chapter, only the piles that were tied together and formed group 1 and 2 are discussed. One of the limitations of this model is that the program does not allow the addition of the helical plates onto the pile shafts, and it assumes that all piles within a group have the same geometry. The skid in the experiment (model structure) was simulated as a lumped mass directly in the top center of the group of piles. The properties of the superstructure, such as spring stiffness (see Figure 5.2), damping ratio, structural mass and height of the structure, external forces and moments in three directions (horizontal,

vertical, rotational), were defined. The skid in the experiment was simulated as the lumped mass on top of the pile head which is the model structure herein; so that, weight and height of the skid were used in the model. Damping ratios of this model structure were obtained and introduced from Shahbazi et al. (2019)'s study; in their study, the damping ratios were achieved by developing hysteresis load-displacement curves from each skid's recorded accelerations (Figure 5.1) and the damping ratios were achieved for each condition (Eq. (5-2)):

$$\zeta = \frac{E_D}{4\pi E_s} \qquad 5\text{-}2$$

where E_D is the hysteresis loop area, which manifests energy loss and E_S represents the maximum strain energy.

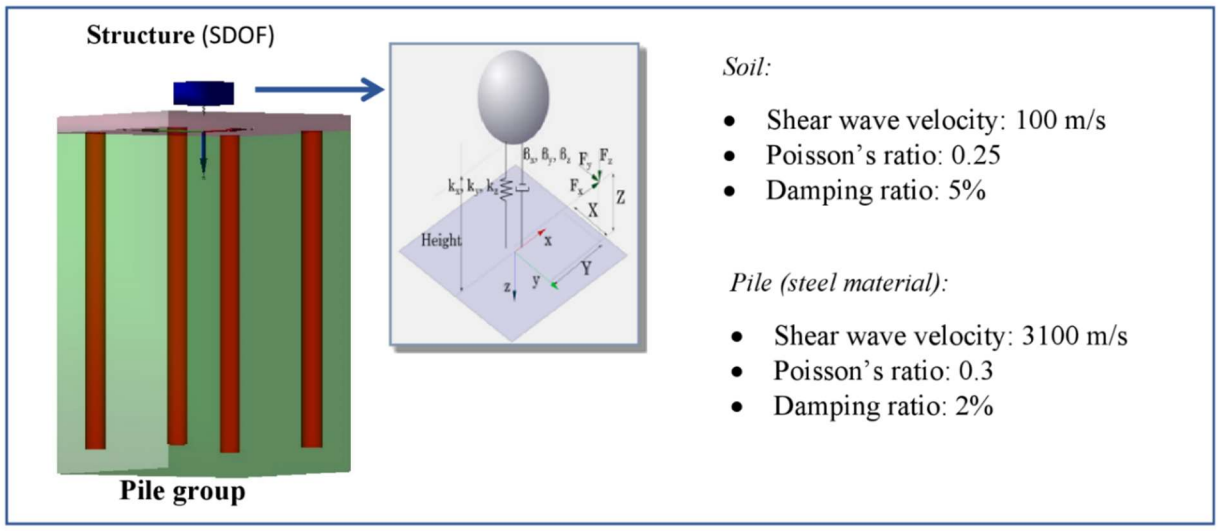

Figure 5.2. The schematic model in DynaPile

Shear wave velocity, shear modulus and damping values of soil were assumed to be constant during each loading. Throughout the testing sequence, pulses were transmitted through the soil bed between each earthquake shake to assess changes in soil shear wave velocity. Since the shear wave velocity change was negligible, possibly due to the high stiffness of dense sand,

ignoring the variation of shear modulus during the test was an appropriate decision. Regarding damping values, the hysteresis loops and subsequently damping values were changing during each shake. Instead of allowing this dynamic input, the model considers only constant damping values, which is another model limitation. The earthquake time histories used in the shake table testing were input as ground motion at the base of the model. Since the focus of this program is soil and foundation, the forces and moment generated at the lumped mass and at the base due to the earthquake motion should be calculated and input manually. To calculate the horizontal input loading, the mass of the skid was multiplied by the maximum acceleration of the earthquake motion. The fixed connection was simulated by applying a moment at the base, which is horizontal force multiplied by the distance of the center of mass to the pile head. In a pinned connection, the moment was assumed to be zero at the pile head. The model was updated iteratively by adjusting the stiffness values of the springs connecting the structure to the pile cap (e.g. k_x, k_y, k_z) in order to achieve the best match with the measured response during the shake table test (e.g. maximum structural displacement). A similar iteration calibration was conducted by Shamsabadi and Taciroglu (2013) on an instrumented long span bridge in California using Dynapile software. Thus, the equivalent structural stiffness compatible with the obtained skid displacement was achieved for a given ground motion and the corresponding configuration. Thus, the model structure's stiffness for various conditions has been determined and the calibrated model was created (Table 5.1).

Table 5.1 compares the dynamic structural lateral stiffness (k_x) obtained from the experimental results with the values obtained from the DynaPile model, which corresponded to the same experimental displacement, for all configurations and loading conditions studied. It is worth mentioning that these values are for the lumped mass (or skid in the experiment) that

inherently includes the effects of the pile foundation and soil. The comparison shows that the stiffness values obtained from DynaPile are higher than the stiffness values back calculated from the experimental results. This difference is significant in a few cases, which indicates that DynaPile may not properly consider the pile-soil-structure interaction from the field in those specific conditions because this model doesn't does not specifically include allow the inclusion of helices of on piles. The presence of helices in the experiment provided more lateral stiffness for the system; thus, to achieve a compatible displacement within the numerical analysis, a higher lateral stiffness was required. Moreover, the skid used in the experiment may not be simulated properly as a lumped mass in this model (e.g. the skid didn't behave the same as a lumped mass would). In general, the pile group with a fixed head connection may exhibit higher stiffness for the structure compared to pinned head connections. There are some exceptions to this observation, which might be due to the imperfect pinned connection in our tests. The pinned connection was simulated by using one bolt in the pile cap, which allowed the pile to rotate about one axis. As was expected, the pile group (Group 2) with a lower slenderness ratio (pile length (l)/pile diameter (d)) (see Table 3.2) seems to be stiffer than more slender piles.

By analyzing the time history responses of soil-pile system to the white noise signals recorded by strain gages and accelerometers in the frequency domain using Fast Fourier Transform (FFT), the natural frequency (f_n) of piles was obtained. As a result, single piles in group 1 (piles 1 to 4) were found to have average natural frequency around 2.1 HZ and larger single piles in group 2 (piles 7 to 10) had average natural frequency around 1.9 HZ. In our study, the natural frequencies of the piles were generally within the frequency content of the Takatori earthquake, which may create resonance and nonlinearity in the soil behavior due to the gap formation between the top of the pile and the soil. This resonance and gapping may cause reduction in stiffness, which

was quantified in the experimental results when the Takatori earthquake revealed a smaller structural stiffness than when the structure was subjected to the Northridge earthquake. In addition, a decline in stiffness occurs when the load intensity increases from 50% to 100% of the original ground motion's peak acceleration. This again occurs due to nonlinear system behavior, such as gapping between the soil and pile (which is not considered directly in the calibrated DynaPile model), under motions with larger acceleration amplitudes.

5.5 Comparing lateral stiffness of pile foundation from model with well-known theoretical equations

The lateral stiffness of the foundation obtained from the numerical model is compared with predictions of available theoretical solutions.

Wolf (1985) proposed a theoretical model for equivalent horizontal spring stiffness of piles. In order to use this method in our case for a grouped pile foundation, the equivalent radius for the pile groups was calculated (Poulos et al. 1993; Randolph 1994; Loria and Laloui 2017). The equations are given by:

$$k_x = \frac{8Gr}{1-\upsilon} \tag{5-3}$$

$$r = \frac{D_{eq}}{2} \tag{5-4}$$

$$A_g = [(\sqrt{n_p} - 1)S + D]^2 \tag{5-5}$$

in which ν is the Poisson's ratio of the soil, r is the equivalent radius of a pile foundation, and G is the dynamic shear modulus of a soil corresponding to a significant strain level in surrounding soil and is commonly given by, $G = \rho_s V_s^2$; where ρ_s is the mass density of the soil and V_s is the shear wave velocity of the soil measured from the test. Assuming a constant shear wave velocity

value of 100 m/s for the entire soil bed provides a constant value of G equal to 19.5 MPa, which was applied in Eq. (5-3). D_{eq} is representative of equivalent grouped pile diameter. n_p, S and D, are number of piles, distance between piles and individual pile diameter, respectively.

Novak (1974) developed a solution for the horizontal stiffness of a pile considering plane strain conditions for an infinitely long pile embedded in a visco-elastic soil medium, which is given by:

$$k_x = (\frac{E_p I_p}{r^3}) f_{11,1} \quad 5\text{-}6$$

where E_p is Young's modulus of the pile material, *r is* the individual radius of the pile, I_p is the moment of inertia of the pile cross-section about the centroidal axis perpendicular to the direction of the motion, and $f_{11,1}$ is a factor that depends on soil stiffness variation along the pile shaft, pile-soil relative rigidity and pile head and toe fixity conditions. The values of $f_{11,1}$ can be found in related tables provided by Novak (1974). The pile-soil-pile interaction is considered in the analysis using equations suggested by Novak (1974), even though the pile shaft spacing was more than 8D and pile interaction could be reduced due to nonlinearity (Arya and Arya 1991; El Naggar and Novak (1995). Thus, in order to estimate the stiffness of a pile group, the stiffness for each single pile using its properties (e.g. E, I, r) in Eq. (5-6) was computed and a coefficient (Eq. (5-8) and (5-9)) based on the relative spacing between the piles was applied in summation of individual pile stiffness (Eq. (5-7)).

$$k_x^g = \frac{\sum_1^{np} k_x}{\sum_1^{np} \alpha_1} \quad 5\text{-}7$$

$$\alpha_{1f} = 0.6 \rho_c [E_p G_c]^{1/7} (\frac{r}{s})(1 + \cos^2 \beta_p) \quad 5\text{-}8$$

$$\alpha_{1H} = 0.4 \rho_c [E_p G_c]^{1/7} (\frac{r}{s})(1 + \cos^2 \beta_p) \quad 5\text{-}9$$

α_{lf} = horizontal interaction factor for fixed headed piles (no head rotation), and α_{lH} = horizontal interaction factor for the case where rotation is allowed. Here $\rho_c = G_z/G_{av}$; G_z = Shear modulus at depth $l_c/4$; l_c which is critical length of pile = $2r[E_p/G_c]^{2/7}$; G_c = Average shear modulus over the critical length of the pile. βp = Angle between a pile with respect to the reference pile. If calculated interaction factor α exceeds 1/3, the correction should be made, and the value needs to be replaced by $\alpha = 1 - 2/\sqrt{(27\alpha)}$.

The pile group stiffness values are obtained using the methodology described above with considering the pile properties and soil used in the tests. The calculated pile group stiffness values are presented in Table 5.2, along with those obtained from the Dynapile output. The results presented in Table 5.2 demonstrate that DynaPile reveals pile group stiffness values close to those generated using Novak's mathematical model. Wolf's model seems not to be suitable for grouped piles using the equivalent pile method. The model by Novak (1974) accounts for the pile geometry, pile material properties (e.g., E and I) and soil properties ($f_{11,1}$) (Eq. (7)) as well as pile interactions more precisely. Therefore, the calibrated DynaPile model yield more realistic values due to the close agreement with the Novak's model. In addition, Nogami and Novak (1977) and Medina et al. (2013) pointed out that at lower excitation frequency, the pile with a higher slenderness ratio reveals lower stiffness. This finding agrees with our results shown in Table 5.2.

Table 5.2. Maximum horizontal equivalent pile group spring stiffness, k_x

Model	k_x (MN/m)	
	Group1	Group2
Wolf (1985)	68	71
Novak (1974)	220	267
DynaPile (2016)	200	250

5.6 Natural frequency of a pile-soil system

The importance of a systems' natural frequency (f_n) emerges when the vibration force frequency is equivalent to its f_n. This results in response amplitude augmentation (i.e., resonance) that may cause irreversible damage to the structure (Kramer 1996). Thus, f_n of a foundation should be considered in design and must be different from the dominant frequency range of a potential future earthquake or machine loading. Several factors such as pile geometry (e.g. length and diameter), soil density, load magnitude, pile condition and physical structure influence the f_n of a soil-pile-structure system (Puri and Prakash 1992; Halling et al. 2000; Tamori et al. 2001; Boominathan and Ayothiraman 2005; Yang et al. 2010). The condition of the pile and the physical state of the structure, which may be altered after an initial strong motion and/or erosion around a pile, are other parameters affecting the natural frequency of a system (Halling et al. 2000; Prendergast et al. 2013; Shirgir et al. 2017). Two common approaches to obtain f_n are developing FFT or FRF in frequency domain using the time history response of a soil-pile system to a white noise motion. The corresponding frequency at which the amplitude peak occurs is extracted as f_n. Therefore, the natural frequency (f_n) of the entire system was calculated based on peaks in either of the two following plots: Fast Fourier Transform (FFT) and Frequency Response Function (FRF) (bandwidth method) using recorded time history from the accelerometers attached to the skid

(Figure 5.3). The results from these two methods were also compared. Table 5.3 shows the natural frequency of the two groups pile foundation system from various approaches. The natural frequency for the system with a stiffer pile group (Group 2) (larger k), which supports a heavier structure (greater m), reveals a smaller f_n. The natural frequency of a SDOF system oscillated by harmonic vibration is commonly calculated by $f_n = \frac{1}{2\pi}\sqrt{\frac{k}{m}}$; thus, the contribution of both mass and stiffness cause Group 1 to have a greater natural frequency. This is due to the different l/d ratios as Boominathan and Ayothiraman (2005) concluded.

Table 5.3. Natural frequency of structure-pile system

Method	Foundation type	Natural frequency (Hz)	
		Fixed connection	Pinned connection
FFT/ Experiment	Group 1	5.5	5.2
	Group 2	4.9	4.7
FRF/ Experiment	Group 1	5.7	4.6
	Group 2	4.4	4.2
FRF/ DynaPile	Group 1	5.2	4.7
	Group 2	4.5	4.3

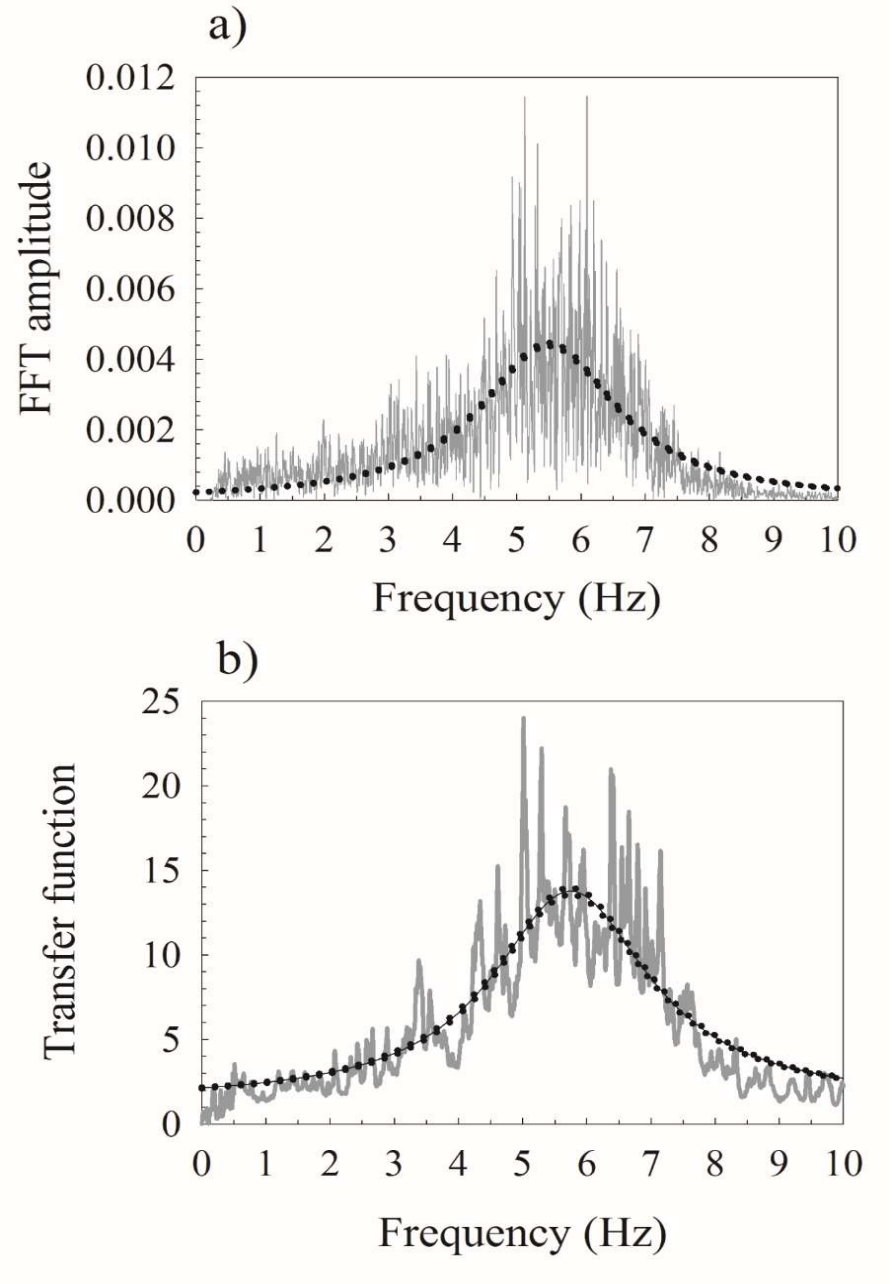

Figure 5.3. Determination of natural frequency from experimental records of accelerometer using a) FFT and b) FRF

In terms of how pile head connections affect a system's natural frequency, the pinned connection seems to reduce the f_n. It can also be seen that the method to calculate f_n does not make a remarkable difference. Hence, FFT can be an alternative to FRF when calculating f_n. These results indicate that the natural frequency from Dynapile agrees with those from the experiments.

5.7 Evaluating the effect of contributed parameters in the seismic response of soil-pile system

The engineering characteristics of soil, foundations and structures have notable impact on each other's response to the ground motion, which ultimately influences the final response of the whole system to the vibration. Therefore, in the current study an effort is made to investigate these interactions. In this regard, various conditions were created in the calibrated DynaPile model to monitor how the changes in individual element properties can vary the response or dynamic property of another element. Mainly, the effect of variation in soil shear wave velocity, structural stiffness, damping ratio and slenderness ratio on the outputs (e.g. structure displacement at center-of-mass, pile group stiffness and pile-head displacement) have been studied. The mentioned parameters either increased or decreased by as much as 20% when keeping the other parameters consistent. All parameter variations were made under the Northridge 100% input motion. The results are discussed in the following:

5.7.1 The effect of soil

Soil is the first medium to propagate the earthquake waves coming from far field. The shear wave velocity (V_s) is one of the seismic properties of soil that basically controls how surrounding soil may transfer the seismic motion to the foundation and finally to the building. Thus, the effect of varying the V_s on the response of a structure and foundation has been studied (Figure 5.4 (a, b and c)) when subject to the same loading (Northridge 100%). Natural frequency, as one of the dynamic properties calculated using records of acceleration under white noise, have also been presented (Figure 5.4 (d and e)).

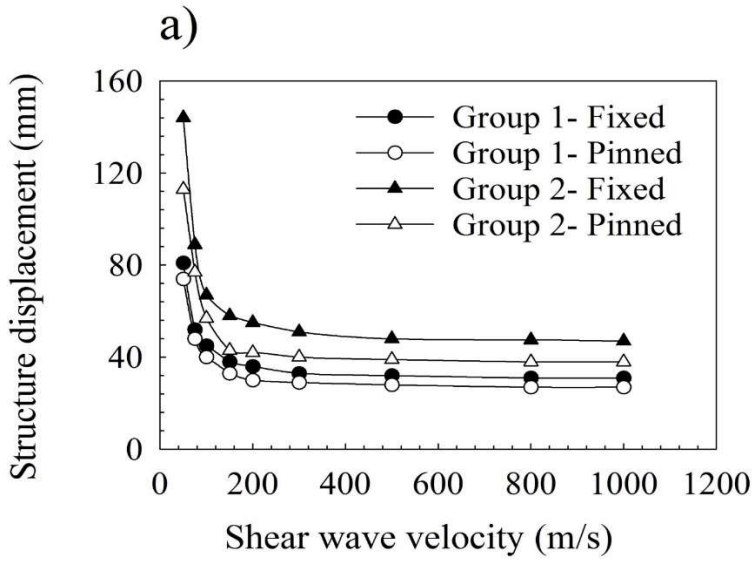
a)
Structure displacement (mm)
160
120
80
40
0
0
200
400
600
800
1000
1200
Shear wave velocity (m/s)
Group 1- Fixed
Group 1- Pinned
Group 2- Fixed
Group 2- Pinned

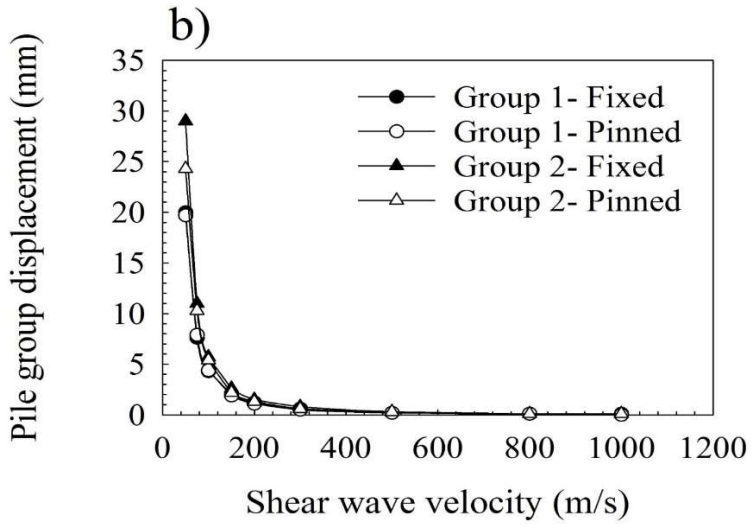
b)
Pile group displacement (mm)
35
30
25
20
15
10
5
0
0
200
400
600
800
1000
1200
Shear wave velocity (m/s)
Group 1- Fixed
Group 1- Pinned
Group 2- Fixed
Group 2- Pinned

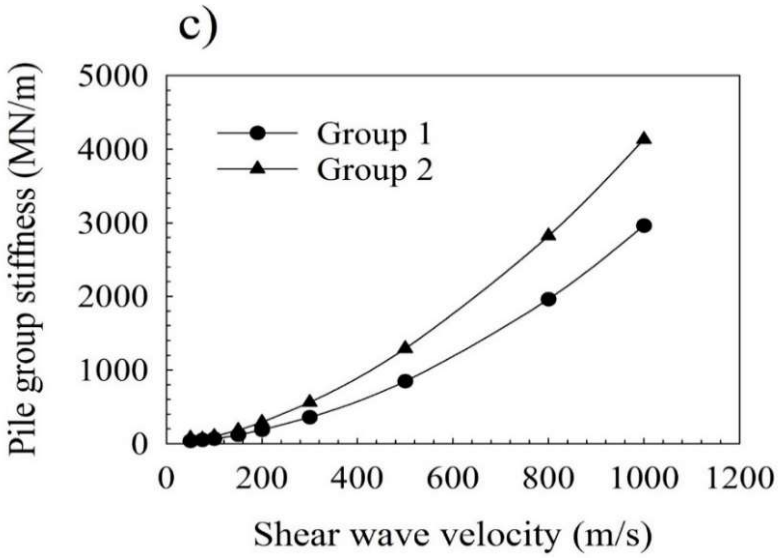
c)
Pile group stiffness (MN/m)
5000
4000
3000
2000
1000
0
0
200
400
600
800
1000
1200
Shear wave velocity (m/s)
Group 1
Group 2

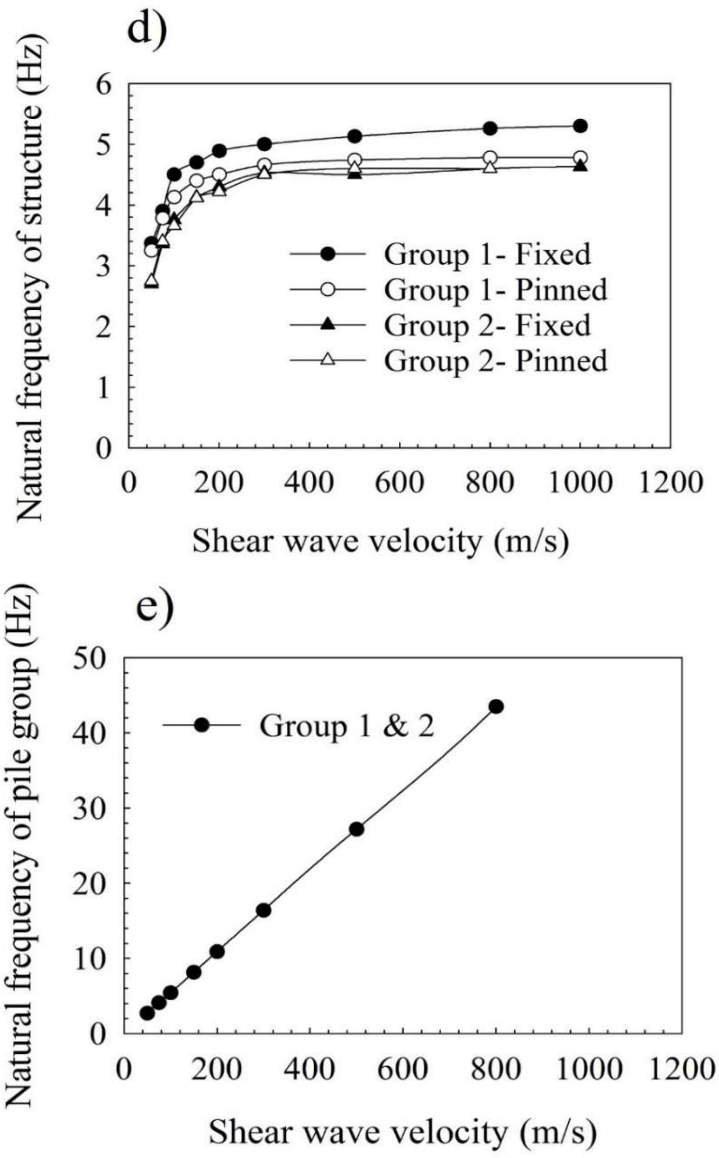

Figure 5.4. Effect of soil shear wave velocity on response and dynamic properties of structure-foundation

When the soil medium is integrated as a homogeneous solid, the shear wave velocity (V_s) increases, which causes a drop in the structural and pile group displacement. This trend is not linear, such that beyond a velocity of 200 m/s, the changes are negligible. In other words, the variation of V_s under 200 m/s is more important to be considered when designing foundations and structural systems. When the soil surrounding the pile is more cohesive and coherent, exhibiting a

higher V_s, it clearly intensifies the pile group's natural frequency and stiffness. This stiffer soil and higher V_s impact on a pile groups' f_n and stiffness is more perceptible in a longer pile group. Raising a soil's V_s to an approximate limit of 200 m/s would also increase the f_n of the superstructure.

Additionally, in a layered soil profile consisting of a dense soil layer (density: 2000 kg/m^3, V_s:200 m/s) extending to the middle of the pile overlying a loose soil (e.g., density: 1400 kg/m^3, V_s: 80 m/s) that continues below the pile, structural displacement was minimal. This can be associated with the higher damping values (higher energy dissipation) occurring through the looser soil where the ground motion vibrations first reach.

5.7.2 The effect of structure

The effect of soil underneath a structure was discussed previously. In order to evaluate the effect of the superstructure's dynamic properties on the pile group supporting it, its stiffness and damping ratio were varied within a wide range (Figures 5.5 and 5.6). Apparently, the stiffer structure with a higher damping ratio should mitigate structural displacement, but there is a limit; when the stiffness exceeds an optimum value, the impact is not noticeable. On the other hand, a stiff superstructure does increase the movement of the pile group. This might be due to a contrast between the stiff (e.g. structure) versus flexible components (e.g. pile) in the system. When the structural damping values decrease by 80% of their original values, the pile group and structural displacement will be approximately 1.8 and 2.8 times greater for fixed and pinned connections, respectively. Changes in structural damping showed greater impact on displacement than the same variation in structural stiffness. In addition to dynamic properties, the geometry of the structure is also crucial. The deflection and displacement of both structure and pile group increases when

height to width ratio (slenderness ratio) of a structure expands (Figure 5.7).

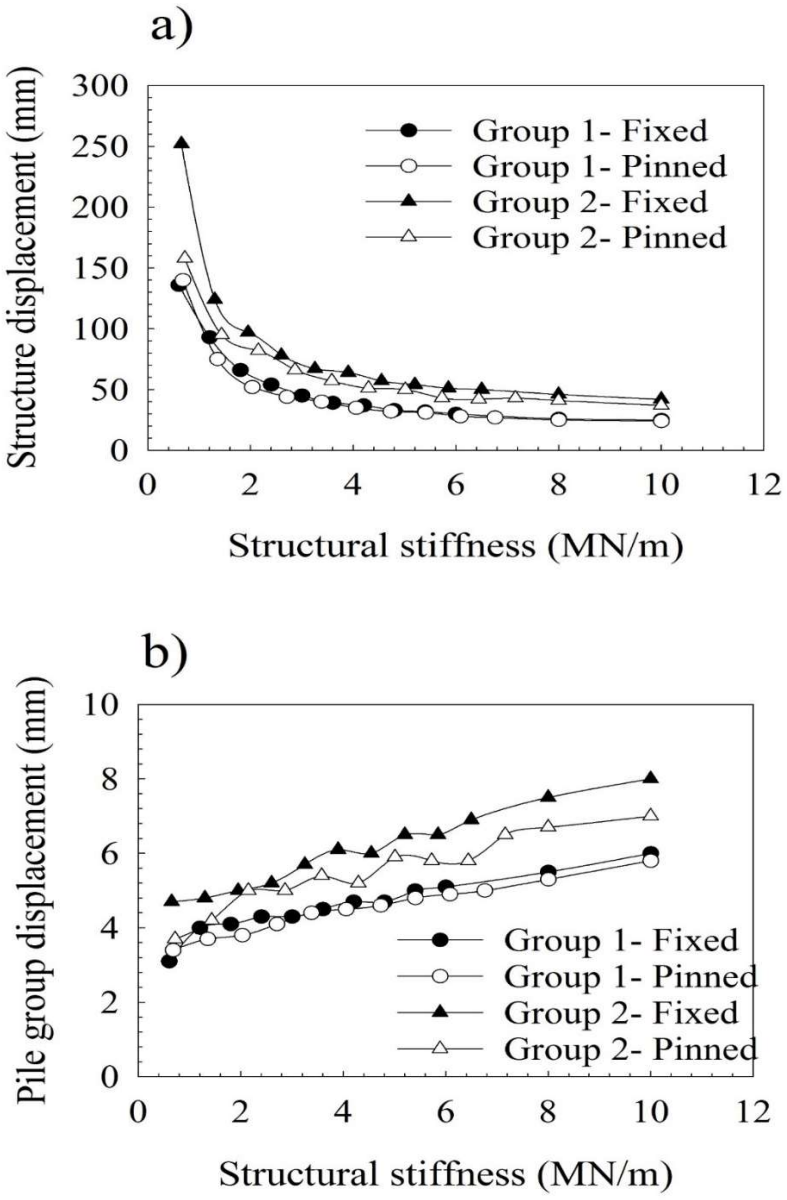

Figure 5.5. Effect of structural stiffness on response of the structure-foundation system

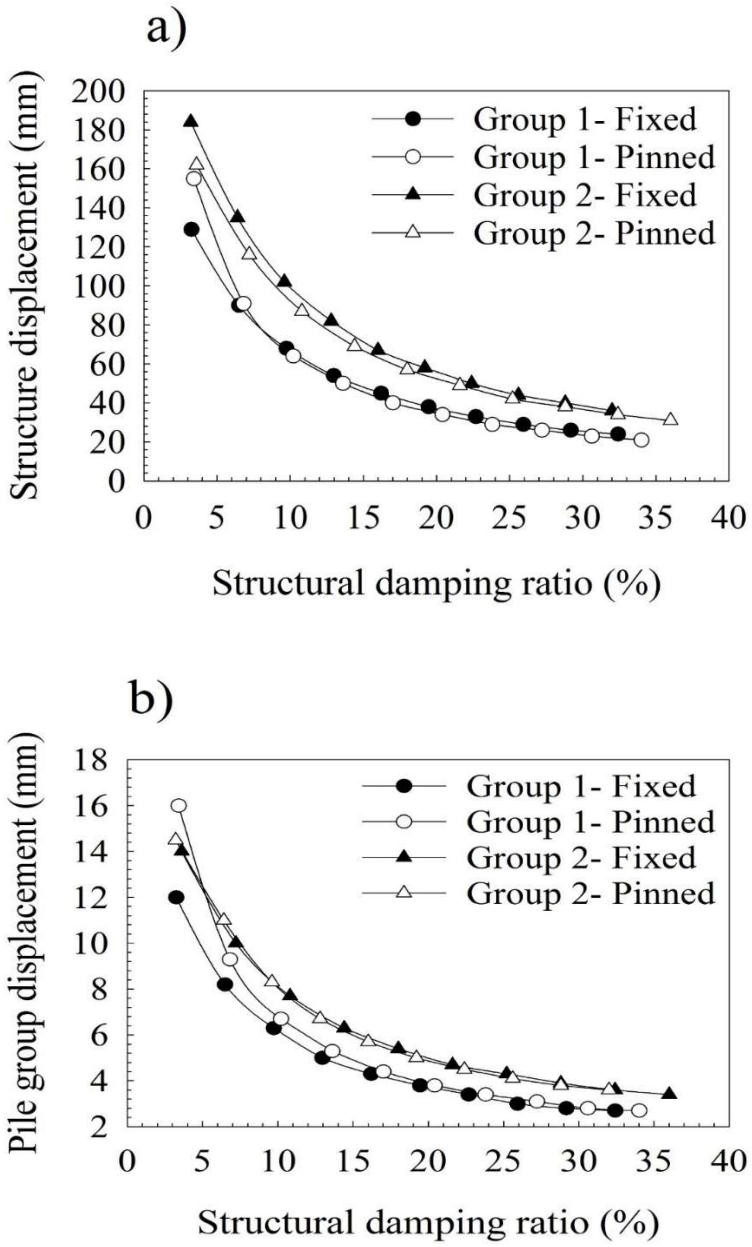

Figure 5.6. Effect of structural damping ratio on response of the structure-foundation system

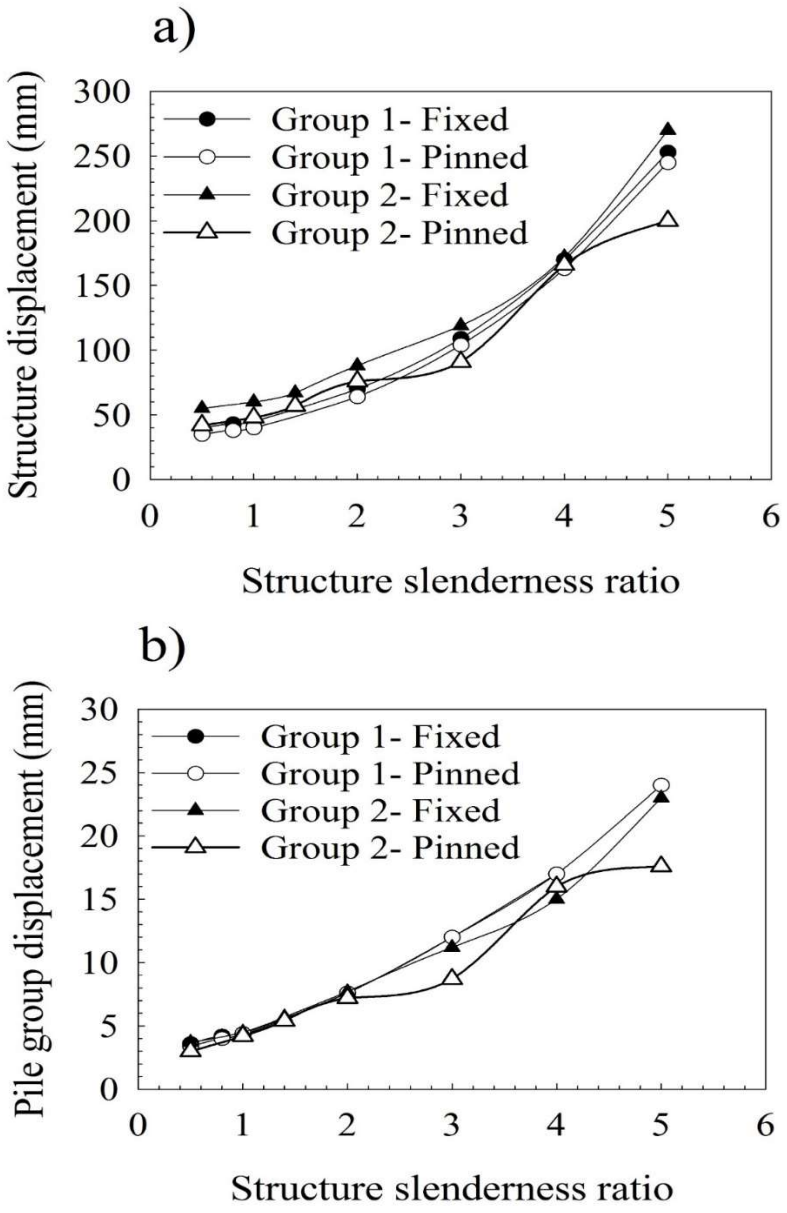

Figure 5.7. Effect of structural slenderness ratio on response of the structure-foundation system

It is worth mentioning that Figs 5.5-5.7 present just the trend of effective parameters on the seismic response of either structure or piles. Due to the user limitations in DynaPile in modeling helices and other previously discussed factors, the values provided in these figures relate exclusively to this specific case study.

5.7.3 Relative properties of soil to structure

Regarding the structure-to-soil stiffness ratio, a flexible structure founded on stiff soil seems to provide less displacement regardless of pile head connections, while a stiff structure on soft soil shows greater displacement. In the first case, ignoring SSI can lead to a conservative design (Givens et al. 2012; Stewart et al. 2012), but in the second case, ignoring SSI could lead to failure. In conclusion, neglecting SSI in the design of a stiff structure can cause underestimation of displacement, which is what the studies conducted by De Carlo et al. (2000) and Papalou et al. (2012) found.

5.8 Conclusions

An investigation of the seismic behavior of helical pile groups with varying parameters subjected to white noise and two replicated earthquakes was performed. Results of the full-scale experimental soil-helical pile-structure system performed on the outdoor shake table at UCSD were used to create and calibrate a model in DynaPile. This calibrated Dynapile model was able to provide realistic results that engineers can use when determining the effect of SSI on soil-pile-structure systems. Experimentally testing full-scale systems within the full range of what could be encountered in the field can be costly and therefore it is imperative that computer models be created and calibrated with high quality experimental testing results to help engineers simulate a wide range of parameters on seismic performance. The stiffness of the tested structure and pile group have been discussed and the quantitative results are developed accordingly. The interaction of soil and helical pile-supported structures have also been analyzed and discussed. The highlighted conclusions include the following:

- The increase in a soil's shear wave velocity influences the seismic response of building and foundation positively and minimizes their displacements; this effect becomes negligible beyond a V_s of 200 m/s in our study.
- Similarly, with a higher structural damping ratio, less displacement occurs in both the building and at the pile foundation.
- Increasing the structural stiffness reduces the displacement of a building but it may cause a slight increase in the pile group's movement.
- Regarding the structure's geometry, the building with a larger slenderness ratio provides more system freedom in movement under lateral loads.

In terms of displacement, the behavior of a flexible structure founded on stiff soil seems to fare better than a stiff structure founded on soft soil. When designing stiff buildings on soft soils, SSI should be considered. In a layered soil profile consisting of a stiffer soil underlain by a looser soil, the underlying looser soil contributes to the mitigation and dissipation of the ground motion's energy. If that looser soil can support the pile and structure without excessive settlement, potential bearing capacity failure, or liquefaction concerns, it may be beneficial to embed the piles into this type of soil to take advantage of its energy dissipation assets.

5.9 References

Allotey, N., and M. H. El Naggar. 2008. "Generalized dynamic Winkler model for nonlinear soil–structure interaction analysis." Canadian Geotechnical Journal, 45(4), 560-573.

Allred, S. M. 2018. "Seismic performance of grouped helical piles in fixed and pinned connections." University of Oklahoma.

Arya, A., and A. S. Arya. 1991. "Pile Group Stiffness for Seismic Soil-Structure Interaction." 2nd International Conferences on Recent Advances in Geotechnical Earthquake Engineering and Soil Dynamics, Missouri University of Science and Technology Scholars' Mine, Missouri.

Badry, P., and N. Satyam. 2017. "Seismic soil structure interaction analysis for asymmetrical buildings supported on piled raft for the 2015 Nepal earthquake." Journal of Asian Earth Sciences, 133, 102-113.

Beltrami, C., C. G. Lai, and A. Pecker. 2005. "A Kinematic Interaction Model For a Large-Diameter Shaft Foundation: An Application to Seismic Demand Assesment of a Bridge Subject to Coupled Swaying-Rocking Excitation." Journal of Earthquake Engineering, 9(spec02), 355-393.

Boominathan, A., and R. Ayothiraman. 2005. "Dynamic behaviour of laterally loaded model piles in clay." Proceedings of the Institution of Civil Engineers-Geotechnical Engineering, 158(4), 207-215.

Borja, R. I., and W.-H. Wu. 1994. "Vibration of foundations on incompressible soils with no elastic region." Journal of geotechnical engineering, 120(9), 1570-1592.

Boulanger, R. W., C. J. Curras, B. L. Kutter, D. W. Wilson, and A. Abghari. 1999. "Seismic Soil-Pile-Structure Interaction Experiments and Analyses " J. Geotech. Geoenviron. Eng., 125(9), 750-759.

Carbonari, S., M. Morici, F. Dezi, F. Gara, and G. Leoni. 2017. "Soil-structure interaction effects in single bridge piers founded on inclined pile groups." Soil Dynamics and Earthquake Engineering, 92, 52-67.

Cerato, A., T. Vargas, and S. Allred. 2017. "A critical review: State of knowledge in seismic behaviour of helical piles." DFI Journal-The Journal of the Deep Foundations Institute, 11(1), 39-87.

Chatzigogos, C. T., A. Pecker, and J. Salençon. 2009. "Macroelement modeling of shallow foundations." Soil Dynamics and Earthquake Engineering, 29(5), 765-781.

Chowdhury, I., and S. Dasgupta 2008. "Dynamics of structure and foundation - A unified approach "Taylor & Francis Group, London, UK.

Cox, W. R., L. C. Reese, and B. R. Grubbs. 1974. "Field testing of laterally loaded piles in sand." Proc., Offshore Technology Conference, Offshore Technology Conference.

Cremer, C., A. Pecker, and L. Davenne. 2001. "Cyclic macro-element for soil–structure interaction: material and geometrical non-linearities." International Journal for Numerical and Analytical Methods in Geomechanics, 25(13), 1257-1284.

De Carlo, G., M. Dolce, and D. Liberatore. 2000. "Influence of Soil–Structure Interaction on the Seismic Response of Bridge Piers." Proc., Proceeding of the 12th World Conference on Earthquake Engineering/Auckland, New Zealand.

Ebeido, A. A. 2019. "Lateral-Spreading Effects on Pile Foundations: Large-scale Testing and Analysis." UC San Diego.

El-sawy, M. 2017. "Seismic performance of steel helical pile." Master of science, The University of Western Ontario.

El Sawy, M. K., M. H. El Naggar, A. B. Cerato , and A. W. Elgamal. 2019. "Seismic performance of helical piles in dry sand from large scale shake table tests." Geotechnique, 18-P-001.

Elkasabgy, M., and M. H. El Naggar. 2013. "Dynamic response of vertically loaded helical and driven steel piles." Canadian Geotechnical Journal, 50(5), 521-535.

Elkasabgy, M., and M. H. El Naggar. 2018. "Lateral Vibration of Helical and Driven Steel Piles Installed in Clayey Soil." Journal of Geotechnical and Geoenvironmental Engineering, 144(9), 06018009.

Far, H. 2019. "Advanced computation methods for soil-structure interaction analysis of structures resting on soft soils." International Journal of Geotechnical Engineering, 13(4), 352-359.

Gajan, S., P. Raychowdhury, T. C. Hutchinson, B. L. Kutter, and J. P. Stewart. 2010. "Application and validation of practical tools for nonlinear soil-foundation interaction analysis." Earthquake Spectra, 26(1), 111-129.

Gazetas, G., and R. Dobry. 1984. "Horizontal response of piles in layered soils." Journal of Geotechnical engineering, 110(1), 20-40.

Ghosh, B., and S. P. G. Madabhushi. 2007. "Centrifuge modelling of seismic soil structure interaction effects." Nuclear Engineering and Design, 237(8), 887-896.

Givens, M. J., J. P. Stewart, C. B. Haselton, and S. Mazzoni. 2012. "Assessment of soil-structure interaction modeling strategies for response history analysis of buildings." UCLA Civil and Environmental Engineering.

Guan, Z., X. Chen, and J. Li. 2018. "Experimental investigation of the seismic performance of bridge models with conventional and rocking pile group foundations." Engineering Structures, 168, 889-902.

Halling, M. W., K. C. Womack, I. Muhamad, and K. M. Rollins. 2000. "Vibrational testing of a full-scale pile group in soft clay." Proc. 12th World Conference on Earthquake Engineering, Auckland.

Han, Y., and M. Novak. 1988. "Dynamic behaviour of single piles under strong harmonic excitation." Canadian Geotechnical Journal, 25(3), 523-534.

Houlsby, G. T., and M. J. Cassidy. 2002. "A plasticity model for the behaviour of footings on sand under combined loading." Géotechnique, 52(2), 117-129.

Jeremic, B., G. Z. Jie, M. Preisig, and N. Tafazzoli. 2009. "Time domain simulation of soil-foundation-structure interaction in non-uniform soils." Journal of Earthquake Engineering and Structural Dynamics, 38, 699-718.

Kagawa, T., M. Sato, C. Minowa, A. Abe, and T. Tazoh. 2004. "Centrifuge simulations of large-scale shaking table tests: case studies." Journal of Geotechnical and Geoenvironmental Engineering, 130(7), 663-672.

Kaynia, A. M. 1982. "Dynamic stiffness and seismic response of pile groups." Massachusetts Institute of technology.

Kaynia, A. M., and S. Mahzooni. 1996. "Forces in pile foundations under seismic loading." Journal of Engineering mechanics, 122(1), 46-53.

Kramer, S. 1996. "Geotechnical Earthquake Engineering. Prentice-Hall, Inc." New Jersey, 348-422.

Liang, F., Y. Jia, L. Sun, W. Xie, and H. Chen. 2017. "Seismic response of pile groups supporting long-span cable-stayed bridge subjected to multi-support excitations." Soil Dynamics and Earthquake Engineering, 101, 182-203.

Loria, A. F. R., and L. Laloui. 2017. "The equivalent pier method for energy pile groups." Géotechnique, 67(8), 691-702.

Lou, M., H. Wang, X. Chen, and Y. Zhai. 2011. "Structure–soil–structure interaction: Literature review." Soil Dynamics and Earthquake Engineering, 31(12), 1724-1731.

Lysmer, J., and F. E. Richart. 1966. "Dynamic response of footings to vertical loading." Journal of Soil Mechanics & Foundations Div.

Matlock, H. 1970. "Correlations for design of laterally loaded piles in soft clay." Offshore Technology in Civil Engineering Hall of Fame Papers from the Early Years, 77-94.

Matlock, H., and S. H. Foo. 1978. "Simulation of lateral pile behavior under earthquake motion." Proc., From Volume I of Earthquake Engineering and Soil Dynamics, Proceedings of the ASCE Geotechnical Engineering Division Specialty Conference, Pasadena, California.

Medina, C., J. J. Aznárez, L. A. Padrón, and O. Maeso. 2013. "Effects of soil–structure interaction on the dynamic properties and seismic response of piled structures." Soil Dynamics and Earthquake Engineering, 53, 160-175.

Michel, P., C. Butenweg, and S. Klinkel. 2018. "Pile-grid foundations of onshore wind turbines considering soil-structure-interaction under seismic loading." Soil Dynamics and Earthquake Engineering, 109, 299-311.

Miura, F. 1997. "Lessons from the damage caused by past earthquakes." Proc., International Workshop on Micropiles, Seattle.

Mylonakis, G., and G. Gazetas. 2000. "Seismic soil-structure interaction: beneficial or detrimental?" Journal of Earthquake Engineering, 4(3), 277-301.

Mylonakis, G., A. Nikolaou, and G. Gazetas. 1997. "Soil–pile–bridge seismic interaction: kinematic and inertial effects. Part I: soft soil." Earthquake Engineering & Structural Dynamics, 26(3), 337-359.

Naggar, M. H. E., M. A. Shayanfar, M. Kimiaei, and A. A. Aghakouchak. 2005. "Simplified BNWF model for nonlinear seismic response analysis of offshore piles with nonlinear input ground motion analysis." Canadian Geotechnical Journal, 42, 365-380.

Nghiem, H. M. 2009. "Soil-Pile-Structure Interaction Effects on High rise Under Seismic Shaking." Doctor of Philosophy, University of Colorado Denver.

Nogami, T., and M. Novak. 1977. "Resistance of soil to a horizontally vibrating pile." Earthquake Engineering & Structural Dynamics, 5(3), 249-261.

Nogami, T., J. Otani, K. Konagai, and H.-L. Chen. 1992. "Nonlinear soil-pile interaction model for dynamic lateral motion." Journal of Geotechnical Engineering, 118(1), 89-106.

Nova, R., and L. Montrasio. 1991. "Settlements of shallow foundations on sand." Géotechnique, 41(2), 243-256.

Novak, M. 1974. "Dynamic stiffness and damping of piles." Canadian Geotechnical Journal, 11(4), 574-598.

Novak, M., and R. F. Grigg. 1976. "Dynamic experiments with small pile foundations." Canadian Geotechnical Journal, 13(4), 372-385.

Novak, M., and T. Nogami. 1977. "Soil-pile interaction in horizontal vibration." Earthquake Engineering & Structural Dynamics, 5(3), 263-281.

Papalou, A., J. Bielak, and E. Bazán. 2012. "Effects of Isolated Spread Footings on the Dynamics of Soil-Structure Interaction." Journal of Geotechnical and Geoenvironmental Engineering, 138(8), 1033-1036.

Pecker, A., and C. T. Chatzigogos. 2010. "Non Linear Soil Structure Interaction: Impact on the Seismic Response of Structures "Dordrecht: Springer Netherlands, Dordrecht.

Penzien, J. 1970. "Soil-pile foundation interaction." Earthquake engineering, 11.

Poulos, H. G. 1993. "Settlement Prediction for Bored Pile Groups "University of Sydney, Centre for Geotechnical Research.

Prendergast, L. J., D. Hester, K. Gavin, and J. O'sullivan. 2013. "An investigation of the changes in the natural frequency of a pile affected by scour." Journal of Sound and Vibration, 332(25), 6685-6702.

Puri, V. K., and S. Prakash. 1992. "Observed and predicted response of piles under dynamic loads." Proc., Piles under dynamic loads, ASCE, 153-169.

Randolph, M. F. 1994. "Design methods for pile group and piled rafts." Proc. 13th Int. Conf. on SMFE, 5, 61-82.

Raychowdhury, P., and T. C. Hutchinson. 2009. "Performance evaluation of a nonlinear Winkler-based shallow foundation model using centrifuge test results." Earthquake Engineering & Structural Dynamics, 38(5), 679-698.

Richart, F. E., R. D. Wood, and J. R. Hall. 1970. "Vibrations of soils and foundations

Ridgley, N. 2015. "Practice Note 28: Screw Piles: Guidelines for Design, Construction & Installation." The Institution of Professional Engineers New Zealand Inc.

Rovithis, E., K. Pitilakis, and G. Mylonakis. 2009. "Seismic analysis of coupled soil-pile-structure systems leading to the definition of a pseudo-natural SSI frequency." Soil Dynamics and Earthquake Engineering, 29(6), 1005-1015.

Sáez, E., F. Lopez-Caballero, and A. Modaressi-Farahmand-Razavi. 2013. "Inelastic dynamic soil–structure interaction effects on moment-resisting frame buildings." Engineering structures, 51, 166-177.

Seed, H. B., and J. Lysmer. 1978. "Soil-structure interaction analyses by finite elements—State of the art." Nuclear Engineering and Design, 46(2), 349-365.

Shahbazi, M., A. B. Cerato, S. Allred, M. H. El Naggar, and A. Elgamal. 2019. "Damping Characteristics of Full-Scale Grouped Helical Piles in Dense Sands Subject to Small and Large Shaking Events." Canadian Geotechnical Journal.

Shamsabadi, A., and E. Taciroglu. 2013. "A Frequency-Time Domain Handshake Method For Seismic Soil-Foundation-Structure Interaction Analysis of Long-Span Bridges." 7th National Seismic Conference on Bridges and Highways.

Shirato, M., Y. Nonomura, J. Fukui, and S. Nakatani. 2008. "Large-scale shake table experiment and numerical simulation on the nonlinear behavior of pile-groups subjected to large-scale earthquakes." Soils and foundations, 48(3), 375-396.

Shirgir, V., A. Ghanbari, M. Amiri, and A. Derakhshandi. 2017. "Effect of Pile Foundation on Natural Frequency of Soil Layer." Journal of Engineering Geology, 10(4), 3839.

Stewart, J., C. B. Crouse, T. C. Hutchinson, B. Lizundia, F. Naeim, and F. Ostadan 2012. " Soil-Structure Interaction for Building Structures " National Institute of Standards and Technology (NIST).

Talukder, M. K. 2009. "Seismic response of pile foundation in saturated sand using Beam on Nonlinear Winkler Foundation approach." Master of Engineering, Memorial University of Newfoundland, Canada.

Tamori, S. i., M. Iiba, and Y. Kitagawa 2001. "A Simplified Method for Dynamic Response Analysis of Soil-Pile-Building Interaction System in Large Strain Levels of Soils-Analysis for Building with Embedment and Pile." Proceedings Third UJNR Workshop on Soil-Structure Interaction, California, USA.

Ting, J. M., C. R. Kauffman, and M. Lovicsek. 1987. "Centrifuge static and dynamic lateral pile behaviour." Canadian Geotechnical Journal, 24(2), 198-207.

Ubilla, J., T. Abdoun, and R. Dobry. 2011. "Centrifuge scaling laws of pile response to lateral spreading." International Journal of Physical Modelling in Geotechnics, 11(1), 2-22.

Vargas Castilla, T. M. 2017. "Understanding the seismic response of single helical piles in dry sand using a large-scale shake table test." Master of science, University of Oklahoma.

Veletsos, A. S., and V. Nair. 1975. "Seismic interaction of structures on hysteretic foundations." Journal of the Structural Division, 101(1), 109-129.

Wilson, D. 1998. "Soil-pile-superstructure interaction in soft clay and liquefiable sand." Rep. No. UCD/CGM-98, 4.

Wolf, J. P. 1985. "Dynamic soil-structure interaction "Englewood Cliffs (N.J.) : Prentice-Hall.

Yang, E.-K., J.-I. Choi, S.-Y. Kwon, and M.-M. Kim. 2011. "Development of dynamic py backbone curves for a single pile in dense sand by 1g shaking table tests." KSCE Journal of Civil Engineering, 15(5), 813.

Yang, E.-K., S.-Y. Kwon, J.-I. Choi, and M. M. Kim 2010. "Natural Frequency Calculation of a Pile-Soil System in Dry Sand Under an Earthquake Loading." 5th International Conference on Recent Advances in Geotechnical Earthquake Engineering and Soil Dynamics, Missouri University of Science and Technology Scholars' Mine.

Chapter 6 : SEISMIC RISK ANALYSIS OF PILE-SOIL-STRUCTURE

6.1 Abstract

Designing structures to be the least vulnerable within earthquake-prone areas is a serious challenge for structural engineers. One common and useful tool that structural engineers use to predict the vulnerability of a structure during an earthquake is a fragility curve. However, most structural fragility curves do not take into consideration the contribution of pile foundation systems in the structural vulnerability. Therefore, this study aims to modify existing fragility curves of a six-story fixed-base steel frame hospital building with buckling-restrained braces (BRBs), to incorporate the effect of helical pile group behavior on the fragility of the structure. To that end, a finite element model of the investigated structure was modified with results from a full-scale shake table test performed on two groups of helical piles embedded in dense sand supporting a superstructure. The primary results show that fixed base design may not be conservative for all conditions and soil-foundation interaction should be considered when creating fragility curves, especially for a stiff structure on soft soils where a high-intensity earthquake is anticipated.

6.2 Introduction

Seismic fragility curves are considered the primary approach for assessing risk and vulnerability of structures to extreme events. For seismic events, the curves represent the probability of exceeding a certain performance (damage) level for increased intensity of ground motions (Porter 2016; Karim and Yamazaki 2001; Mekki et al. 2016). The literature on this topic has been

extensively discussed in Chapter 2.

Most of the fragility analyses performed to date have assumed a fixed connection with the ground. However, it is well known that many structures, including high rise buildings, are mostly supported by deep foundations and those deep foundations affect how the structure reacts to the earthquake. Soil incorporates the final response of a structure to an earthquake, which means structural stiffness in design will vary based on the type and behavior of the soil and foundation; the designed structure might experience different levels of damage (Nakhaei and Ghannad 2008) depending on the interaction between the soil, foundation and structure. Therefore, assessing how the stiffness of a structure or the softness of a soil influence the structure vulnerability is important. Therefore, consideration of soils and foundations during both linear and nonlinear soil response is important because it influences the seismic vulnerability of structures. Typically, several assumptions are made to model simplified soil-pile-structure systems. When assumptions are used, inaccuracies can occur, and the design should be justified by experimental observations.

An authentic response of a soil-pile-structure system subjected to an earthquake motion would better predict the level of damage than assuming a fixed base or a simplified soil-foundation model in all cases. Having this type of real data for all combinations of different building and pile types is unrealistic, but it will be a significant engineering development to adjust existing fragility curves to properly account for the foundation system's influence. Thus, this study aims to perform a sensitivity study on existing fragility curves using the full-scale experimental data set on soil-helical pile groups to assist deep foundation designers in effectively predicting how the soil-pile system could affect the behavior of a structure under future earthquake loading.

The experimental setup (the full-scale experimental tests) on helical pile groups have been explained completely in Chapter 3. For soil, pile, loading and other relevant properties review that chapter.

6.3 Model calibration summary

The data from the experiment were analyzed to find the response of piles and both sand-filled skids. The single accelerometer at the center of mass of each skid recorded the acceleration of the box with time for each specific condition. These recorded accelerations multiplied by the weight of the box produced the horizontal load. Double integration of the acceleration time history produced the horizontal displacement. Then, the hysteresis load-displacement curves were developed using MATLAB (Shahbazi et al. 2019). From these curves the maximum lateral displacement of the box was determined for each shake. These results were employed to calibrate a model using ENSOFT's Dynapile (2016). The grouped pile foundation and surrounding soil medium were modeled in this software package to be similar to the physical test model. The skids were modeled as a lumped mass on top of each pile group and the height was the same as the height of the center of the skid in the shake table experiment.

The dynamic properties of the piles and soil (Table 6.1) were introduced to the program. The applied earthquake time histories in the experiment were entered into the program as the ground motion loading. The mass of the skid multiplied by the maximum acceleration of the earthquake motion was entered as horizontal force. This horizontal force multiplied by the distance of the center of mass from the base was applied to simulate the generated moment at the base due to the fixed connection. More details on this model can be found in Chapter 5. The modeling process is summarized and simplified in Figure 6.1.

Table 6.1. Material properties in DynaPile model

Material properties in model	Soil	Steel pile
Shear wave velocity (m/s)	100	3100
Poisson's ratio	0.25	0.3
Damping ratio (%)	5	2

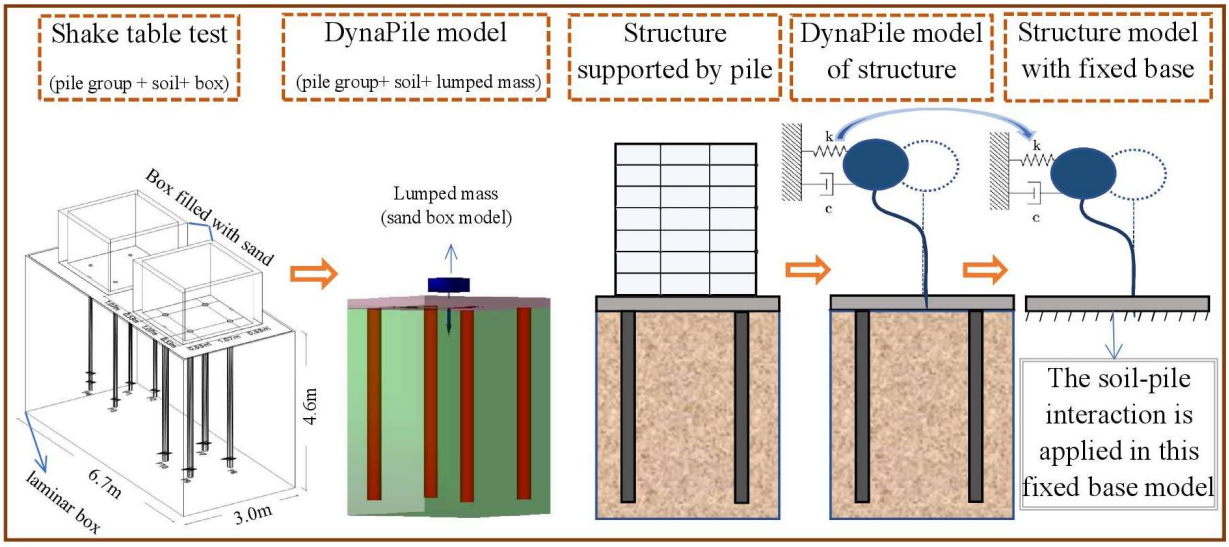

Figure 6.1. Schematic process of modeling

The skid stiffness was then modified, and the model was updated (e.g. k_x) each time to achieve the same response (e.g. maximum skid displacement) observed during the experiment. This iterative process was used to develop a calibrated model that is based on the experimental results. The obtained stiffness for the skid was assumed to be the total structural stiffness with consideration of soil and pile response. Then, two different models, including stiff skid (lumped mass as structure) on soft soil and flexible skid on stiff soil, with varying soil and structure properties presented in Table 6.2, were simulated using the basic calibrated model. In these models, the stiffness and damping ratio were designed to acquire the response regarding the allowable displacement for the steel frame (ASCE 1988): Typical total building drift limit is found

acceptable between H/100 (flexible structure) to H/600 (stiff structure) where Δ/H= total building drift; Δ= deflection of the most occupied floor; H= height of building. The weight of the skid in the experiment was compatible with a three-story building. Thus, the allowable total building displacement (lumped mass) for design was estimated to be 10 cm for a three-story building, when applying the deflection amplification factor suggested by NEHRP (Uang and Maarouf 1994). Finally, the stiffnesses of the superstructures in these two models that correlated with an allowable three-story structure drift were obtained. The stiffness for each story was estimated and then updated for a six-story building to be utilized in an available fixed base FE model in order to modify it to account for soil and pile response. Then, the 15 scaled earthquakes were loaded in the DynaPile model to achieve the stiffness for each specific motion based on allowable displacement. This latter data was used in IDA analysis for evaluation of vulnerability, which will be discussed in the following section.

Table 6.2. Condition and properties of models

Model conditions:	Original fixed base	Enhanced model on Winkler soil	Modified flexible structure on stiff soil	Modifed stiff structure on soft soil
k_x of six-story structure (MN/m)	60	60	40	88
Structural damping ratio	0.03	0.03	0.1	0.05
Soil shear wave velocity (m/s)	270	270	270	180

Note: Soil-pile interaction is not considered in the original model; in the modified model the structural properties are modified in order to take soil-pile interaction into account in fixed base condition.

6.4 Modifying the existing finite element model

Hassan and Mahmoud (2017) and Hassan and Mahmoud (2018), developed several numerical finite element models of a six-story steel frame hospital building with buckling-restrained braces

(BRBs), located in Memphis, Tennessee, using OpenSees, to evaluate the seismic performance of the structure. The structural frame consists of six bays in the North-South (N-S) direction and five bays in the East-West (E-W) direction. The total height of the building is 31.70 m (104 ft). The general 3D view of frame in both directions is depicted in Figure 6.2. A seismic design category of D, risk category of IV, and importance factor of 1.5 are used in the design. Seismic loading and design have been performed based on criteria in ASCE. The full design details of this hospital are specified in Hassan and Mahmoud (2018)'s study. The soil underneath the building was a weak soil, therefore it was replaced with stiff sand (NIST). They developed two models: 1) basic fixed base and 2) an enhanced model accounting for strain hardening and fatigue damage considering soil interaction using Beam on Nonlinear Winkler Foundation (BNWF).

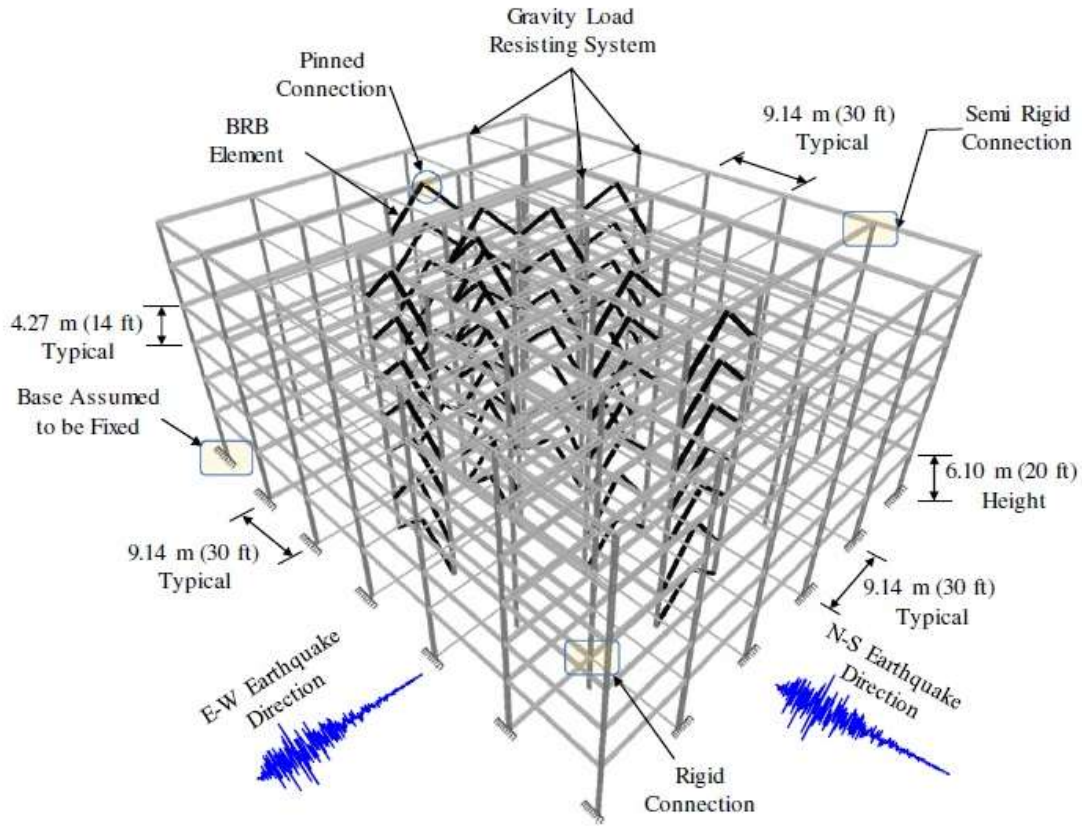

Figure 6.2. 3D view of modeled building frame (Hassan and Mahmoud 2017)

The results of the Dynapile model, which was calibrated based on a full scale experimental shake table test, were integrated into the fixed base 2D elastic-plastic FEM model of a lateral load resisting frame (without strain hardening and fatigue damage) from Hassan and Mahmoud (2017)'s study. In the FEM model, the same damping ratio as was used in DynaPile was implemented, while the structural stiffness was modified to achieve an equivalent DynaPile structural stiffness value. The structural stiffness in their model was achieved by running the pushover analysis. The slope of the generated load-displacement curve was assigned as total building stiffness. In this regard, the modulus of elasticity for steel were modified in the FEM model in order to reach the obtained stiffness from the dynamic model in Dynapile for each scaled earthquake motion. These modified models for two conditions (stiff structure on soft soil and flexible structure on stiff soil) were supposed to reflect the soil and pile interaction. Modifications were not made to the connections and the bracing systems, since they are the source of non-linearity in the structure and alteration of their properties could impact the sequence of plastic hinge formation in the system as a whole (Mahmoud 2011 and Mahmoud et al. 2013).

6.5 Developing fragility curves for the modified models

Seismic vulnerability and risk assessment of buildings and other structures requires characterization of earthquake hazards, usually by a suite of appropriate ground motions, determination of structural response (structural demand), identification of performance limits (structural capacity), and degrees of structural damage and losses associated with specific damage states.

The fragility curves were generated with the following steps: 1) 15 far field ground motion time histories with distances greater than 10 km were derived from FEMA P695 (2009); Shome et

al. (1998) have shown that for mid-rise buildings, ten to twenty records are usually enough to provide enough accuracy in the estimation of seismic demands. 2) earthquake records were scaled to different excitation levels to obtain elastic to collapse response in accordance with FEMA P695 (2009); 3) the analytical fixed base model was developed in OpenSees by Hassan and Mahmoud (2018); 4) the scaled ground motion records were applied to the system; 5) damage state limits were found for a mid-rise steel structure of hospital occupancy class (COM6) and high code seismic design level from Hazus- MH 2.1 (2003); slight, moderate, extensive and complete damage states are categorized by an inter-story drift ratio (IDR) of 0.0033, 0.0067, 0.02 and 0.0533, respectively; 6) the maximum IDRs as structural response for each excitation level (peak ground acceleration (PGA)) of each earthquake were obtained from the IDA analysis; 7) the corresponding exact PGA of each earthquake for each threshold drift from the previous step was determined by interpolation between two close values. Thus, for each damage limit, several values of PGAs were achieved; 8) for each damage state, a lognormal cumulative distribution function (CDF) was used to fit the curve on a lognormal probability scale using the EasyFit program and the fragility curve for each damage state was developed. The whole process is summarized in Figure 6.3.

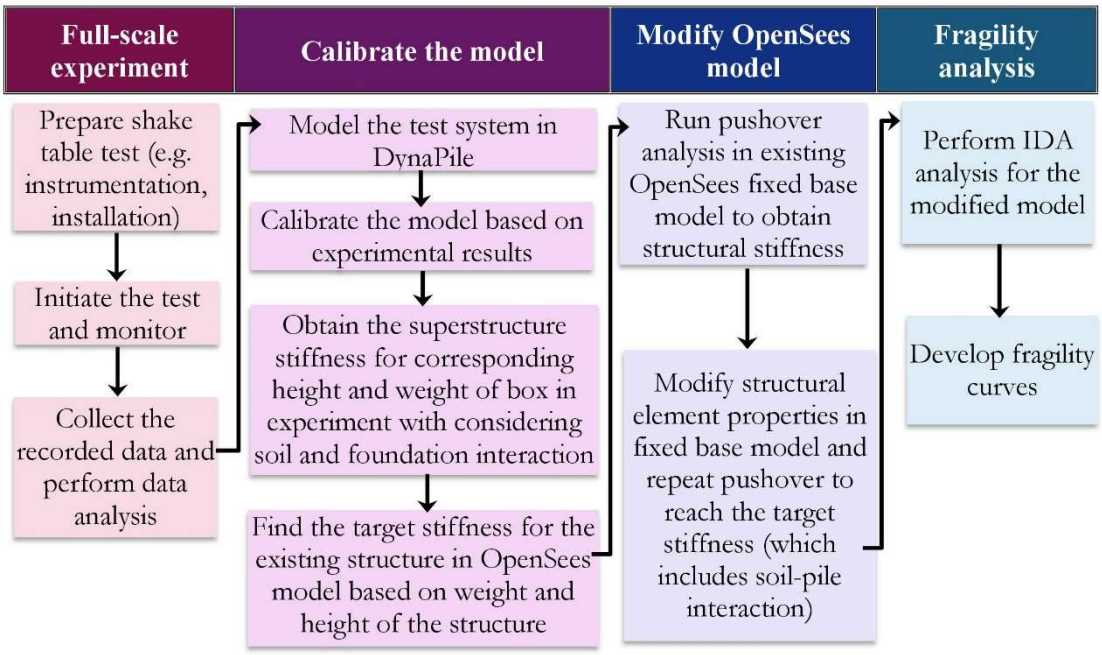

Figure 6.3. Flowchart of fragility curve development from physical and finite element model

6.6 Results and discussion

The vulnerability of two structural conditions (stiff or flexible) subject to seismic loading are discussed and compared with fixed base with and without the effect of soil.

6.6.1 Incremental dynamic analysis (IDA) curves

IDA curves were developed to evaluate the impact of different designs on the structural response. In these curves, the ranges of maximum acceleration of earthquake motions that cause each damage state can be observed and the earlier results can be seen more clearly. In Figure 6.4 a and b, the IDA curves for each of the 15 earthquakes (light gray lines) as well as the mean IDA curve (thick black line) are plotted for flexible and stiff structures, respectively. It is apparent that during a lower intensity earthquake (S_a < 0.5 g), inter story drift ratio (IDR) is higher for a flexible structure under the same motion compared to stiff structure. Under stronger ground motions (S_a >

0.75g) a stiff structure founded on soft soil shows a higher IDR and reaches the complete damage state, while the flexible structure reaches just the extensive damage limit state boundary. Figure 6.4 c, illustrates the comparison of mean IDA for three types of design conditions (fixed base; flexible structure on stiff soil and stiff structure on soft soil). The fixed base design below Sa ≈ 0.8g appears to be a conservative design, while under higher ground accelerations, the stiff structure on soft soil shows greater interstory drift (damage) and is more vulnerable. These results agree with the results of a study performed by Karapetrou et al. (2015). The corresponding Sa to reach each damage limit based on IDR are also presented in Table 6.3 for each model type.

Table 6.3. Ground motion acceleration (Sa(g)) limits to reach each damage state in each model

	Slight	Moderate	Extensive	Complete
Basic model	0.13	0.21	0.45	1.11
Modified flexible structure	0.18	0.24	0.40	1.09
Modified stiff structure	0.20	0.30	0.64	0.96

6.6.2 Flexible structure versus stiff structure

Fragility curves created using the IDA method, of both flexible and stiff structures in modified models are displayed in Figure 6.5 for each damage state. During a strong shaking event, it is less probable for a flexible structure on stiff soil to reach a complete damage state than a stiff structure on soft soil. This phenomenon reverses when the damage limit definition changes to slight, moderate and/or extensive. The damping ratio, which is higher in the flexible model, seems to be an effective factor in dissipating the energy of strong motions and decreasing the vulnerability of a structure under a complete damage state. Although stiffer structures may be more stable under static loading, in seismic design the more flexible structure might be less vulnerable to collapse.

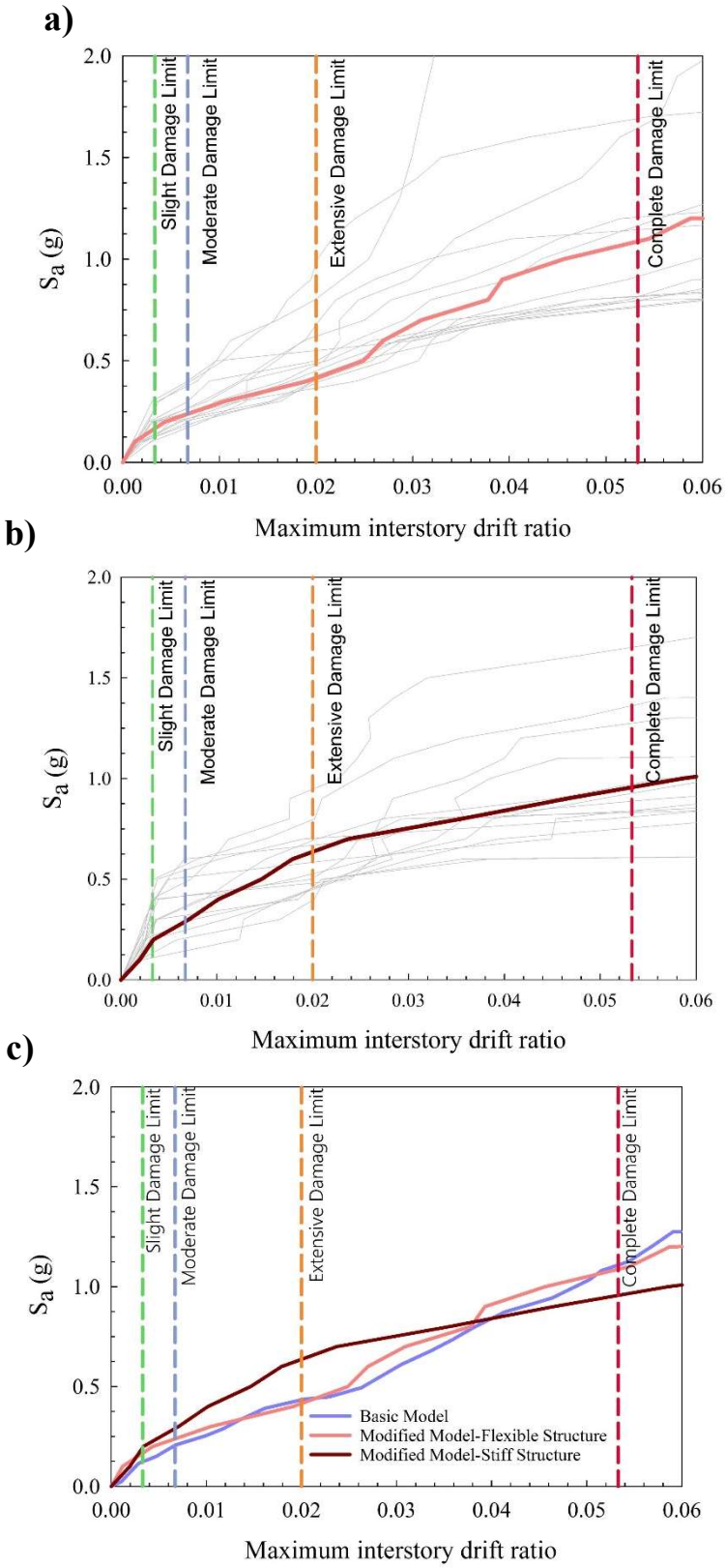

Figure 6.4. IDA curves for a) flexible structure on stiff soil; b) stiff structure on soft soil; c) all three models

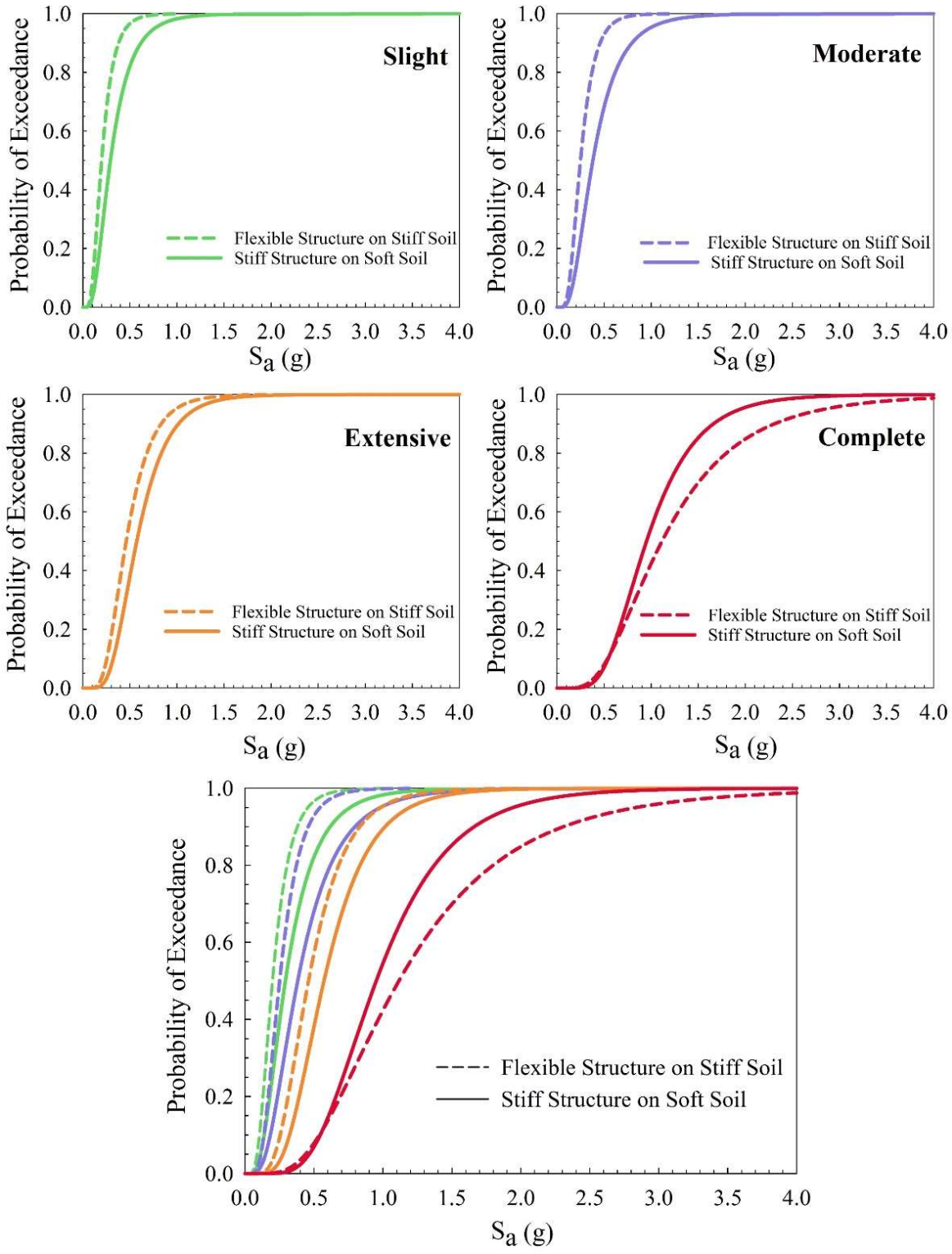

Figure 6.5. Comparing fragility curves for flexible structure on stiff soil versus stiff structure on soft soil at each damage limit

6.6.3 Fixed base design versus modified design considering pile and soil

Figure 6.6 demonstrates fragility curves for the fixed base model, the enhanced model that considered soil using the Winkler method (structure on Winkler soil), and the superstructure founded on pile groups with dynamic properties designed in DynaPile (modified fixed base accounting for soil-foundation-structure interaction (SFSI)). The conventional fixed base design may be conservative for slight and moderate damage states. In the case of the modified model (based on DynaPile), which includes the effect of soil and pile interaction, the probability of exceedance between the slight to extensive damage states is similar to, but always lower at higher accelerations than the fixed base structural response. In the complete damage state where collapse is probable, the modified fixed base structure at Sa<1.5g and the enhanced model on Winkler soil at Sa>1.5g show the highest risk of collapse. This might be due to the high nonlinear behavior of soil under strong earthquakes. Therefore, taking soil and pile foundation interaction into consideration when determining the structural response of a building, should be considered in design of structures within earthquake prone areas.

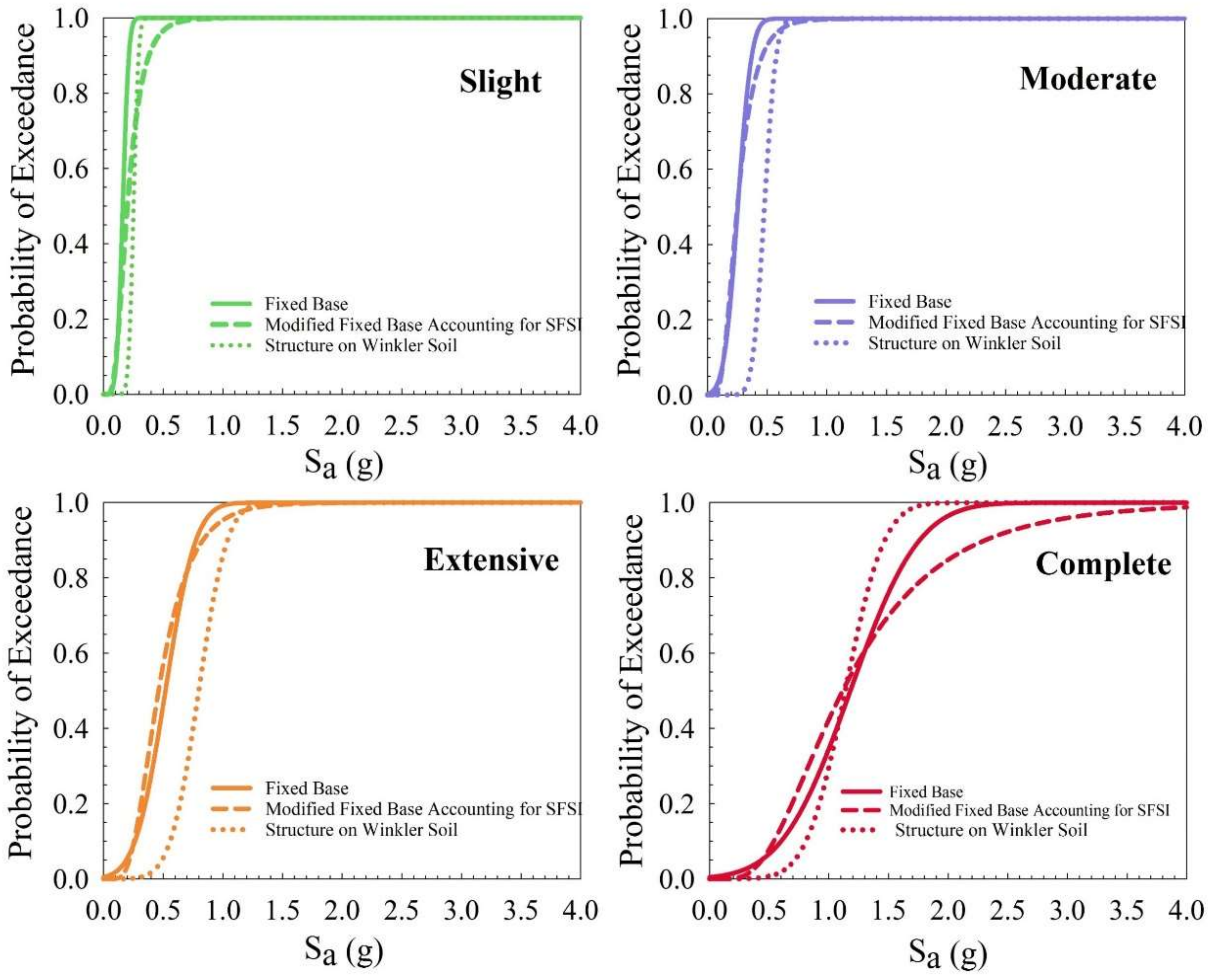

Figure 6.6. Comparing the design models in fragility of structure (Note: "SFSI" is Soil-Foundation-Structure interaction)

6.7 Conclusions

The vulnerability of a six-story steel frame building with buckling-restrained braces, including the effects of soil-structure interaction, was investigated. An existing fixed-base finite element model was modified based on the results of an experimental full-scale shake table test on helical pile group in dense sand to observe the effect of soil-pile behavior on seismic structural response in terms of fragility functions. The results were verified by IDA curves, which provides quantitative

correlation between ground acceleration and the corresponding inter story drift ratio and subsequently the damage states of three types of six-story hospital building designs.

The following highlighted results can be concluded:

- Although a flexible structure on stiff soil seems to be more vulnerable for possible slight, moderate, or extensive damage states, a stiff structure on soft soil is more likely to experience complete damage in a high intensity earthquake. The key consideration is whether the structure is flexible, and a weak earthquake is probable, or a structure is stiff and strong ground motion is anticipated in the location of construction.
- Soil and pile foundation interaction with structural response should be considered in the design within earthquake prone areas.

6.8 References

Allred, S. M. (2018). "Seismic performance of grouped helical piles in fixed and pinned connections." Master of Science, University of Oklahoma.

El-sawy, M. (2017). "Seismic performance of steel helical pile." Master of science, Master of science, The University of Western Ontario.

Federal Emergency Management Agency. FEMA 577: (2000). Recommended seismic evaluation and upgrade criteria for existing welded steel moment-frame buildings, Washington, DC.

Federal Emergency Management Agency. FEMA P695: (2009). Quantification of building seismic performance factors, Washington, DC.

Federal Emergency Management Agency. FEMA P-58-1 (2012). Seismic performance assessment of buildings. *Applied Technology Council (ATC)*.

Hassan, E. M., and Mahmoud, H. (2017). "Modeling resolution effects on the seismic response of a hospital steel building." *Journal of Constructional Steel Research*, 139, 254-271.

Hassan, E. M., and Mahmoud, H. (2018). "A framework for estimating immediate interdependent functionality reduction of a steel hospital following a seismic event." *Engineering Structures*, 168, 669-683.

HAZUS-MH 2.1 (2003). "Multi-hazard loss estimation methodology earthquake model."Washington, DC: FEMA-National Institute of Building Sciences.

Karapetrou, S. T., Fotopoulou, S. D., and Pitilakis, K. D. (2015). "Seismic vulnerability assessment of high-rise non-ductile RC buildings considering soil–structure interaction effects." *Soil Dynamics and Earthquake Engineering*, 73, 42-57.

Karim, K. R., and Yamazaki, F. (2001). "Effect of earthquake ground motions on fragility curves of highway bridge piers based on numerical simulation." *Earthquake Engng Struct. Dyn., John Wiley & Sons*, 30, 1839–1856.

Kinali, K. (2007). "Seismic Fragility Assessment of Steel Frames in the Central and Eastern United States." Doctor of Philosophy, Georgia Institute of Technology, Georgia Institute of Technology.

Kinali, K., and Ellingwood, B. R. J. E. s. (2007). "Seismic fragility assessment of steel frames for consequence-based engineering: A case study for Memphis, TN." 29(6), 1115-1127.

Mahmoud, H. N. (2011). "Seismic behavior of semi-rigid steel frames." Doctor of Philosophy, University of Illinois at Urbana-Champaign.

Mahmoud, H. N., Elnashai, A. S., Spencer Jr, B. F., Kwon, O.-S., and Bennier, D. J. (2013). "Hybrid simulation for earthquake response of semirigid partial-strength steel frames." *Journal of structural engineering*, 139(7), 1134-1148.

Mekki, M., Elachachi, S. M., Breysse, D., and Zoutat, M. (2016). "Seismic behavior of R.C. structures including soil-structure interaction and soil variability effects." *Engineering Structures*, 126, 15-26.

Mouroux, P., and Brun, B. L. (2003). *RISK-UE. An advanced approach to earthquake risk scenarios with applications to different European towns*.

Nakhaei, M., and Ghannad, M. A. (2008). "The effect of soil–structure interaction on damage index of buildings." *Engineering Structures*, 30(6), 1491-1499.

Nielson, B. G. (2005). "Analytical Fragility Curves for Highway Bridges in Moderate Seismic Zones." Doctor of Philosophy, Georgia Institute of Technology.

Padgett, J. E. (2007). "Seismic Vulnerability Assessment of Retrofitted Bridges Using Probabilistic Methods." Doctor of Philosophy, Georgia Institute of Technology.

Park, Y.-J. (1985). "Seismic Damage Analysis and Damage-Limiting Design for R/c Structures (Earthquake, Building, Reliability, Design)." University of Illinois at Urbana-Champaign.

Park, Y.-J., Ang, A. H.-S., and Wen, Y. K. (1985). "Seismic damage analysis of reinforced concrete buildings." *J Struct Eng ASCE*, 111(4), 740-757.

Porter, K. (2016). "A Beginner's Guide to Fragility, Vulnerability, and Risk."University of Colorado Boulder

Rajeev, P., and Tesfamariam, S. (2012). "Seismic fragilities of non-ductile reinforced concrete frames with consideration of soil structure interaction." *Soil Dynamics and Earthquake Engineering*, 40, 78-86.

Shahbazi, M., Cerato, A. B., Allred, S., El Naggar, M. H., and Elgamal, A. (2019). "Damping Characteristics of Full-Scale Grouped Helical Piles in Dense Sands Subject to Small and Large Shaking Events." *Canadian Geotechnical Journal*.

Shahbazi, M., Rowshanzamir, M., Abtahi, S. M., & Hejazi, S. M. J. A. C. S. (2017). "Optimization of carpet waste fibers and steel slag particles to reinforce expansive soil using response surface methodology". *142*, 185-192.

Shinozuka, M., Feng, M. Q., Lee, J., and Naganuma4, T. (2000). "Statistical Analysis of Fragility Curves." *J. Eng. Mech., ASCE*, 126(12), 1224-1231.

Shome, N., Cornell, C. A., Bazzurro, P., and Carballo, J. E. (1998). "Earthquakes, Records, and Nonlinear Responses." *Earthquake Spectra*, 14(3), 469-500.

Tang, Y., and Zhang, J. (2011). "Probabilistic seismic demand analysis of a slender RC shear wall considering soil–structure interaction effects." *Engineering Structures*, 33(1), 218-229.

Tehrani, M. H., and Harvey, P. S. (2019). "Generation of synthetic accelerograms for telecommunications equipment: fragility assessment of a rolling isolation system." *Bulletin of Earthquake Engineering*, 17(3), 1715-1737.

Uang, C.-M., and Maarouf, A. (1994). "Deflection amplification factor for seismic design provisions." *Journal of structural engineering*, 120(8), 2423-2436.

Vamvatsikos, D., Cornell, C. A. J. E. E., and Dynamics, S. (2002). "Incremental dynamic analysis." 31(3), 491-514.

Chapter 7 : CONCLUSIONS AND RECOMMENDATIONS

7.1 Overview

A full-scale field study on the seismic behavior of helical piles with varying parameters subjected to white noise and two replicated earthquakes was performed in dense sands using the outdoor shake table at UCSD. The experimental results were analyzed to determine dynamic properties of individual and grouped helical piles. These properties were used to better understand the seismic behavior of helical pile groups and study the effect of several parameters on behavior, including strain magnitude, instrumentation type and location, pile-structure connection, pile slenderness ratio and soil depth.

The results of experimental soil-helical pile-structure system were used to create and calibrate a model in DynaPile. This calibrated Dynapile model was able to provide realistic results that engineers can use when determining the effect of SSI on soil-pile-structure systems. Experimentally testing full-scale systems within the full range of what could be encountered in the field can be costly and therefore it is imperative that computer models be created and calibrated with high quality experimental testing results to help engineers simulate a wide range of parameters on seismic performance. The stiffness of the tested structure and pile group have been discussed and the quantitative results are developed accordingly. The interaction of soil and helical pile-supported structures have also been analyzed and discussed.

The vulnerability of a structure including the effects of helical piles behavior was also investigated. The existing fixed-base finite element model in OpenSees was modified based on the

results of an experimental full-scale shake table test on helical pile group in dense sand to observe the effect of soil-pile behavior on seismic structural response in terms of fragility. The results were verified by IDA curves, which provides the quantitative data on ground acceleration and corresponding inter story drift ratio and subsequently the damage states of three types of six-story hospital building designs.

The following highlighted results can be concluded:

7.2 Highlighted conclusions

1. Each damping calculation method has its own limitations, assumptions and approximations. Using data from this study, however, suggest that these methods are all valid to be used in assessing the seismic behavior of a soil-pile system, based on specific conditions. The log decrement method appeared to be appropriate for smaller strain applications during the pulse input motions. The half power bandwidth method seems to work well for a wider range of strain responses for a soil-pile system, but not for a soil system alone, due to the development of increasing nonlinear behavior. The energy method, in which the corresponding maximum deflection loop is considered in calculations, provides a good estimation of "equivalent" maximum damping for both small and large vibrations on piles and through soil when it is compared to values from other methods. Finally, modal analysis does not seem to show reasonable results on the tested soil-pile system during either white noise or earthquake input motions. There is not one method that is appropriate for all conditions, and therefore, a careful consideration of how to match each method with experimental data set is warranted.

2. ζ increases regardless of structure type when motions become increasingly vigorous, which is attributed to the incremental increase in deflection. Thus, greater deflection contributes to greater

ζ. This deflection depends on the intensity and frequency content of load and natural frequency of system.

3. When comparing the results of damping ratios calculated from individual pile strain gauges and single accelerometers at the center of a structure mass, it was found that the individual pile strain gauges produced a much larger damping ratio than using the center-of-mass group accelerometer. When deciding on instrumentation needs on a large-scale foundation project, it may be appropriate to consider that a single accelerometer may provide results with less errors than using a mathematical fitting method through multiple pile strain gauges.

4. The type of connection between the pile and structure significantly affect the performance of the structure, quantified by damping ratio. Both pile groups on Day 4 (Fixed connection) exhibit stiffer behavior (lower ζ and greater stiffness) compared to the same pile group on Day 5 (pinned connection) in all applied methods regardless of the amount of deformation.

5. All piles in this study, regardless of their geometries, demonstrate more flexible behavior (higher ζ) when they act individually. However, pile groups were observed to show higher energy dissipation overall compared with single piles.

6. On both Day 4 (fixed connection) and Day 5 (pinned connection), the pile group (Group 1) containing piles with higher slenderness ratios (83-91) demonstrated a greater ζ and lower stiffness values than group 2 (piles with slenderness ratios of 61). The higher the slenderness ratio, the higher the flexibility, which allows the pile more deflection and energy dissipation. This trend was true as well for individual piles. Adding a second helix, while not changing the slenderness ratio, increases the stiffness and as a result, the damping ratio decreased 12% approximately.

7. In general, shear strain initially increases with soil depth and then decreases. ζ varies with shear strain and the maximum occurs at the maximum shear strain. Shaking the laminar box containing just dense sand demonstrates significantly lower γ and ζ compared to Days 2-5, when there were piles in the soil. In other words, installing 10 piles in the laminar box filled with dense sand, increased damping ratio of soil by 17%.

8. The increase in a soil's shear wave velocity influences the seismic response of building and foundation positively and minimizes their displacements; this effect becomes negligible beyond a V_s of 200 m/s in our case of study.

9. Similarly, with a higher structural damping ratio, less displacement occurs in both the building and at the pile foundation.

10. Increasing the structural stiffness reduces the displacement of a building but it may cause a slight increase in the pile group's movement.

11. Regarding the structure's geometry, the building with a larger slenderness ratio provides more system freedom in movement under lateral loads.

12. In terms of displacement, the behavior of a flexible structure founded on stiff soil seems to fare better than a stiff structure founded on soft soil. When designing stiff buildings on soft soils, SSI should be considered. In a layered soil profile consisting of a stiffer soil underlain by a looser soil, the underlying looser soil contributes to the mitigation and dissipation of the ground motion's energy. If that looser soil can support the pile and structure without excessive settlement, potential bearing capacity failure, or liquefaction concerns, it may be beneficial to embed the piles into this type of soil to take advantage of its energy dissipation assets.

13. Although a flexible structure on stiff soil seems to be more vulnerable for possible slight, moderate, or extensive damage states, a stiff structure on soft soil is more likely to experience complete damage in a high intensity earthquake. The key consideration is whether the structure is flexible and a weak earthquake is probable, or a structure is stiff and strong ground motion is anticipated in the location of construction.

14. Soil and pile foundation interaction with structural response should be considered in the design within earthquake prone areas.

7.3 Recommendations for future studies

- This research provided the quantitative results on seismic behavior of helical piles in dense dry sand. Similar experimental tests would be suggested to be performed in different soil type (e.g. clay) and under different condition (e.g. saturated, unsaturated, liquefiable) to obtain more comprehensive view on seismic behavior of helical piles.
- In a numerical model (DynaPile), it may be useful to investigate the effect of varying the soil Poisson's ratio on the seismic behavior of a soil-pile system as it enters the inelastic zone.
- The sensitivity study for different conditions can be conducted by modeling (e.g. in DynaPile, DIANA FEA, OpenSees) different soil types (e.g. density, shear wave velocity, Poisson's ratio), pile material and pile arrangement in a group (e.g. yield strength, pile to pile distance), and integrating the results into a structural model.
- The lateral spacing between piles in this test was at the recommended spacing (3D) (Diameter of the helix, not shaft) to ignore pile interactions when loaded axially. Theoretically, because the diameter of the helix is used, which is typically much greater than the shaft diameter, when determining center-to-center spacing, the pile interaction within a pile group is considered

negligible. However, there have been no studies performed on this. It is recommended to further investigate helical pile group reduction factors when the pile group is loaded laterally. The effect of pile group interaction when loaded laterally can be assessed by varying the pile to pile distance in experiments and numerical models.

- The connection between the pile and the structure has been shown to significantly affect the super-structural behavior. A comprehensive study investigating this connection detail would be essential to better quantify the pile-system's effect on the structure. Simulating the exact helical pile-head connection with an equivalent replicated head connection in OpenSees, or another robust FEM program (e.g. DIANA FEA), is recommended. If the pile-head connection could be effectively modeled, then the modeled system would be a better representation of the experimental conditions and better able to produce realistic results with the existing fixed base structural model in OpenSees. Subsequently, the fragility curves extracted from this modeling effort will be able to accurately consider the effect of not only varying the size of the helical pile or soil type in the design but varying the pile head connections.
- When developing fragility curves and seismic risk assessment of structures, it is recommended that spectral velocity be investigated along with spectral acceleration

Appendix A

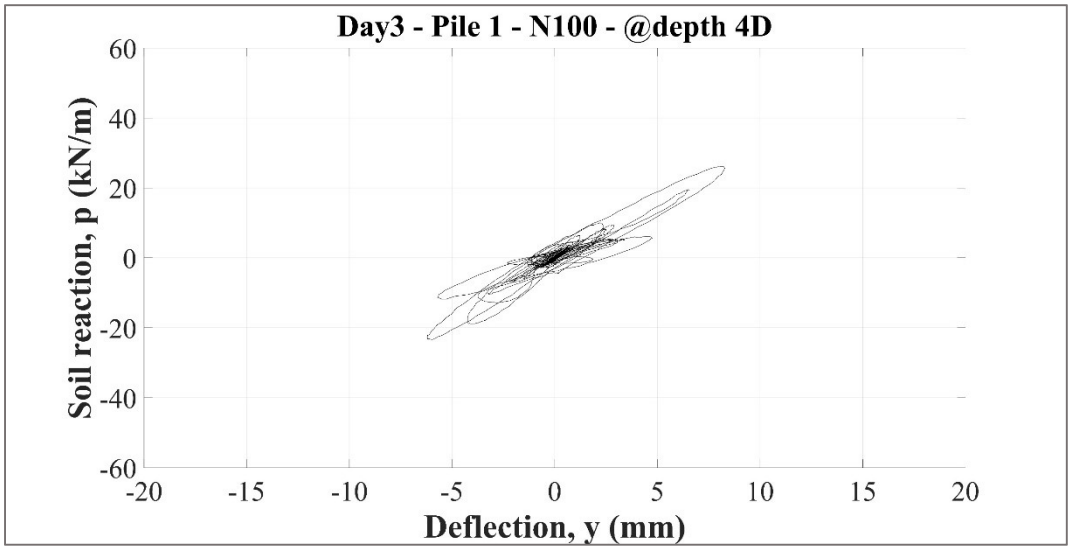
Day3 - Pile 1 - N100 - @depth 4D
Soil reaction, p (kN/m)
60
40
20
0
-20
-40
-60
-20
-15
-10
-5
0
5
10
15
20
Deflection, y (mm)

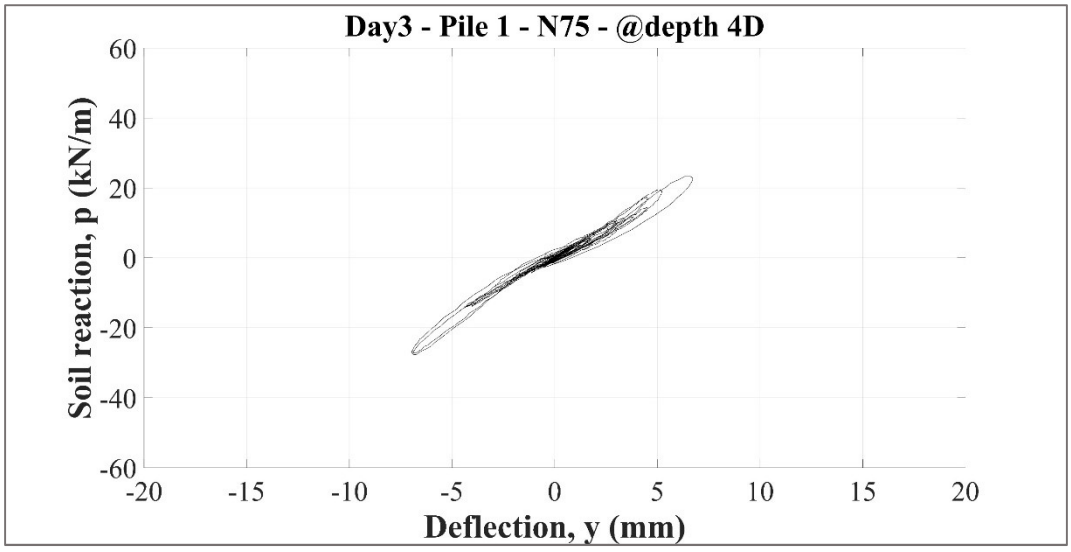
Day3 - Pile 1 - N75 - @depth 4D
Soil reaction, p (kN/m)
60
40
20
0
-20
-40
-60
-20
-15
-10
-5
0
5
10
15
20
Deflection, y (mm)

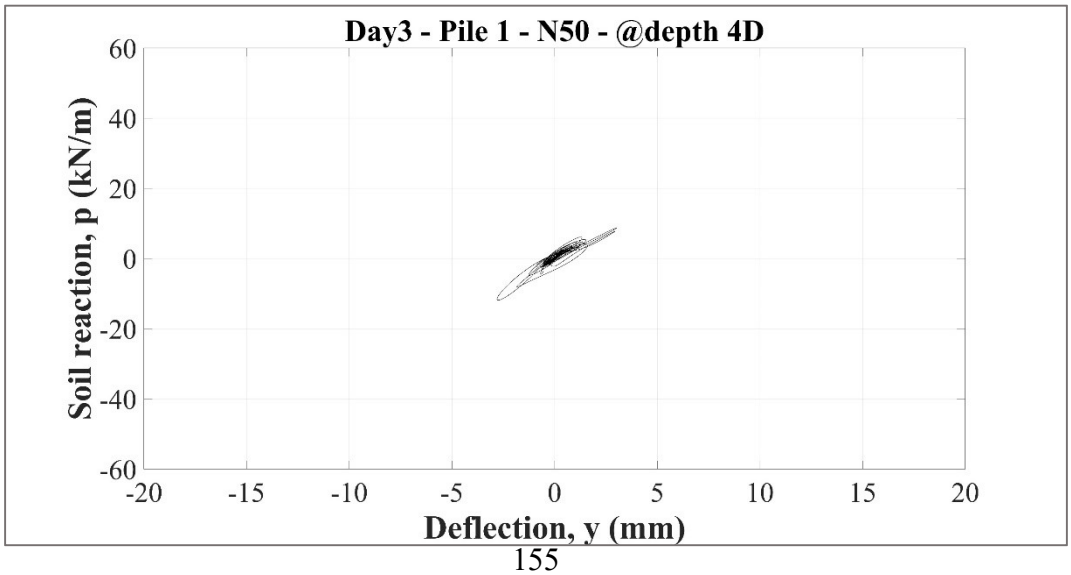
Day3 - Pile 1 - N50 - @depth 4D
Soil reaction, p (kN/m)
60
40
20
0
-20
-40
-60
-20
-15
-10
-5
0
5
10
15
20
Deflection, y (mm)

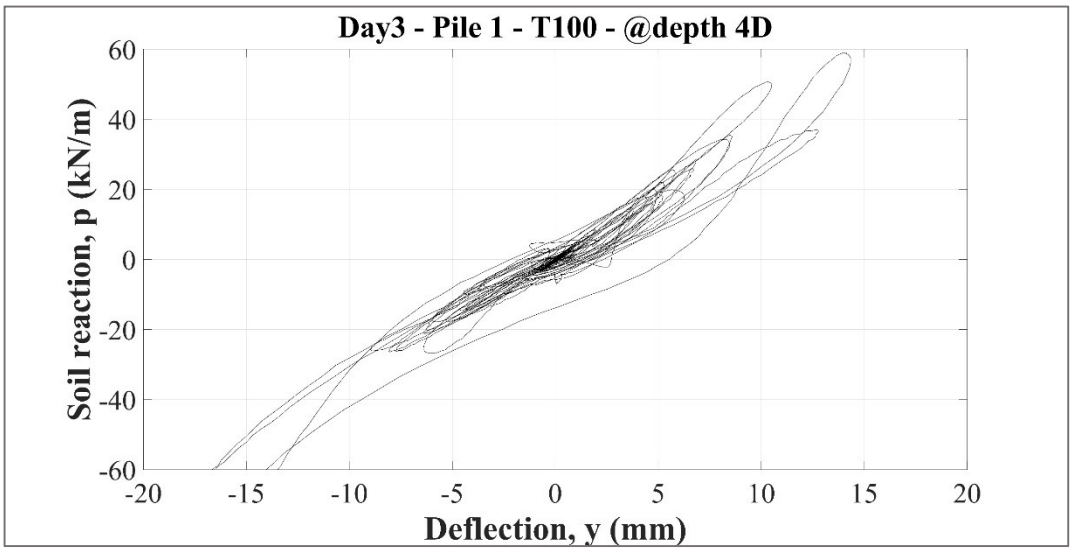
Day3 - Pile 1 - T100 - @depth 4D
Soil reaction, p (kN/m)
Deflection, y (mm)
60
40
20
0
-20
-40
-60
-20
-15
-10
-5
0
5
10
15
20

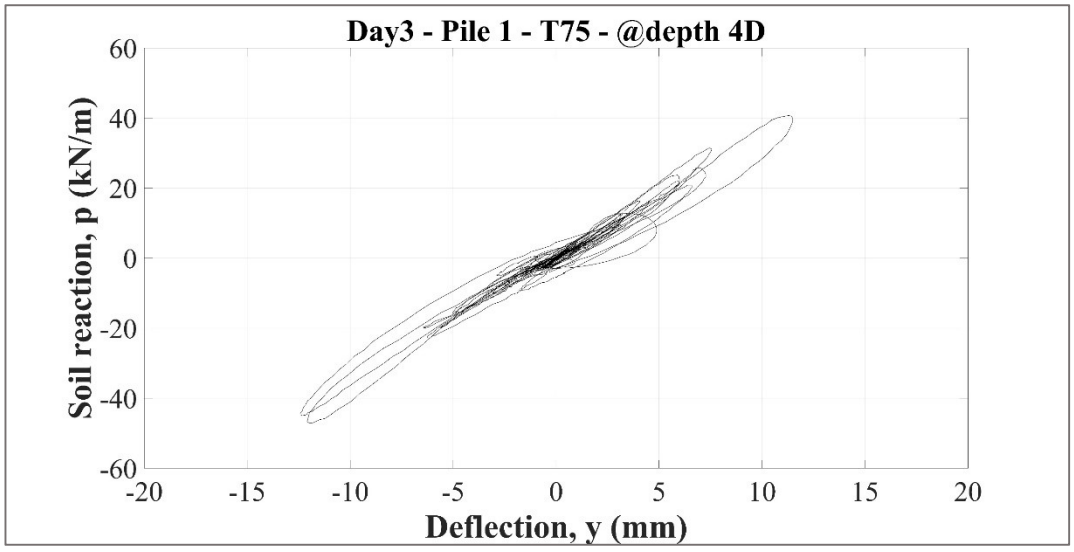
Day3 - Pile 1 - T75 - @depth 4D
Soil reaction, p (kN/m)
Deflection, y (mm)
60
40
20
0
-20
-40
-60
-20
-15
-10
-5
0
5
10
15
20

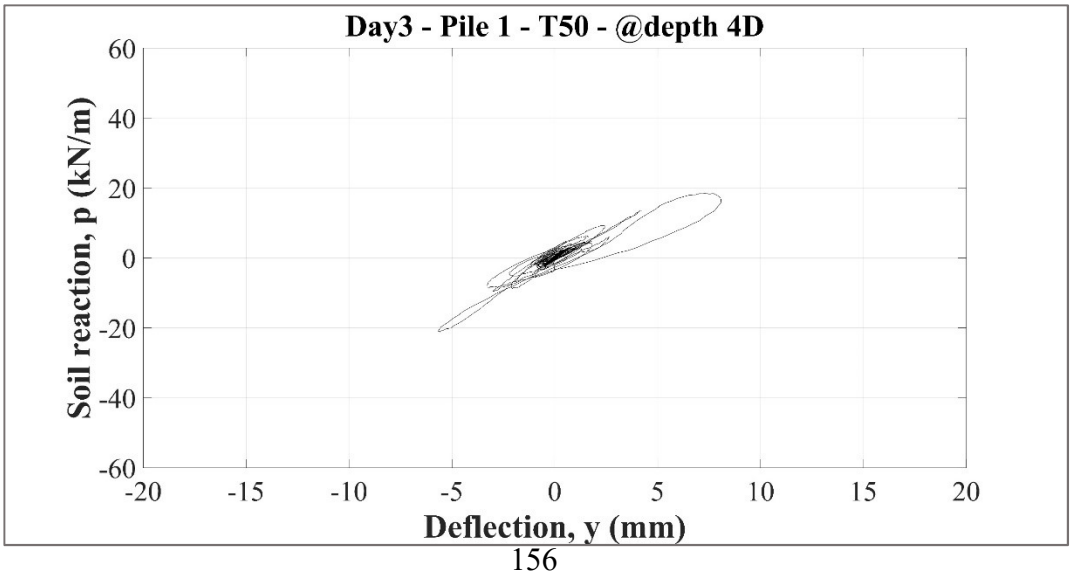
Day3 - Pile 1 - T50 - @depth 4D
Soil reaction, p (kN/m)
Deflection, y (mm)
60
40
20
0
-20
-40
-60
-20
-15
-10
-5
0
5
10
15
20

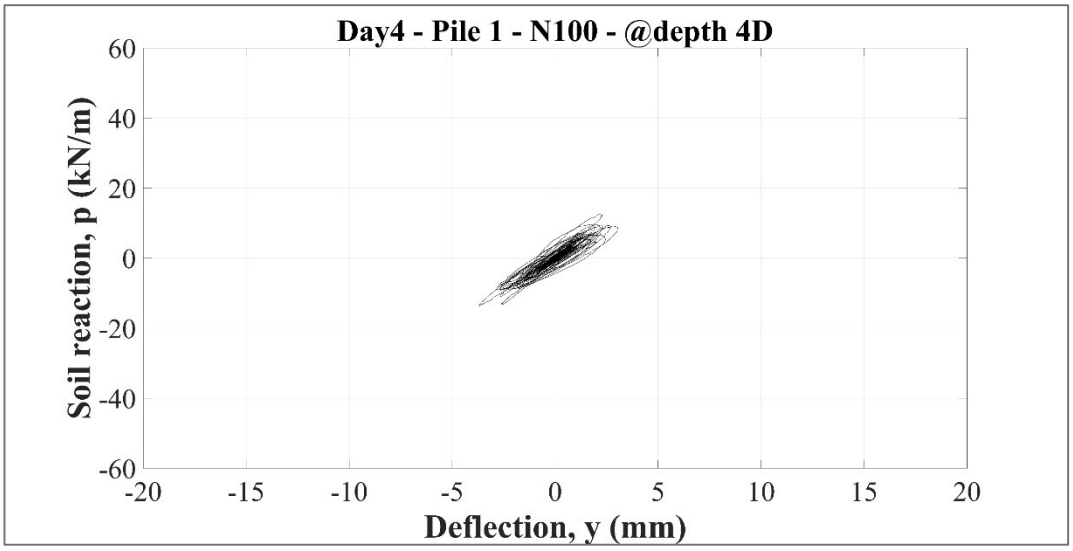
Day4 - Pile 1 - N100 - @depth 4D
Soil reaction, p (kN/m)
60
40
20
0
-20
-40
-60
-20
-15
-10
-5
0
5
10
15
20
Deflection, y (mm)

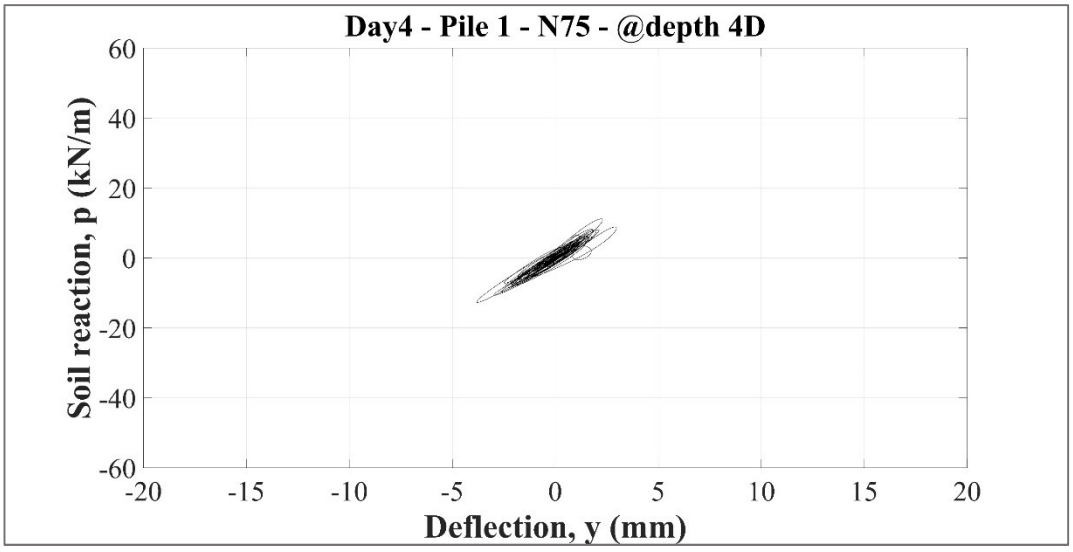
Day4 - Pile 1 - N75 - @depth 4D
Soil reaction, p (kN/m)
60
40
20
0
-20
-40
-60
-20
-15
-10
-5
0
5
10
15
20
Deflection, y (mm)

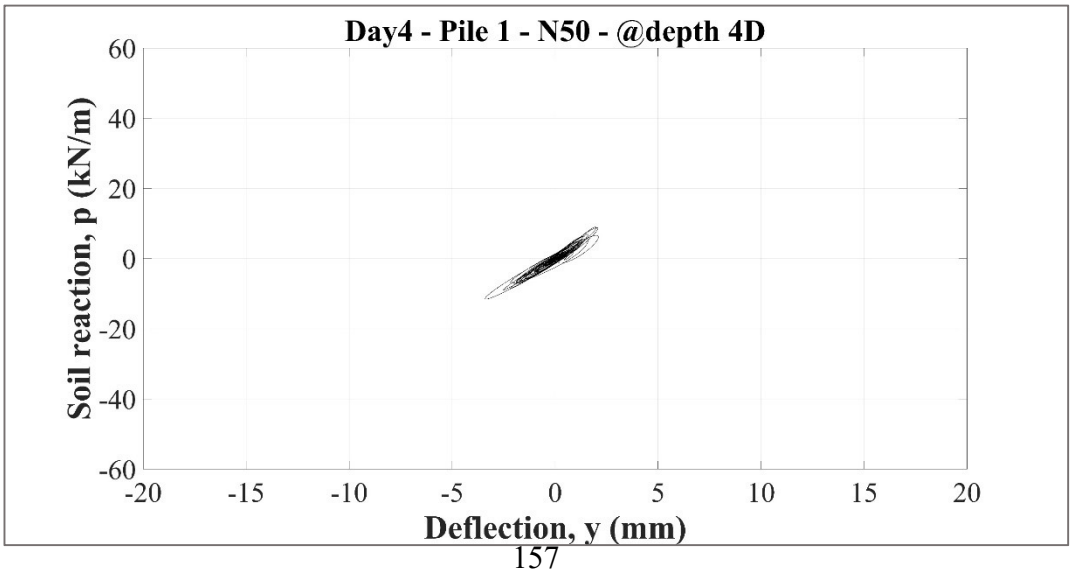
Day4 - Pile 1 - N50 - @depth 4D
Soil reaction, p (kN/m)
60
40
20
0
-20
-40
-60
-20
-15
-10
-5
0
5
10
15
20
Deflection, y (mm)

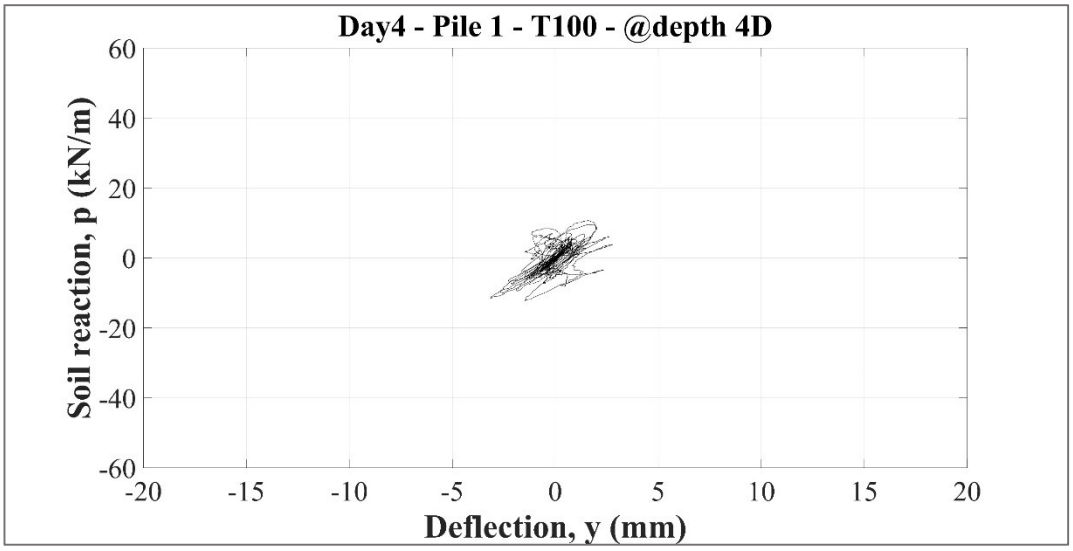
Day4 - Pile 1 - T100 - @depth 4D
Soil reaction, p (kN/m)
60
40
20
0
-20
-40
-60
-20
-15
-10
-5
0
5
10
15
20
Deflection, y (mm)

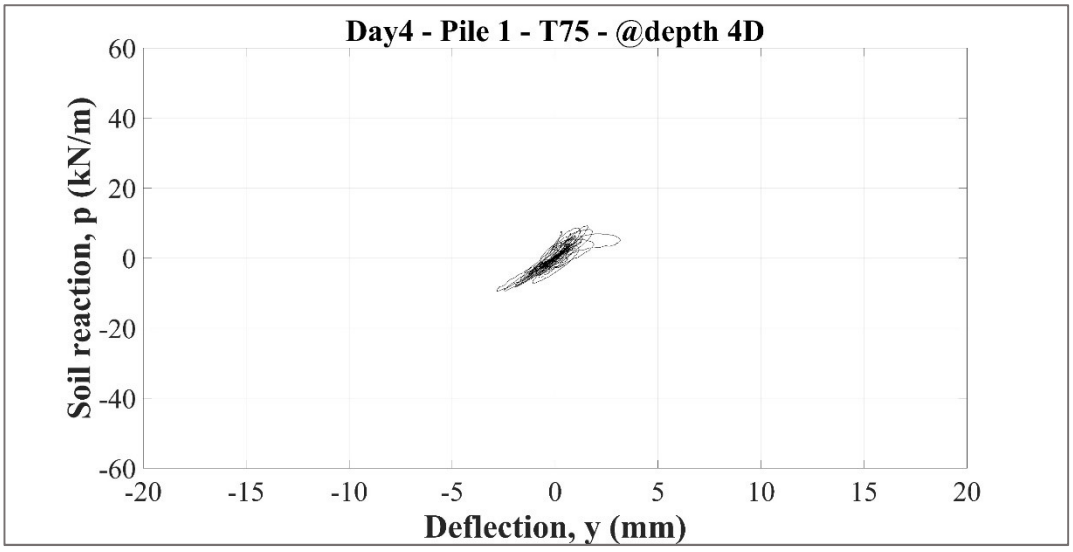
Day4 - Pile 1 - T75 - @depth 4D
Soil reaction, p (kN/m)
60
40
20
0
-20
-40
-60
-20
-15
-10
-5
0
5
10
15
20
Deflection, y (mm)

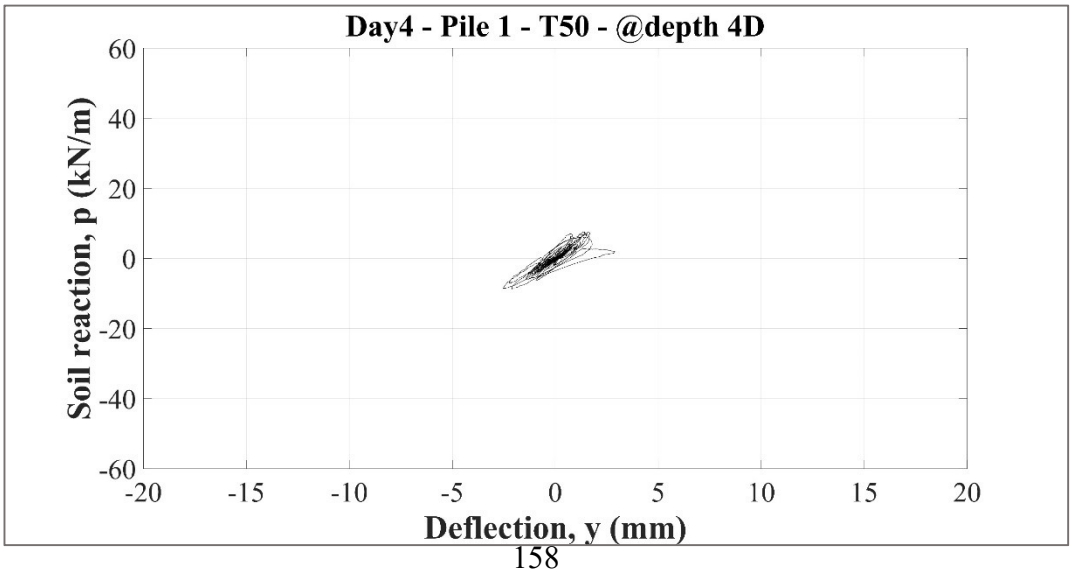
Day4 - Pile 1 - T50 - @depth 4D
Soil reaction, p (kN/m)
60
40
20
0
-20
-40
-60
-20
-15
-10
-5
0
5
10
15
20
Deflection, y (mm)

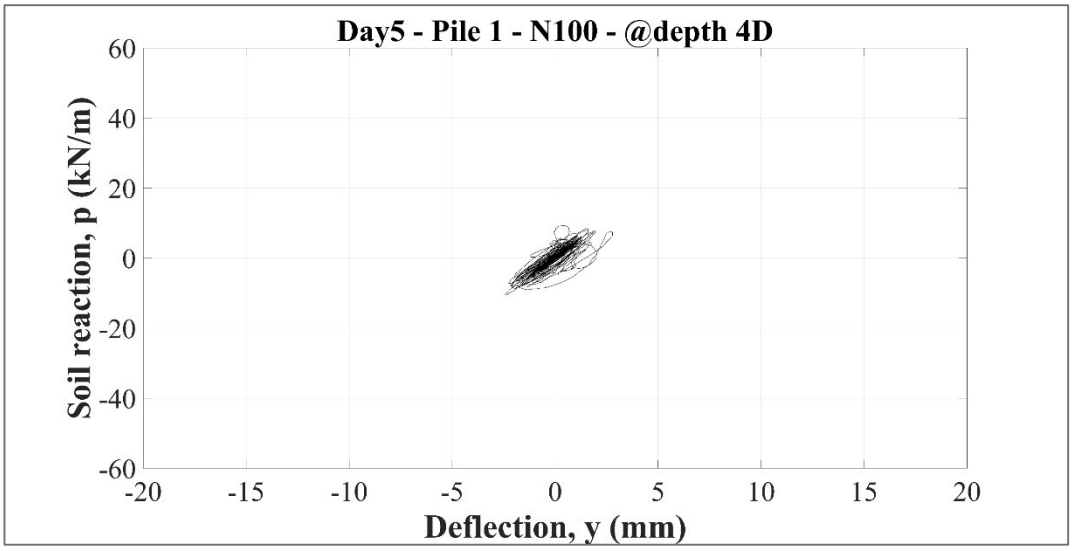
Day5 - Pile 1 - N100 - @depth 4D
Soil reaction, p (kN/m)
60
40
20
0
-20
-40
-60
-20
-15
-10
-5
0
5
10
15
20
Deflection, y (mm)

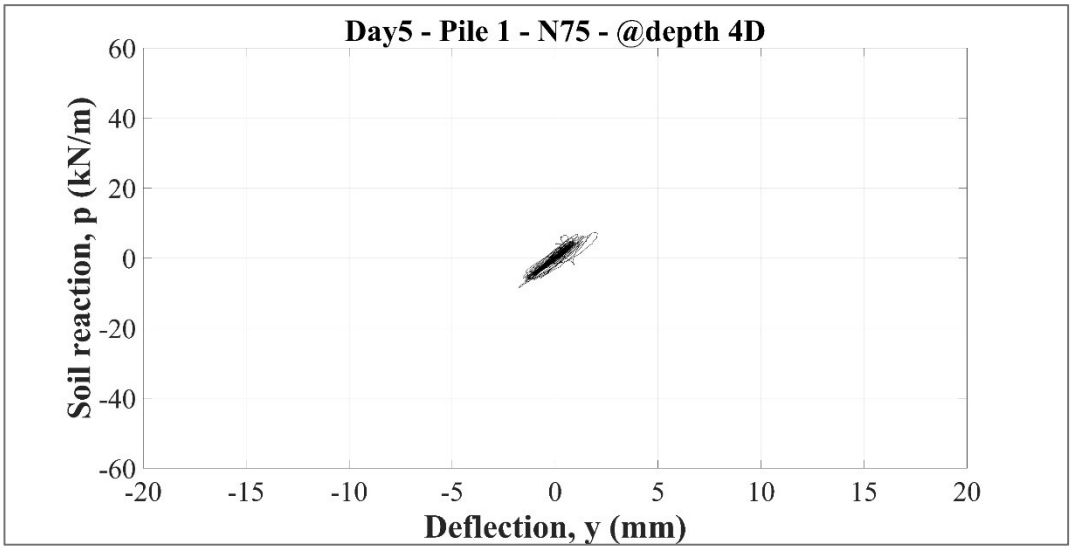
Day5 - Pile 1 - N75 - @depth 4D
Soil reaction, p (kN/m)
60
40
20
0
-20
-40
-60
-20
-15
-10
-5
0
5
10
15
20
Deflection, y (mm)

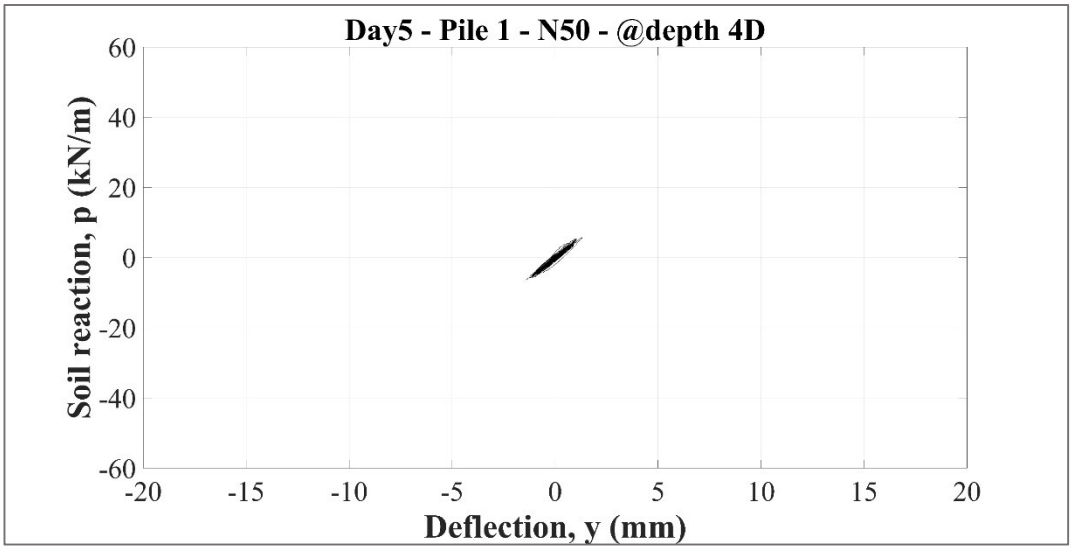
Day5 - Pile 1 - N50 - @depth 4D
Soil reaction, p (kN/m)
60
40
20
0
-20
-40
-60
-20
-15
-10
-5
0
5
10
15
20
Deflection, y (mm)

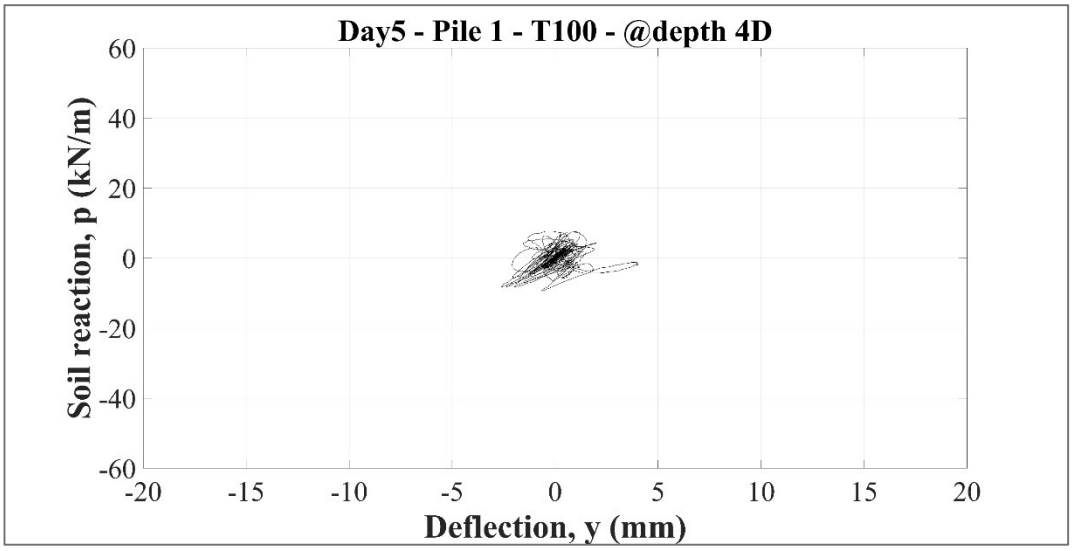
Day5 - Pile 1 - T100 - @depth 4D
Soil reaction, p (kN/m)
60
40
20
0
-20
-40
-60
-20
-15
-10
-5
0
5
10
15
20
Deflection, y (mm)

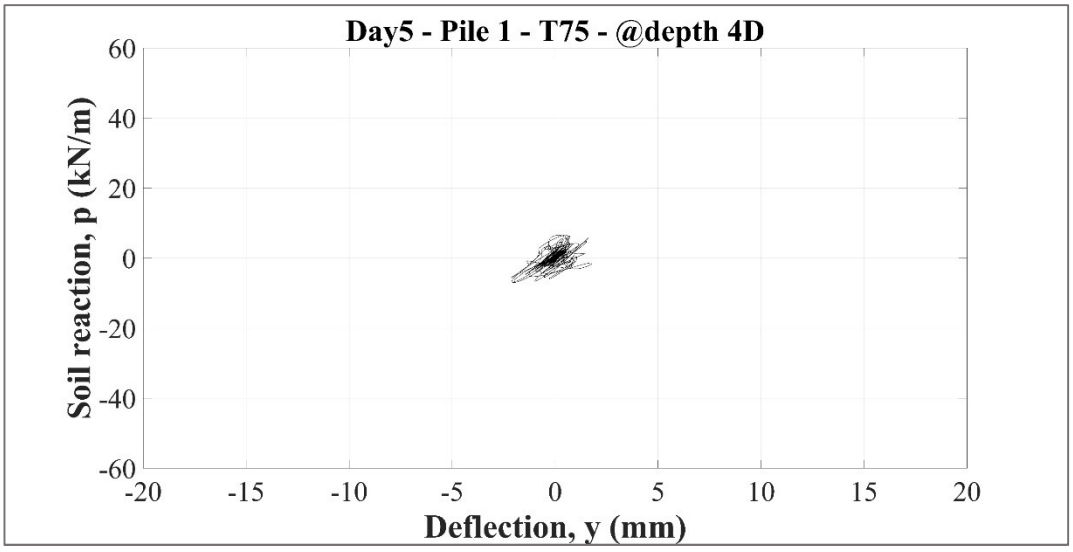
Day5 - Pile 1 - T75 - @depth 4D
Soil reaction, p (kN/m)
60
40
20
0
-20
-40
-60
-20
-15
-10
-5
0
5
10
15
20
Deflection, y (mm)

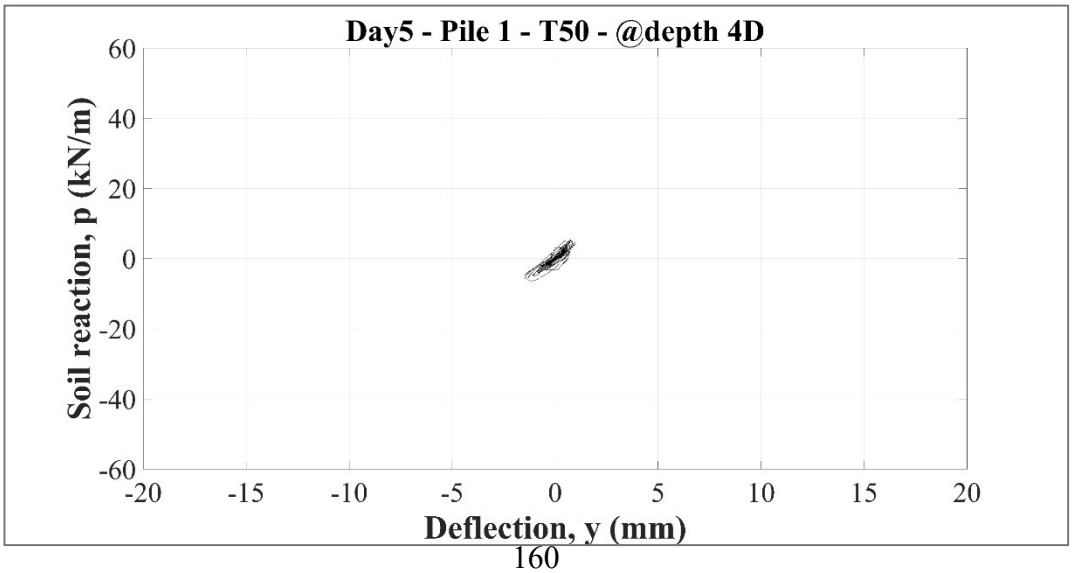
Day5 - Pile 1 - T50 - @depth 4D
Soil reaction, p (kN/m)
60
40
20
0
-20
-40
-60
-20
-15
-10
-5
0
5
10
15
20
Deflection, y (mm)

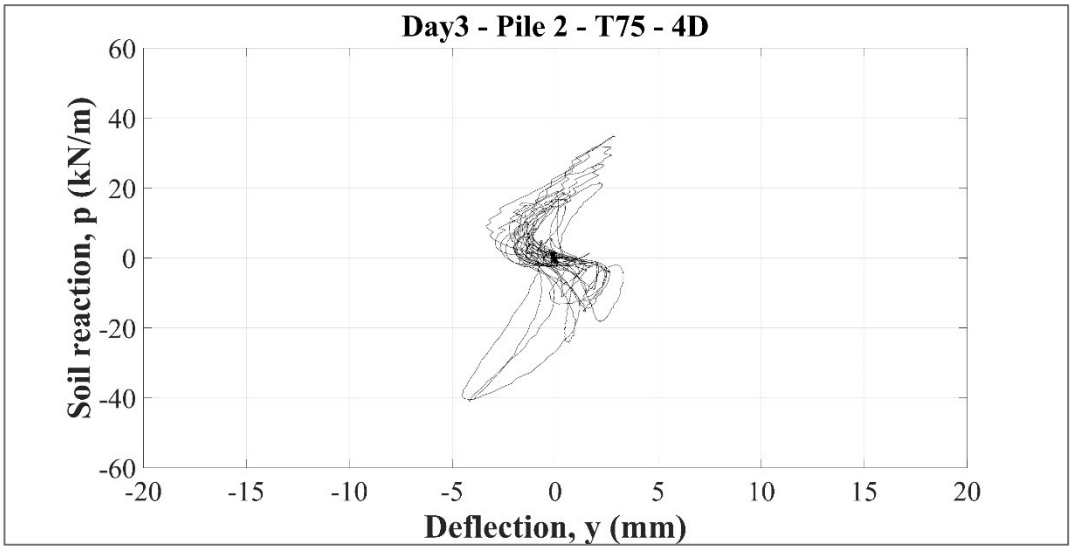
Day3 - Pile 2 - T75 - 4D
Soil reaction, p (kN/m)
60
40
20
0
-20
-40
-60
-20
-15
-10
-5
0
5
10
15
20
Deflection, y (mm)

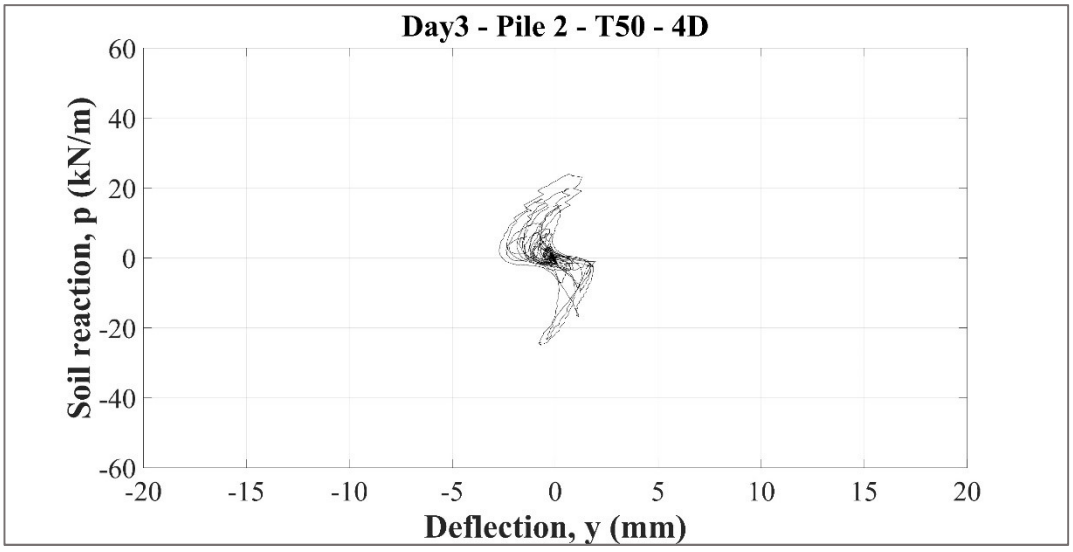
Day3 - Pile 2 - T50 - 4D
Soil reaction, p (kN/m)
60
40
20
0
-20
-40
-60
-20
-15
-10
-5
0
5
10
15
20
Deflection, y (mm)

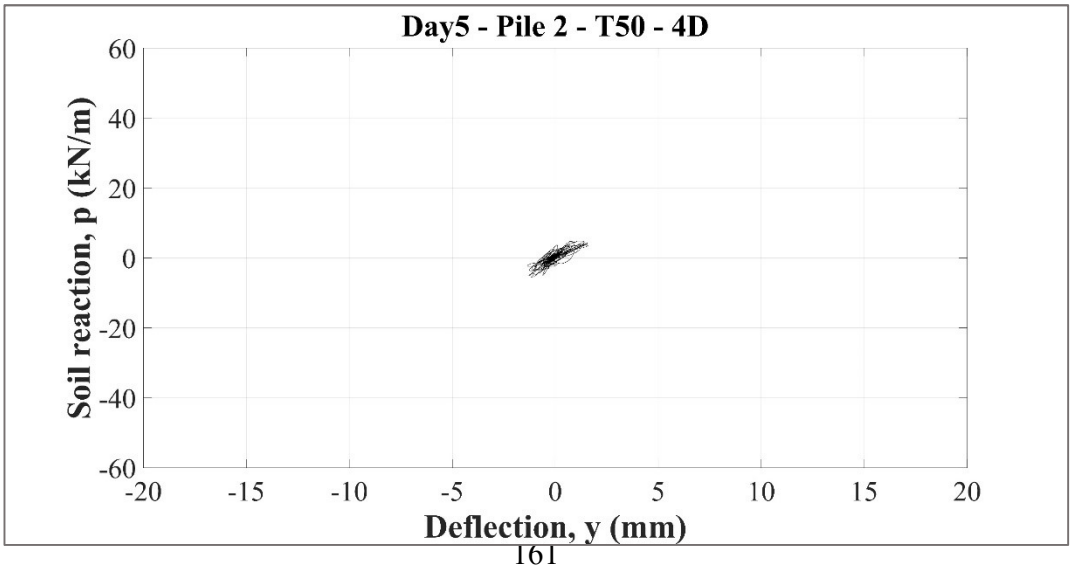
Day5 - Pile 2 - T50 - 4D
Soil reaction, p (kN/m)
60
40
20
0
-20
-40
-60
-20
-15
-10
-5
0
5
10
15
20
Deflection, y (mm)

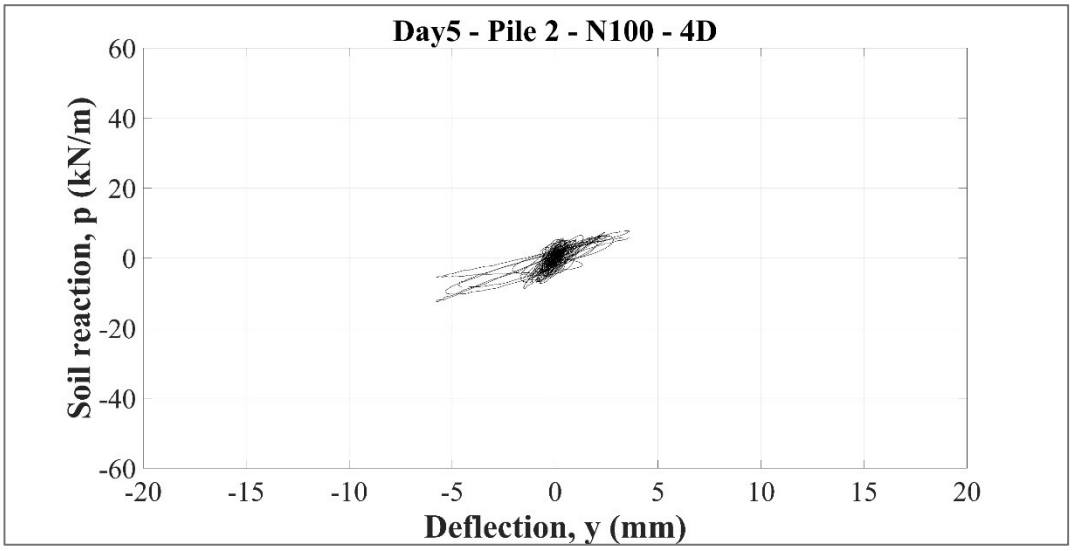
Day5 - Pile 2 - N100 - 4D
Soil reaction, p (kN/m)
60
40
20
0
-20
-40
-60
-20
-15
-10
-5
0
5
10
15
20
Deflection, y (mm)

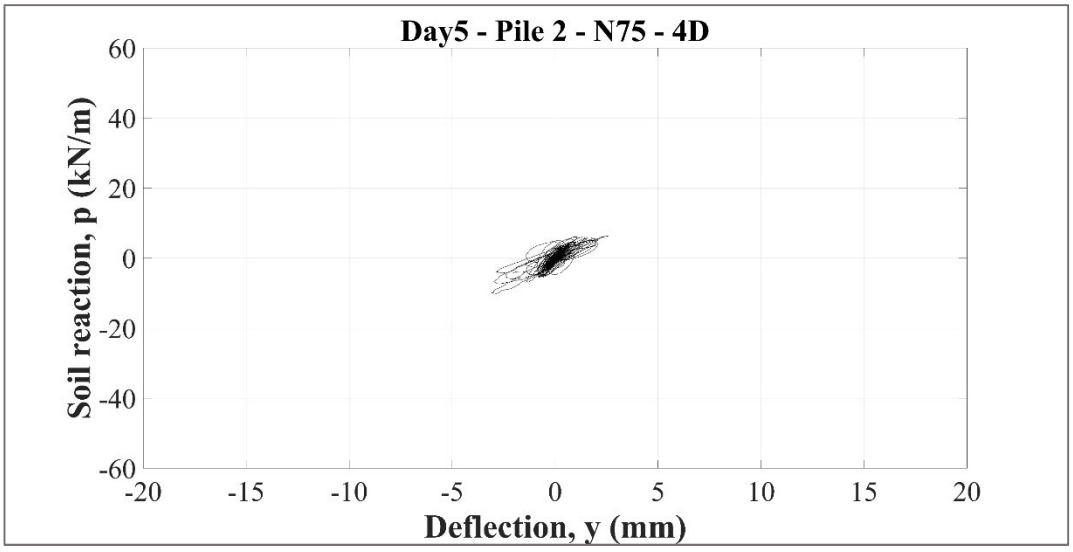
Day5 - Pile 2 - N75 - 4D
Soil reaction, p (kN/m)
60
40
20
0
-20
-40
-60
-20
-15
-10
-5
0
5
10
15
20
Deflection, y (mm)

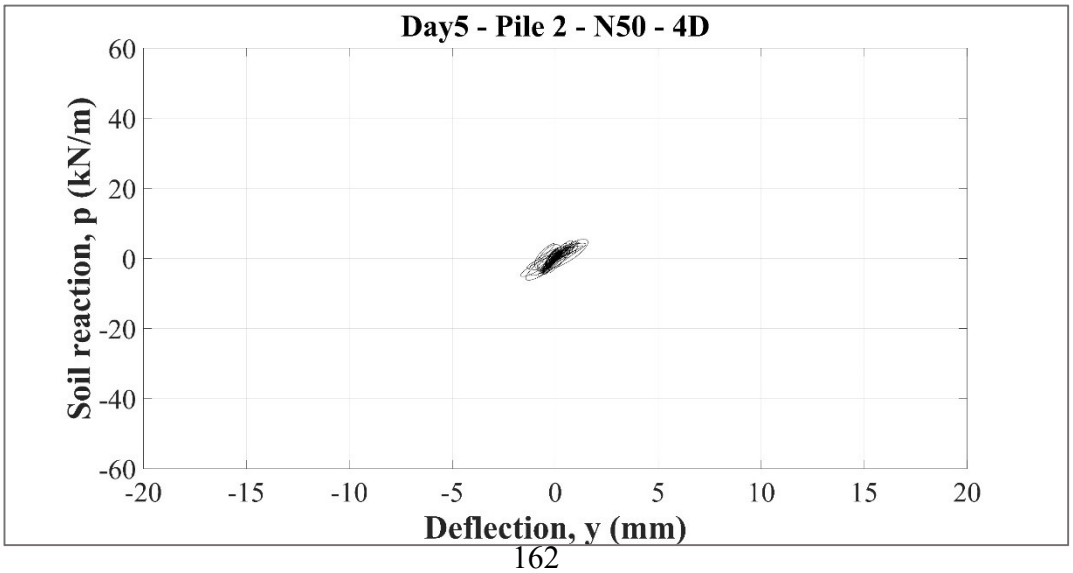
Day5 - Pile 2 - N50 - 4D
Soil reaction, p (kN/m)
60
40
20
0
-20
-40
-60
-20
-15
-10
-5
0
5
10
15
20
Deflection, y (mm)

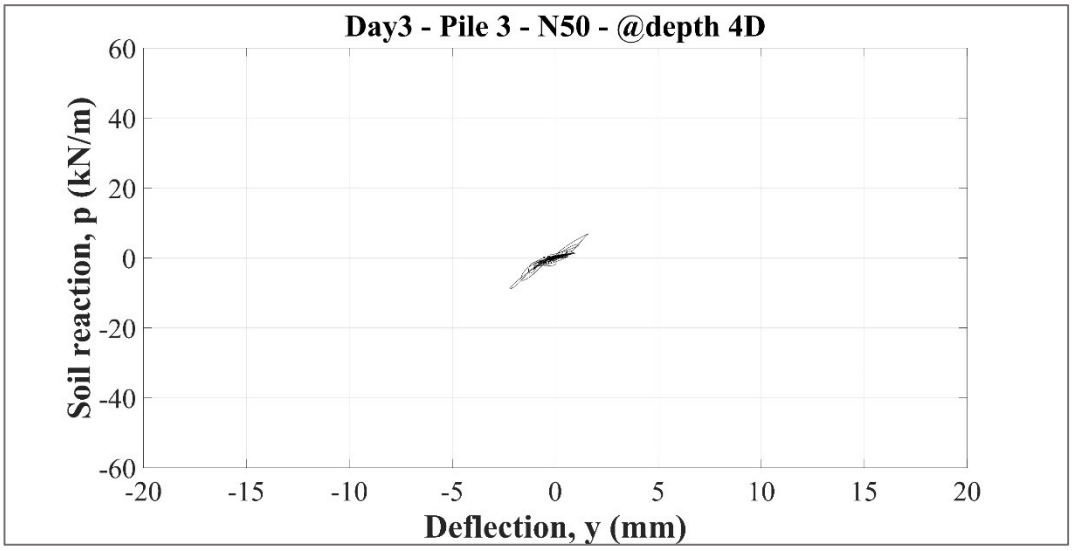
Day3 - Pile 3 - N50 - @depth 4D
Soil reaction, p (kN/m)
60
40
20
0
-20
-40
-60
-20
-15
-10
-5
0
5
10
15
20
Deflection, y (mm)

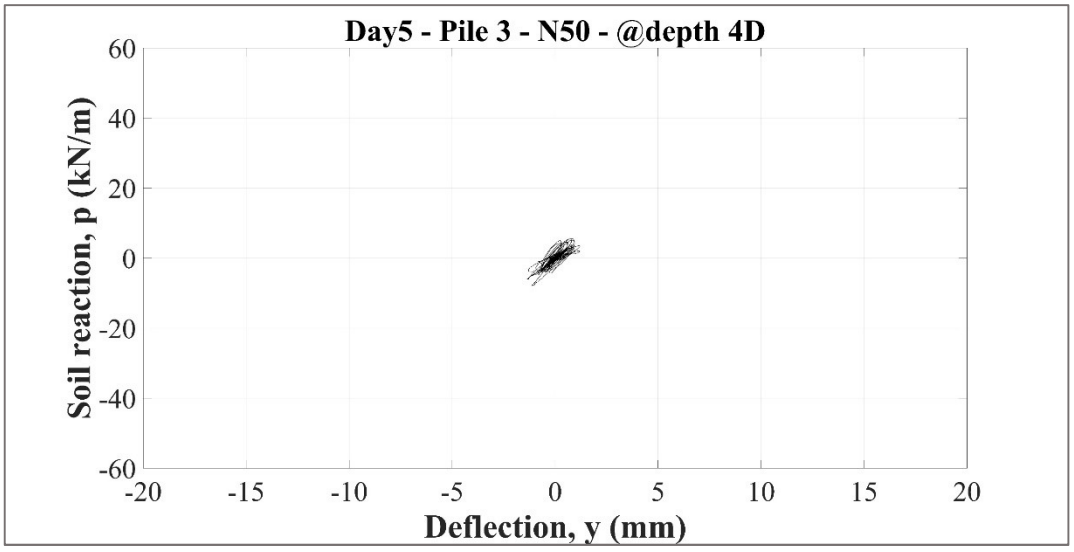
Day5 - Pile 3 - N50 - @depth 4D
Soil reaction, p (kN/m)
60
40
20
0
-20
-40
-60
-20
-15
-10
-5
0
5
10
15
20
Deflection, y (mm)

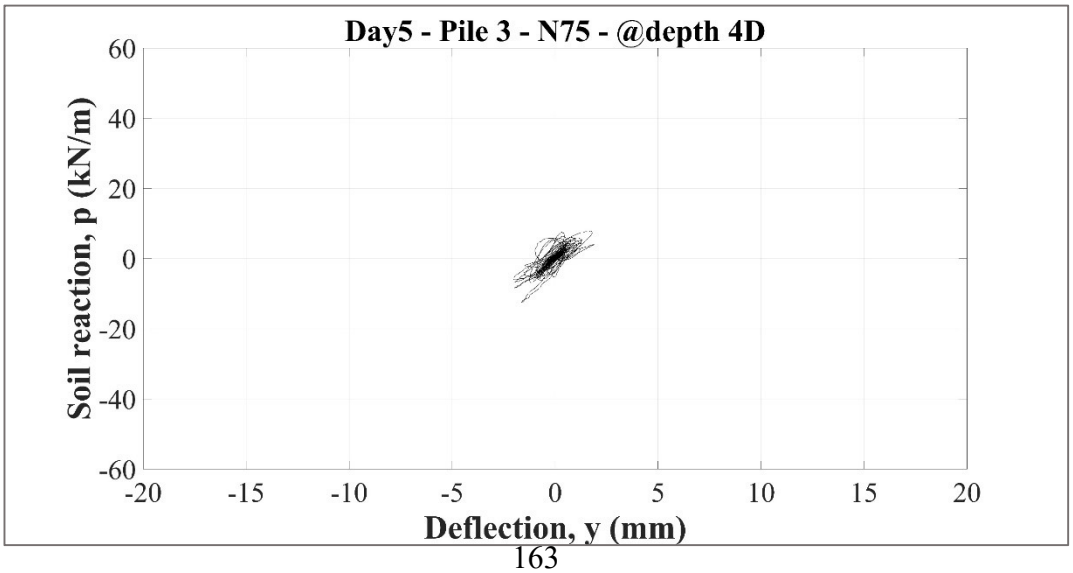
Day5 - Pile 3 - N75 - @depth 4D
Soil reaction, p (kN/m)
60
40
20
0
-20
-40
-60
-20
-15
-10
-5
0
5
10
15
20
Deflection, y (mm)

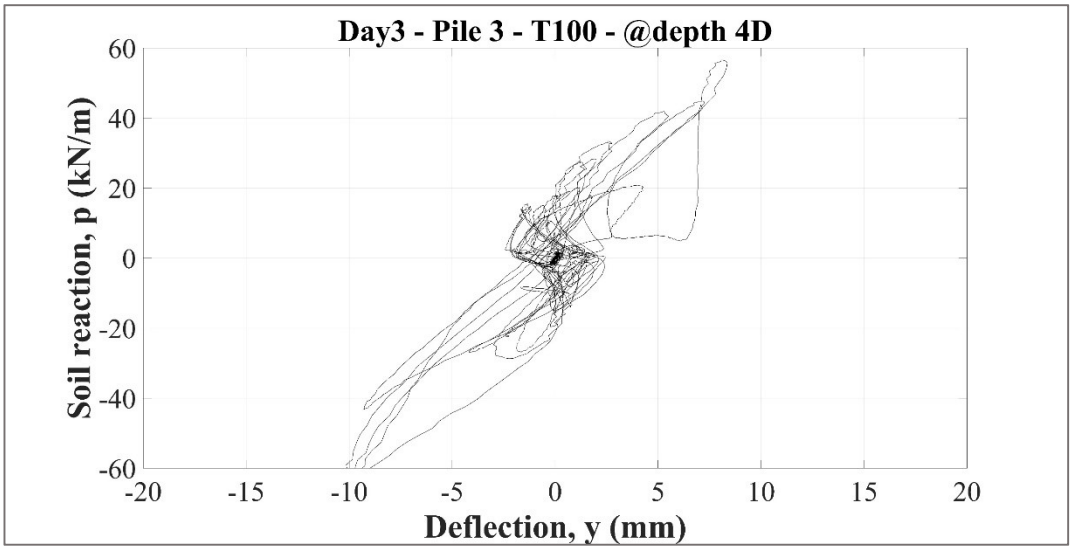
Day3 - Pile 3 - T100 - @depth 4D
Soil reaction, p (kN/m)
Deflection, y (mm)
60
40
20
0
-20
-40
-60
-20
-15
-10
-5
0
5
10
15
20

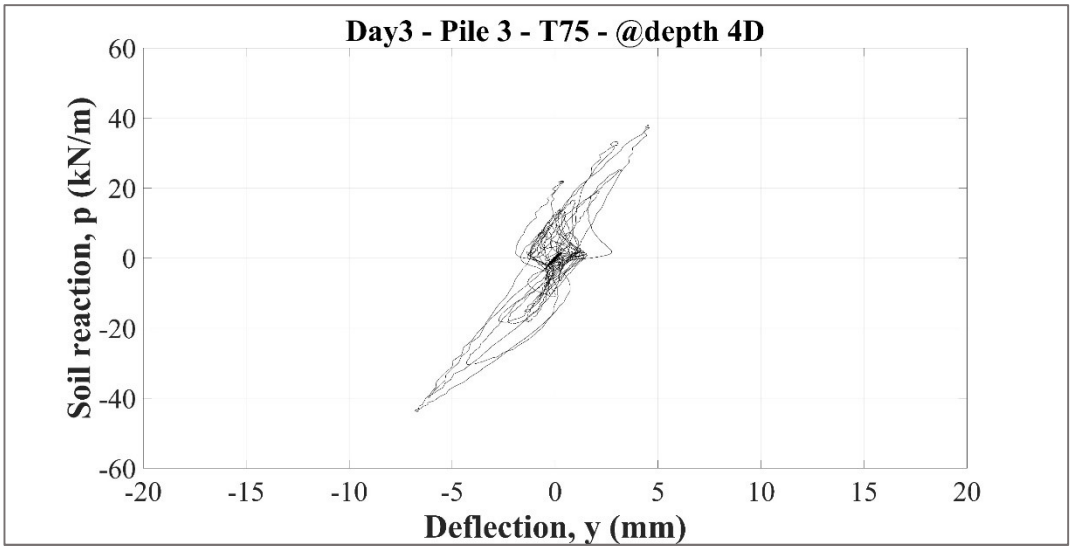
Day3 - Pile 3 - T75 - @depth 4D
Soil reaction, p (kN/m)
Deflection, y (mm)
60
40
20
0
-20
-40
-60
-20
-15
-10
-5
0
5
10
15
20

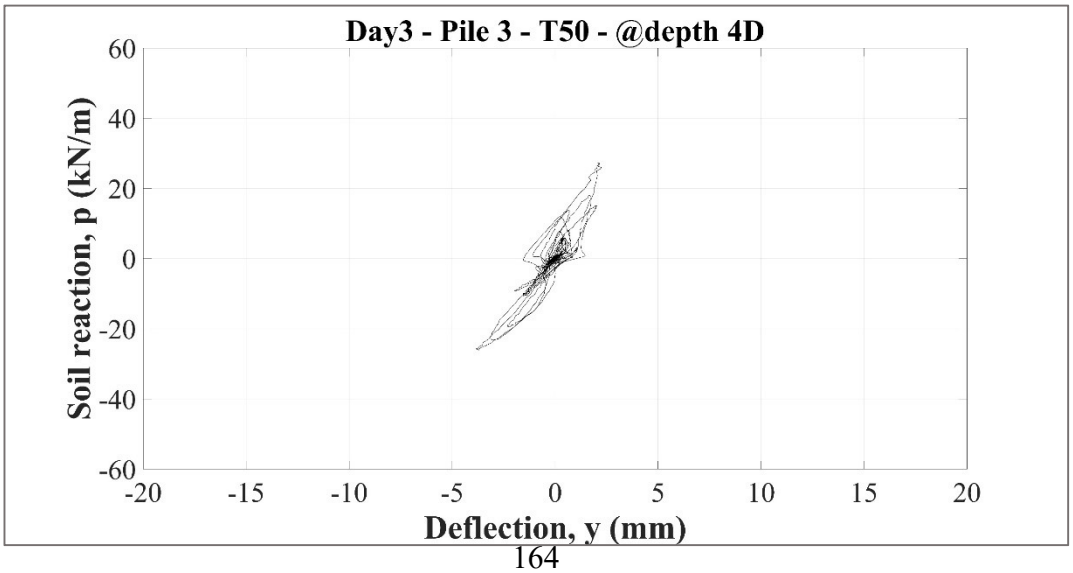
Day3 - Pile 3 - T50 - @depth 4D
Soil reaction, p (kN/m)
Deflection, y (mm)
60
40
20
0
-20
-40
-60
-20
-15
-10
-5
0
5
10
15
20

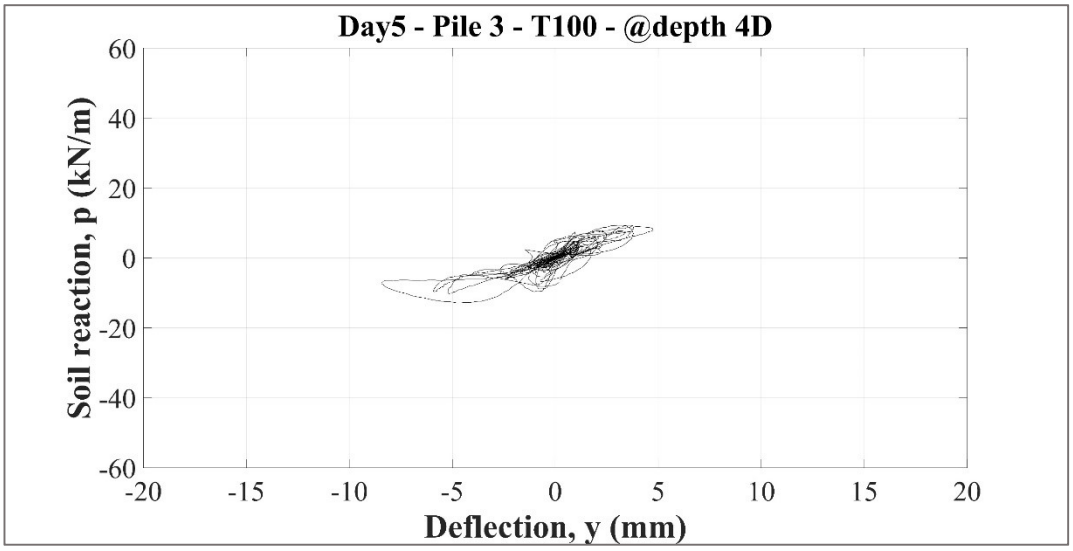
Day5 - Pile 3 - T100 - @depth 4D
Soil reaction, p (kN/m)
60
40
20
0
-20
-40
-60
-20
-15
-10
-5
0
5
10
15
20
Deflection, y (mm)

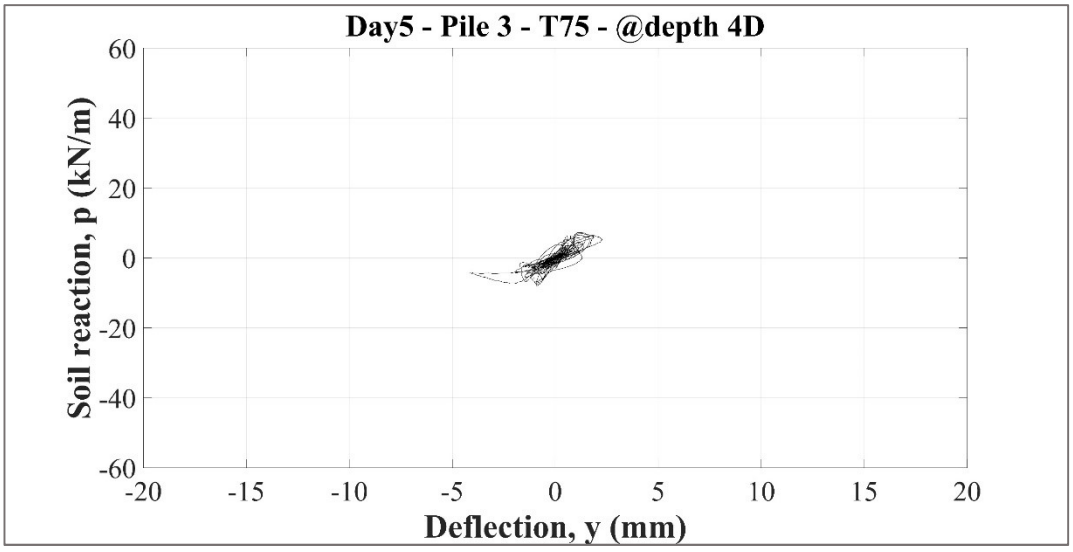
Day5 - Pile 3 - T75 - @depth 4D
Soil reaction, p (kN/m)
60
40
20
0
-20
-40
-60
-20
-15
-10
-5
0
5
10
15
20
Deflection, y (mm)

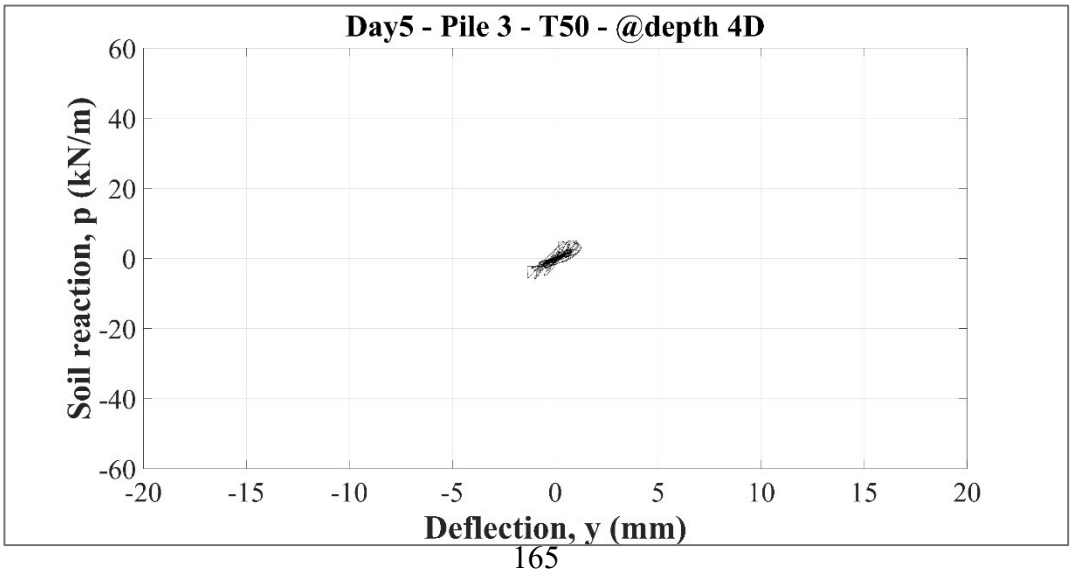
Day5 - Pile 3 - T50 - @depth 4D
Soil reaction, p (kN/m)
60
40
20
0
-20
-40
-60
-20
-15
-10
-5
0
5
10
15
20
Deflection, y (mm)

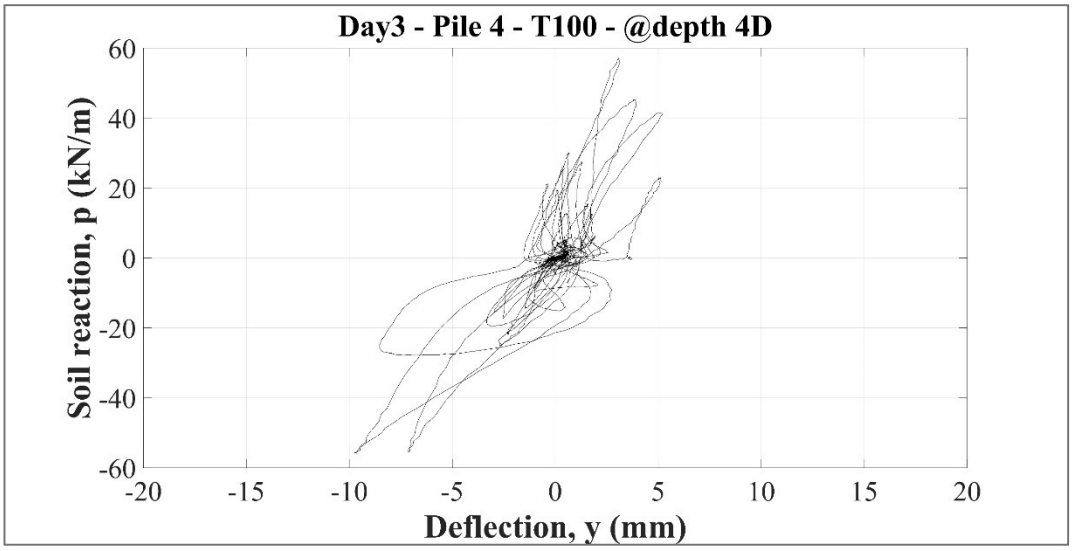
Day3 - Pile 4 - T100 - @depth 4D
Soil reaction, p (kN/m)
60
40
20
0
-20
-40
-60
-20
-15
-10
-5
0
5
10
15
20
Deflection, y (mm)

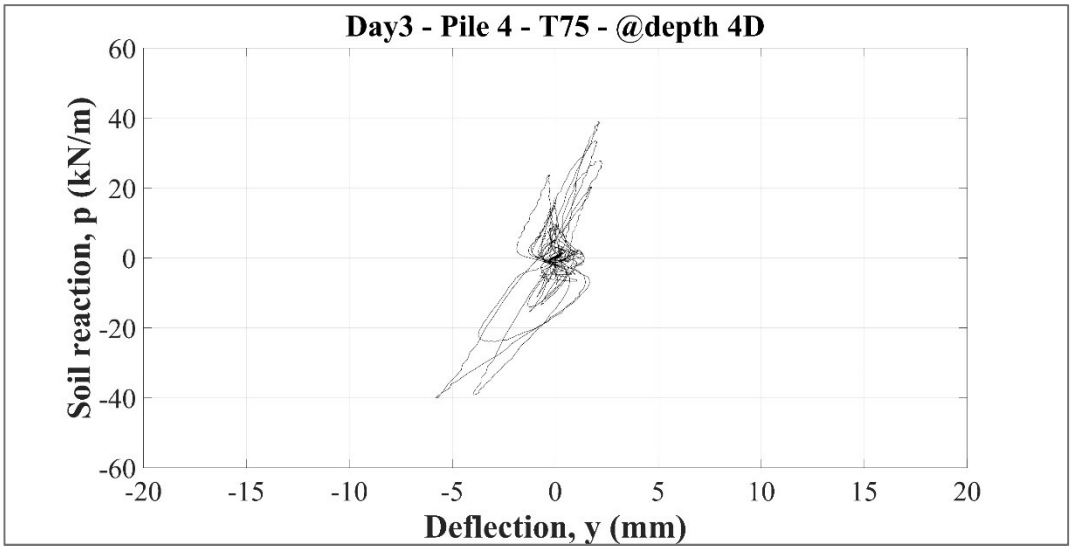
Day3 - Pile 4 - T75 - @depth 4D
Soil reaction, p (kN/m)
60
40
20
0
-20
-40
-60
-20
-15
-10
-5
0
5
10
15
20
Deflection, y (mm)

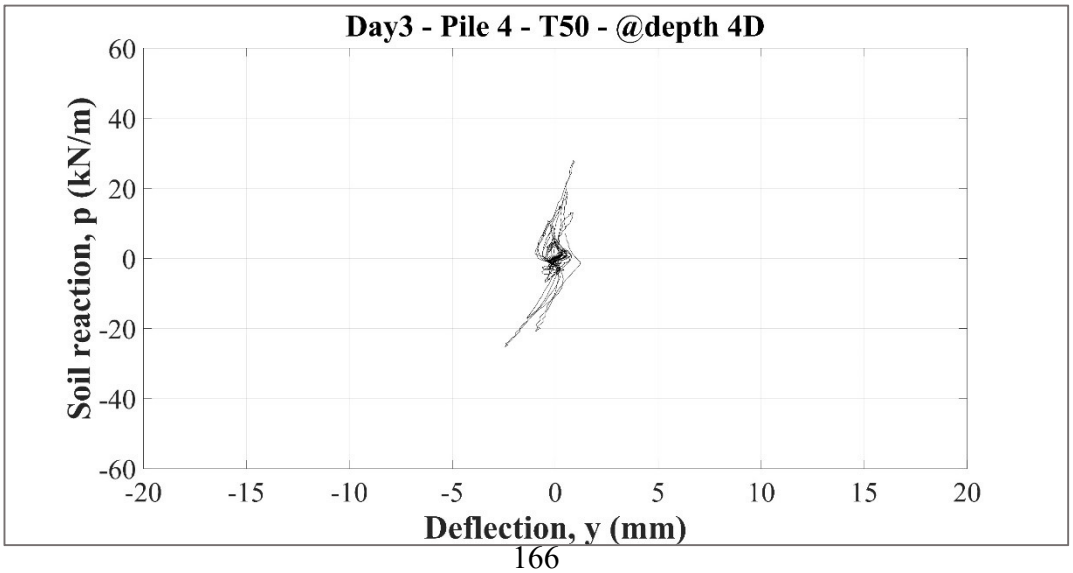
Day3 - Pile 4 - T50 - @depth 4D
Soil reaction, p (kN/m)
60
40
20
0
-20
-40
-60
-20
-15
-10
-5
0
5
10
15
20
Deflection, y (mm)

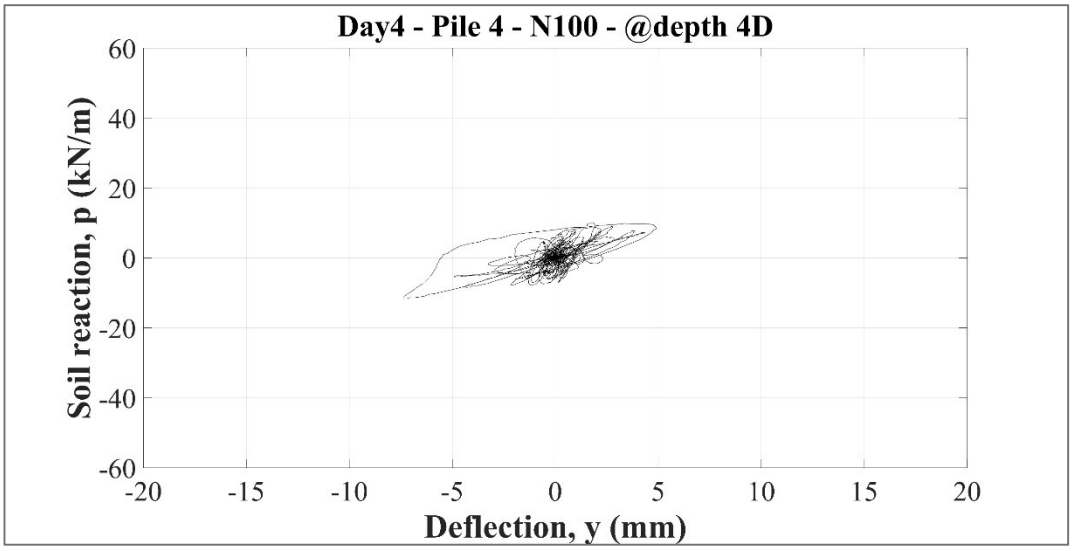
Day4 - Pile 4 - N100 - @depth 4D
Soil reaction, p (kN/m)
60
40
20
0
-20
-40
-60
-20
-15
-10
-5
0
5
10
15
20
Deflection, y (mm)

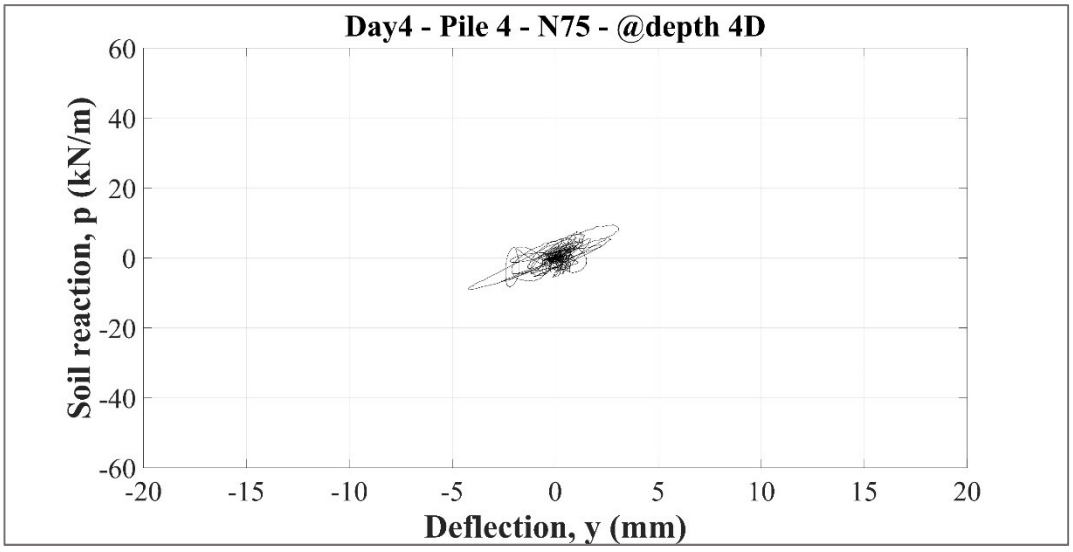
Day4 - Pile 4 - N75 - @depth 4D
Soil reaction, p (kN/m)
60
40
20
0
-20
-40
-60
-20
-15
-10
-5
0
5
10
15
20
Deflection, y (mm)

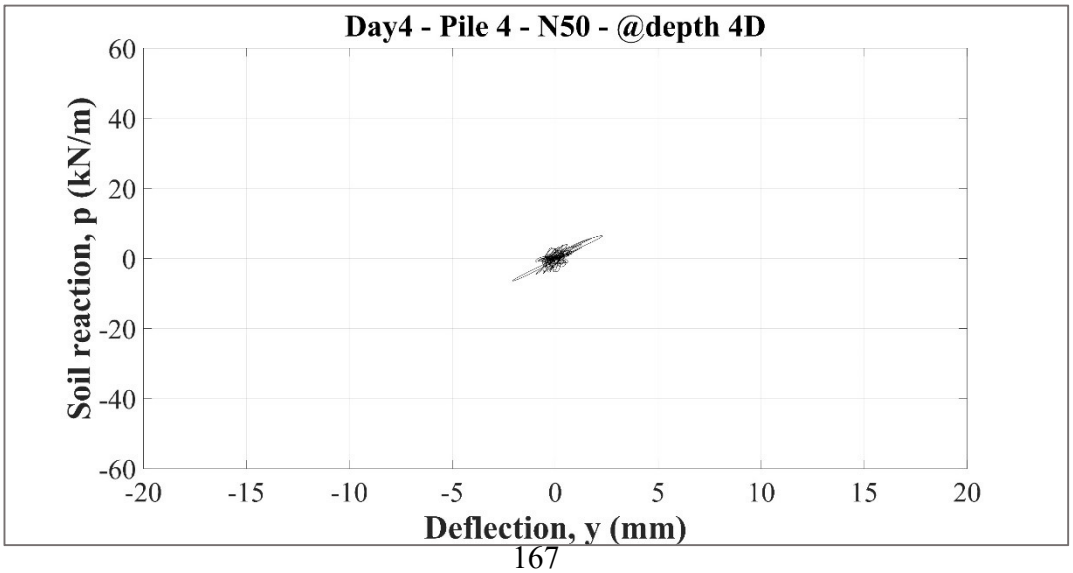
Day4 - Pile 4 - N50 - @depth 4D
Soil reaction, p (kN/m)
60
40
20
0
-20
-40
-60
-20
-15
-10
-5
0
5
10
15
20
Deflection, y (mm)

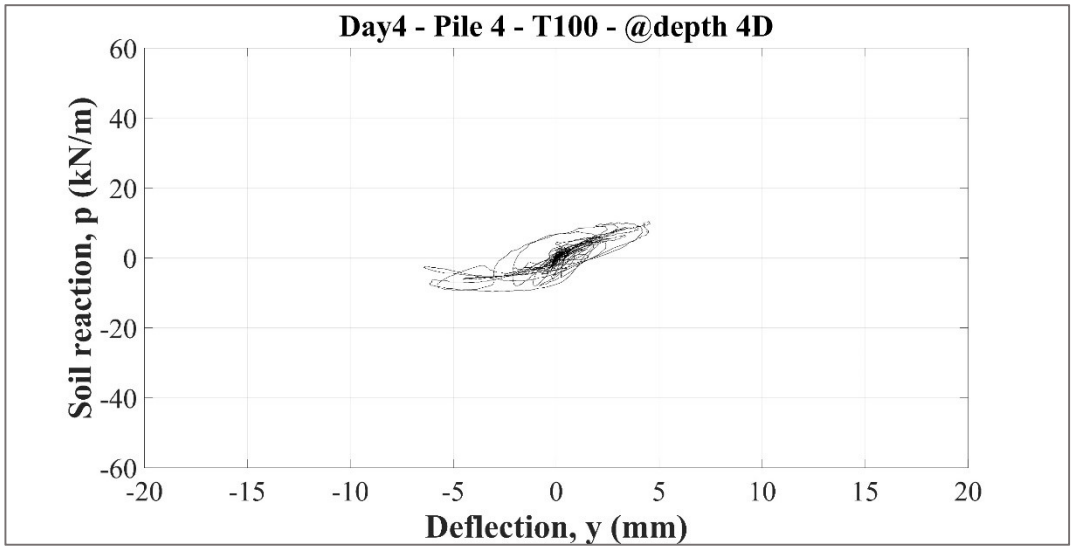
Day4 - Pile 4 - T100 - @depth 4D
Soil reaction, p (kN/m)
Deflection, y (mm)
60
40
20
0
-20
-40
-60
-20
-15
-10
-5
0
5
10
15
20

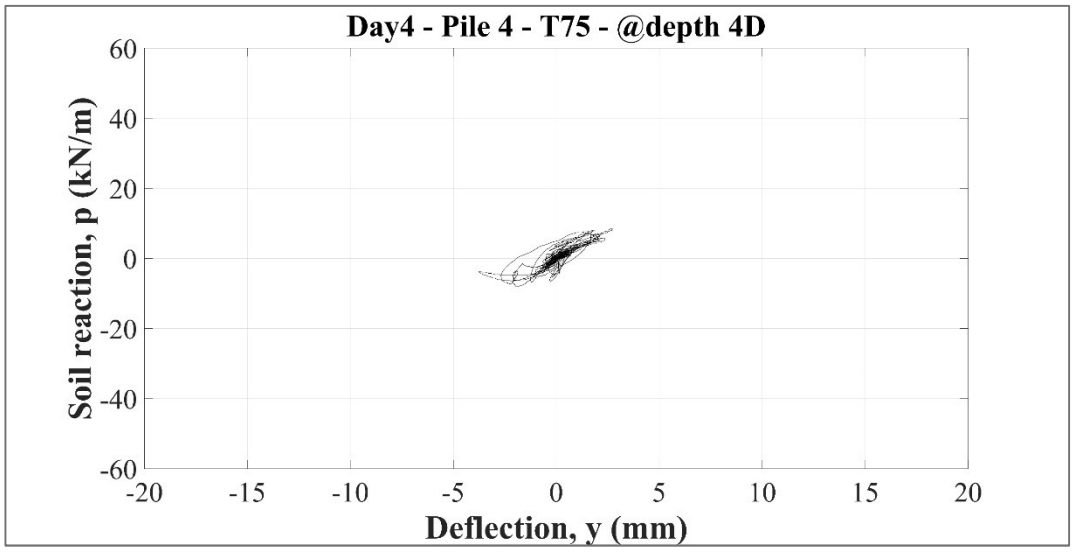
Day4 - Pile 4 - T75 - @depth 4D
Soil reaction, p (kN/m)
Deflection, y (mm)
60
40
20
0
-20
-40
-60
-20
-15
-10
-5
0
5
10
15
20

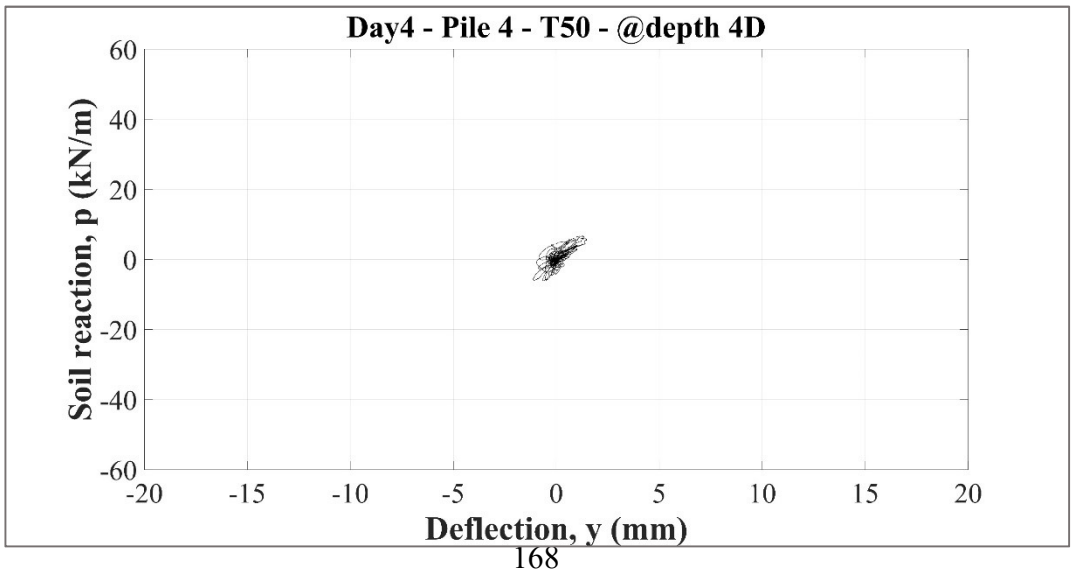
Day4 - Pile 4 - T50 - @depth 4D
Soil reaction, p (kN/m)
Deflection, y (mm)
60
40
20
0
-20
-40
-60
-20
-15
-10
-5
0
5
10
15
20

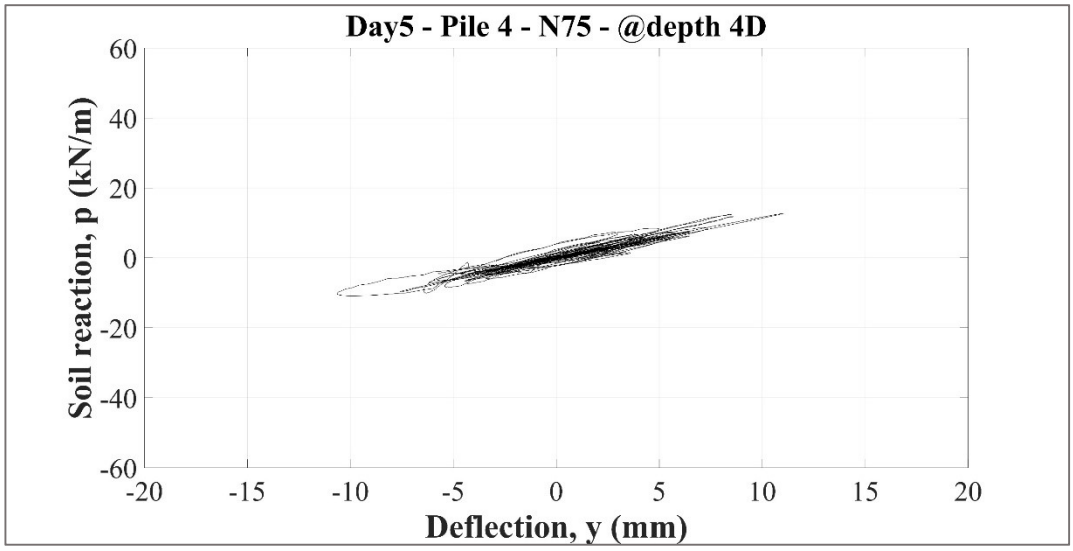
Day5 - Pile 4 - N75 - @depth 4D
Soil reaction, p (kN/m)
60
40
20
0
-20
-40
-60
-20
-15
-10
-5
0
5
10
15
20
Deflection, y (mm)

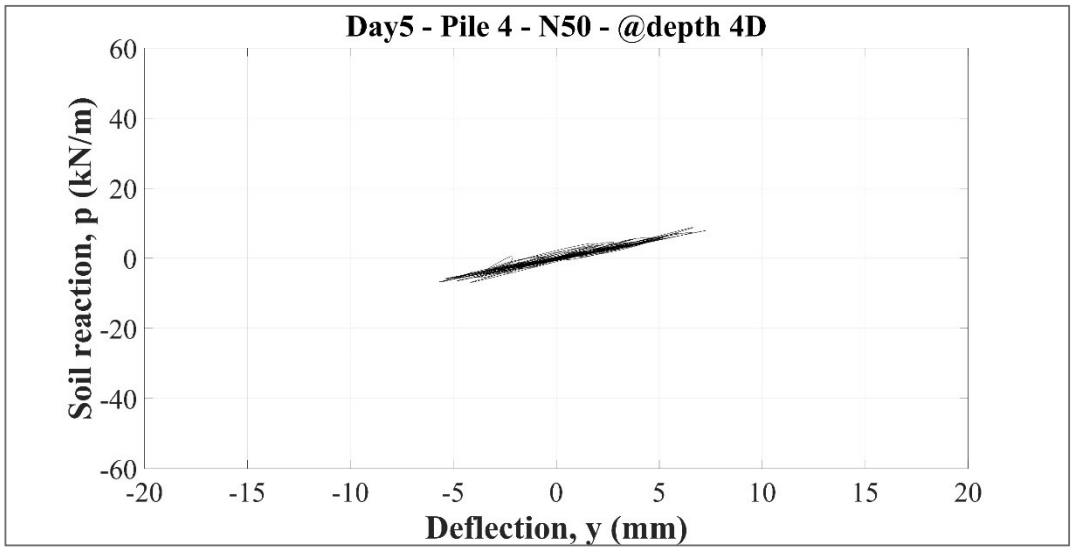
Day5 - Pile 4 - N50 - @depth 4D
Soil reaction, p (kN/m)
60
40
20
0
-20
-40
-60
-20
-15
-10
-5
0
5
10
15
20
Deflection, y (mm)

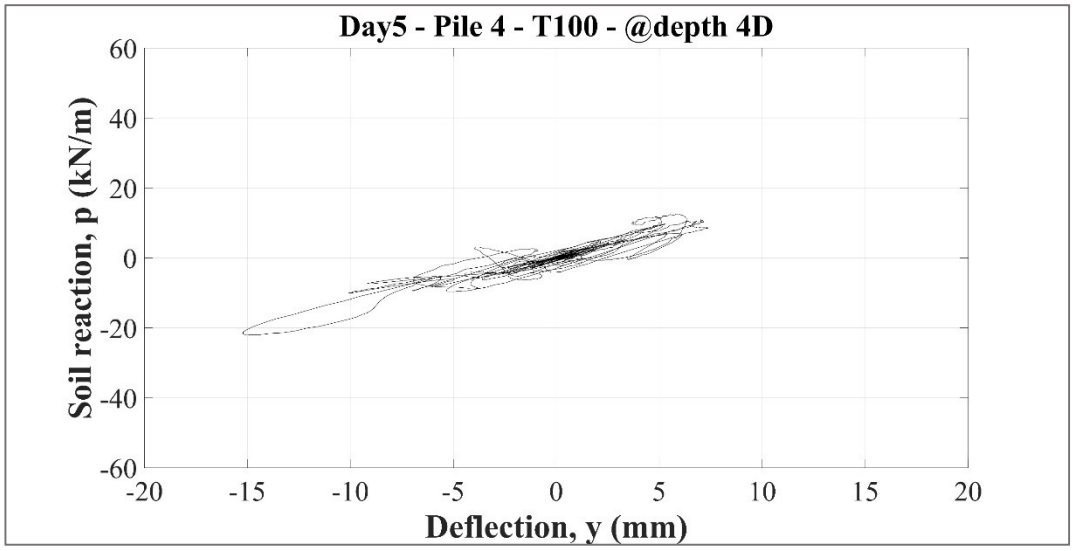
Day5 - Pile 4 - T100 - @depth 4D
Soil reaction, p (kN/m)
60
40
20
0
-20
-40
-60
-20
-15
-10
-5
0
5
10
15
20
Deflection, y (mm)

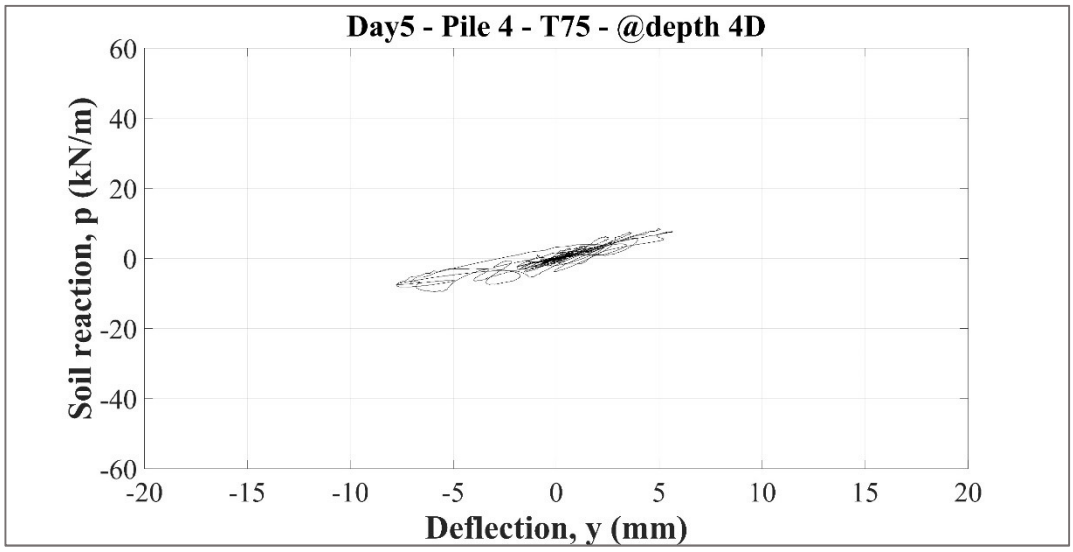
Day5 - Pile 4 - T75 - @depth 4D
Soil reaction, p (kN/m)
60
40
20
0
-20
-40
-60
-20
-15
-10
-5
0
5
10
15
20
Deflection, y (mm)

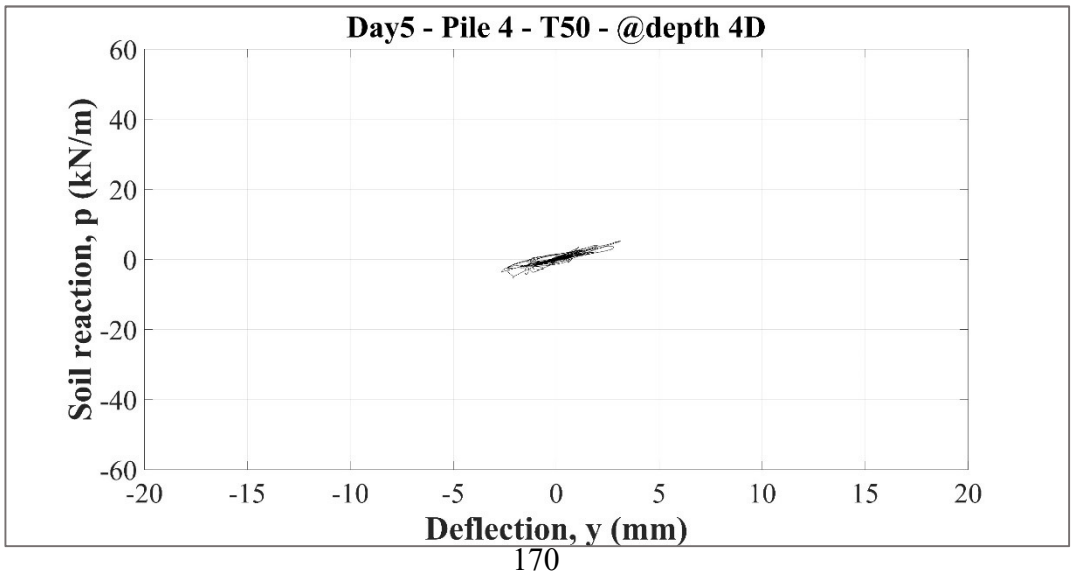
Day5 - Pile 4 - T50 - @depth 4D
Soil reaction, p (kN/m)
60
40
20
0
-20
-40
-60
-20
-15
-10
-5
0
5
10
15
20
Deflection, y (mm)

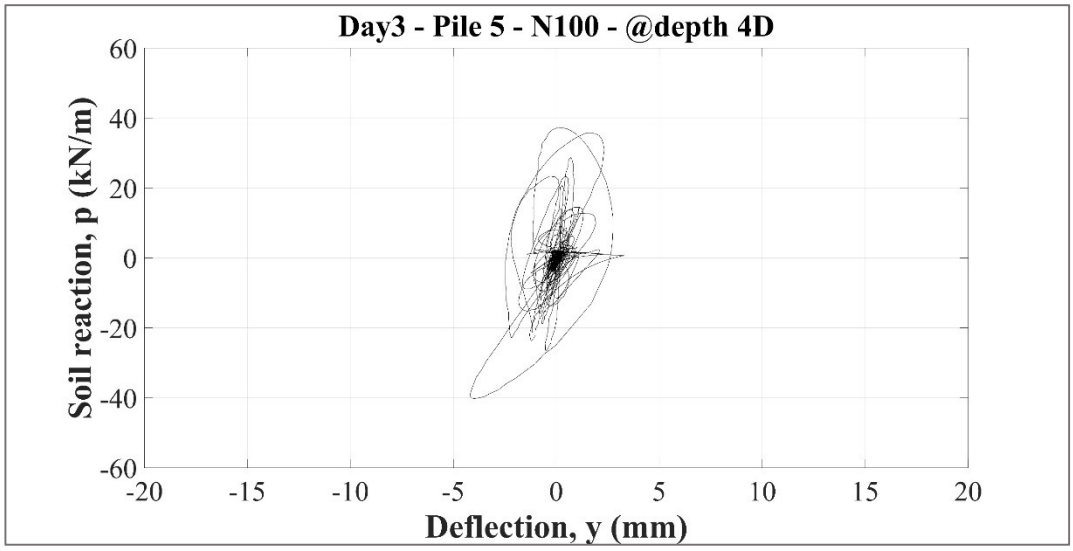
Day3 - Pile 5 - N100 - @depth 4D
Soil reaction, p (kN/m)
60
40
20
0
-20
-40
-60
-20
-15
-10
-5
0
5
10
15
20
Deflection, y (mm)

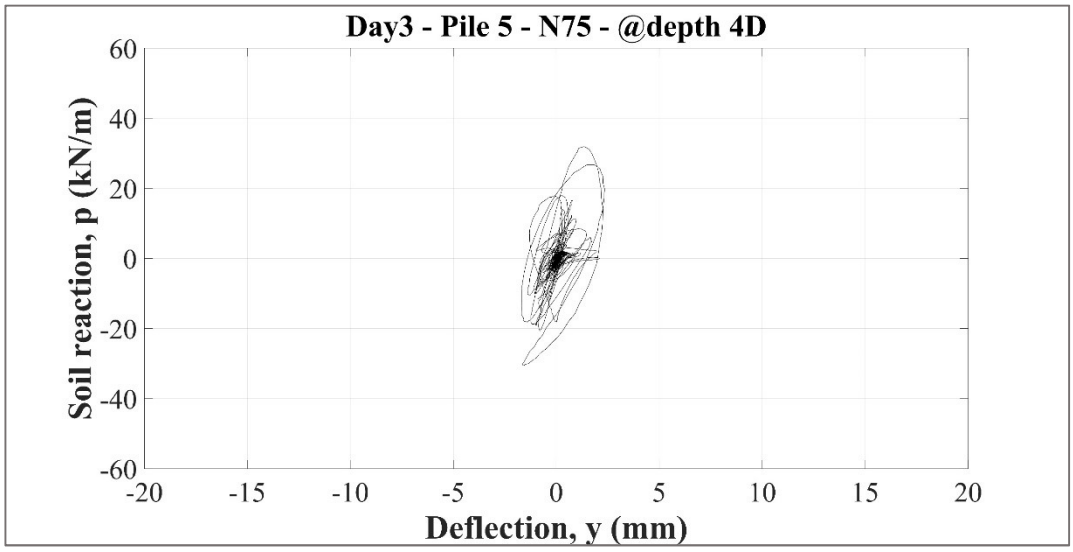
Day3 - Pile 5 - N75 - @depth 4D
Soil reaction, p (kN/m)
60
40
20
0
-20
-40
-60
-20
-15
-10
-5
0
5
10
15
20
Deflection, y (mm)

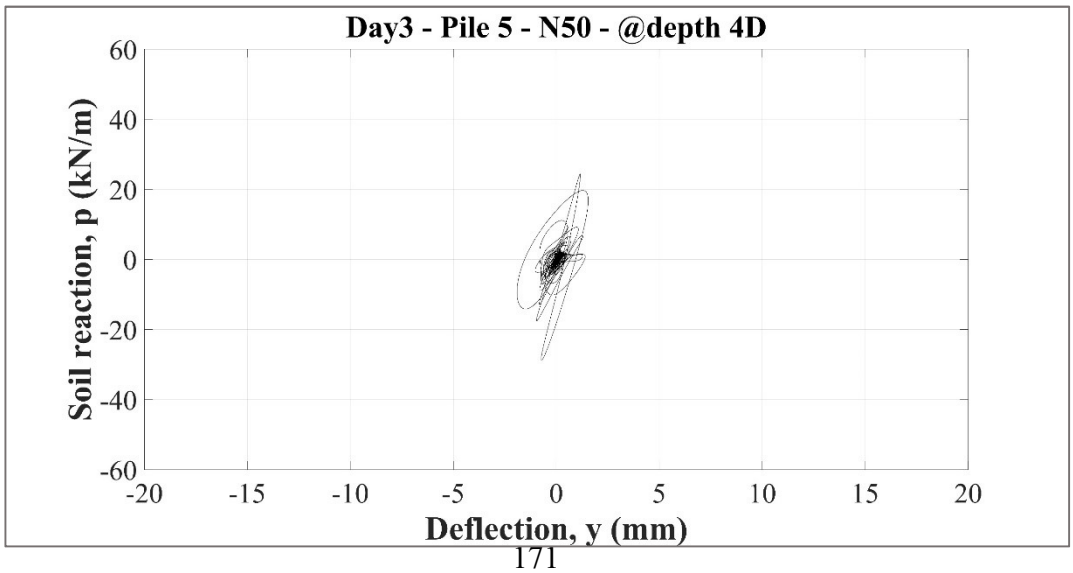
Day3 - Pile 5 - N50 - @depth 4D
Soil reaction, p (kN/m)
60
40
20
0
-20
-40
-60
-20
-15
-10
-5
0
5
10
15
20
Deflection, y (mm)

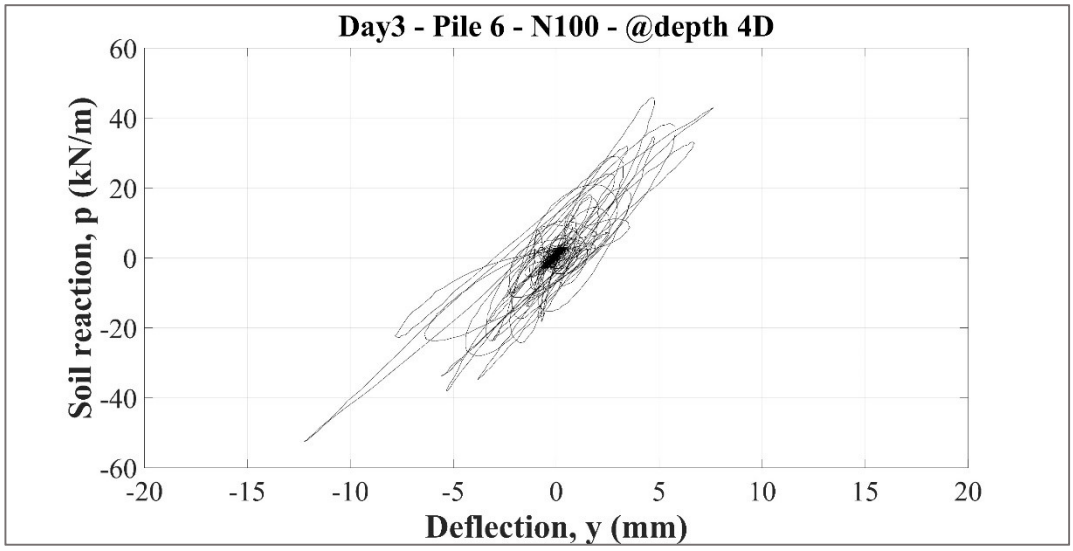
Day3 - Pile 6 - N100 - @depth 4D
Soil reaction, p (kN/m)
Deflection, y (mm)
60
40
20
0
-20
-40
-60
-20
-15
-10
-5
0
5
10
15
20

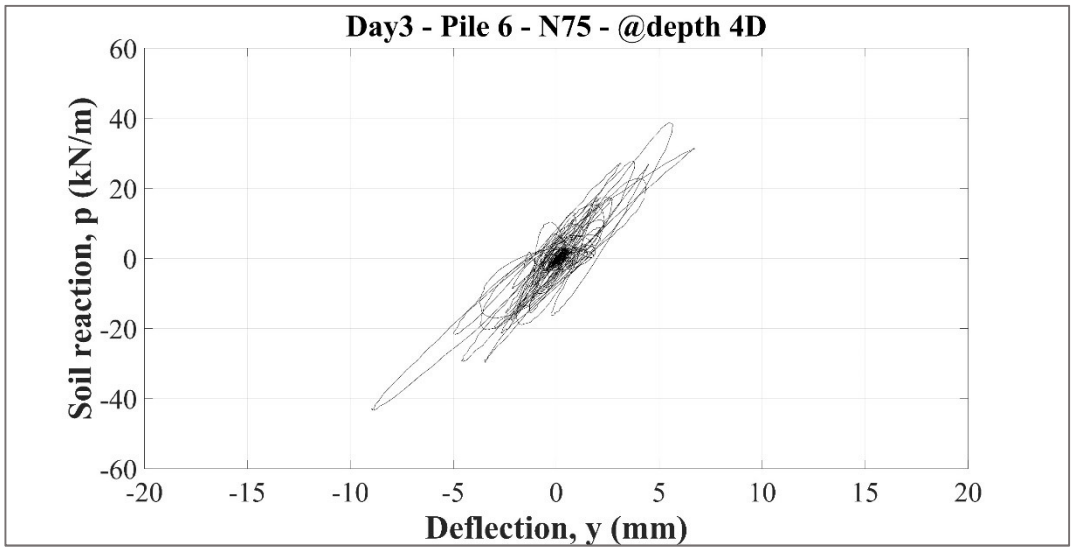
Day3 - Pile 6 - N75 - @depth 4D
Soil reaction, p (kN/m)
Deflection, y (mm)
60
40
20
0
-20
-40
-60
-20
-15
-10
-5
0
5
10
15
20

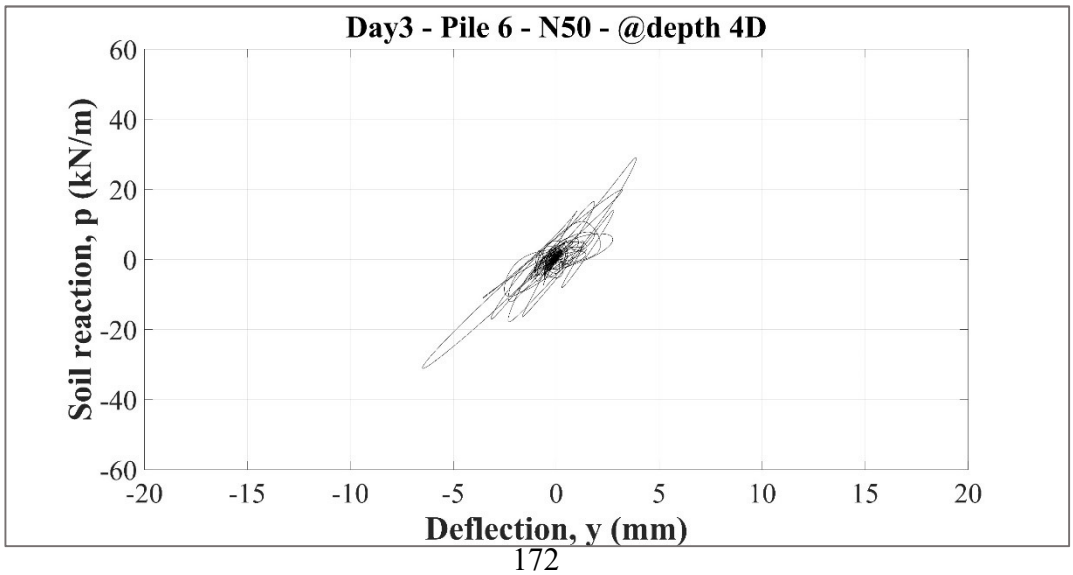
Day3 - Pile 6 - N50 - @depth 4D
Soil reaction, p (kN/m)
Deflection, y (mm)
60
40
20
0
-20
-40
-60
-20
-15
-10
-5
0
5
10
15
20

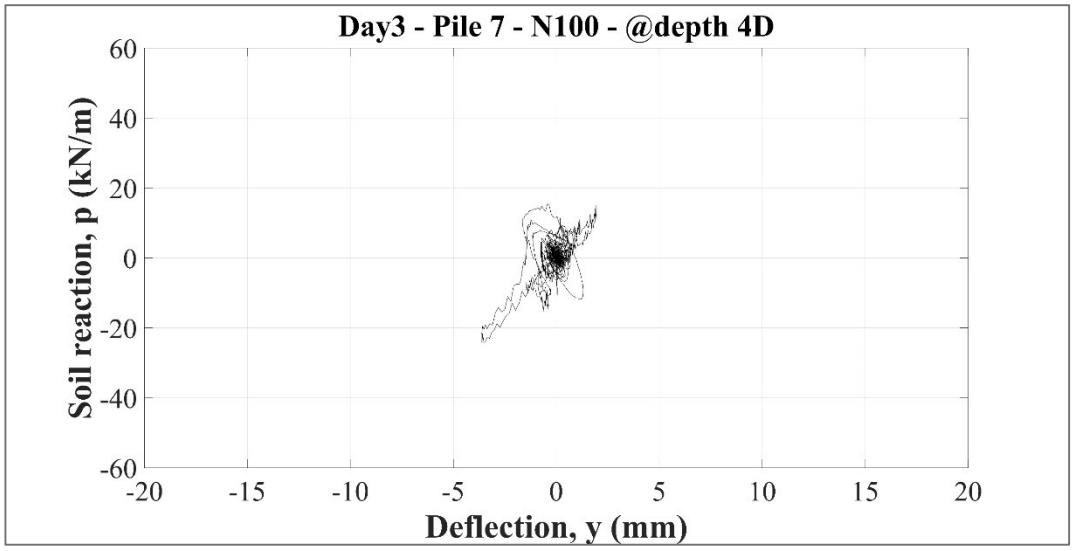
Day3 - Pile 7 - N100 - @depth 4D
Soil reaction, p (kN/m)
60
40
20
0
-20
-40
-60
-20
-15
-10
-5
0
5
10
15
20
Deflection, y (mm)

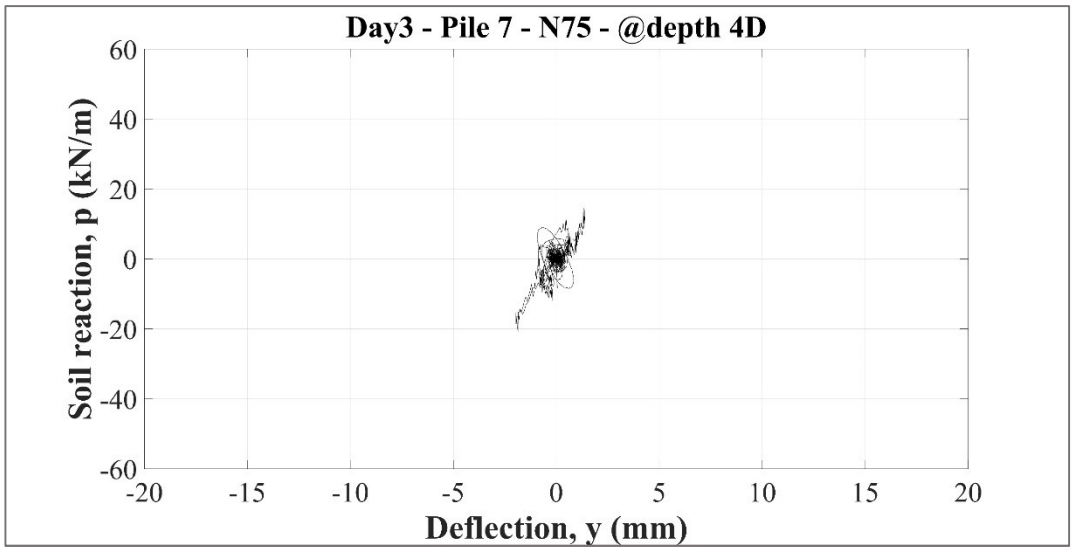
Day3 - Pile 7 - N75 - @depth 4D
Soil reaction, p (kN/m)
60
40
20
0
-20
-40
-60
-20
-15
-10
-5
0
5
10
15
20
Deflection, y (mm)

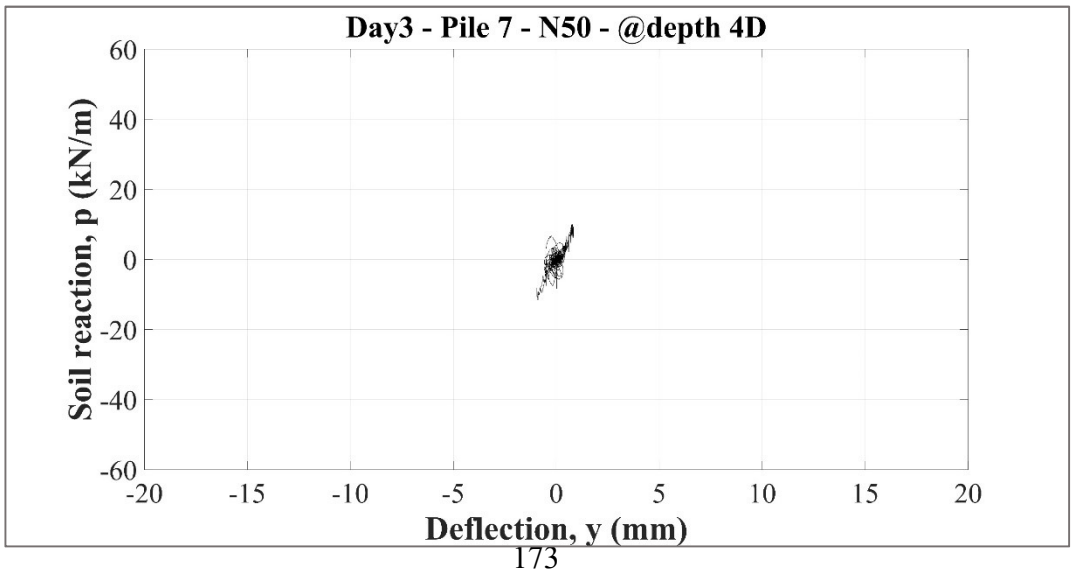
Day3 - Pile 7 - N50 - @depth 4D
Soil reaction, p (kN/m)
60
40
20
0
-20
-40
-60
-20
-15
-10
-5
0
5
10
15
20
Deflection, y (mm)

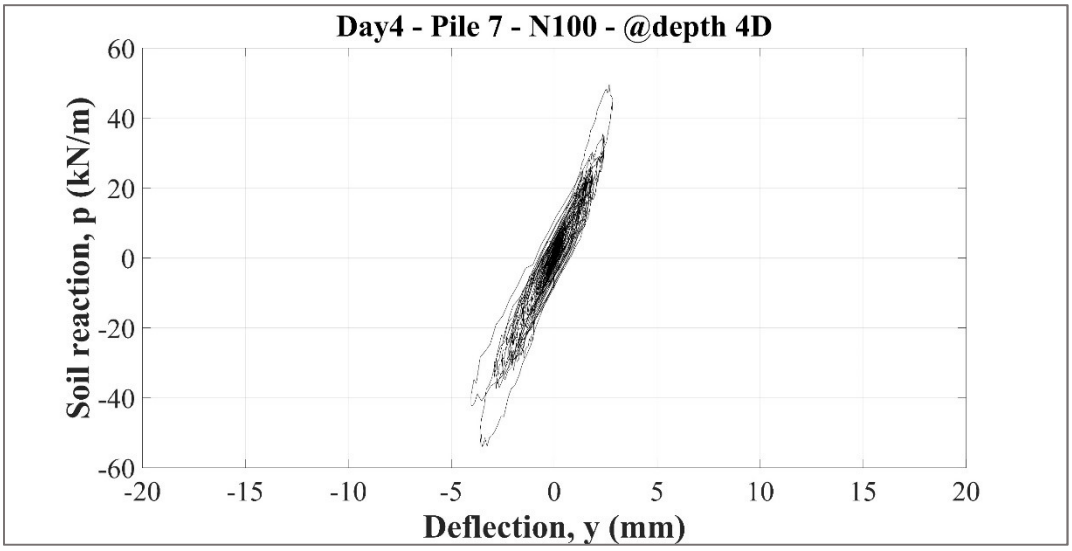
Day4 - Pile 7 - N100 - @depth 4D
Soil reaction, p (kN/m)
Deflection, y (mm)
60
40
20
0
-20
-40
-60
-20
-15
-10
-5
0
5
10
15
20

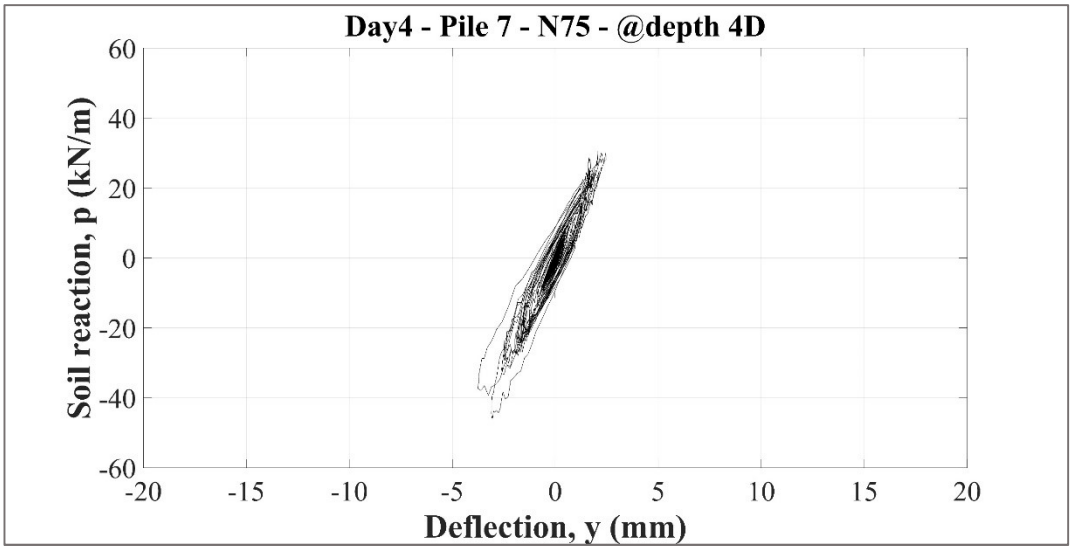
Day4 - Pile 7 - N75 - @depth 4D
Soil reaction, p (kN/m)
Deflection, y (mm)
60
40
20
0
-20
-40
-60
-20
-15
-10
-5
0
5
10
15
20

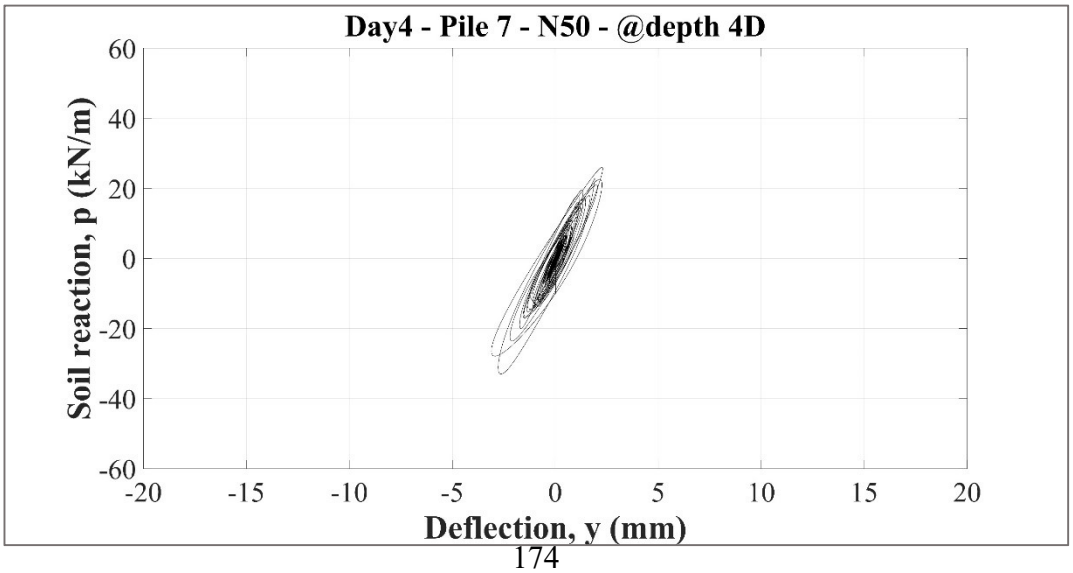
Day4 - Pile 7 - N50 - @depth 4D
Soil reaction, p (kN/m)
Deflection, y (mm)
60
40
20
0
-20
-40
-60
-20
-15
-10
-5
0
5
10
15
20

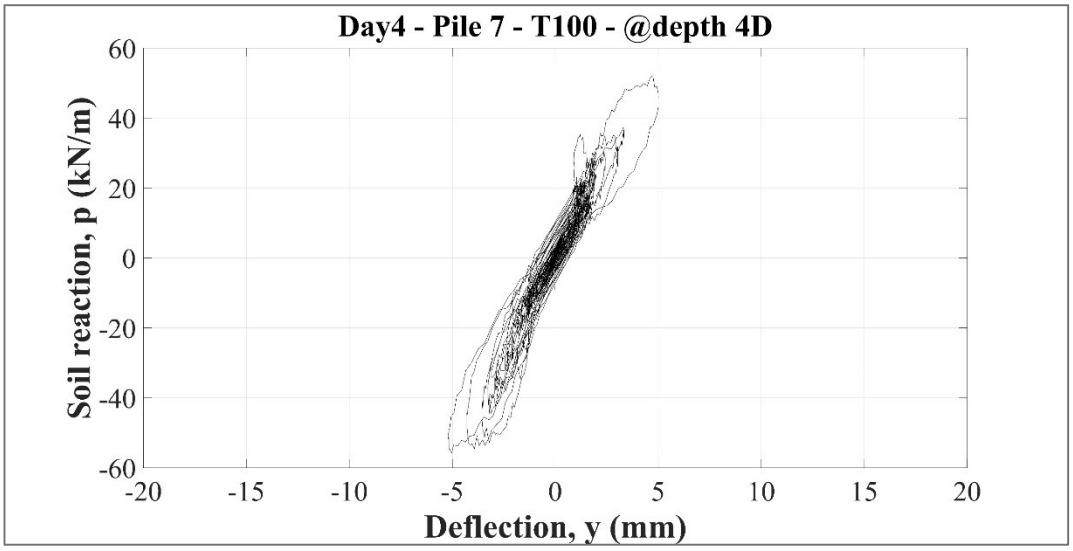
Day4 - Pile 7 - T100 - @depth 4D
Soil reaction, p (kN/m)
Deflection, y (mm)
60
40
20
0
-20
-40
-60
-20
-15
-10
-5
0
5
10
15
20

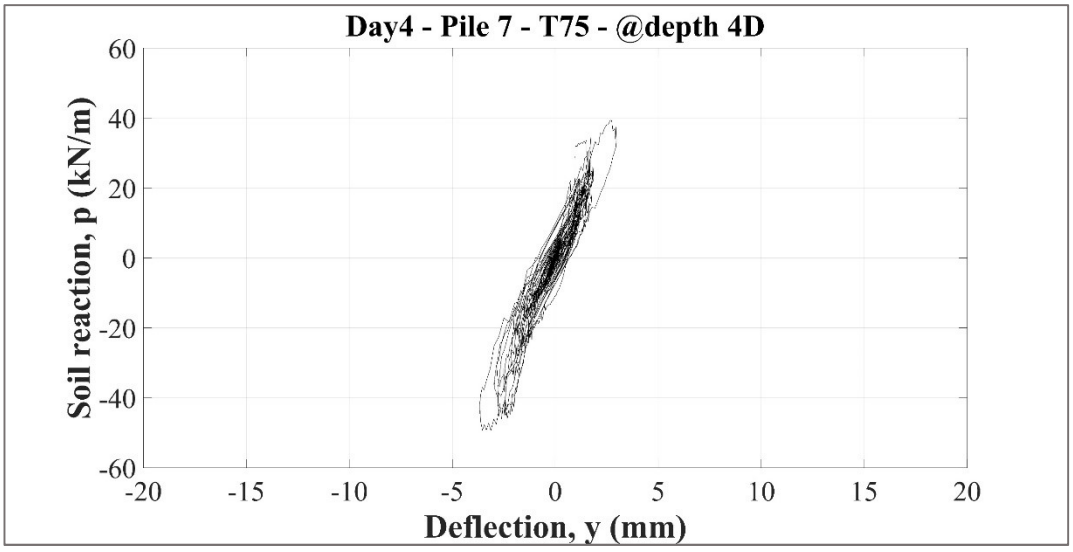
Day4 - Pile 7 - T75 - @depth 4D
Soil reaction, p (kN/m)
Deflection, y (mm)
60
40
20
0
-20
-40
-60
-20
-15
-10
-5
0
5
10
15
20

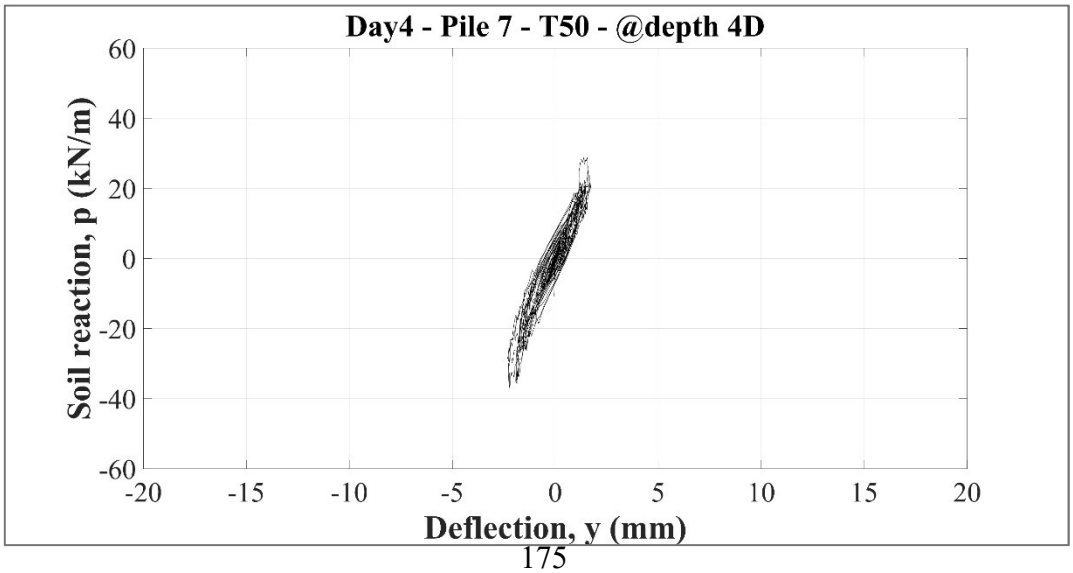
Day4 - Pile 7 - T50 - @depth 4D
Soil reaction, p (kN/m)
Deflection, y (mm)
60
40
20
0
-20
-40
-60
-20
-15
-10
-5
0
5
10
15
20

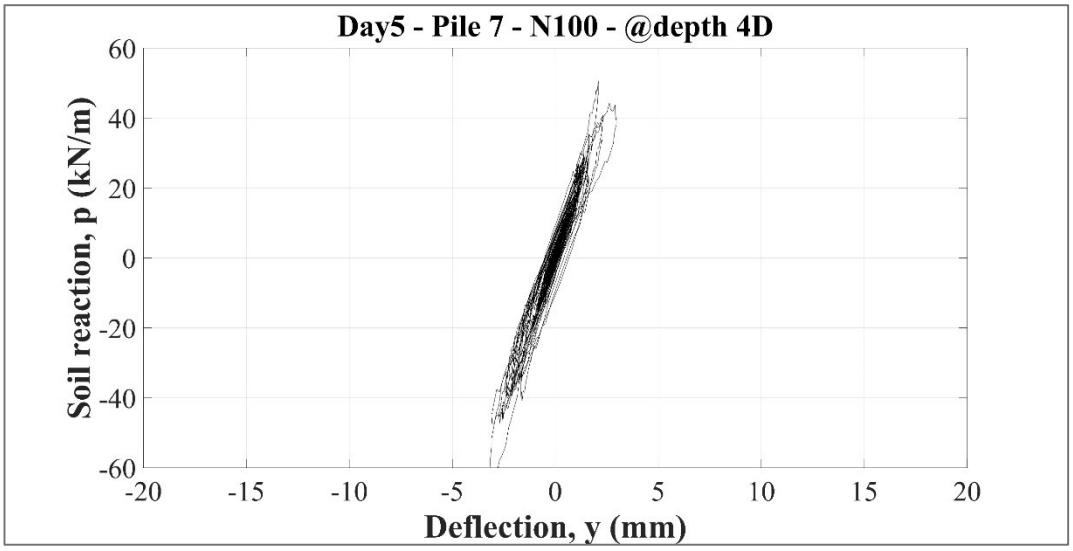
Day5 - Pile 7 - N100 - @depth 4D
Soil reaction, p (kN/m)
Deflection, y (mm)
60
40
20
0
-20
-40
-60
-20
-15
-10
-5
0
5
10
15
20

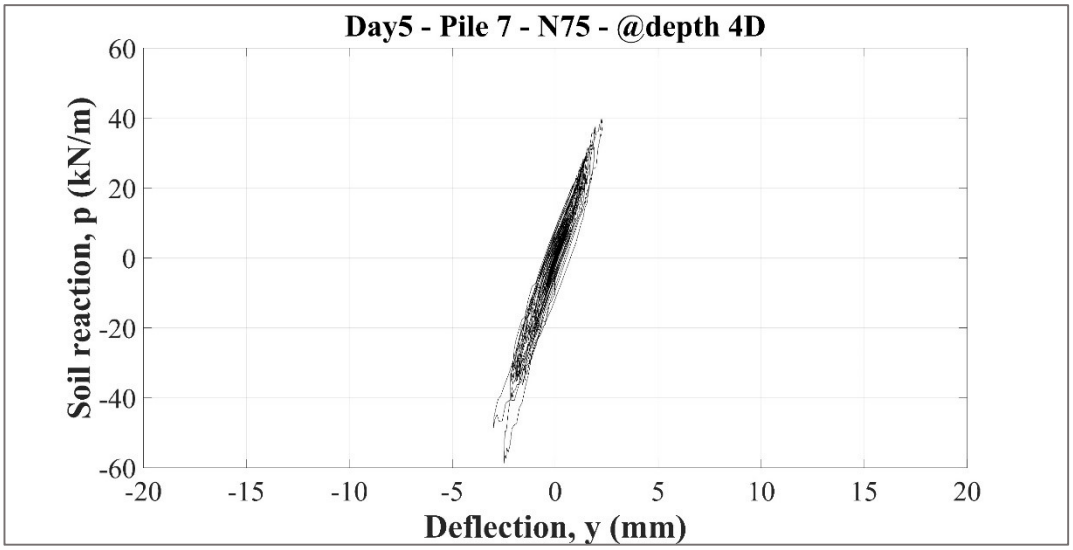
Day5 - Pile 7 - N75 - @depth 4D
Soil reaction, p (kN/m)
Deflection, y (mm)
60
40
20
0
-20
-40
-60
-20
-15
-10
-5
0
5
10
15
20

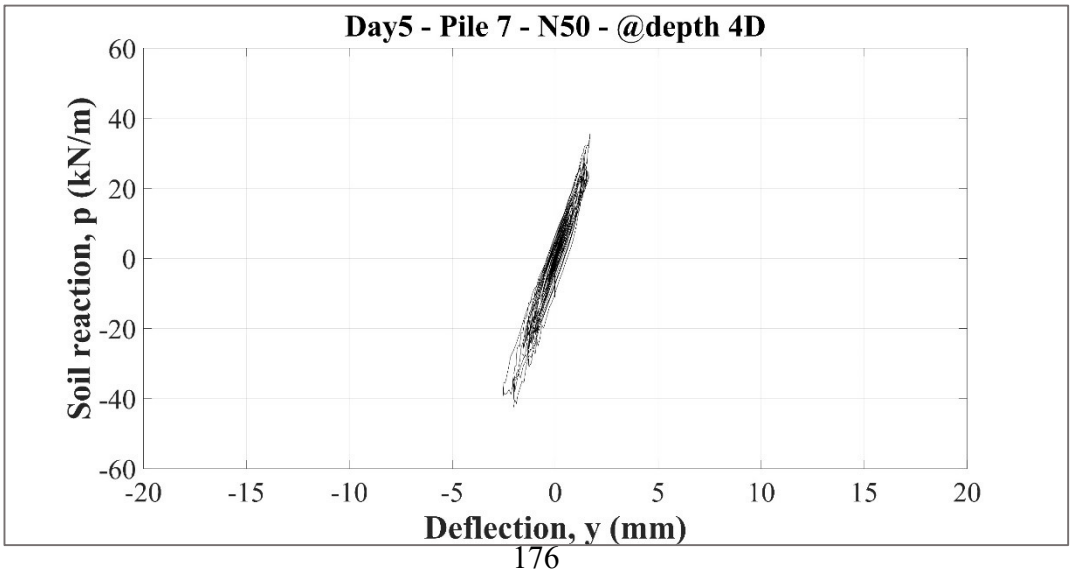
Day5 - Pile 7 - N50 - @depth 4D
Soil reaction, p (kN/m)
Deflection, y (mm)
60
40
20
0
-20
-40
-60
-20
-15
-10
-5
0
5
10
15
20

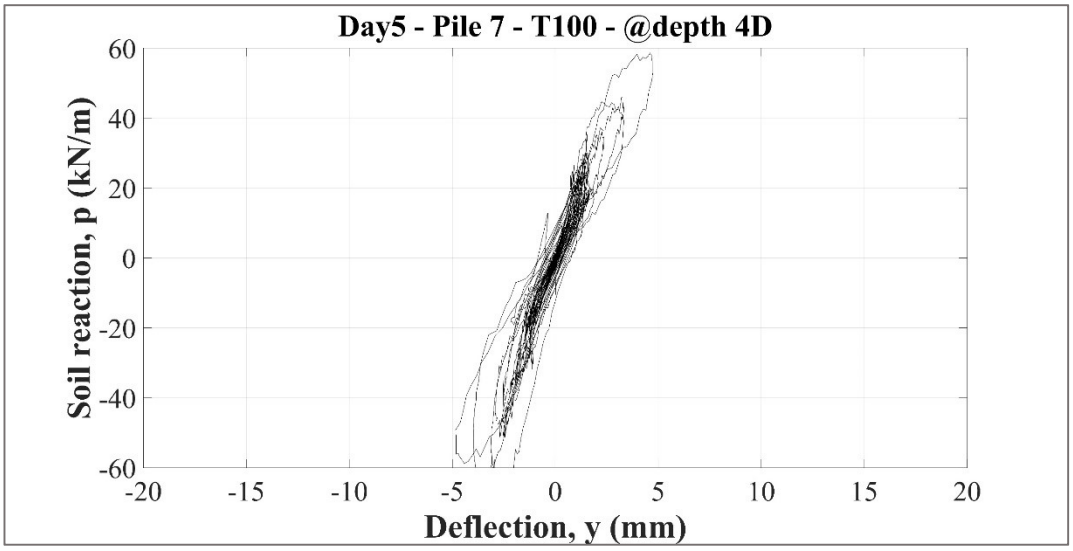
Day5 - Pile 7 - T100 - @depth 4D
Soil reaction, p (kN/m)
Deflection, y (mm)
60
40
20
0
-20
-40
-60
-20
-15
-10
-5
0
5
10
15
20

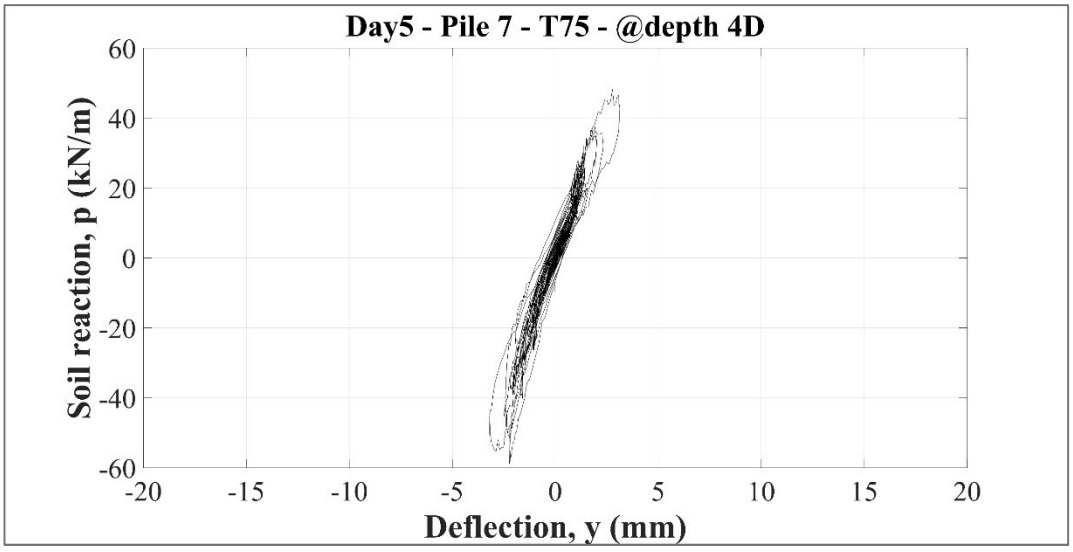
Day5 - Pile 7 - T75 - @depth 4D
Soil reaction, p (kN/m)
Deflection, y (mm)
60
40
20
0
-20
-40
-60
-20
-15
-10
-5
0
5
10
15
20

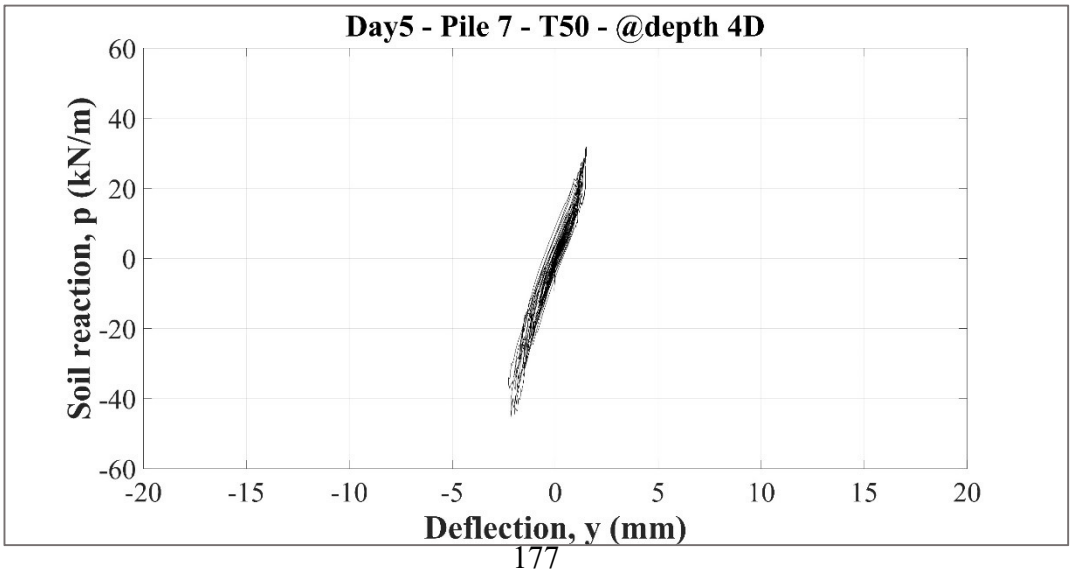
Day5 - Pile 7 - T50 - @depth 4D
Soil reaction, p (kN/m)
Deflection, y (mm)
60
40
20
0
-20
-40
-60
-20
-15
-10
-5
0
5
10
15
20

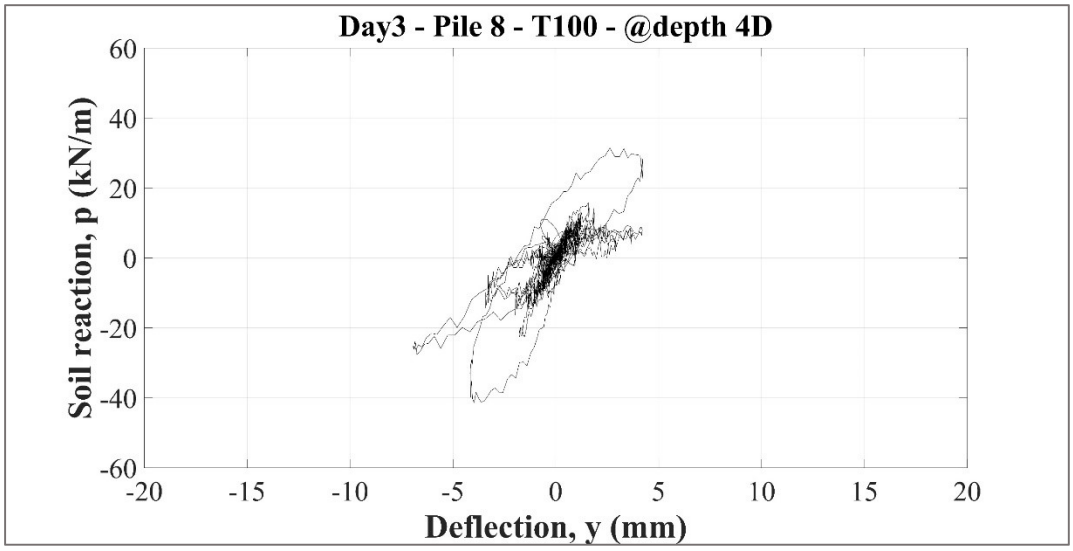
Day3 - Pile 8 - T100 - @depth 4D
Soil reaction, p (kN/m)
60
40
20
0
-20
-40
-60
-20
-15
-10
-5
0
5
10
15
20
Deflection, y (mm)

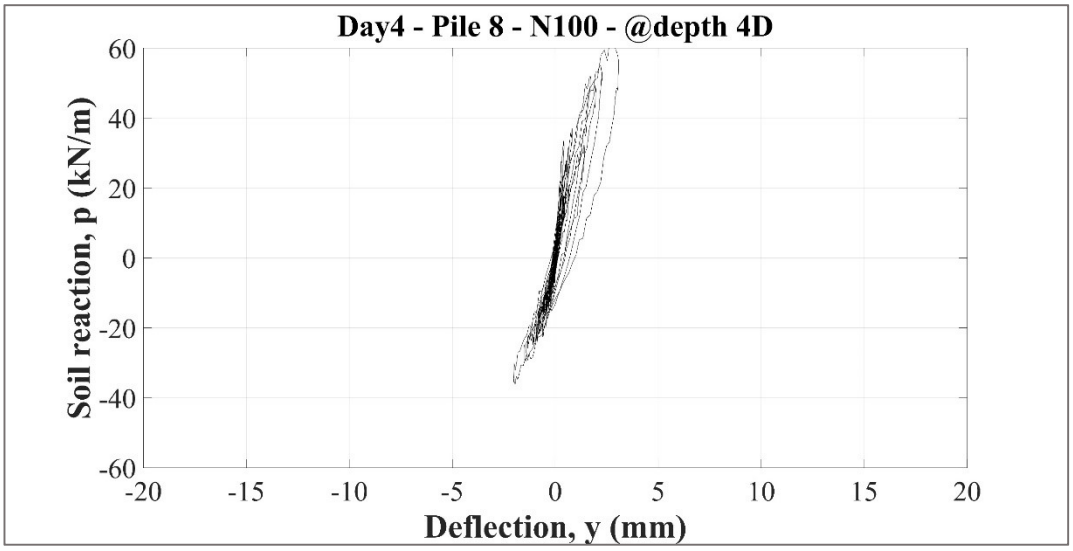
Day4 - Pile 8 - N100 - @depth 4D
Soil reaction, p (kN/m)
60
40
20
0
-20
-40
-60
-20
-15
-10
-5
0
5
10
15
20
Deflection, y (mm)

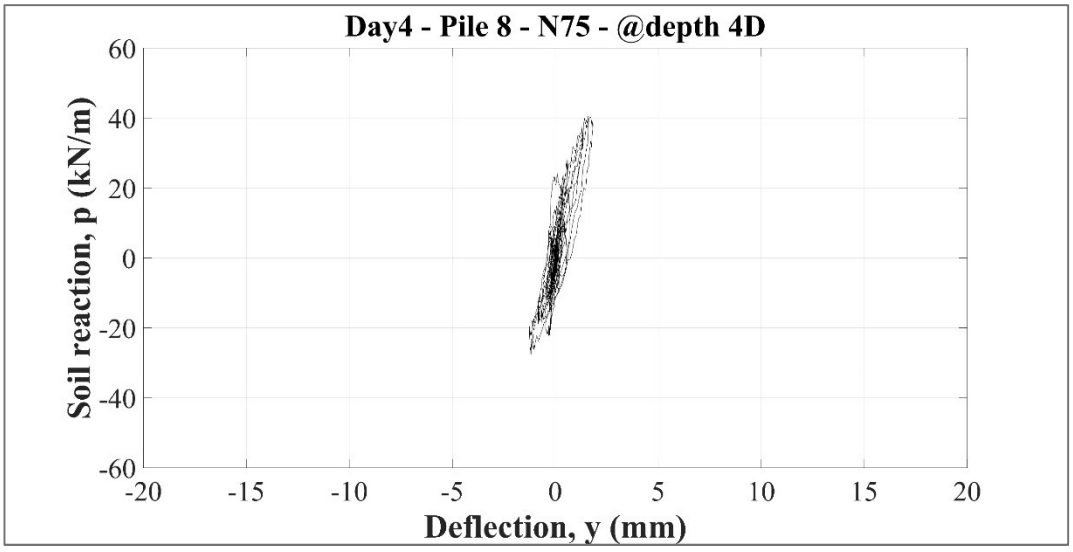
Day4 - Pile 8 - N75 - @depth 4D
Soil reaction, p (kN/m)
60
40
20
0
-20
-40
-60
-20
-15
-10
-5
0
5
10
15
20
Deflection, y (mm)

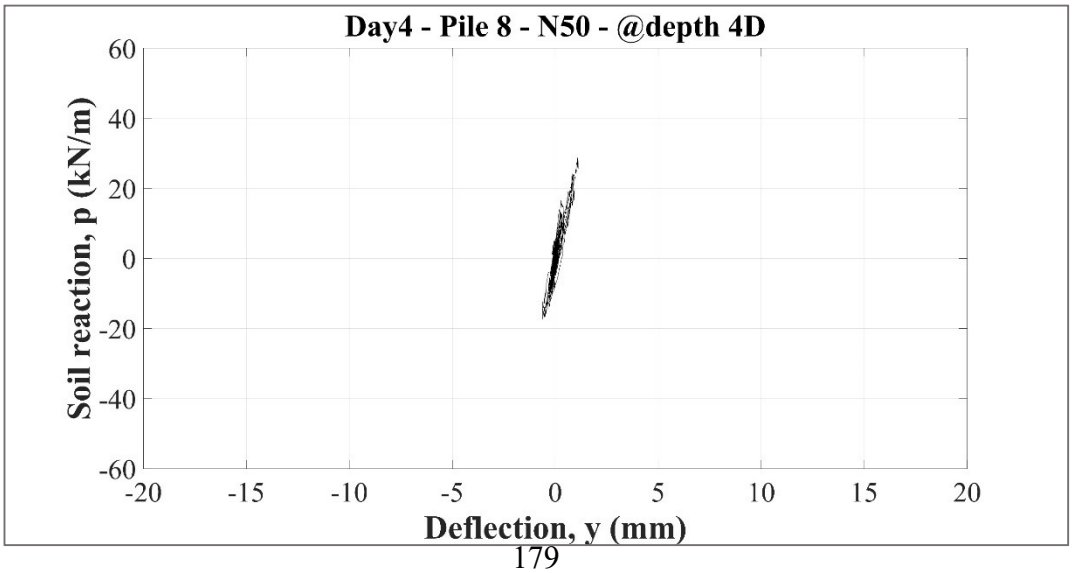
Day4 - Pile 8 - N50 - @depth 4D
Soil reaction, p (kN/m)
60
40
20
0
-20
-40
-60
-20
-15
-10
-5
0
5
10
15
20
Deflection, y (mm)

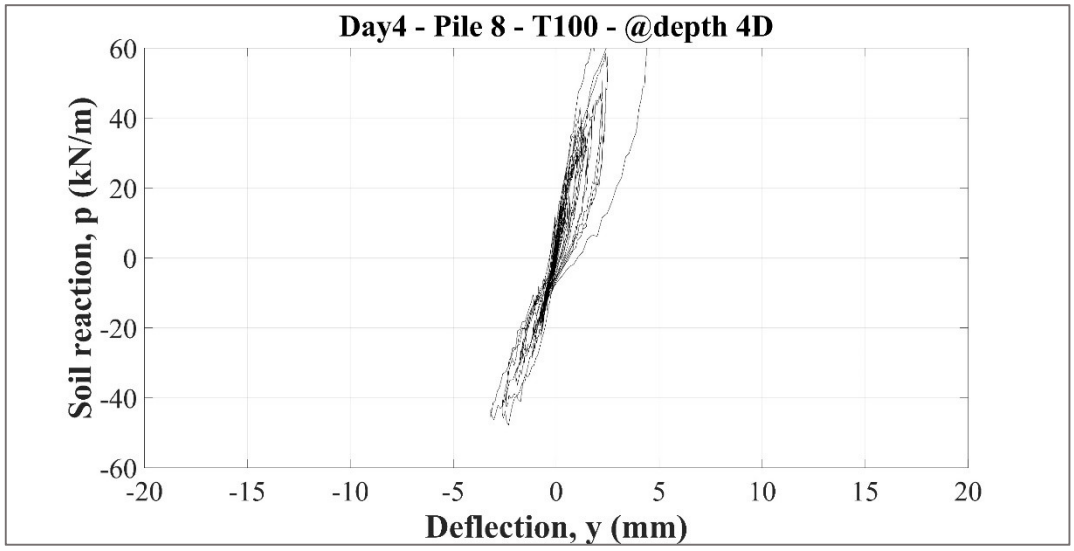
Day4 - Pile 8 - T100 - @depth 4D
Soil reaction, p (kN/m)
Deflection, y (mm)
60
40
20
0
-20
-40
-60
-20
-15
-10
-5
0
5
10
15
20

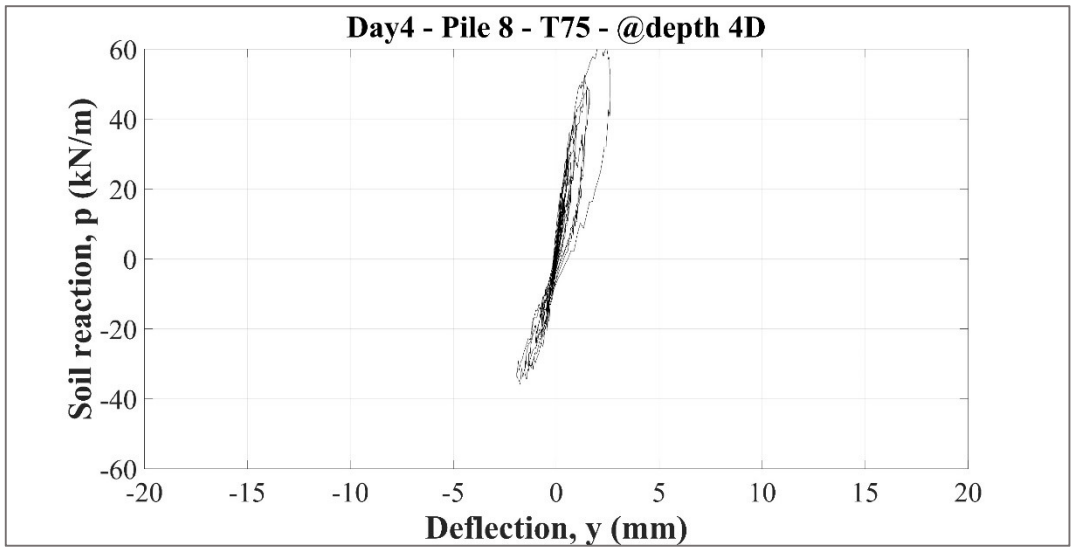
Day4 - Pile 8 - T75 - @depth 4D
Soil reaction, p (kN/m)
Deflection, y (mm)
60
40
20
0
-20
-40
-60
-20
-15
-10
-5
0
5
10
15
20

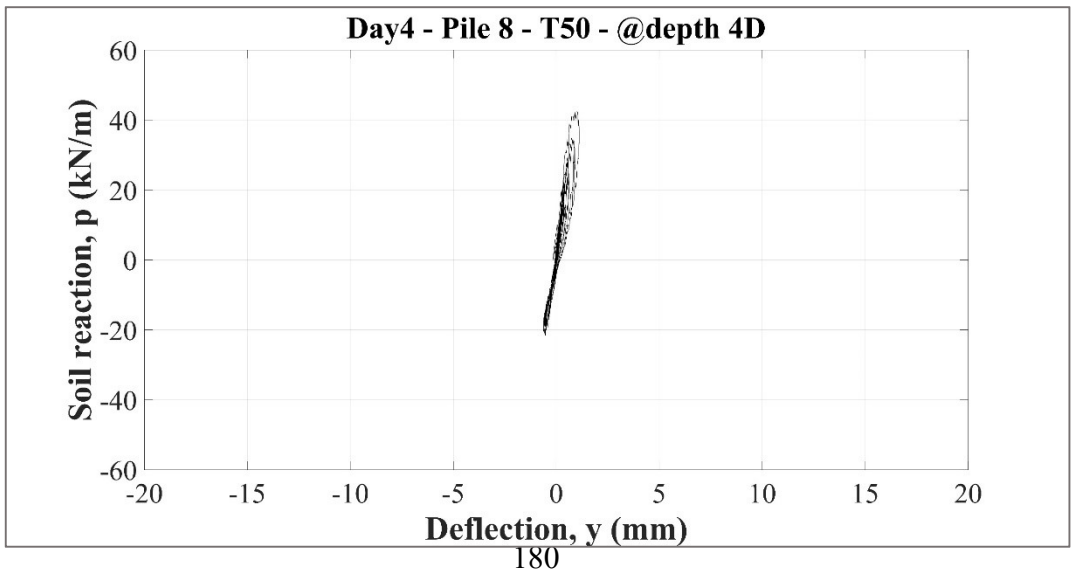
Day4 - Pile 8 - T50 - @depth 4D
Soil reaction, p (kN/m)
Deflection, y (mm)
60
40
20
0
-20
-40
-60
-20
-15
-10
-5
0
5
10
15
20

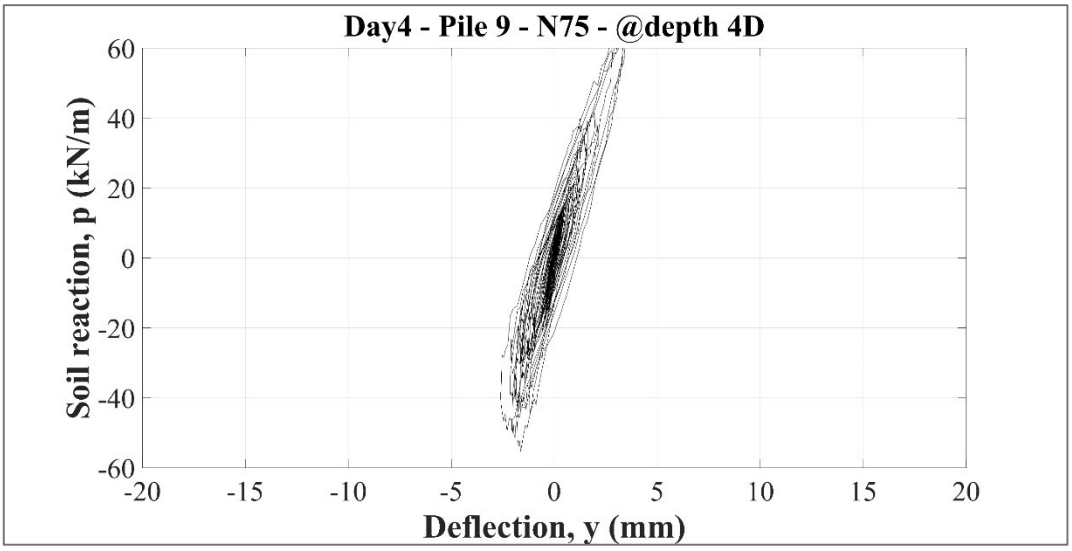
Day4 - Pile 9 - N75 - @depth 4D
Soil reaction, p (kN/m)
60
40
20
0
-20
-40
-60
-20
-15
-10
-5
0
5
10
15
20
Deflection, y (mm)

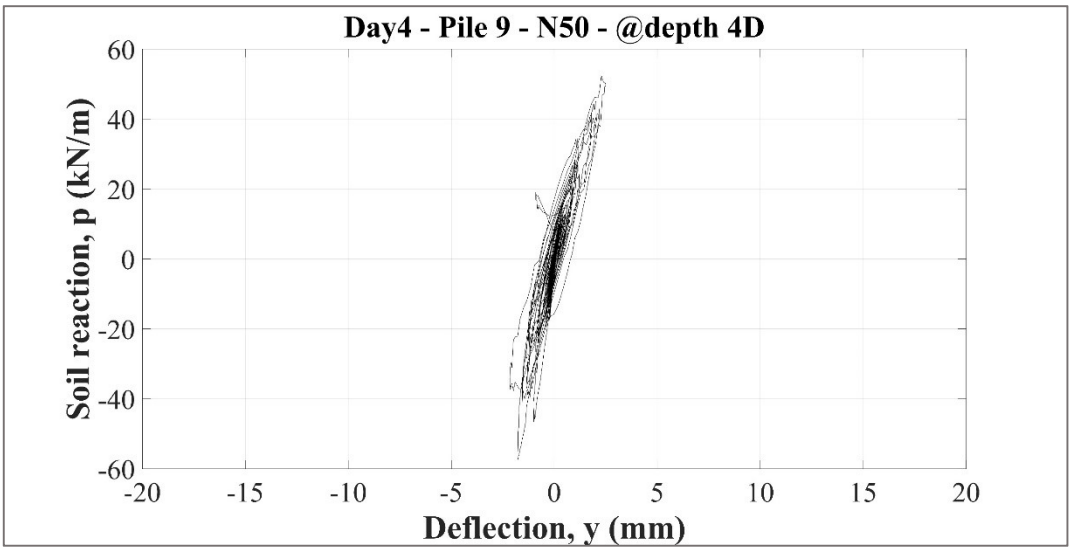
Day4 - Pile 9 - N50 - @depth 4D
Soil reaction, p (kN/m)
60
40
20
0
-20
-40
-60
-20
-15
-10
-5
0
5
10
15
20
Deflection, y (mm)

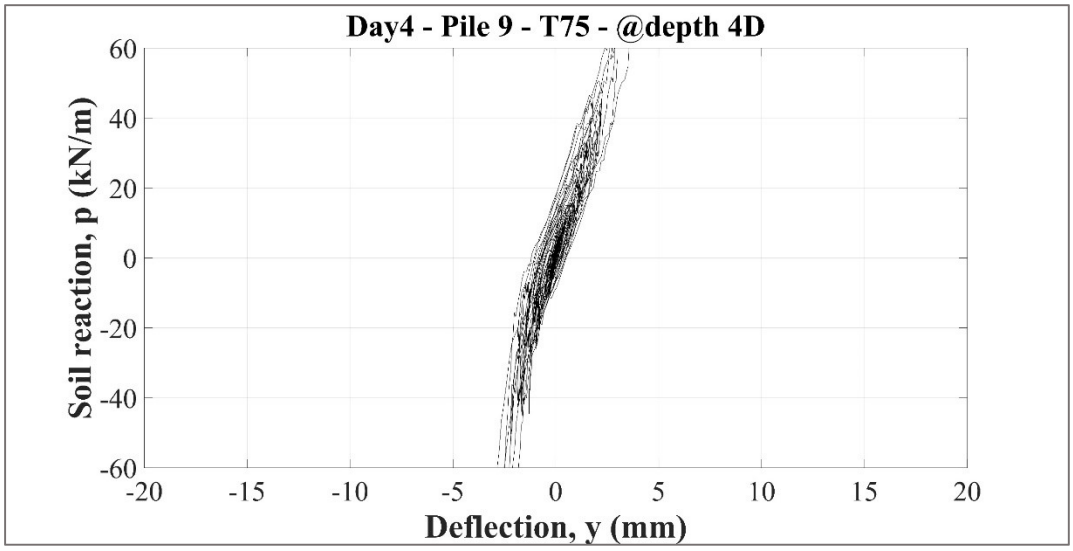
Day4 - Pile 9 - T75 - @depth 4D
Soil reaction, p (kN/m)
60
40
20
0
-20
-40
-60
-20
-15
-10
-5
0
5
10
15
20
Deflection, y (mm)

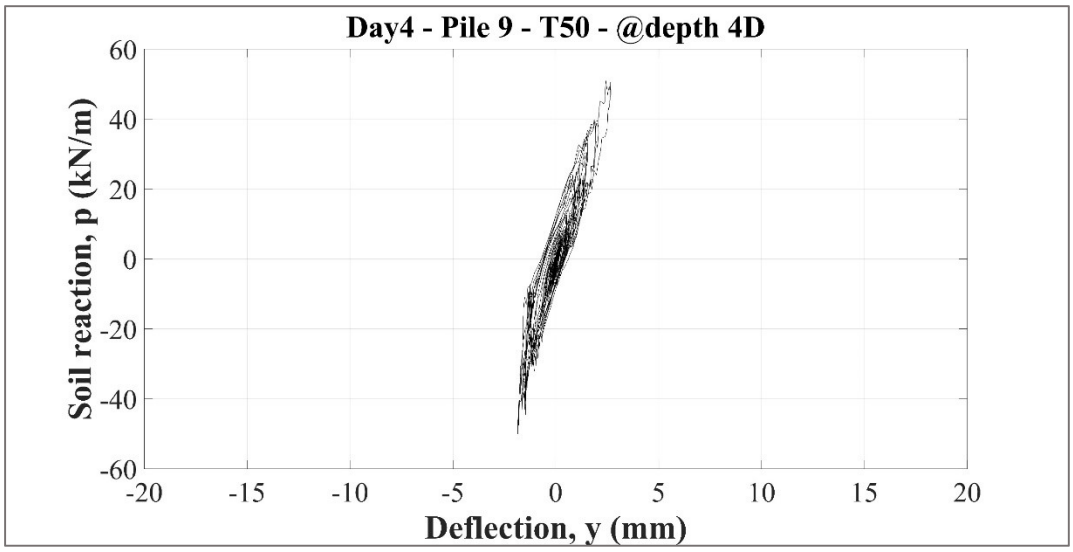
Day4 - Pile 9 - T50 - @depth 4D
Soil reaction, p (kN/m)
60
40
20
0
-20
-40
-60
-20
-15
-10
-5
0
5
10
15
20
Deflection, y (mm)

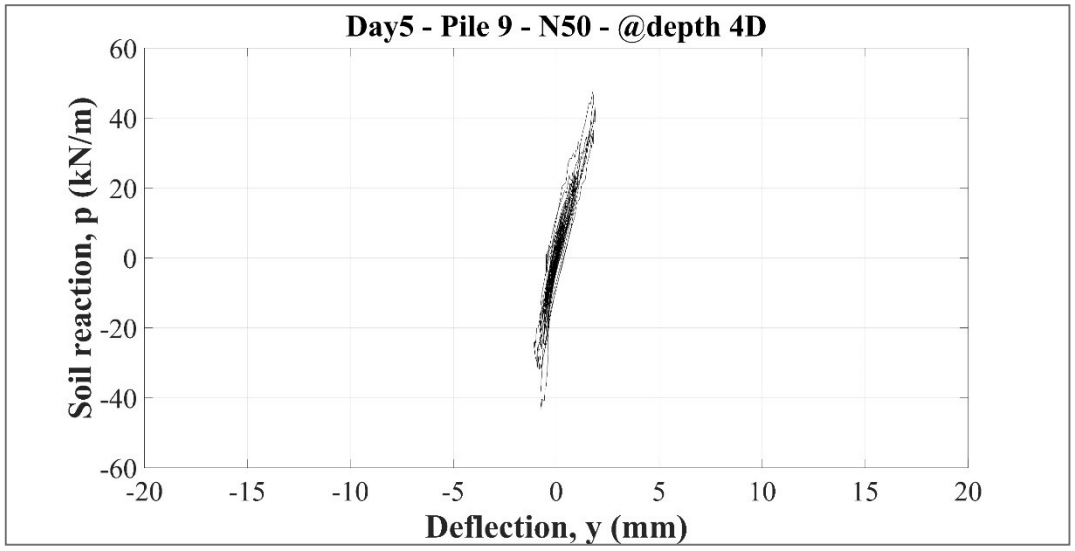
Day5 - Pile 9 - N50 - @depth 4D
Soil reaction, p (kN/m)
60
40
20
0
-20
-40
-60
-20
-15
-10
-5
0
5
10
15
20
Deflection, y (mm)

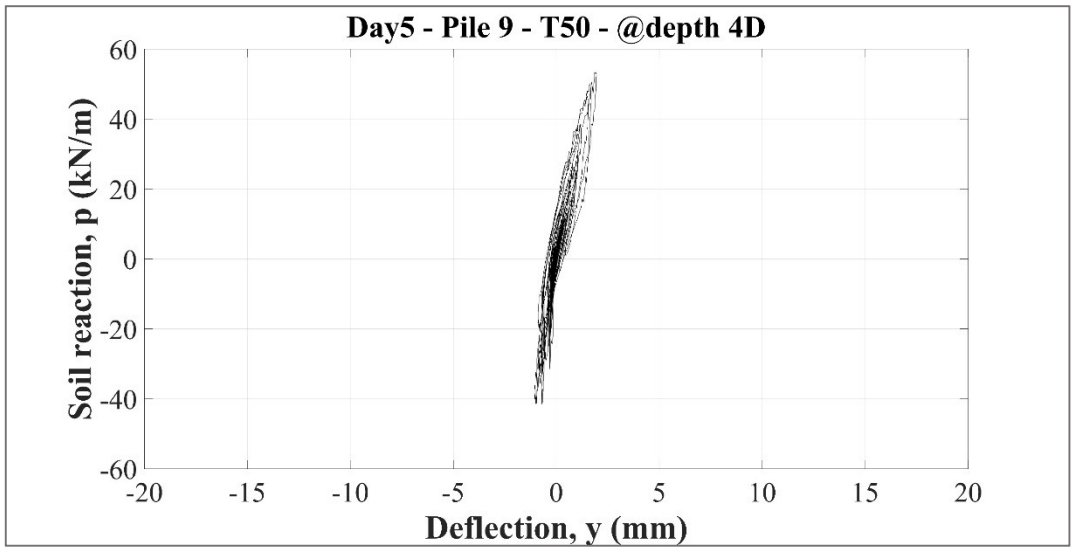
Day5 - Pile 9 - T50 - @depth 4D
Soil reaction, p (kN/m)
60
40
20
0
-20
-40
-60
-20
-15
-10
-5
0
5
10
15
20
Deflection, y (mm)

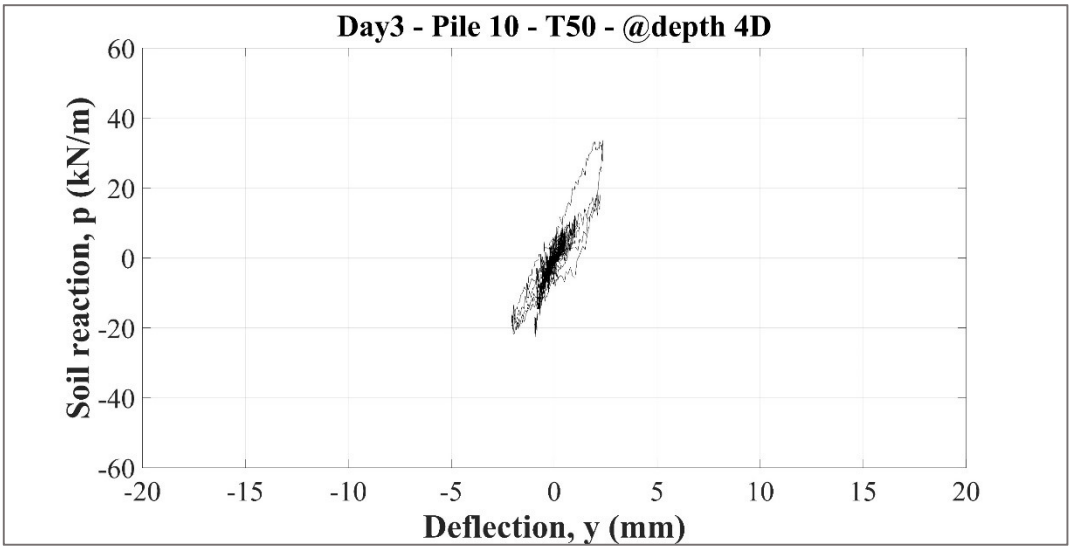
Day3 - Pile 10 - T50 - @depth 4D
Soil reaction, p (kN/m)
60
40
20
0
-20
-40
-60
-20
-15
-10
-5
0
5
10
15
20
Deflection, y (mm)

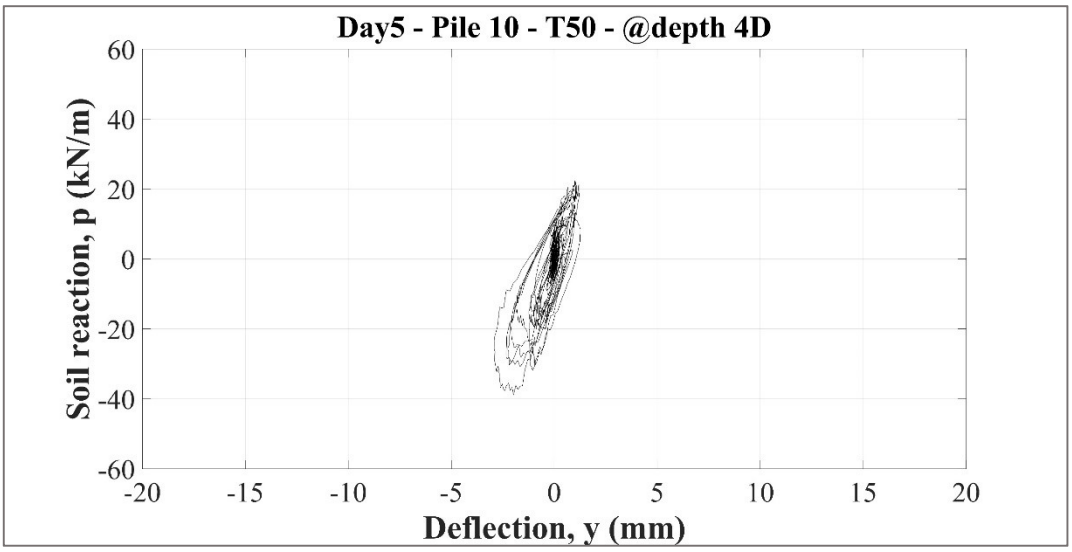
Day5 - Pile 10 - T50 - @depth 4D
Soil reaction, p (kN/m)
60
40
20
0
-20
-40
-60
-20
-15
-10
-5
0
5
10
15
20
Deflection, y (mm)

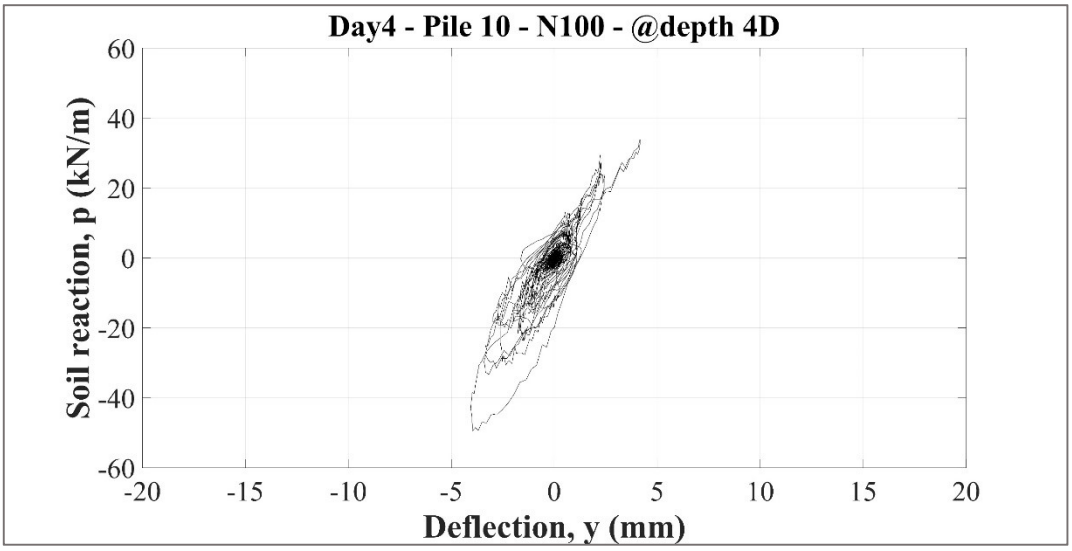
Day4 - Pile 10 - N100 - @depth 4D
Soil reaction, p (kN/m)
60
40
20
0
-20
-40
-60
-20
-15
-10
-5
0
5
10
15
20
Deflection, y (mm)

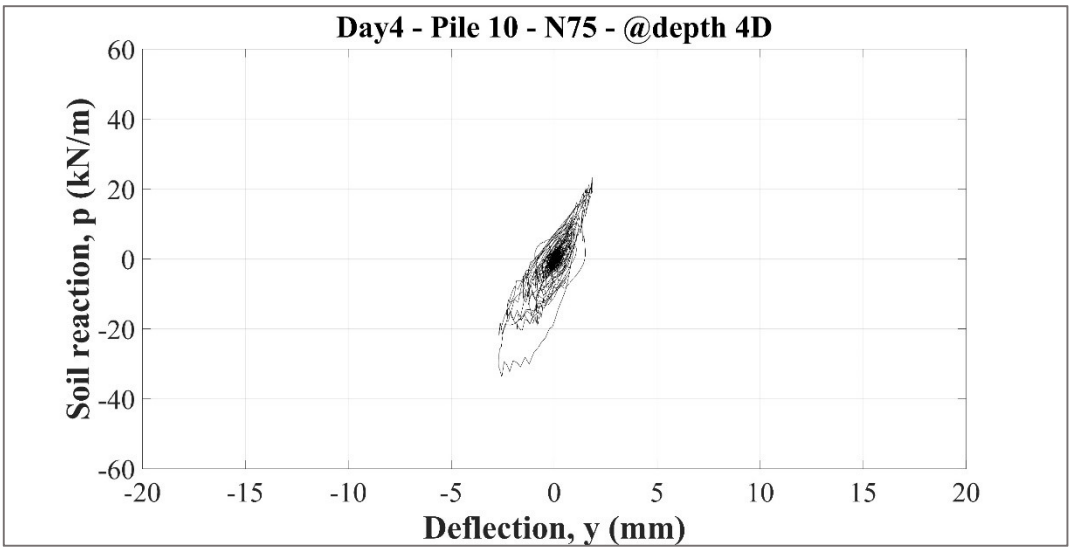
Day4 - Pile 10 - N75 - @depth 4D
Soil reaction, p (kN/m)
60
40
20
0
-20
-40
-60
-20
-15
-10
-5
0
5
10
15
20
Deflection, y (mm)

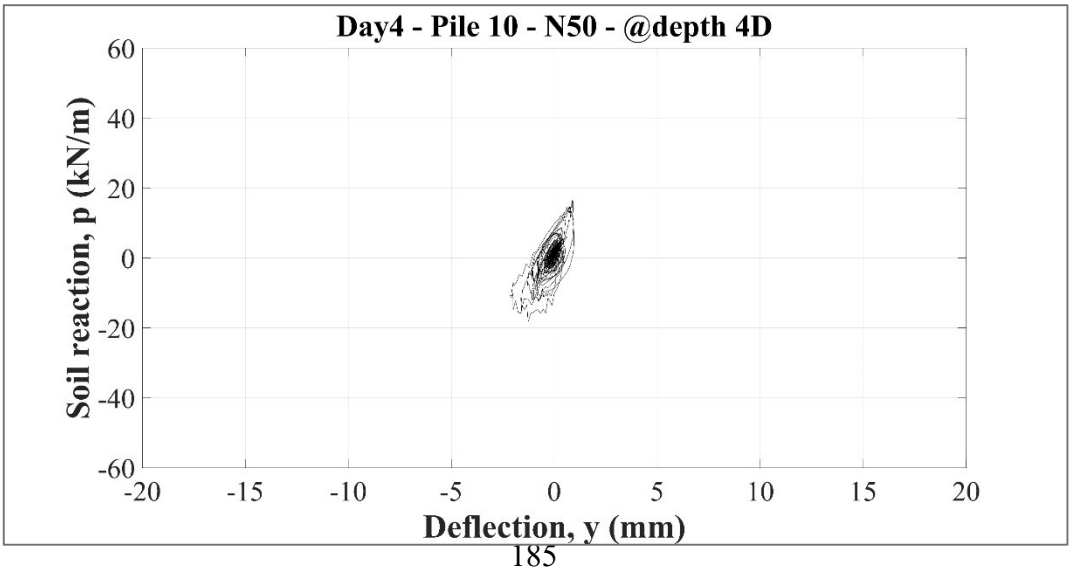
Day4 - Pile 10 - N50 - @depth 4D
Soil reaction, p (kN/m)
60
40
20
0
-20
-40
-60
-20
-15
-10
-5
0
5
10
15
20
Deflection, y (mm)

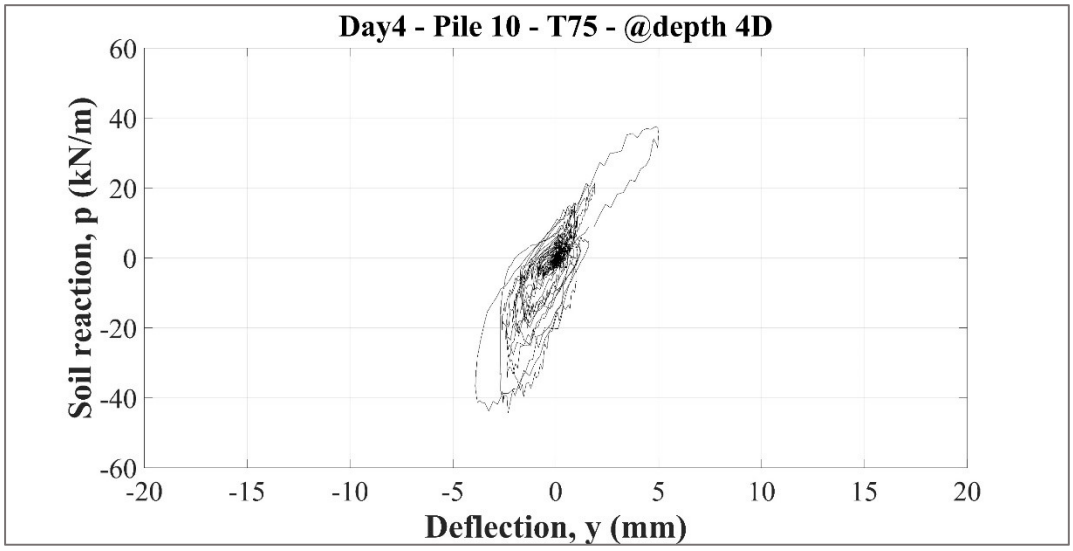
Day4 - Pile 10 - T75 - @depth 4D
Soil reaction, p (kN/m)
60
40
20
0
-20
-40
-60
-20
-15
-10
-5
0
5
10
15
20
Deflection, y (mm)

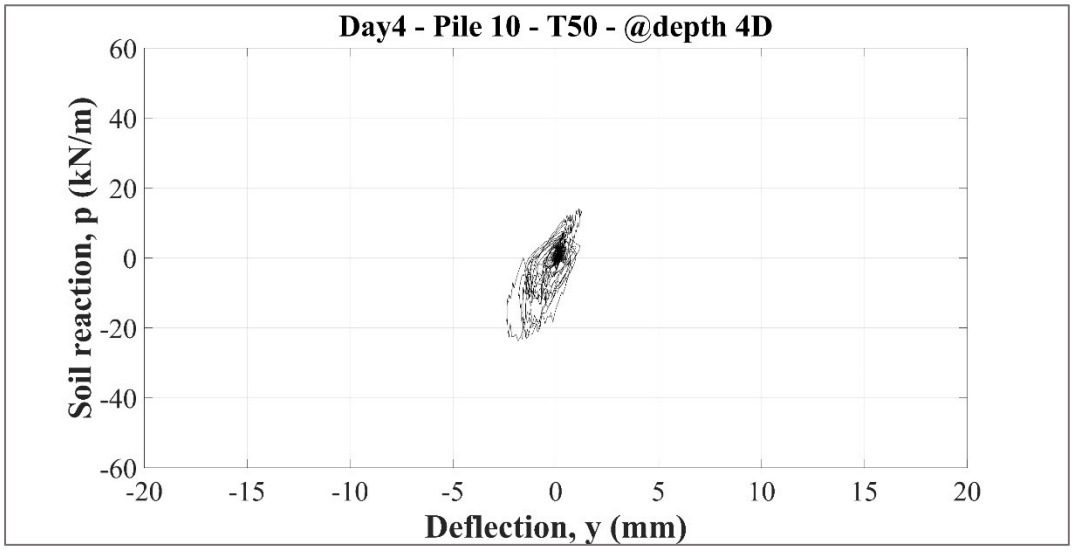
Day4 - Pile 10 - T50 - @depth 4D
Soil reaction, p (kN/m)
60
40
20
0
-20
-40
-60
-20
-15
-10
-5
0
5
10
15
20
Deflection, y (mm)

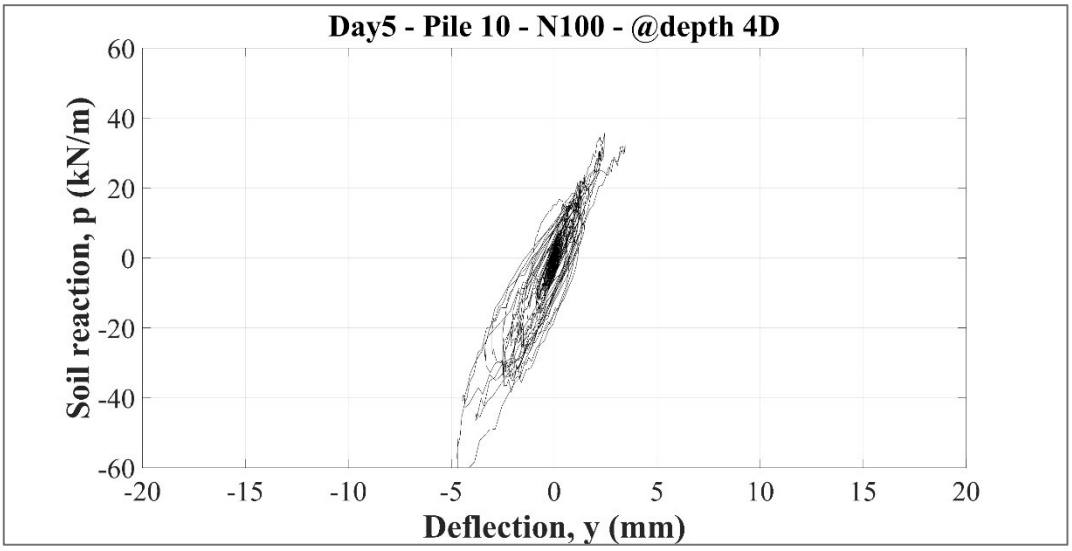
Day5 - Pile 10 - N100 - @depth 4D
Soil reaction, p (kN/m)
Deflection, y (mm)
60
40
20
0
-20
-40
-60
-20
-15
-10
-5
0
5
10
15
20

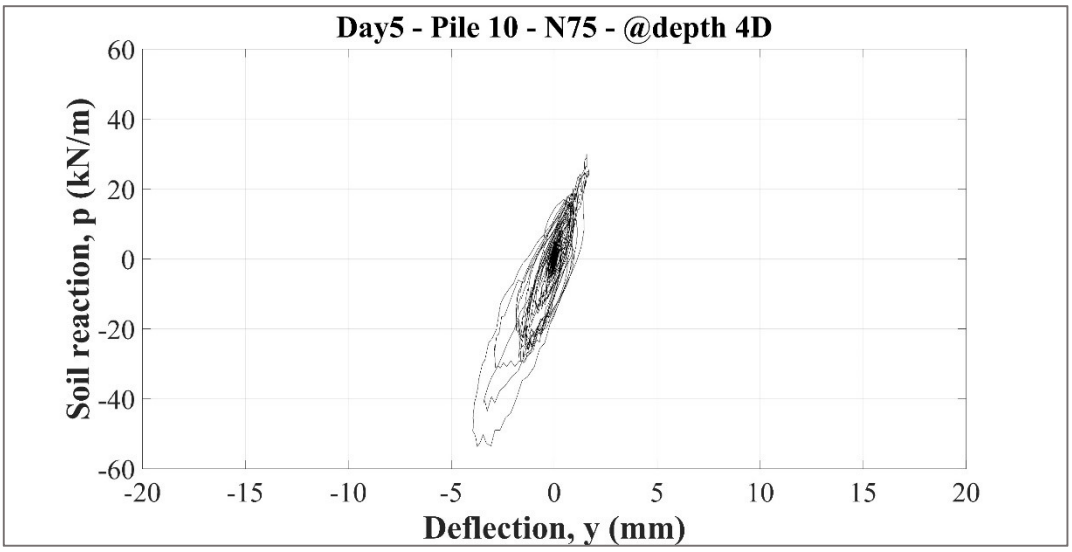
Day5 - Pile 10 - N75 - @depth 4D
Soil reaction, p (kN/m)
Deflection, y (mm)
60
40
20
0
-20
-40
-60
-20
-15
-10
-5
0
5
10
15
20

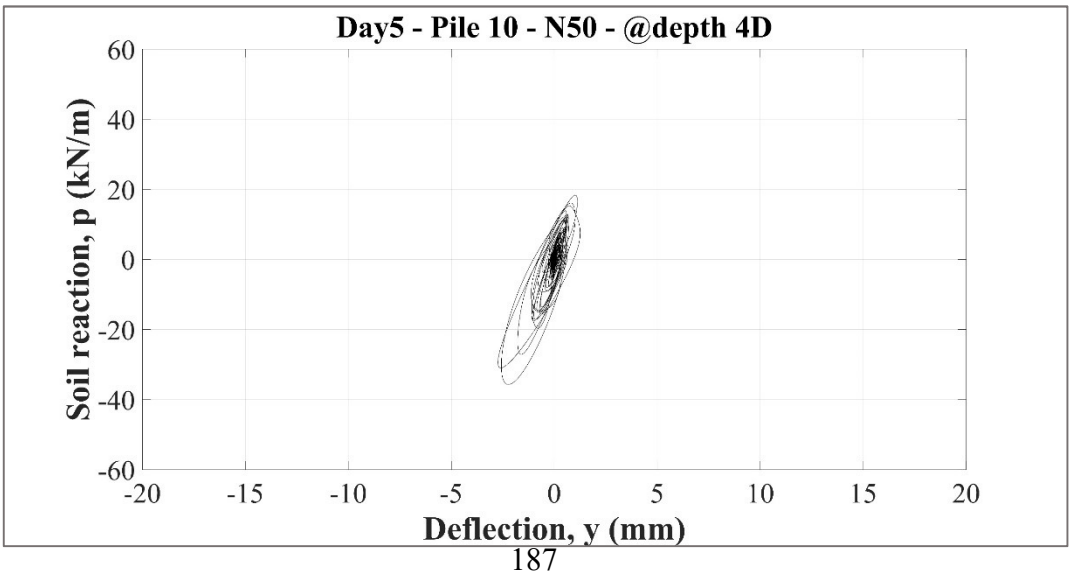
Day5 - Pile 10 - N50 - @depth 4D
Soil reaction, p (kN/m)
Deflection, y (mm)
60
40
20
0
-20
-40
-60
-20
-15
-10
-5
0
5
10
15
20